

COMPLEX BEHAVIOR OF SWITCHING POWER CONVERTERS

Chi Kong Tse



CRC PRESS

Boca Raton London New York Washington, D.C.

Library of Congress Cataloging-in-Publication Data

Tse, Chi Kong.

Complex behavior of switching power converters / by Chi Kong Tse.

p. cm. — (Power electronics and applications series)

Includes bibliographical references and index.

ISBN 0-8493-1862-9 (alk. paper)

1. Electric current converters. 2. Semiconductor switches. 3. Switching power supplies.

I. Title. II. Series.

TK7872.C8T74 2003

621.31'7—dc21

2003053187

This book contains information obtained from authentic and highly regarded sources. Reprinted material is quoted with permission, and sources are indicated. A wide variety of references are listed. Reasonable efforts have been made to publish reliable data and information, but the author and the publisher cannot assume responsibility for the validity of all materials or for the consequences of their use.

Neither this book nor any part may be reproduced or transmitted in any form or by any means, electronic or mechanical, including photocopying, microfilming, and recording, or by any information storage or retrieval system, without prior permission in writing from the publisher.

The consent of CRC Press LLC does not extend to copying for general distribution, for promotion, for creating new works, or for resale. Specific permission must be obtained in writing from CRC Press LLC for such copying.

Direct all inquiries to CRC Press LLC, 2000 N.W. Corporate Blvd., Boca Raton, Florida 33431.

Trademark Notice: Product or corporate names may be trademarks or registered trademarks, and are used only for identification and explanation, without intent to infringe.

Visit the CRC Press Web site at www.crcpress.com

© 2004 by CRC Press LLC

No claim to original U.S. Government works

International Standard Book Number 0-8493-1862-9

Library of Congress Card Number 2003053187

Printed in the United States of America 1 2 3 4 5 6 7 8 9 0

Printed on acid-free paper

To Belinda and Eugene

*P*refac*e*

Power electronics, as an application-oriented discipline, has been developed to address specific power conversion problems in industrial, commercial, residential and aerospace environments. In the past three decades, motivated by the burgeoning demand of delivering electric power in various specific forms, this branch of electrical engineering has undergone an intense development in many areas of technology, including power devices, control methods, circuit design, computer-aided analysis, passive components, packaging techniques, and so on. The principal focus in power electronics has been to fulfill the functional requirements of the intended applications. Because practical applications are the prime concerns, it often turns out that a particular circuit topology or system implementation has found widespread applications long before it has been thoroughly analyzed. For instance, switching power converters have been used for more than half a century, but analytical models that allow systematic circuit design (e.g., averaged models and sampled-data models) have been available only since the late 1970s.

Power electronics circuits, being nonlinear, exhibit a variety of complex behavior such as sudden change of operating regime, chaotic operation, occasional instability (in certain parameter windows), intermittent subharmonic or chaotic operation, etc. Power electronics engineers are always dealing with these problems in the course of developing power electronics products. Since the engineers' job is to make the circuit work in the expected operating regime, the usual treatment is to find ways to eliminate any unwanted behavior, often in some quick and heuristic manner such as adjusting circuit components and parameters through a trial-and-error procedure. However, as the field of power electronics gains maturity, the quest for better design, functionality and reliability has made it necessary for engineers to understand thoroughly the behavior of the systems being designed under all possible practical conditions. For example, *bifurcation*, a behavior characterized by a sudden change of operating regime when a parameter is varied intentionally or unintentionally, can be catastrophic, leading possibly to unexpected expansion of operating ranges which can damage semiconductor devices. Thus, knowing *when* (under what conditions) and *how* (in what way) a bifurcation occurs should be of fundamental importance. Such knowledge, however, requires appropriate modeling methodology and in-depth analysis.

This book is concerned with the study of complex behavior of switching power converters. The objective is to provide a systematic treatment procedure for observation, identification and diagnosis of the complex behavior

exhibited by switching power converters. The essential techniques for capturing complex behavior on the computer and in the laboratory are explained, along with application examples describing the key procedure for diagnosing complex behavior such as chaos and bifurcation. The target audience includes graduate students, researchers and engineers who work in the field of power electronics and have the need or interest to understand complex behavior in switching power converters. Furthermore, in presenting the techniques of investigation and the various findings, a conscientious effort has been made to emphasize circuit operation rather than mathematical abstraction, and whenever possible, phenomena will be explained in terms of the physical circuit operation with a minimal amount of mathematics. With this, we hope this book can also be useful as a start-up guide for graduate students and researchers who wish to grasp the essentials for analyzing complex behavior in power converters, as well as a readable reference for engineers who wish to understand such complex behavior.

We begin in [Chapter 1](#) with an overview of the complex behavior of switching power converters, outlining some important findings and research methodologies. We will also introduce some salient concepts of nonlinear dynamical systems that are essential to the study of complex behavior in switching converters. In [Chapter 2](#), we introduce specific computer and laboratory techniques for studying complex behavior. In [Chapter 3](#), we describe the key modeling approaches for switching converters which are capable of retaining the salient nonlinear properties and hence can be used to study complex behavior. Our formal investigation of the nonlinear dynamics of switching converters begins in [Chapter 4](#), where we test-drive a discrete-time analysis method on a simple first-order system. The purpose is to illustrate the key procedure involved in the analysis of period-doubling bifurcation, which is a commonly found phenomenon in switching converters. In [Chapter 5](#), we take a detailed look at the basic phenomenology for power electronics circuits, which is characterized by the interaction of smooth and non-smooth bifurcations. In describing this important basic phenomenon, we emphasize the physical mechanism that prevents a switching converter from operating “smoothly.” Specifically, from a circuit operational viewpoint, we explain the mechanism of the so-called *border collision*, and make an attempt to predict its occurrence. In [Chapter 6](#), we move on to a high-order converter, known as the Ćuk converter. The bifurcation behavior of this converter is studied for two different control configurations. Our aim is to highlight the importance of choosing the appropriate models for analysis. This issue is again addressed in [Chapters 7](#) and [8](#), where two different types of parallel-connected switching converters are treated with different modeling approaches. In [Chapter 9](#), we consider an application of bifurcation analysis to a practical power-factor-correction switching converter where we uncover a possible but rarely known fast-scale instability. In [Chapter 10](#), we investigate the problem of intermittent operation in switching converters. By using an appropriate model that incorporates a mechanism that couples spurious signals into a power converter, we explain

a possible origin for intermittent chaotic or subharmonic operations.

For the successful completion of this book, I am indebted to a number of people, institutions and organizations. First of all, in the course of my research in this field, I have been constantly stimulated, challenged and inspired by my students. Among them, special credits must go to my former graduate students and postdoctoral assistants, William Chan, Octavian Dranga, Herbert Iu and Yufei Zhou, not only for their diligent work which has added materially to this book, but also for their inquiring minds which have prompted me to pay attention to many important but easily overlooked problems. I also wish to express my sincere appreciation to Prof. Soumitro Banerjee, who has read a large part of an earlier version of this book and has made many valuable suggestions and comments. Excellent opportunities and environments for pursuing this writing project were kindly provided by Prof. Hiroshi Kawakami of Tokushima University and Prof. Leon Chua of UC Berkeley while I spent my sabbatical in their laboratories during last fall and spring. Furthermore, I have been particularly fortunate to have the opportunities to discuss research problems with many brilliant researchers and colleagues. Among them, Mario di Bernardo, Ron Chen, Martin Chow, Tetsuro Endo, Yuk-Ming Lai, Francis Lau, Yim-Shu Lee, István Nagy, Shui-Sheng Qiu, Toshimichi Saito, Michael Small, Tetsushi Ueta and Siu-Chung Wong deserve my most grateful thanks. I would also like to thank the editor of this series, Prof. Muhammad Rashid, and the staff of the CRC Press at Boca Raton for their professional and enthusiastic support of this project.

Last, but by no means least, I must thank the Hong Kong Research Grant Council and the Research Committee of Hong Kong Polytechnic University for funding my research work.

Hong Kong

C. K. Tse

Contents

Preface

1 Introduction

- 1.1 Overview of Power Electronics Circuits
 - 1.1.1 Switching Power Converters
 - 1.1.2 Voltage-Mode Control
 - 1.1.3 Current-Mode Control
 - 1.1.4 Complexity of Operation
- 1.2 Overview of Modeling Strategies for Switching Converters
 - 1.2.1 From Nonlinear Models to Linear Models
 - 1.2.2 Back to Nonlinear Models
- 1.3 Overview of Nonlinear Dynamical Systems
 - 1.3.1 Qualitative Behavior of Dynamical Systems
 - 1.3.2 Bifurcation
 - 1.3.3 Deterministic Chaos
 - 1.3.4 Quantifying Chaos
 - 1.3.5 Routes to Chaos
- 1.4 Complex Behavior in Power Electronics

2 Computer and Laboratory Techniques for Studying Nonlinear Behavior in Switching Power Converters

- 2.1 The Use and Misuse of Computer Simulations
 - 2.1.1 Improper Choice of Models
 - 2.1.2 Insufficient Resolution
- 2.2 Accuracy of Models: Does It Matter?
- 2.3 Mode of Investigation
- 2.4 Capturing Complex Behavior on Computers
 - 2.4.1 Time-Evolution Behavior under Fixed Parameters
 - 2.4.2 Bifurcation Behavior under Varying Parameters
- 2.5 Test for Chaos: The Lyapunov Exponent
 - 2.5.1 Computing Lyapunov Exponents from Iterative Maps
 - 2.5.2 Computing Lyapunov Exponents from Time Series
- 2.6 Laboratory Investigation
 - 2.6.1 Capturing Waveforms, Phase Portraits and Frequency Spectra
 - 2.6.2 Capturing Poincaré Sections on Oscilloscopes

- 2.6.3 Plotting Bifurcation Diagrams on Oscilloscopes
 - 2.6.4 Alternative Methods of Plotting Bifurcation Diagrams in the Laboratory
 - 2.7 Roles of Laboratory Experiments and Computer Simulations
- 3 Modeling of Switching Power Converters for Nonlinear Dynamical Analysis**
- 3.1 A Glimpse at Discrete-Time Modeling
 - 3.1.1 Ad Hoc Derivation of the Discrete-Time Iterative Map for the Boost Converter
 - 3.1.2 Steady-State Solution
 - 3.1.3 Approximation by Series Expansion
 - 3.2 General Procedure for Derivation of Discrete-Time Iterative Maps for the Basic Switching Converters
 - 3.2.1 Continuous Conduction Mode
 - 3.2.2 Discontinuous Conduction Mode
 - 3.3 Approximation of Iterative Maps by Series Expansions
 - 3.4 Approximate Iterative Maps for the Boost and Buck Converters
 - 3.4.1 Continuous Conduction Mode
 - 3.4.2 Discontinuous Conduction Mode
 - 3.5 The Method of Averaging
 - 3.5.1 General Procedure
 - 3.5.2 Averaged Models for the Boost and Buck Converters
 - 3.5.3 Steady-State Solutions
 - 3.5.4 Averaged Circuit Models
 - 3.6 Control Law to Complete the Model
 - 3.7 Determination of the Boundary of Operating Modes
 - 3.8 Border Collision: A Trivial Case
 - 3.9 Pros and Cons of the Models
- 4 Analysis of Period-Doubling Bifurcation in Switching Converters Operating in Discontinuous Conduction Mode**
- 4.1 Review of the Derivation of Iterative Maps
 - 4.2 The Closed-Loop System and Control Equation
 - 4.3 Period-Doubling Bifurcation
 - 4.4 Computer Simulations
 - 4.5 Experimentation
 - 4.5.1 Circuit Operation
 - 4.5.2 Experimental Observations
 - 4.6 Recapitulation of Basic Phenomenology

5 Bifurcation Behavior in Switching Power Converters: Smooth versus Non-Smooth Bifurcations

- 5.1 A Quick Glimpse at Complexity
 - 5.1.1 Buck Converter Operating in Continuous Conduction Mode under Simple Voltage Feedback Control
 - 5.1.2 Bifurcation Behavior from Simulations and Measurements
 - 5.1.3 A Zoo of Complex Behaviors
 - 5.1.4 “Skipped” Cycles and Border Collision
- 5.2 Current-Mode Controlled Switching Converters
 - 5.2.1 Overview of Operation
 - 5.2.2 Derivation of the Describing Iterative Map
- 5.3 Initial Simulation Study of the Boost Converter under Current-Mode Control
- 5.4 Bifurcation Behavior of the Open-Loop Current-Mode Controlled Boost Converter
 - 5.4.1 Analysis via the Iterative Map
 - 5.4.2 Bifurcation Diagrams Based on the Iterative Map
 - 5.4.3 Bifurcation Diagrams Based on Circuit Simulations
 - 5.4.4 Experimental Verification
- 5.5 Theoretical Analysis of Period-Doubling Bifurcation and Border Collision
 - 5.5.1 Analysis of Period-Doubling
 - 5.5.2 Analysis of Border Collision
- 5.6 Bifurcation Behavior of the Closed-Loop Current-Mode Controlled Boost Converter
- 5.7 Border Collision: Is It Important?

6 Nonlinear Dynamics of the Ćuk Converter

- 6.1 Review of the Ćuk Converter and Its Operation
- 6.2 Bifurcation Behavior for Fixed-Frequency Operation
 - 6.2.1 Fixed-Frequency Current-Mode Control
 - 6.2.2 Analysis of Bifurcation Behavior
 - 6.2.3 Verification by Computer Simulations
 - 6.2.4 Interim Conclusion on the Basic Phenomenology
- 6.3 Bifurcation Behavior for Free-Running Operation
 - 6.3.1 Autonomous System Modeling
 - 6.3.2 Dimensionless Equations
 - 6.3.3 Stability of Equilibrium Point and Hopf Bifurcation
 - 6.3.4 Local Trajectories from Describing Equation
 - 6.3.5 Computer Simulations
- 6.4 Recapitulation

- 7 Bifurcation Behavior of Parallel-Connected Buck Converters via Discrete-Time Models**
 - 7.1 Parallel-Connected Switching Converters
 - 7.1.1 The Basic Issue of Current Sharing
 - 7.1.2 The Master-Slave Scheme for Current Sharing
 - 7.2 State Equations for Two Parallel Buck Converters
 - 7.3 Initial Simulation Study
 - 7.4 Experimentation
 - 7.5 Analysis of Period-Doubling Bifurcation
 - 7.5.1 Derivation of the Discrete-Time Map
 - 7.5.2 Derivation of the Jacobian
 - 7.5.3 Characteristic Multipliers and Period-Doubling Bifurcation
 - 7.6 Analysis of Border Collision
 - 7.7 A Remark on Modeling: Can It Be Simpler?
- 8 Slow-Scale Bifurcation Behavior of Parallel-Connected Boost Converters via Averaged Models**
 - 8.1 The System of Parallel-Connected Boost Converters
 - 8.2 Initial Experimentation
 - 8.3 Averaged Model for Two Parallel Boost Converters
 - 8.3.1 Derivation of State Equations
 - 8.3.2 Dimensionless Equations
 - 8.3.3 Equilibrium Point Calculation
 - 8.4 Stability of Equilibrium Point and Hopf Bifurcation
 - 8.5 Local Trajectories from the Averaged Equations
 - 8.6 Computer Simulation Study
 - 8.7 Usefulness of Averaged Models
- 9 Fast-Scale Bifurcation Analysis of Power-Factor-Correction Boost Converters**
 - 9.1 Bifurcation Analysis of Boost Converters under Current-Mode Control with Ramp Compensation
 - 9.1.1 Review of Basic Operation
 - 9.1.2 Review of Period-Doubling Bifurcation
 - 9.1.3 Ramp Compensation from a Bifurcation Control Viewpoint
 - 9.2 Application to Power-Factor-Correction Boost Converter
 - 9.2.1 Bifurcation Analysis
 - 9.2.2 Fast-Scale Instability by Computer Simulations
 - 9.3 A Note on Fast-Scale and Slow-Scale Instabilities

10 Intermittent Chaotic Operation in Switching Power Converters

- 10.1 Simplified Model of Spurious Signal Intrusion
- 10.2 Quick Glimpse at “Intermittent” Chaos
- 10.3 Time-Bifurcation Diagrams – A Closer Look
 - 10.3.1 Sinusoidal Intruding Source
 - 10.3.2 Rectangular Pulse Intruding Source
- 10.4 Experimental Observations
- 10.5 Parameters Affecting the Occurrence of “Intermittent” Chaos
- 10.6 Summary of the Basic Phenomenon

Glossary

Bibliography

1

Introduction

Research in *nonlinear systems and complexity* had made remarkable progress in the 1970's and 1980's, leading to discoveries which were not only new, but also revolutionary in the sense that some of our traditional beliefs regarding the behavior of deterministic systems were relentlessly challenged [63, 64, 79, 92]. Most striking of all, simple deterministic systems can behave in a "random-like" fashion and their solution trajectories can deny "long-term predictability" even if the initial conditions are practically known [29, 54, 76, 109]. Such behavior is now termed *chaos*, which underlies the *complexity* and subtle *order* exhibited by real-world systems. Scientists, mathematicians and engineers from a diverging range of disciplines have found remarkably similar complex behavior in their systems. The root cause of such complex behavior has been identified collectively as *nonlinearity*. Precisely, without exception, all systems in the real world are nonlinear. In this book, we are concerned with a particular class of engineering systems, known as power electronics, which by virtue of its rich nonlinearity exhibits a variety of complex behavior.

In this introductory chapter we will take a quick tour of power electronics circuits and dynamical systems. Our aim is to introduce the basic types of switching converters, their salient operating features, modeling approaches and nonlinear behavior. We will also introduce some basic concepts of nonlinear dynamics that are necessary for understanding the complex behavior of switching converters to be described in the later chapters.

1.1 Overview of Power Electronics Circuits

The basic operation of any power electronics circuit involves toggling among a set of linear or nonlinear circuit topologies, under the control of a feedback system [33, 78, 81, 99, 100, 118, 128]. As such, they can be regarded as *piecewise switched* dynamical systems. For example, in simple switching converters, such as the ones shown in Figure 1.1, an inductor (or inductors) is/are "switched" between the input and the output through an appropriate switching element (labelled as S in the figure). The way in which the inductor(s) is/are switched determines the output voltage level and transient behavior. Usually, a semiconductor switch and a diode are used to implement

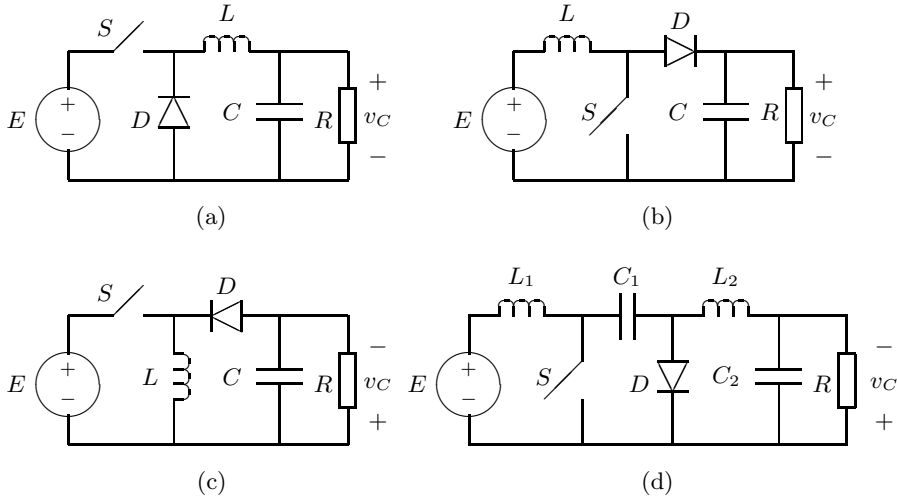


FIGURE 1.1

Examples of simple switching converters. (a) Buck converter; (b) boost converter; (c) buck-boost converter; (d) boost-buck (Cuk) converter.

such switching. Through the use of a feedback control circuit, the relative durations of the various switching intervals are continuously adjusted. Such feedback action effectively controls the transient and steady-state behaviors of the circuit. Thus, both the circuit topology and the control method determine the dynamical behavior of a power electronics circuit.

1.1.1 Switching Power Converters

Most power converters are constructed on the basis of the simple converters shown in Figure 1.1 [128]. Typically, the switch and the diode are turned on and off in a cyclic and complementary manner. The switch is directly controlled by a pulse-width modulated signal which is derived from a feedback circuit. The diode turns on and off depending upon its terminal condition. When the switch is closed, the diode is reverse biased and hence open. Under this condition, the inductor current ramps up. When the switch is turned off, the diode is forward biased and behaves as a short circuit. This causes the inductor current to ramp down. The process repeats cyclically. The system can therefore be plainly described by a set of state equations, each responsible for one particular switch state. For the operation described above, we have two state equations:

$$\dot{x} = \mathbf{A}_1 x + \mathbf{B}_1 E \quad \text{switch on and diode off} \quad (1.1)$$

$$\dot{x} = \mathbf{A}_2 x + \mathbf{B}_2 E \quad \text{switch off and diode on} \quad (1.2)$$

where \mathbf{x} is the state vector usually consisting of all capacitor voltages and inductor currents, the \mathbf{A} 's and \mathbf{B} 's are the system matrices, and E is the input voltage. Furthermore, because the conduction of the diode is determined by its own terminal condition, there is a possibility that the diode can turn itself off even when the switch is off. This happens when the diode current becomes zero and is not permitted to reverse its direction. In the power electronics literature, this operation has been termed *discontinuous conduction mode*, as opposed to *continuous conduction mode* where the switch and the diode operate strictly in a complementary fashion.* Clearly, we have another state equation for the situation where both switch and diode are off.

$$\dot{\mathbf{x}} = \mathbf{A}_3\mathbf{x} + \mathbf{B}_3E \quad \text{switch off and diode off.} \quad (1.3)$$

In practice, the choice between continuous and discontinuous conduction modes of operation is often an engineering decision. Continuous conduction mode is more suited for high power applications, whereas discontinuous conduction mode is limited to low power applications because of the relatively high device stresses. On the other hand, discontinuous conduction mode gives a more straightforward control design and generally yields faster transient responses. Clearly, a number of factors determine whether the converter would operate in continuous or discontinuous conduction mode. For instance, the size of the inductance determines how rapidly the current ramps up and down, and hence is a determining factor for the operating mode. We will postpone the detailed discussion of the operating modes to [Chapter 3](#).

We now examine the control of switching converters. First, as in all control systems, a control input is needed. For switching converters, the usual choice is the *duty cycle*, d , which is defined as the fraction of a repetition period, T , during which the switch is closed, i.e.,

$$d = \frac{t_c}{T} \quad (1.4)$$

where t_c is the time duration when the switch is held closed. In practice, the duty cycle is continuously controlled by a feedback circuit that aims to maintain the output voltage at a fixed level even under input and load variations. In the steady state, the output voltage is a function of the duty cycle and the input voltage. For the buck converter operating in continuous conduction mode, for example, the volt-time balance for the inductor requires that the following be satisfied in the steady state:

$$(E - V_C)DT = V_C(1 - D)T \Rightarrow V_C = DE \quad (\text{buck converter}) \quad (1.5)$$

where uppercase letters denote steady-state values of the respective variables. Likewise, for the other converters shown in [Figure 1.1](#) operating in continuous

*For simplicity, we omit details of the other operating modes which can possibly happen in the Cuk converter [143].

conduction mode, we have

$$V_C = \frac{E}{1 - D} \quad (\text{boost converter}) \quad (1.6)$$

$$V_C = \frac{ED}{1 - D} \quad (\text{buck-boost converter}) \quad (1.7)$$

$$V_C = \frac{ED}{1 - D} \quad (\text{Cuk converter}) \quad (1.8)$$

Thus, we see that as long as the duty cycle and input voltage are fixed, the output voltage will converge to a value given in the above formulas. Moreover, in the event of a transient in the load or the input voltage, the output voltage will experience a corresponding transient before it settles back to the steady-state value. Furthermore, in the event of an input voltage shift, the duty cycle value must be changed accordingly if the same output voltage is to be maintained. Clearly, we need a control circuit for output voltage regulation.

We may imagine that the simplest feedback method compares the output voltage with a reference and sends a control signal to adjust the duty cycle so as to minimize the error. Alternatively, a full state feedback can be considered. For instance, in the second-order buck, boost and buck-boost converters, both the output voltage and the inductor current can be used by the feedback circuit. In practice, two particular implementations have become the industry standard for controlling switching converters, namely, voltage feedback control and current-programmed control, also known as *voltage-mode* and *current-mode* control, respectively [83]. The former uses only the output voltage in the feedback process, and the latter uses both the output voltage and the inductor current.

1.1.2 Voltage-Mode Control

A typical voltage-mode controlled buck converter is shown in [Figure 1.2 \(a\)](#). The key feature of this control is the presence of a feedback loop which keeps track of the output voltage variation and adjusts the duty cycle accordingly. Precisely, in this control scheme, the difference between the output voltage, v_C , and a reference signal, V_{ref} , is processed by a compensation network which generates a control signal, v_{con} , i.e.,

$$v_{\text{con}}(t) = g(V_{\text{ref}} - v_C) \quad (1.9)$$

where $g(\cdot)$ is a function determined by the compensation network. This control signal effectively tells how the duty cycle has to be changed in order to give the best transient dynamics for the output voltage. In a typical implementation, this control signal is compared with a periodic ramp signal, $V_{\text{ramp}}(t)$, to generate a pulse-width modulated signal which drives the switch. The ramp signal typically takes the form:

$$V_{\text{ramp}}(t) = V_L + (V_U - V_L) \left(\frac{t}{T} \bmod 1 \right), \quad (1.10)$$

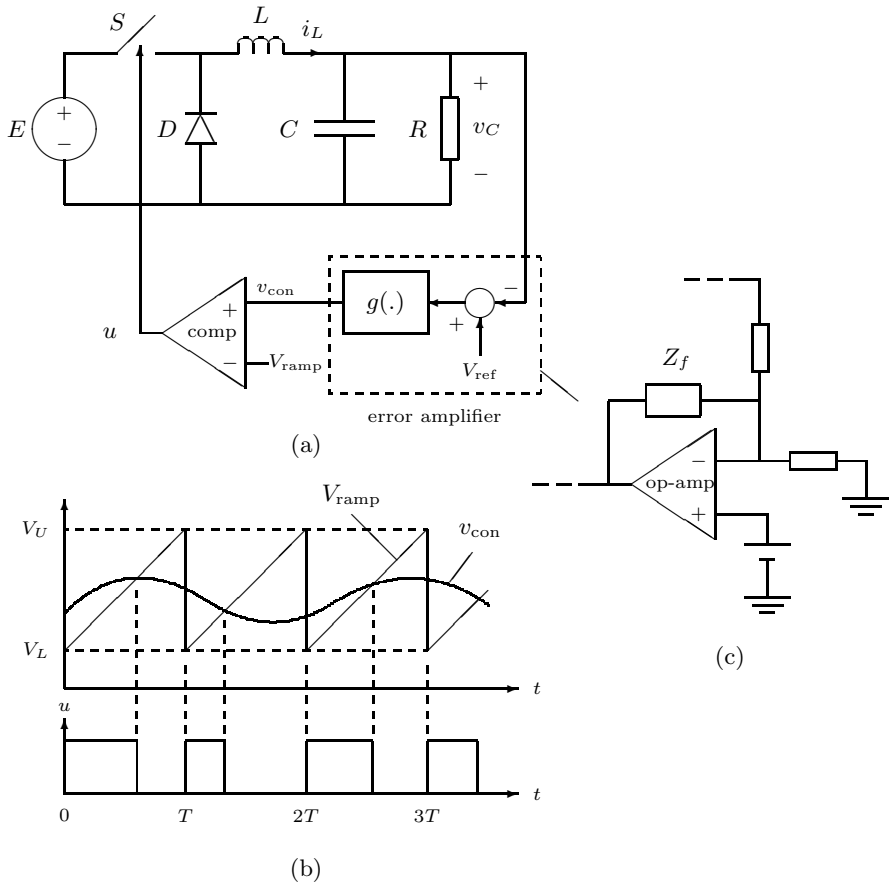


FIGURE 1.2

Voltage-mode controlled buck converter. (a) Circuit schematic; (b) waveforms of control signal and ramp signal; (c) possible implementation of error amplifier.

where V_L and V_U are the lower and upper thresholds of the ramp signal. Figure 1.2 (b) shows the interaction of the control signal and the ramp signal. Suppose the control signal moves in the opposite direction as the output voltage, i.e., v_{con} goes up when the output voltage decreases, and vice versa. Then, the output voltage can be regulated with the following switching rule:

$$\text{Switch} = \begin{cases} \text{on} & \text{if } V_{\text{ramp}}(t) \leq v_{\text{con}}(t) \\ \text{off} & \text{if } V_{\text{ramp}}(t) > v_{\text{con}}(t) \end{cases} \quad (1.11)$$

which can be easily implemented by a comparator, as shown in [Figure 1.2 \(a\)](#). Thus, the duty cycle at the n th switching period, d_n , is given implicitly by

$$v_{\text{con}}((d_n + n)T) = V_{\text{ramp}}((d_n + n)T). \quad (1.12)$$

We can easily verify in this case that if the control signal goes up as a result of an output voltage drop, the duty cycle increases.* Thus, the feedback action regulates the output voltage, and the closed-loop dynamics can be shaped by the compensation network.

1.1.3 Current-Mode Control

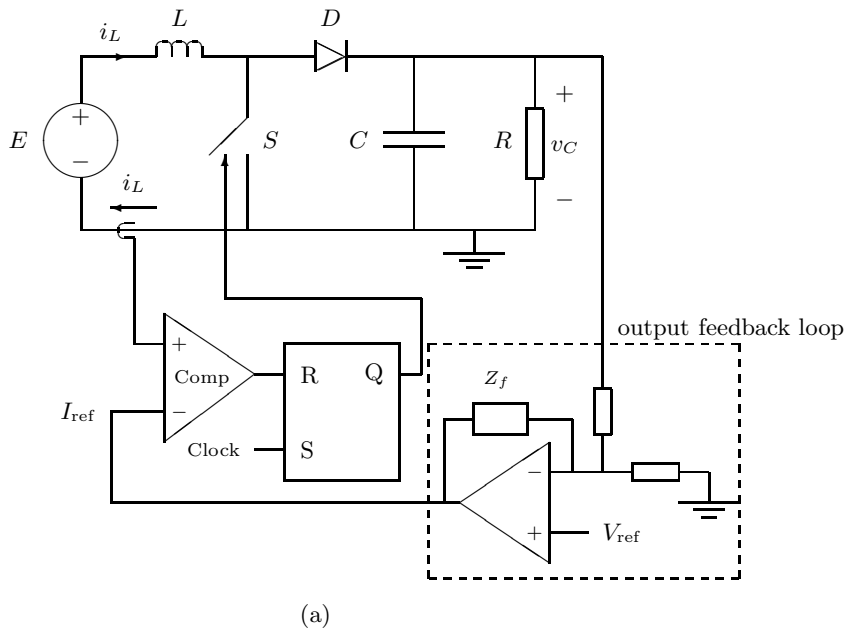
For current-mode control, an inner current loop is used in addition to the voltage feedback loop. The aim of this inner loop is to force the inductor current to follow some reference signal provided by the output voltage feedback loop. The result of current-mode control is a faster response. This kind of control is mainly applied to boost and buck-boost converters which suffer from an undesirable non-minimum phase response [83, 128]. A simplified schematic is shown in [Figure 1.3 \(a\)](#). The circuit operation of the inner loop can be described as follows. Suppose the switch is now turned on by a clock pulse. The inductor current thus rises up, and as soon as it reaches the value of the reference current I_{ref} , the comparator output goes momentarily high and turns off the switch. The inductor current then ramps down. The process repeats as the next clock pulse turns the switch back on. [Figure 1.3 \(b\)](#) describes the typical inductor current waveform. By inspecting the waveform, we can write the duty cycle at the n th switching period implicitly as

$$d_n = \frac{I_{\text{ref}}((d_n + n)T) - i_L(nT)}{(E/L)T} \quad (1.13)$$

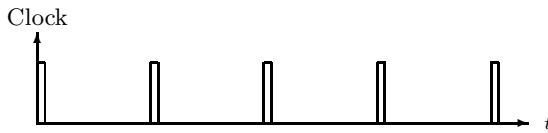
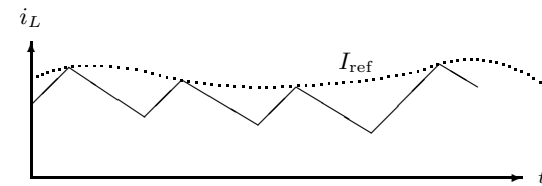
To achieve output voltage regulation, an output voltage loop is needed, as shown in [Figure 1.3 \(a\)](#). This loop senses the output voltage error and adjusts the value of I_{ref} accordingly. In practice, the inner current loop is a much faster loop compared to the output voltage loop. Thus, when we study the inner current loop dynamics, we may assume that I_{ref} is essentially constant or varying slowly. Details of the analysis of this system are left to [Chapter 5](#).

With the inductor current taken into account, current-mode control generally performs better. In practice, however, the application of current-mode control to the buck converter does not gain much benefit over voltage-mode control. This is because the inductor current information can be readily derived from the output voltage in the case of the buck converter. Thus, with

*Depending on how the error amplifier is connected, the control voltage can be designed to react in the same or opposite direction as the output voltage. If the control signal goes in the same direction as the output voltage, the switching rule (1.11) must be reversed in order to regulate the output voltage. The choice is arbitrary.



(a)



(b)

FIGURE 1.3

Current-mode controlled boost converter. (a) Circuit schematic; (b) waveforms of inductor current and reference current.

an appropriate design of the compensation circuit, voltage-mode control can achieve comparable performance as current-mode control. When applied to the boost or buck-boost converter, the benefits of current-mode control becomes significant. Essentially, since the inductor current is programmed to follow a reference current (which is in turn derived from the output voltage), its averaged dynamics is “destroyed.” Thus, for frequencies much below the switching frequency, the inductor current dynamics becomes insignificant,

making the design of the compensator much easier to perform. Besides, with the absence of the low-frequency inductor current dynamics, the inherent non-minimum phase problem associated with the boost and buck-boost converters is automatically eliminated. However, current-mode control is not completely free from stability problems. In fact, it has been shown that high-frequency instability in the form of subharmonics and chaos is possible in current-mode controlled converters, as will be detailed in [Chapter 5](#).

1.1.4 Complexity of Operation

Up till now, switching power converters have always been designed to operate in only one specific type of periodic operation, commonly known as *period-1* operation, in which all waveforms repeat at the same rate as the driving clock. Most converter circuits are thus expected to work stably in this regime under all possible disturbances. However, period-1 operation is not the only possibility. For instance, under certain conditions, the circuit may operate in a period- n regime in which the periods of all waveforms are exactly n times that of the driving clock. We can immediately appreciate the complexity in the operation of switching converters, where a variety of operational regimes exist and a large number of parameters may affect the stability of a particular regime. As parameters vary, the operation can go from one regime to another, sometimes in an abrupt manner. Such a phenomenon, where one regime fails to operate (e.g., as a result of a loss of stability) and another one picks up, is termed *bifurcation*.^{*} Thus, even when a converter is well designed to work in a particular (desired) regime, it could fail to operate as expected if some parameters are varied, causing it to assume another regime. If the newly assumed regime is an undesirable one, locating the bifurcation boundary becomes imperative. A few basic questions are often posed to the engineers:

1. What determines the operating regime of a given system?
2. How can we guarantee that a circuit operates in a desired regime?
3. When a system fails to operate in its desired operating regime, what is then the operating regime it would assume?

To answer these questions, we need to develop appropriate simulation and experimental tools (see [Chapter 2](#)). We also need to derive appropriate models to facilitate analysis (see [Section 1.2](#) and [Chapter 3](#)). Most importantly, we have to identify the basic phenomenology associated with each system under study. For nonlinear systems, there is no stereotypical result that fits all. We have to tackle each system separately.

*Bifurcation literally means splitting into two parts. In nonlinear dynamics, the term has been used to mean splitting of the behavior of a system at a threshold parameter value into two qualitatively different behaviors, corresponding to parameter values below and above the threshold [65].

1.2 Overview of Modeling Strategies for Switching Converters

As mentioned before, switching converters are essentially piecewise switched circuits. The number of possible circuit topologies is usually fixed, and the switching is done in a cyclic manner (but not necessarily periodically because of the feedback action). This results in a nonlinear time-varying operating mode, which naturally demands the use of nonlinear methods for analysis and design.

1.2.1 From Nonlinear Models to Linear Models

Power electronics engineers are always dealing with nonlinear problems and have attempted to explore methods not normally used in other circuit design areas, e.g., state-space averaging [98], phase-plane trajectory analysis [108], Lyapunov based control [126], Volterra series approximation [159], etc. However, in order to expedite the design of power electronics systems, “adequate” simplifying models are imperative. In the process of deriving models, accuracy is often traded off for simplicity for many good practical reasons. Since closed-loop stability and transient responses are basic design concerns in practical power electronics systems, models that can permit the direct application of conventional small-signal approaches will present obvious advantages. Thus, much research in modeling power electronics circuits has been directed toward the derivation of linearized models that can be applied in a small-signal analysis, the limited validity being the price to pay. (The fact that most engineers are trained to use linear methods is also a strong motivation for developing linearized models.) The use of linearized models for analysis is relatively mature in power electronics. However, it falls short of predicting any nonlinear behavior.

1.2.2 Back to Nonlinear Models

Since our purpose here is nonlinear analysis, we will not consider linearization right at the start of the analysis, which effectively suppresses all nonlinear terms. In fact, linearization is a useful technique only when we need to characterize the system behavior locally around a point in the state space. The major modeling step prior to linearization is the derivation of a suitable nonlinear model. In this book we will focus on two particularly useful modeling approaches:

1. Continuous-time averaging approach
2. Discrete-time iterative mapping approach (or simply discrete-time approach)

Averaging Approach

Probably the most widely adopted modeling approach for switching converters is the averaging approach which was developed by R.D. Middlebrook in the 1970s [98]. This modeling approach effectively removes the time-varying dependence from the original time-varying model. The ultimate aim is to produce a continuous-time state equation which contains no time-varying terms. The key idea in this approach lies in discarding the switching details of the state variables and retains only their “average” dynamics. In the modeling process, the state equations corresponding to all possible stages are first written down, and the final model is simply the weighted average of all the state equations. The weightings are determined from the relative durations of the stages. Typically, an averaged model takes the form:

$$\frac{d\mathbf{x}}{dt} = \left(\sum_{i=1}^N d_i \mathbf{A}_i \right) \mathbf{x} + \left(\sum_{i=1}^N d_i \mathbf{B}_i \right) E \quad (1.14)$$

where \mathbf{x} is the state vector, N is the number of stages in a period, d_i is the fractional period (duty cycle) of the i th stage, \mathbf{A}_i and \mathbf{B}_i are the system matrices for the i th stage. Finally, we need to state the control law in order to complete the model. This is usually given as a set of equations defining explicitly or implicitly the quantities d_j . The general form of such a set of equations is

$$\begin{cases} G_1(d_1, d_2, \dots, E, \mathbf{x}) = 0 \\ G_2(d_1, d_2, \dots, E, \mathbf{x}) = 0 \\ \dots \end{cases} \quad (1.15)$$

Note that the above equations generally define the duty cycles d_j as nonlinear functions of the system states and parameters. Thus, despite its appearance, the averaged model is nonlinear. Clearly, the averaged model so derived has left out all high-frequency details, and hence is not suitable for characterizing high-frequency or fast-scale dynamics. As a rule, we should only use an averaged model for analysis or characterization of phenomena which occur as fast as an order of magnitude below the switching frequency.

Discrete-Time Mapping Approach

Another modeling approach that provides fuller dynamical information is the discrete-time iterative mapping approach. Here, we aim to model the dynamics in a discrete manner. We take the value of the state vector at the start of a period, say \mathbf{x}_n , follow its trajectory through all the N stages, and find its value at the end of the period. The ultimate aim is to produce a difference equation of the form:

$$\mathbf{x}_{n+1} = \mathbf{f}(\mathbf{x}_n, \mathbf{d}, E) \quad (1.16)$$

where \mathbf{x}_n is the state vector at $t = nT$, E is the input voltage, \mathbf{d} is the vector of the duty cycles, i.e., $\mathbf{d} = [d_1 \ d_2 \ \dots \ d_N]^T$. To complete the model, a

control equation similar to (1.15) is needed. It is worth noting that the above description assumes the sampling period be equal to the switching period. Thus, the model so obtained is capable of describing the dynamical variation up to the switching frequency.

Needless to say, the two modeling approaches have their own advantages and disadvantages. Intuitively, the averaged model should be quite easy to obtain (involving less algebraic manipulation) whereas the discrete-time iterative model would probably involve more tedious algebra. They also deviate in their capabilities of characterizing dynamical behavior of a given system. Generally speaking, the averaged model is good for slow-scale (low-frequency) characterization whereas the discrete-time model is good for fast-scale (high-frequency) characterization. In [Chapter 3](#), we will take a detailed look at the modeling processes and their capabilities.

1.3 Overview of Nonlinear Dynamical Systems

As we have seen in the foregoing section, switching power converters can be modeled by a continuous-time differential equation or a discrete-time difference equation. In general, any system that can be put in such a form is a dynamical system in the sense that its behavior varies as a function of time [44, 55, 56]. More precisely, what constitutes a dynamical system is

- a set of independent state variables; and
- a function which connects the rates of change of the state variables with the state variables themselves and other inputs.

In an electrical circuit, for example, the inductor currents and capacitor voltages form a set of independent state variables.* The basic constitutive laws of all elements (i.e., $v = iR$ for resistors, $L(di/dt) = v$ for inductors, $C(dv/dt) = i$ for capacitors, and other possible nonlinear laws), together with the relevant independent Kirchhoff's law equations, give the connecting function [144]. Thus, with a set of state variables and a connecting function, we can describe a dynamical system. Further, we may assume that the following form is universal for describing a dynamical system:

$$\frac{d\mathbf{x}(t)}{dt} = \mathbf{f}(\mathbf{x}(t), \mu, t) \quad (1.17)$$

*We emphasize “independent” here. If a circuit contains dependent inductor currents and/or capacitor voltages, the number of state variables should be less than the number of inductors and capacitors. In the circuit theory literature, there are well established rules to identify independent state variables. See for example the texts by Rohrer [124] and Tse [144].

where \mathbf{x} is the vector consisting of the state variables, \mathbf{f} is the connecting function, and μ is a vector of parameters. The above system, with \mathbf{f} being dependent upon time, is called a *non-autonomous* system. Moreover, if the time dependence is absent in \mathbf{f} , i.e.,

$$\frac{d\mathbf{x}(t)}{dt} = \mathbf{f}(\mathbf{x}(t), \mu), \quad (1.18)$$

the system is *autonomous*.

In switching converters, distinction between non-autonomous and autonomous systems can be made conveniently by the presence or absence of a fixed frequency driving clock. In the past, most converters were constructed in a free-running mode, typically using a hysteretic or self-oscillating control circuit. Such systems are therefore autonomous. Nowadays, with the advent of integrated circuits (ICs), fixed frequency oscillators are easily implemented and most switching converters are designed to operate periodically under a fixed frequency clock which comes with most control ICs. Such systems are therefore non-autonomous. For example, the circuits shown in Figures 1.2 and 1.3 are non-autonomous systems.

1.3.1 Qualitative Behavior of Dynamical Systems

The afore-described dynamical systems are often called *deterministic systems*, in the sense that the exact way in which they evolve as time advances is fully determined by the describing differential equations [4, 53]. Precisely, given an initial condition, the solution of the system, also known as the *trajectory*, is completely determined. For linear systems, we know that closed-form solutions can be found. But for nonlinear systems, closed-form solutions are almost always unavailable, and numerical solutions must be sought.

After an initial transient period, the system soon enters its steady state. The solution in the steady state can be regarded as an *equilibrium solution*, in the sense that if the system starts at a point on this solution, it stays permanently on that solution. Thus, we may conceive that there could be many equilibrium solutions which may or may not be steady-state solutions. When the system is let go from a point outside these equilibrium solutions, it converges to only one of them. The equilibrium solution to which the system converges is called an *attracting equilibrium solution* or simply an *attractor*. In nonlinear systems, the behavior can be further complicated by the selective convergence to an equilibrium solution depending upon the initial point. In other words, there may be two or more competing attractors, and depending on the initial condition, the system converges selectively to one of them. Thus, to determine the steady-state behavior of a system, we have to know the possible attractors as well as their respective *basins of attraction*.

For ease of visualization, we refer to a 3-dimensional state space in the following discussion of attractors. In general, we may classify attractors under the following categories:

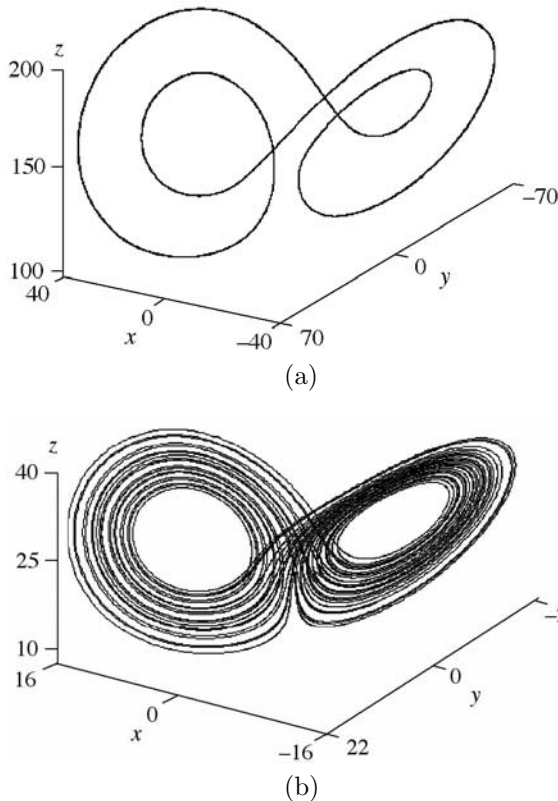


FIGURE 1.4

Attractors from the Lorenz system [134]: $\dot{x} = 10(y - x)$, $\dot{y} = -xz + rx - y$ and $\dot{z} = xy - 8z/3$. (a) Limit cycle with $r = 160$; (b) chaotic attractor with $r = 25$.

1. *Fixed point*: The solution is a point in the state space.
2. *Limit cycle or periodic orbit*: The trajectory moves along a closed path in the state space. Furthermore, this motion is associated with a finite number of frequencies, which are related to one another by rational ratios. The motion is periodic. An example is shown in Figure 1.4 (a).
3. *Chaotic attractor*: The trajectory appears to move randomly in the state space. Moreover, the trajectory is bounded and the motion is non-periodic. An example is shown in Figure 1.4 (b). We will discuss the properties of chaos in more detail in Section 1.3.3.
4. *Quasi-periodic orbit*: The trajectory moves on the surface of a torus, as illustrated in Figure 1.5. The motion is associated with a finite number

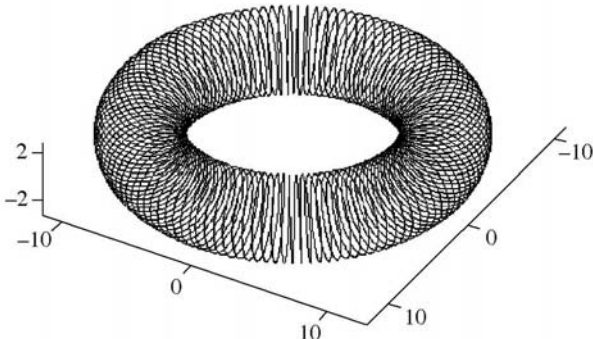


FIGURE 1.5

Quasi-periodic orbit. The trajectory moves on the surface of the torus and eventually visits every point on that surface. The motion is characterized by two rotations, one around the large circumference at frequency f_1 and the other around the cross section of the torus at frequency f_2 . The ratio of f_1 to f_2 is irrational.

of frequencies, which are related to one another by irrational ratios. The motion appears “almost periodic” but is not exactly periodic.

1.3.2 Bifurcation

As mentioned before, a dynamical system can have multiple equilibrium solutions. For a given set of parameters and initial condition, the system converges to one of the equilibrium solutions. This equilibrium solution is the attractor. If the parameters are allowed to vary, the system may relinquish its presently assumed equilibrium solution and pick up another equilibrium solution. For instance, as the parameters vary, the presently assumed equilibrium solution becomes unstable and the system is attracted to another stable equilibrium solution. This phenomenon is termed *bifurcation*, as we have briefly mentioned before. In general, bifurcation can be regarded as a sudden change of qualitative behavior of a system when a parameter is varied. We may therefore classify bifurcation according to the type of qualitative change that takes place when a parameter is varied. In the following we briefly summarize some commonly observed bifurcations in physical and engineering systems [1, 2, 3, 65, 85, 104, 109].

1. *Saddle-node bifurcation*: This type of bifurcation is characterized by a sudden loss or acquisition of a stable equilibrium solution as a parameter moves across a critical value. Systems that exhibit a saddle-node bifurcation can be “normalized” to the form $\dot{x} = \mu \pm x^2$, where μ is the

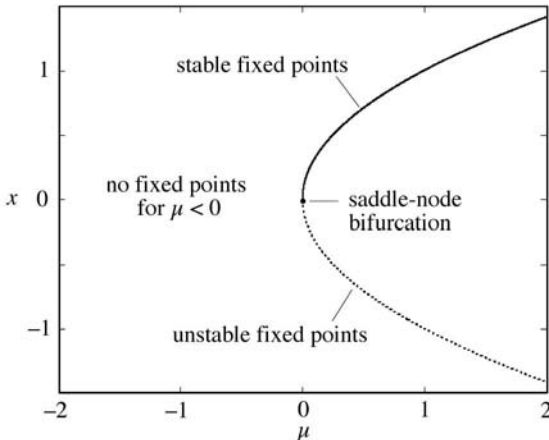


FIGURE 1.6

Saddle-node bifurcation of the system $\dot{x} = \mu - x^2$. As μ goes from negative to positive, a stable fixed point suddenly appears. Conversely, as μ goes from positive to negative, the stable fixed point suddenly disappears.

parameter and its critical parameter value is 0.* Figure 1.6 illustrates this bifurcation.

2. *Transcritical bifurcation:* This type of bifurcation is characterized by an exchange of stability status of two equilibrium solutions, as illustrated in Figure 1.7. Precisely, the system initially has one stable equilibrium solution and one unstable equilibrium solution. As a parameter is varied and reaches a critical value, the stable equilibrium solution becomes unstable, while the unstable equilibrium one becomes stable and takes over. The form of the system equation that exhibits a transcritical bifurcation can be normalized to $\dot{x} = \mu x \pm x^2$. The critical value of μ is again 0.
3. *Supercritical pitchfork bifurcation:* This type of bifurcation is characterized by splitting of a stable equilibrium solution into two stable equilibrium solutions at the critical parameter value. Precisely, the system exchanges stability status between one equilibrium solution and another pair of equilibrium solutions. Systems exhibiting this type of bifurcation

*From the center manifold theorem [53, 77, 138], any local bifurcation of an N -dimensional system can be analyzed by examining the so-called center manifold at the point of bifurcation, which is an M -dimensional ($M < N$) subspace tangential to the eigenspace corresponding to zero eigenvalue(s) of the Jacobian evaluated at the bifurcation point. The normalized system equation shown above describes the dynamics on this center manifold.

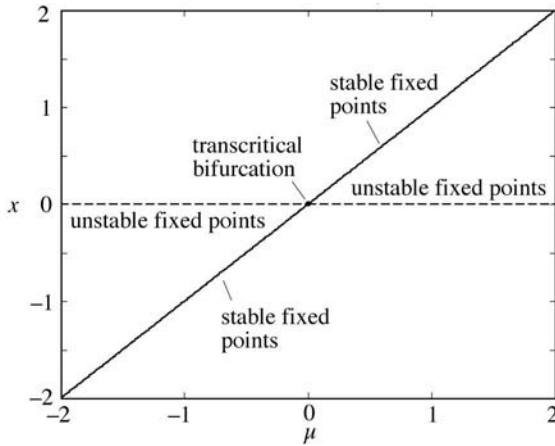


FIGURE 1.7

Transcritical bifurcation of the system $\dot{x} = \mu x - x^2$. As μ moves across zero, stability suddenly exchanges between two fixed points.

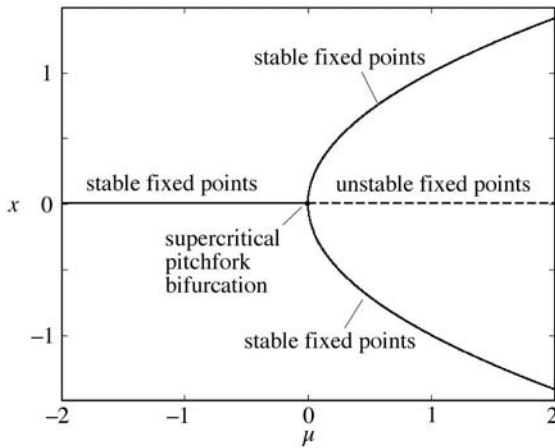


FIGURE 1.8

Supercritical pitchfork bifurcation of the system $\dot{x} = \mu x - x^3$. As μ goes from negative to positive, the stable fixed point suddenly forks off into two stable fixed points. The system is then attracted to one of the stable fixed points.

can be normalized to the form $\dot{x} = \mu x - x^3$, where $\mu = 0$ is the critical parameter value. Figure 1.8 illustrates this bifurcation.

4. *Subcritical pitchfork bifurcation:* This type of bifurcation is characterized by a sudden explosion of a stable equilibrium solution as a pa-

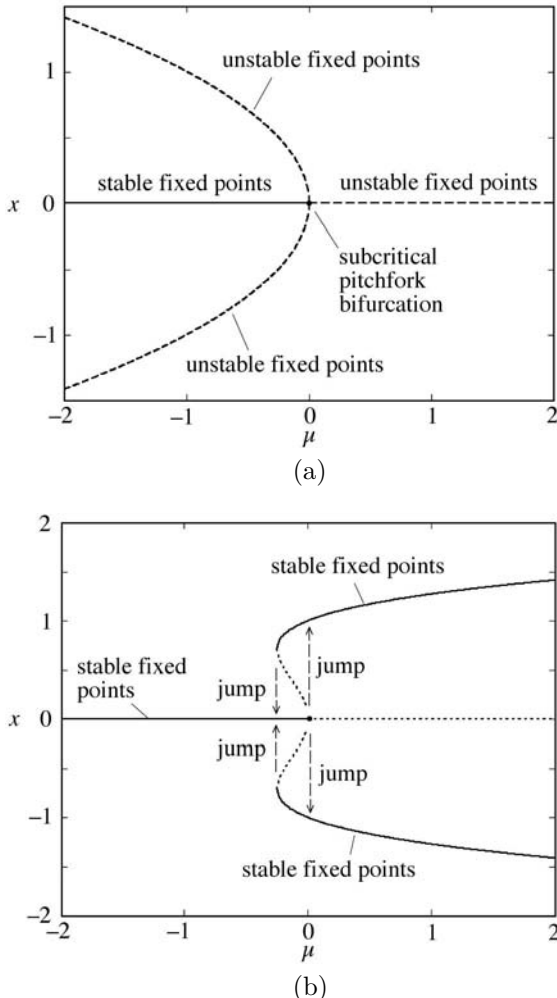


FIGURE 1.9

(a) Subcritical pitchfork bifurcation of the system $\dot{x} = \mu x + x^3$. As μ goes from negative to positive, the stable fixed point suddenly blows up; (b) sudden “jump” in real systems due to the presence of higher order terms $\dot{x} = \mu x + x^3 - x^5$. Note that a hysteresis loop exists. When μ moves in backward direction, the jump occurs at a negative value of μ .

parameter moves across a critical value. The normalized equation takes the form of $\dot{x} = \mu x + x^3$, where $\mu = 0$ is the critical parameter value. Figure 1.9 (a) illustrates this bifurcation. In real systems, higher order terms always exist to counteract the explosion, e.g., $\dot{x} = \mu x + x^3 - x^5$.

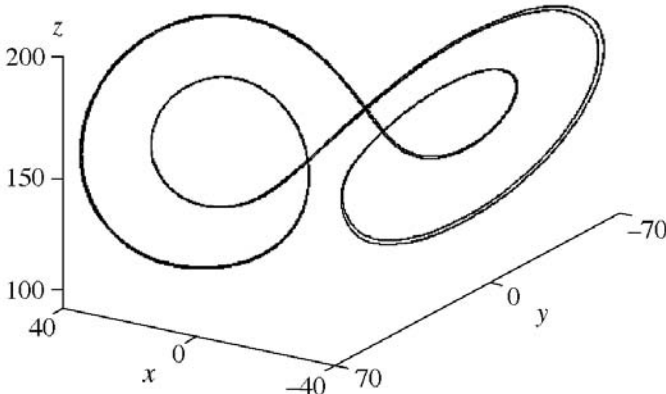
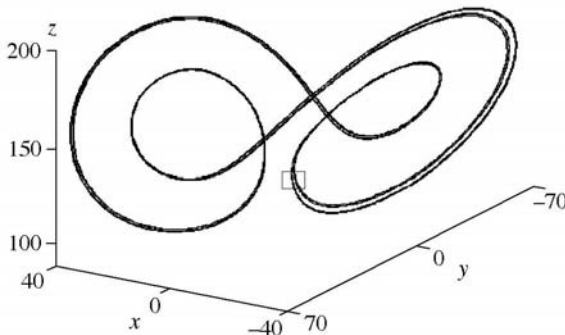


FIGURE 1.10

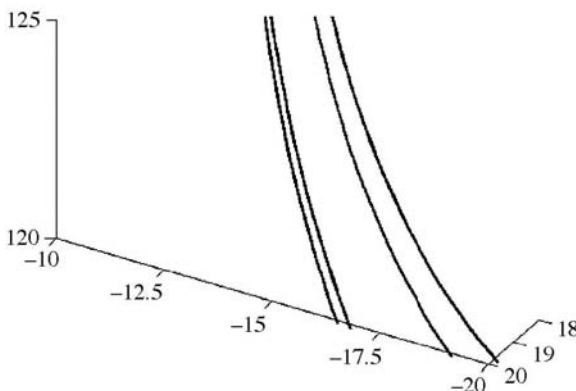
Period-2 orbit with $r = 149$ in the Lorenz system (see caption of Figure 1.4).

In this case, the system does not blow up at $\mu = 0$, but “jumps” to another stable equilibrium solution, as illustrated in Figure 1.9 (b).

5. *Period-doubling bifurcation:* This type of bifurcation is characterized by a sudden doubling of the period of a stable periodic orbit or limit cycle. Using the example of the Lorenz system shown in Figure 1.4, we may observe period-doubling bifurcation by varying the parameter r . Specifically, the periodic orbit shown in Figure 1.4 loses stability when r is decreased to around 149, and at that point, a period-2 orbit takes over, as shown in Figure 1.10. Further decreasing r to about 147, the period doubles again, as shown in Figure 1.11.
6. *Hopf bifurcation:* This type of bifurcation is characterized by a sudden expansion of a stable fixed point to a stable limit cycle. Systems that exhibit this bifurcation can be normalized to a second-order equation of the form $\dot{x} = -y + x[\mu - (x^2 + y^2)]$, $\dot{y} = x + y[\mu - (x^2 + y^2)]$. For $\mu < 0$, the system has a stable fixed point ($x = y = 0$), which is associated with a pair of complex eigenvalues having negative real parts. As μ goes from negative to positive, the pair of complex eigenvalues move across the imaginary axis, i.e., the real parts become positive. Thus, the fixed point loses stability. However, due to the second-order terms, the system has a stable limit cycle of radius $\sqrt{\mu}$ for $\mu > 0$.
7. *Border collision:* This type of bifurcation occurs in dynamical systems where two or more structurally different systems operate for different parameter ranges. When a parameter is varied across the boundary of two structurally different systems, an abrupt change in behavior occurs.



(a)



(b)

FIGURE 1.11

(a) Period-4 orbit with $r = 147$ in the Lorenz system; (b) enlargement of the small framed area.

This is known as border collision. The exact type of behavioral change depends on the dynamics of the systems corresponding to the two sides of the boundary.

It is worth noting that with the exception of border collision, the afore-described types of bifurcation do not involve structural changes of the system. They are sometimes called *smooth bifurcation* or *standard bifurcation*. The meaning of the adjective “smooth” has a mathematical origin, which relates to the differentiability of the function that describes the system. Coincidentally, the term “non-smooth” fits well with the appearance of the bifurcation diagrams which manifest rather unusual transitions not resembling

TABLE 1.1

Qualitative differences between “smooth” (standard) bifurcations and border collisions.

Characteristics	“Smooth” (standard) bifurcations e.g., period-doubling, Hopf, etc.	Border collisions
Cause	Loss of stability	Alteration of circuit operation
Structure of system	Structurally unchanged (topological sequence unchanged)	Structurally changed (topological sequence altered)
Manifestation in bifurcation diagrams	Appearance as typified in bifurcation diagrams of standard types	Abrupt transitions not resembling any standard bifurcation (e.g., abrupt bendings, discontinuities, jumps)

those in standard bifurcations, as we will see in later chapters.* Furthermore, a “smooth” bifurcation is normally associated with the loss of stability of one solution and the picking up of another, whereas border collision is characterized by abrupt alteration of the detailed operating principle. In other words, a “smooth” bifurcation occurs at a stability boundary, whereas border collision occurs at an operation boundary where the system experiences an operational change. We will discuss what we mean by an operational change more precisely in [Section 1.4](#). [Table 1.1](#) summarizes the basic differences between these two classes of bifurcations.

1.3.3 Deterministic Chaos

As mentioned earlier in [Section 1.3.1](#), chaos is a particular qualitative behavior of nonlinear systems, which is characterized by an aperiodic and apparently random trajectory [115]. In addition, the trajectory is unpredictable in the long term, meaning that knowing the trajectory at this time gives no information about where exactly the trajectory will be in the far future. Note that the dynamics of any deterministic system can be theoretically described by differential equations, although the derivation of such differential equations may prove to be difficult for very complicated systems. A classic example of an apparently random system is the flipping of a coin. The final outcome, either a head or a tail, appears to be unpredictable. However, the process of

*Here, we may regard bifurcation diagrams as summary charts of behavioral changes, which typically record the change of behavior of a system as some parameter(s) is/are varied.

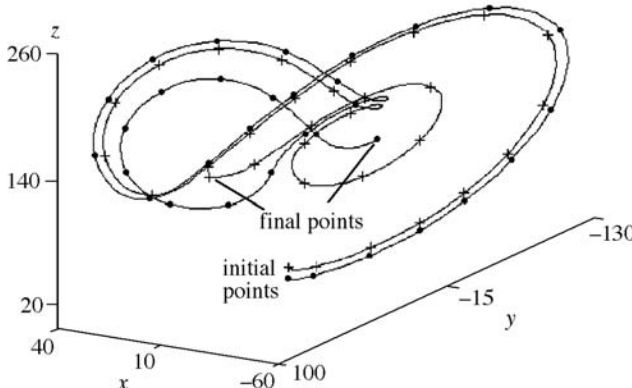


FIGURE 1.12

Two trajectories of the Lorenz system: $\dot{x} = 10(y - x)$, $\dot{y} = -xz + 25x - y$ and $\dot{z} = xy - 8z/3$. At $t = 0$, the trajectory labelled with “+” starts at $(0, -5, 15)$, and the one labelled with “•” starts at $(1, -6, 16)$. The final points are taken at $t = 1$. Note that if the initial points are set closer, a longer time is needed to observe the divergence of the two trajectories.

generating any particular outcome in this system is unarguably deterministic. First, the initial position of the coin can theoretically be known. Then, the initial velocity, gravitational force, air viscosity, the mass and moment of inertia of the coin, etc. are all theoretically known or knowable. Therefore, deterministic equations can be theoretically written to describe the motion of the coin as it is thrown up and later falls under the force of gravity. Finally, its landing position is also theoretically computable. The question is what makes the outcome random and unpredictable. In fact, this question is shared by all deterministic systems which exhibit apparent randomness and deny long-term predictability.

The answer to the above question lies in a key property of chaotic systems, which is now widely known as *sensitive dependence on initial condition*. In brief, two nearby starting points can evolve into two entirely uncorrelated trajectories. We take the Lorenz system again as an example, and examine two trajectories beginning at two nearby points. As shown in Figure 1.12, the two trajectories initially stay close to each other, but quickly move apart. We should now appreciate the difficulty of predicting where the system will end up eventually. In other words, the trajectory is unpredictable in the long run because there is a limit to which the starting condition can be accurately located. In our earlier example of tossing a coin, we may begin each time with a slightly different initial condition, including the position of the coin, upward velocity, spinning speed, etc. The final landing position is therefore unpredictable, even though the system is deterministic.

1.3.4 Quantifying Chaos

The afore-described property of being sensitively dependent upon initial condition can be taken as a defining property of chaotic systems [41, 65, 162, 167]. Thus, we may test whether a system is chaotic by evaluating its sensitivity to a change of initial condition. To illustrate how the sensitivity to initial condition can be quantified, we consider a first-order system which is defined by

$$\dot{x} = f(x). \quad (1.19)$$

Suppose $x_0(t)$ is the trajectory corresponding to an initial value x_0 . We consider another trajectory which starts at a nearby point, say $x_0 + \epsilon_0$. We simply denote this trajectory by $x(t)$. Clearly, what we are interested in is the difference between $x(t)$ and $x_0(t)$ as time elapses. Let this difference be $s(t)$, i.e.,

$$s(t) = x(t) - x_0(t). \quad (1.20)$$

If we assume that $s(t)$ grows exponentially, we may write $s(t) = s(0)e^{\lambda t}$, where λ can be found empirically to fit the divergence rate. Alternatively, we may describe the dynamics of $s(t)$ by

$$\dot{s} = \lambda s. \quad (1.21)$$

Moreover, the Taylor's expansion of $f(x)$ around x_0 is

$$f(x) = f(x_0) + f'(x_0)(x - x_0) + \frac{1}{2!}f''(x_0)(x - x_0)^2 + \dots \quad (1.22)$$

Thus, ignoring higher-order terms in (1.22), the variable $s(t)$ changes at a rate given by

$$\begin{aligned} \dot{s}(t) &= \frac{d}{dt}(x(t) - x_0(t)) \\ &= f'(x_0)(x - x_0). \end{aligned} \quad (1.23)$$

Now, from (1.21) and (1.23), we get

$$\lambda = f'(x_0). \quad (1.24)$$

Therefore, we may test divergence of the two trajectories, $x(t)$ and $x_0(t)$, by inspecting the sign of λ . Precisely, a positive value of λ indicates that the two trajectories diverge at the point x_0 , whereas a negative value indicates convergence. The quantity λ has been known as the *Lyapunov exponent*. Furthermore, the value of the Lyapunov exponent may change along the trajectory. Thus, we need to look at the average value of the Lyapunov exponent along a sufficiently long segment of the trajectory in order to tell whether nearby trajectories diverge exponentially on the average. The test for chaos should therefore be based on the *average Lyapunov exponent*. In brief, *if the*

average Lyapunov exponent is positive, the system is sensitively dependent upon initial condition and thus is chaotic [77].

The above concept of measuring the divergence rate of two nearby trajectories can be extended to higher-order systems. If we consider an N th order system, the expansion or contraction of $s(t)$ at a specific point must be associated with specific directions. In general, there should be N Lyapunov exponents corresponding to N directions in the state space. We note that $f'(x)$ in the above first-order system is simply the eigenvalue of the system, which describes the divergence rate of the error near x . In an N th order system, the N Lyapunov exponents at a certain point are the N eigenvalues evaluated at that point. Each of these Lyapunov exponents is associated with a direction of expansion or contraction which is given by the corresponding eigenvector. Thus, at a certain point, the trajectory may expand in some direction, and contract in another. If any one of the Lyapunov exponents is positive, nearby trajectories are diverging at that point. Again, we need to take the average of the Lyapunov exponents along a sufficiently long segment of the trajectory. For the higher-order case, we conclude that if the “largest” average Lyapunov exponent is positive, the system is sensitively dependent upon initial condition and thus is chaotic. In [Chapter 2](#), we will describe the computation of the average Lyapunov exponents in some detail.

1.3.5 Routes to Chaos

In the foregoing we have shown that randomness and lack of predictability are the key elements of chaos. However, being random or unpredictable does not necessarily mean that no systematic study can be pursued on the complex behavior of nonlinear systems. In fact, behind the complex behavior, there is always some *subtle order* that governs the way complexity is organized. In particular, in studying chaos, we often try to find some traceable precursors so that we might tell if chaos is likely to happen in an otherwise non-chaotic system. We have seen earlier that nonlinear systems can exhibit a variety of behavior, chaos being one particular type. We have also seen that nonlinear systems can undergo bifurcation whereby qualitative behavior can change from one type to another. In the literature, the term *route to chaos* has been commonly used to refer to the series of bifurcations through which non-chaotic behavior transmutes into chaotic behavior. Here, we summarize a few important routes to chaos [109].

1. *Route to chaos via period-doubling:* As discussed earlier, some nonlinear systems may undergo period-doubling bifurcation as a certain parameter is varied. This doubling of the period may continue to occur when the same parameter is varied in the same direction. Eventually, the behavior becomes chaotic. In fact, the Lorenz system shown earlier exhibits this type of route to chaos, as the parameter r is varied. We recall that when $r = 160$, the steady-state behavior is periodic (i.e., exhibiting a

limit cycle), as shown in [Figure 1.4 \(a\)](#). As we reduce r to about 149, we observe a period-doubling bifurcation, and if we further reduce r to about 147, we observe another period-doubling bifurcation. [Figures 1.10](#) and [1.11](#) show the period-2 and period-4 attractors. In fact, period-doubling bifurcation continues to occur as r is reduced. When r is about 144, the attractor is chaotic.

2. *Route to chaos via quasi-periodicity:* Some nonlinear systems may undergo Hopf bifurcation whereby a stable fixed point changes to a limit cycle as a certain parameter is varied. As the parameter continues to vary, the system admits another periodicity which is not in a rational ratio to that of the first limit cycle. The resulting behavior is quasi-periodic. Under some circumstances, upon further varying the parameter, the behavior becomes chaotic.
 3. *Route to chaos via intermittency:* Some nonlinear systems exhibit chaotic behavior intermittently, with bursts of chaotic behavior separated by long intervals of periodic behavior. Under the variation of a certain parameter, the bursts of chaotic behavior become progressively longer while the intervals of periodic behavior become shorter. Eventually, the behavior becomes fully chaotic.
 4. *Crisis:* Some nonlinear systems may all of a sudden become chaotic when a certain parameter is varied. There is no traceable route to chaos in the form of a sequence of events. Crisis may be encountered, for example, when an attractor “collides” with an unstable chaotic orbit, causing the attractor to span also the unstable chaotic orbit. The result is a sudden expansion to chaos.
-

1.4 Complex Behavior in Power Electronics

Chaos and bifurcation have long been observed by power electronics engineers in the course of developing power electronics circuits [169]. Problems such as subharmonic oscillations, intermittent chaos, quasi-periodic and chaotic operations are not at all uncommon. Because of the complexity of these problems, most practicing engineers have resorted to quick fixes via some trial-and-error procedures, the aim being just to get rid of the undesirable operations. With the success of nonlinear dynamics research in the 1970s, the complex behavior in power electronics has begun to receive some formal treatments since the late 1980s, and much of the reported work has focused on switching power converters. Research in this field has now reached a point where the basic phenomena associated with some commonly used power converters have been

identified. Of particular importance is the identification of bifurcation phenomena, which has played a crucial role in improving our understanding of the complex behavior exhibited by switching converters.

Power electronics can exhibit both smooth bifurcation and border collision, depending upon whether a structural change is involved. It should be noted that the switching between one topology to another during the normal operation of a power converter should not be considered as structural change (for the purpose of distinguishing between smooth bifurcation and border collision). Precisely, our definition of structural change as applied to switching converters is as follows.

A switching converter is said to be structurally changed if its topological sequence in a switching period is altered.

When no structural changes are involved, power electronics systems may exhibit a variety of smooth bifurcation such as period-doubling bifurcation, Hopf bifurcation, etc., as will be detailed in later chapters. Moreover, it should be apparent that power electronics systems are prone to border collision since operating boundaries exist to separate various operating modes. Two situations are particularly relevant to switching converters, as illustrated in [Figure 1.13](#).

1. *Change of operating mode:* In any switching converter, a boundary exists between continuous and discontinuous conduction modes of operation. Due to the difference in the topological sequence assumed by the converter for the two conduction modes, the converter undergoes a structural change when its operation changes from one mode to another. Crossing the boundary of the two conduction modes would cause a border collision.
2. *Saturating nonlinearity:* Saturating boundaries naturally exist due to the inherent limitation of the range of some control parameters. At such saturating boundaries, the topological sequence is significantly altered. For example, in the voltage-mode buck converter shown in [Figure 1.2](#), the control signal is supposed to hit the ramp signal once per switching period. If this fails to happen due to an excessively wide swing of the control signal, the topological sequence is altered significantly. A border collision thus occurs.

In the past two decades, a few important basic findings regarding bifurcation in switching converters have been established. Some surveys of published work have been conducted by Hamill [58], Hamill, Banerjee and Verghese [59], Nagy [102], Tse [145], and Tse and di Bernardo [148]. Here, we give a brief summary.

1. Voltage-mode controlled buck converters typically undergo period-doubling bifurcations [27, 48, 60], whereas boost converters are more likely to exhibit Hopf bifurcation [5, 68].

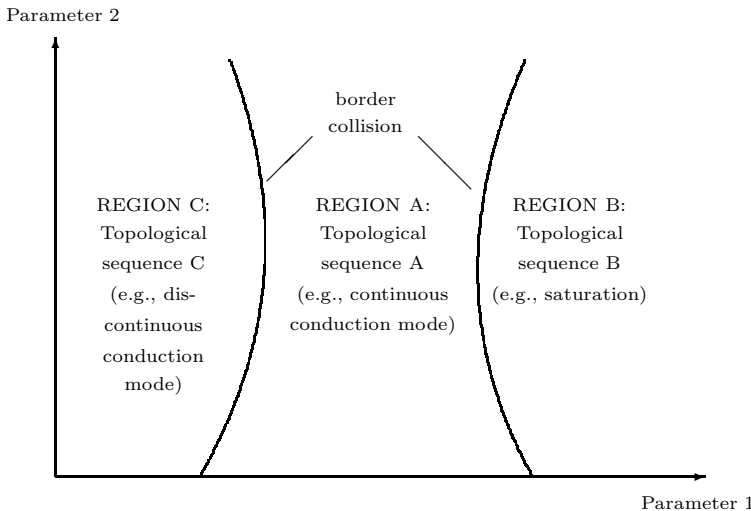


FIGURE 1.13

Operating boundaries on parameter space separating regions with different topological sequences. Border collision occurs at the boundaries where the converter experiences a structural change as its topological sequence is altered.

2. Period-doubling is common in buck or boost-type converters operating in discontinuous conduction mode [141, 142] and current-mode controlled converters [25, 38, 150].
3. A variety of bifurcations are possible when other nonlinear control methods are used, e.g., crisis, saddle-node bifurcation, switching-time bifurcation, etc. [45, 59, 73, 94].
4. Border collision is often present to organize the overall bifurcation pattern [8, 10, 14, 172].

In the rest of this book, we will take a detailed look at the bifurcation phenomena that govern the complex behavior of switching power converters. We will begin in [Chapter 2](#) with some important computer and laboratory tools for studying the dynamics of nonlinear systems, and in [Chapter 3](#) we will proceed with the essential modeling techniques for facilitating nonlinear analysis of switching power converters. From [Chapter 4](#), through the end, we will examine some selected power converters, with emphasis on bifurcation phenomena. In the process of studying complex behavior of the various converters, we try to illustrate the investigational approach that we have found effective in dealing with complex behavior in switching power converters.

2

Computer and Laboratory Techniques for Studying Nonlinear Behavior in Switching Power Converters

Computer simulations and laboratory measurements are indispensable to the investigation of the behavior of nonlinear systems, both for the purpose of verifying certain analytical findings and for making initial observations on how a given system behaves. In capturing the behavior of nonlinear systems, however, the usual techniques employed for the study of linear systems are often found inadequate or inappropriate. For example, chaos and quasi-periodicity are difficult to identify from the standard time-domain simulations or frequency-domain measurements. Furthermore, in order to capture a certain bifurcation scenario by simulation or experimentally, we need to devise an elaborate procedure which may require the use of specific computational or experimental techniques. In this chapter we review the essential techniques for capturing certain complex behavior of nonlinear systems, e.g., bifurcation and chaos, with particular emphasis on switching power converters. We begin with pointing out some common errors in the use of computer simulations for studying complex behavior, which give invalid or inviable verifications of certain findings or even erroneous conclusions about the occurrence of certain phenomena. The specific techniques for computer simulation and laboratory measurement of nonlinear phenomena will be described in detail.

2.1 The Use and Misuse of Computer Simulations

Digital computers have played a pivotal role in the identification of nonlinear phenomena such as chaos and bifurcation. In using digital computers for studying nonlinear behavior, however, it is sometimes easy to come to erroneous conclusions if the results revealed by the simulations are not carefully interpreted. The gist of the problem often lies in how well one understands the objective of the simulation and the limitation of digital computation. In the following we discuss two types of errors which are particularly relevant to the study of complex behavior. The first one originates from an improper

choice of models and the second one is related to insufficient resolution in the simulation.

2.1.1 Improper Choice of Models

The consequence of using an improper model for simulation depends on how the results are to be used. If the results are used for verifying certain analytical findings, improper simulating models may make the verification invalid. Specifically, to verify a certain phenomenon which has been observed from an analytical model, computer simulation should be performed using the empirical system model that emulates the “true” behavior of the system. In the case of power converters, if some discrete-time iterative maps or averaged equations have been used to establish the occurrence of certain phenomena, then computer simulation can provide valid verification only if it is based on the original piecewise switched model.

Moreover, if the simulation results are used to observe phenomena in a given system, the use of an improper model can have profound consequence. For instance, a certain phenomenon such as period-doubling may fail to show up when an averaged model is used to study it. Likewise, the simulation results may erroneously conclude the occurrence of a certain phenomenon which is inconsistent with the system under study.

2.1.2 Insufficient Resolution

Switching power converters are piecewise switched circuits. A typical switching converter operates by toggling its topology according to some external signals as well as the circuit’s own conditions. The determination of the time instants at which the circuit topology changes is crucial to the accuracy of the simulation results. Thus, the algorithm used in the simulation should allow the variation of switching instants to be recorded with sufficient resolution.

A variety of pathological conditions may arise as a result of insufficient resolution. For example, if the duty cycle should converge to 0.42, simulation with a time step equal to one-twentieth of the switching period may give a subharmonic orbit that alternates between 0.40 and 0.45. Some even more serious errors can result from poor resolution. For example, if the supposed switching instants do not “grid” on the simulation time steps, the cumulation of numerical residues may make the simulated operation appear intermittently chaotic while it should have actually been operating in a perfectly stable period-1 orbit. So, stable operation may look chaotic on a digital computer. Moreover, the converse can happen as well. Periodicity may be incorrectly concluded for a chaotic operation if insufficient resolution is used in the simulation, typically due to the time step chosen being too large.

Finally, it should be borne in mind that *no chaos should ever be found by digital computers* in theory. The best we can get is an orbit of a very long

period. But this can be practically regarded as chaos if the observation is complemented by other supporting analytical and experimental evidence.

2.2 Accuracy of Models: Does It Matter?

In performing computer simulations, it is often asked whether the model used should be as accurate as possible. The answer again depends on how the simulation results are to be used. Accurate models are generally preferred for verification purposes because the simulation results should reflect the true behavior of the physical system in order to make the verification valid. Moreover, if the simulation aims to observe certain qualitative behavior such as chaos, then the model need not be very accurate since exact trajectories are never wanted. What is needed is perhaps a simple model that contains adequately the salient nonlinear features of the system under study.*

It should be stressed that computer simulation alone, however, is not completely convincing as a verification or investigation tool since numerical procedures are always subject to round-off errors, however small, and the model used for simulation may not fully describe the system. What we see in the computer simulated waveforms may sometimes contain artifacts due to numerical errors or flaws in the simulating model. Hence, laboratory experiments remain an indispensable form of verification [62, 158].

2.3 Mode of Investigation

Despite the apparent popularity in the use of the traditional “analyze-simulate-experiment” mode of investigation as reported in numerous scientific publications, the actual investigation of complex behavior in physical systems would have been done, mostly, in the reverse order. In fact, experimentation can sometimes be well ahead of any analysis and simulation, especially for many practical electronics systems whose popularity in practical use often precedes any detailed analysis. In that case, experimentation plays an important role in providing important clues to the possible kinds of phenomena that may

*Here we recall our discussion in [Chapter 1](#) concerning the choice between averaged models and discrete-time iterative maps for the analysis of bifurcation phenomena in switching converters. We note that averaged models are simple models and yet adequate for predicting low-frequency bifurcations such as Hopf bifurcation in some switching converters.

occur in a given system. This is like a “pre-analysis” which narrows down the problem area and guides the choice of analysis methods.

On the other hand, it is equally probable that certain phenomena may be observed unintentionally while developing a practical system. Then, the quest for an explanation for the observed unusual behavior motivates in-depth analysis of the underlying mechanism. This in turn calls for appropriate analytical models which fit the observed phenomena and provide adequate analytical basis to predict the occurrence of similar phenomena. As we move on to the study of particular converter systems in later chapters, we will see, in a number of occasions, how initial simulation and experimentation can provide essential clues to the choice of analytical models.

2.4 Capturing Complex Behavior on Computers

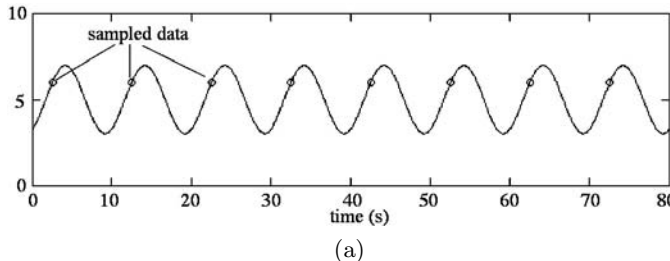
One important process in the study of complex behavior of nonlinear systems is to record the occurrence of representative phenomena. The basic questions are *what to record* and *how to record*. Here, we classify behavioral observations under two categories of conditions, namely, *fixed parameters* and *varying parameters*.

2.4.1 Time-Evolution Behavior under Fixed Parameters

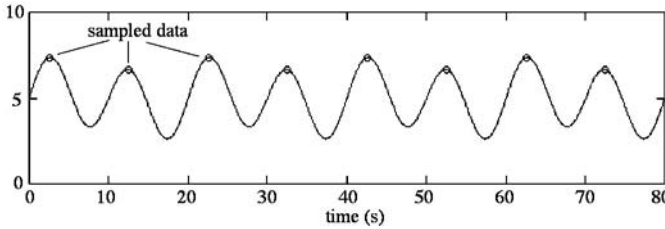
When a system is let go in time with a fixed set of parameters, several properties of its evolution may be of interest, namely, waveforms of selected variables, steady-state trajectories in the state space (also known as *attractors*), and frequency spectra of selected variables in the steady state.

These properties are relatively straightforward to obtain from computer simulations and laboratory measurements. However, in their original forms, these properties may not provide much insight into the behavior of the system. For example, it is not always easy to tell from the waveforms the difference between chaotic operation and quasi-periodic operation. Sometimes, even periodic operation and chaotic operation can be hard to distinguish. However, if these properties are presented in certain formats, identification of a particular behavior can be more easily accomplished. Here, we focus on three specific formats:

- Sampled data or stroboscopic maps.
- Phase portraits or 2-dimensional projections.
- Poincaré sections.



(a)



(b)

FIGURE 2.1

Detecting periodicity by sampling. (a) Period-1 waveform sampled at 10 s intervals giving a fixed point; (b) period-2 waveform sampled at 10 s intervals giving two alternating fixed points.

Sampled Data

For periodically driven (non-autonomous) systems, like most of the fixed-frequency switching converters, information about periodicity can be easily obtained by sampling the waveforms. Essentially, we take a waveform, extract its value at periodic time instants and look for specific patterns. **Figure 2.1** illustrates how this sampling process reveals the periodicity of periodic waveforms.

Typically, by inspecting the sampled data, we can draw the following conclusions regarding the period of the waveform relative to the sampling period.

1. If the sampled data stays at a constant value, the waveform is periodic with its period equal to the sampling period.
2. If the sampled data cycles through N values, the waveform is periodic with its period equal to N times the sampling period.

Moreover, if no clear pattern is observed in the sampled data, no definite conclusion can be drawn. Chaos or quasi-periodicity is possible.

The basic problem with this method is related to the choice of the appropriate sampling frequency. For non-autonomous systems, the driving frequency is a handy choice since any periodic behavior of the system must be related

to the driving frequency. For switching converters, the switching frequency is the natural choice. However, this sampled-data method is in principle not suitable for autonomous systems which do not possess any externally driven periodic source. The phase portrait and Poincaré section will prove to be useful for autonomous systems, as we will see shortly.

Phase Portraits

The use of sampled data, as described above, provides a simple and fast means of identifying the periodicity of a system. However, we should be cautious about its use when the order of the system under study is two or higher since inspecting one particular state variable may not give correct information about the periodicity of the system. One variable may have a period-1 waveform, while another may be period-2, etc. Thus, inspection of the entire attractor is needed to provide complementary information.

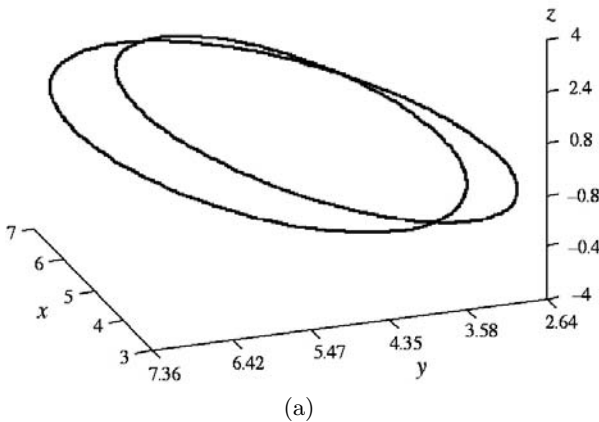
Shown in [Figure 2.2 \(a\)](#) is an attractor of a 3-dimensional system in which variables x and z are period-1 and variable y is period-2. For this attractor, inspecting x or z alone may give a wrong indication about its periodicity. In this case, an effective tool is to project the trajectory on a 2-dimensional plane, for example, the x-y plane, as shown in [Figure 2.2 \(b\)](#). Such projections, also called *phase portraits*, are very useful in uncovering subtle periodicity. In this specific example, we clearly see the double-roller which correctly indicates the period-2 operation of the system.

Poincaré Section

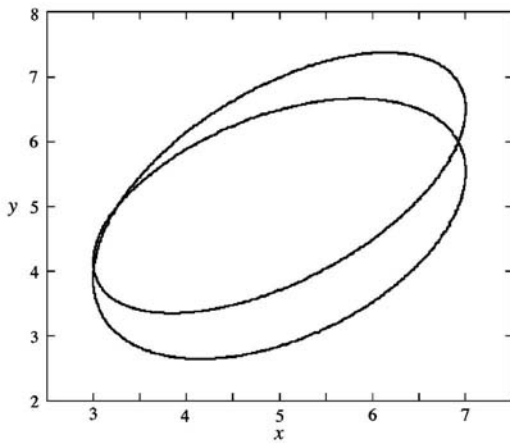
To distinguish between chaos and quasi-periodicity, we need a special tool to uncover the “hidden” information contained in the steady-state trajectory of a system (i.e., attractor). Here, we consider third-order systems for simplicity. Our discussion applies to autonomous and non-autonomous systems. The tool we use is called *Poincaré section*, which is a 2-dimensional plane that intersects the trajectory. By examining the way in which the steady-state trajectory intersects an appropriately chosen Poincaré section, we can tell if the steady-state operation is periodic, quasi-periodic or chaotic [41, 113]. The following is what we can typically conclude from inspecting a Poincaré section.

1. If the Poincaré section contains a finite number of points, the operation is periodic, as illustrated in [Figure 2.3 \(a\)](#).
2. If the Poincaré section contains a closed loop, the attractor is a torus,* i.e., the operation is quasi-periodic, as illustrated in [Figure 2.3 \(b\)](#).

*A torus is topologically equivalent to the surface of a doughnut-like object. A quasi-periodic trajectory moves on the surface of a doughnut, similar to an inductor coil winding around a ferrite ring. If a cross-section of the doughnut surface is examined, the trajectory can be seen going through every point of this cross-section.



(a)



(b)

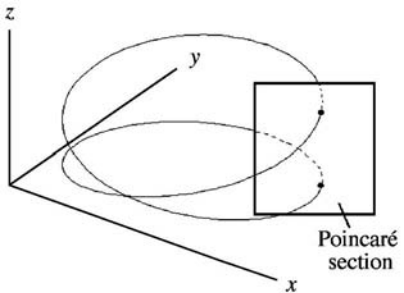
FIGURE 2.2

(a) An attractor from a 3-dimensional system and (b) a phase portrait. x and z are period-1 waveforms, and y is period-2.

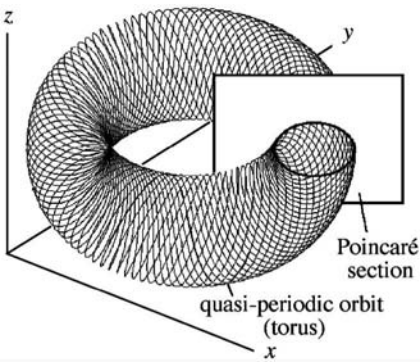
3. If the Poincaré section contains a large number of irregularly and densely located points, the operation is chaotic, as exemplified in [Figure 2.4](#).

2.4.2 Bifurcation Behavior under Varying Parameters

Nonlinear systems can behave in many different ways depending upon the values of the parameters. The transition from one type of behavior to another can happen abruptly when some parameters are varied. We refer to the sudden change in the behavior of a system under parameter variation as *bifurcation*.



(a)



(b)

FIGURE 2.3

Poincaré section of (a) a period-2 orbit; and (b) a quasi-periodic orbit.

Bifurcation can sometimes be catastrophic. For example, a converter may operate nicely when a certain parameter is kept below a certain threshold. Beyond this threshold, a chaotic attractor may suddenly take over, with its trajectory extended to a much wider voltage and current ranges causing damage to the devices. Thus, the study of bifurcation in an engineering system is relevant not only to its functionality but also to reliability and safety.

The most commonly used tool for capturing bifurcation behavior is the *bifurcation diagram*, which is essentially a summary chart of the different types of behavior exhibited by a system when some parameters are varied. The simplest case corresponds to variation of only one parameter. In this case, the bifurcation diagram usually consists of an x - y plot, where sampled data are plotted against the chosen parameter. An example will clarify its construction.

Consider a system which can be represented by an iterative map. Alternatively, we may assume that sampled data are available from sampling the simulated or measured waveforms of the system. For the purpose of illustra-

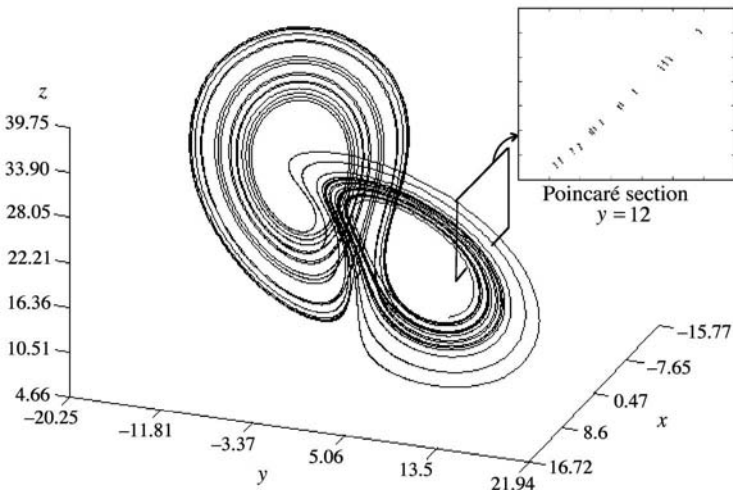


FIGURE 2.4

Chaotic attractor from Lorenz equation and a Poincaré section. Note that when using a digital computer to capture points that hit the Poincaré section, a finite “thickness” or tolerance band must be defined. Here, points that fall in the range $11.99 \leq y \leq 12.01$ are considered to be on the Poincaré section. This may lead to artifacts if the tolerance range is set too wide.

tion, we take the logistic map as the generating system [54]:

$$x_{n+1} = \mu x_n (1 - x_n) \quad (2.1)$$

where μ is a parameter which can be varied. If we use this map to generate a sequence of numbers, we observe behavioral changes of the steady-state sequence as μ is varied. In order to record the changes, we construct the bifurcation diagram as follows:

1. Starting with a small μ , we generate a sufficiently large number of consecutive values of x , e.g., 500, from the iterative map. Discard the initial transient, say the first 100 values. The remaining 400 values of x form one data set.
2. With a slightly larger μ , we again generate 500 consecutive values of x from the iterative map and discard the transient. We then have another data set.
3. We repeat the above process for different values of μ within a chosen range.
4. Suppose we have 200 data sets corresponding to 200 equally spaced values of μ between 2.5 and 4. Then, we simply plot each data set

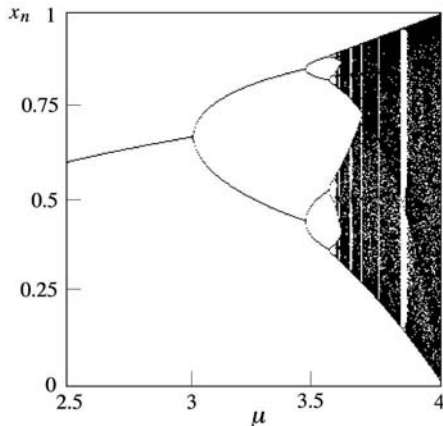


FIGURE 2.5

Bifurcation diagram as a tool for recording the changes of behavior as a parameter is varied. This bifurcation diagram is generated from the logistic map for 200 equally spaced values of μ between 2.5 and 4. For each value of μ , 400 iterates of x are plotted.

against μ . The resulting diagram is shown in Figure 2.5, which is the bifurcation diagram required.

From the bifurcation diagram, we can see clearly the behavioral change of the system within the parameter range of interest.

When two parameters are involved, bifurcation diagrams are usually constructed to show the boundaries of different operating regimes. Thus, in typical bifurcation diagrams with two parameters plotted on both axes, regions of operations are identified and separated by boundary curves.* Finally, when three parameters are involved, although it is theoretically possible to construct bifurcation diagrams as 3-dimensional plots, they are usually too complex to be of practical use. In most cases, it is more helpful to construct multiple bifurcation diagrams for different parameters rather than to put all parameters in the same bifurcation diagram.

*Here, we restrict ourselves to cases where only one parameter needs to be varied in order to cause a bifurcation. Moreover, some systems require variation of two or more parameters simultaneously in order to define a bifurcation. If n parameters must be varied to effect a bifurcation, such a bifurcation is called a co-dimension- n bifurcation [162].

2.5 Test for Chaos: The Lyapunov Exponent

As discussed in [Chapter 1](#), chaos is characterized by divergence of nearby trajectories, which also gives chaos a signature property of *denying long-term predictability*. This property can be used to test chaos and to some extent quantify the “chaoticity” of a system in terms of the rate of divergence of nearby trajectories. Precisely, suppose two nearby trajectories are separated by a distance ϵ_0 initially. Then, if this distance expands or contracts exponentially as time elapses, it may be expressed as

$$\epsilon(t) = \epsilon_0 e^{\lambda t} \quad (2.2)$$

where the sign of λ determines whether the separation is expanding or contracting. Specifically, if $\lambda > 0$, the two trajectories diverge exponentially in time. As discussed in [Chapter 1](#), since the rate of divergence of nearby trajectories measured in this way may vary along the trajectory, we need to look at the average divergence rate over a sufficiently long segment of the trajectory. Also, the choice of initial point may affect the result. Thus, we need to take a large number of measurements and evaluate the *average* λ . We refer to this average λ as the *average Lyapunov exponent* or simply the *Lyapunov exponent*. We also recall from our earlier discussion in [Chapter 1](#) that for systems of second or higher order, there are more than one Lyapunov exponents, each being associated with one particular direction of expansion or contraction. In general, an N th order system has N Lyapunov exponents. If any one of the Lyapunov exponents is positive, the behavior of the system is chaotic. In the following we discuss the methods for computing the Lyapunov exponent.

2.5.1 Computing Lyapunov Exponents from Iterative Maps

First-Order Systems

Suppose we wish to find the Lyapunov exponent of a system which is generated by the first-order iterative map $x_{n+1} = f(x_n)$. A procedure for computing the Lyapunov exponent may be derived from the definition stated above. We consider two trajectories starting at the point x_0 and a nearby point $x_0 + \epsilon_0$. Iterating N times, we get $f^{(N)}(x_0)$ and $f^{(N)}(x_0 + \epsilon_0)$ for the two different initial values. Then, the separation of the two trajectories after N iterations is

$$\epsilon_N = \left| f^{(N)}(x_0 + \epsilon_0) - f^{(N)}(x_0) \right|, \quad (2.3)$$

and the growth of this separation can be evaluated by

$$\frac{\epsilon_N}{\epsilon_0} = \left| \frac{f^{(N)}(x_0 + \epsilon_0) - f^{(N)}(x_0)}{\epsilon_0} \right|. \quad (2.4)$$

If we assume that this ratio increases exponentially with N , then we may write

$$\frac{\epsilon_N}{\epsilon_0} = e^{\lambda N} \quad (2.5)$$

which gives

$$\lambda = \frac{1}{N} \ln \left| \frac{f^{(N)}(x_0 + \epsilon_0) - f^{(N)}(x_0)}{\epsilon_0} \right|. \quad (2.6)$$

The above formula can be used to estimate λ . It basically says that λ is the average of all $\ln |(f^{(N)}(x_0 + \epsilon_0) - f^{(N)}(x_0)) / \epsilon_0|$ along the trajectory. A problem with using this formula is to choose an appropriate value for N . Obviously, N must be large enough to give a “good” average. But we also know that nearby trajectories will not keep diverging exponentially in the long run since the values of the iterates must necessarily be bounded. Thus, N should not be chosen too large to cause ϵ_N to saturate or be folded back. Of course, smaller the value of ϵ_0 , larger the value of N we may choose. We will discuss this issue in more detail when we introduce the time series method for estimating Lyapunov exponents in the next subsection. Here, since the iterative map is available in closed form, we have a better way to find λ , as we will now explain.

For differentiable maps, if we let ϵ_0 tend to zero, we recognize that $(f^{(N)}(x_0 + \epsilon_0) - f^{(N)}(x_0)) / \epsilon_0$ is by definition the x -derivative of $f^{(N)}(x)$ evaluated at x_0 . Thus, we may write

$$\lambda = \frac{1}{N} \ln \left| \frac{df^{(N)}(x)}{dx} \right|_{x=x_0} \quad (2.7)$$

which, upon application of the chain rule, becomes

$$\lambda = \frac{1}{N} \ln |f'(x_0)f'(x_1) \cdots f'(x_{N-1})| = \frac{1}{N} \sum_{i=0}^{N-1} \ln |f'(x_i)| \quad (2.8)$$

where $f'(x) = df(x)/dx$ and x_i is the i th iterate, i.e., $x_i = f^{(i)}(x_0)$. Clearly, from (2.8), λ is the average of all $\ln |f'(x_i)|$ along the trajectory. In order for nearby trajectories to diverge exponentially in time, we require that the average value of $\ln |f'(x_i)|$ be positive, i.e., the average value of $|f'(x_i)|$ be greater than 1. Furthermore, since we have let ϵ_0 tend to zero in this case, N can be chosen as large as possible. In practice, however, a very large N is usually not needed because the improvement in accuracy will quickly saturate and become insignificant to justify the huge computational effort required when a very large N is used.

Finally, we note that the above λ is found only for one initial point. To obtain the average Lyapunov exponent, we have to take the average of λ 's obtained for a number of initial points. As an example, we apply the above procedure to compute the average Lyapunov exponents for the logistic map defined in (2.1). [Figure 2.6](#) shows the results for a range of μ . Here, we can clearly identify regions of chaotic behavior.

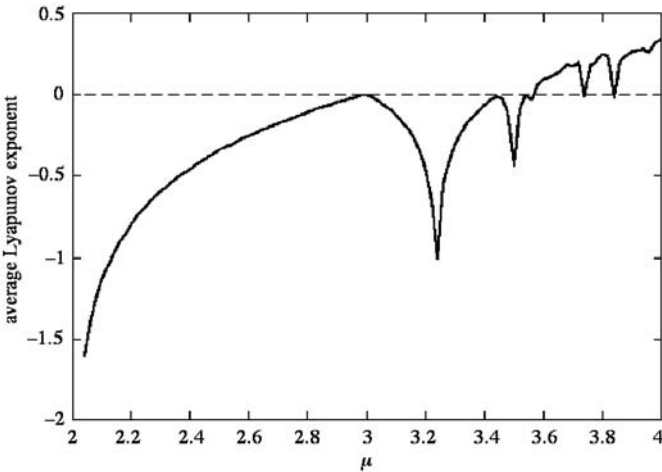


FIGURE 2.6

Average Lyapunov exponents computed for the logistic map for 100 equally spaced values of μ . For each value of μ , 50 iterates are used in the computation of one Lyapunov exponent using (2.8), and an average Lyapunov exponent is taken over 10 Lyapunov exponents found from 10 different initial values.

Second or Higher Dimensional Systems

For second or higher dimensional systems, the procedure for finding the average Lyapunov exponent is in principle the same. However, the formula for λ given in (2.8) has to be modified. Let us consider an m th order iterative map of the form:

$$\mathbf{x}_n = \mathbf{f}(\mathbf{x}_{n-1}) \quad (2.9)$$

where \mathbf{x} is an m -dimensional vector. For this map, as mentioned before, we have m Lyapunov exponents, each corresponding to one direction of expansion or contraction. We have also seen in the first-order case that the Lyapunov exponent is effectively the average of all $\ln |f'(x_i)|$ along the trajectory $\{x_i\}$. Note that $f'(x_i)$ is actually the eigenvalue of $f(x)$ evaluated at x_i . Extending this concept to the m th order iterative map, we may write the m Lyapunov exponents as

$$\lambda_1, \lambda_2, \dots, \lambda_m = \frac{1}{N} \ln |\text{eig} [J(\mathbf{x}_0) J(\mathbf{x}_1) J(\mathbf{x}_2) \cdots J(\mathbf{x}_{N-1})]| \quad (2.10)$$

where eig denotes the eigenvalues of a matrix and $J(\mathbf{x}_i)$ is the Jacobian of $\mathbf{f}(\mathbf{x})$ evaluated at \mathbf{x}_i [65, 115, 162]. Once the Lyapunov exponents are found, we may determine if the system exhibits chaotic behavior according to the sign of the largest Lyapunov exponent. If the largest Lyapunov exponent is

positive, the system is chaotic.*

2.5.2 Computing Lyapunov Exponents from Time Series

In the absence of a closed-form iterative map, the average Lyapunov exponent may still be estimated if a time series or sampled data of a waveform is available from an implicit iterative function or computer simulation. The basic principle of the estimation method follows from the definition of the Lyapunov exponent. Suppose we have a time series $\{x_0, x_1, x_2, \dots\}$. We first select a value in this series, e.g., x_j . Since our purpose is to observe how two nearby trajectories diverge as time elapses, we try to find another value in the time series which is close to x_j . Suppose x_k is very close to x_j . Then, we may simply regard the series beginning at x_j and that beginning at x_k as two nearby trajectories. The initial separation of these two trajectories is

$$\epsilon_0 = |x_j - x_k|. \quad (2.11)$$

We assume that time advances relative to the starting times j and k . The separation after N time steps is

$$\epsilon_N = |x_{j+N} - x_{k+N}|. \quad (2.12)$$

Applying a similar reasoning as in (2.2), we may write $\epsilon_N = \epsilon_0 e^{\lambda N}$, which can be rearranged as

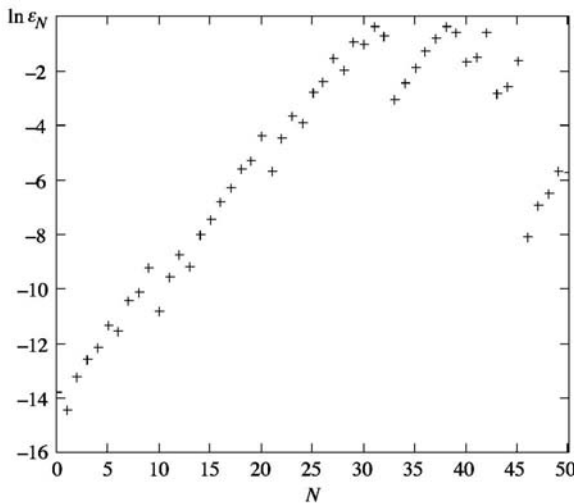
$$\lambda = \frac{1}{N} \ln \frac{\epsilon_N}{\epsilon_0}. \quad (2.13)$$

Finally, let us not forget that the average Lyapunov exponent is what we wish to find. Thus, we need to find λ for a number of x_j chosen along the time series. Preferably, equally spaced points should be chosen for x_j to ensure that the choice of x_j is not biased to a local region. Suppose for each x_j , we get a value for λ , which we denote here by $\lambda(x_j)$. Then, the average Lyapunov exponent is the average of all $\lambda(x_j)$'s.

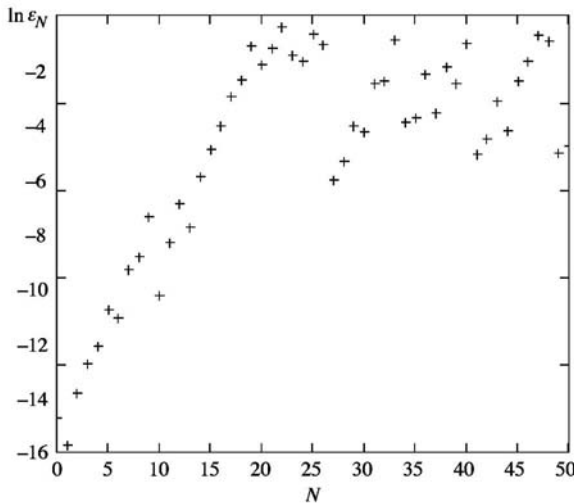
Although the estimation process is rather straightforward, a few problems are worth noting.

- As mentioned before, since all values of the time series are bounded, the choice of N should not be too large to make ϵ_N saturate. As we can see from (2.13), $\ln \epsilon_N$ is supposed to be proportional to N if ϵ_N is below saturation. As shown in Figure 2.7, the proportionality between $\ln \epsilon_N$ and N is maintained only for N below a certain level. In general,

*The formula shown here has been derived directly from the definition of the Lyapunov exponent. It does not necessarily represent the most effective numerical algorithm. In fact, numerous effective algorithms have been developed over the years for computing the Lyapunov exponents for higher dimensional systems. For example, see [115] for an algorithm based on the Gram-Schmitt renormalization method.



(a)



(b)

FIGURE 2.7

Logarithm of trajectory separation versus the number of time steps for a time series generated from the logistic map with $\lambda = 3.8$ and $x_j = 0.57$. (a) Initial separation is 10^{-6} ; (b) initial separation is 10^{-4} .

- smaller the initial separation ϵ_0 , larger the maximum value of N that can be used. A practical rule is to set N to approximately the number of iterates required for ϵ_N to expand to about half of the whole range of x .
2. The second problem is associated with the choice of k . In general, k should be chosen as remote from j as possible. If k is close to j , the two trajectories starting at x_j and x_k may be correlated to some extent. In that case, the Lyapunov exponent found can be deceptively small. A simple way to avoid this problem is to choose k such that significant differences are displayed between the time series segment containing x_j and that containing x_k . In practice, only a crude estimate of the minimum delay $|j - k|$ is needed, and in most cases, it can be found from a quick visual inspection of the time series. The algorithm should then insist that k and j are separated by at least the value of the minimum delay.
 3. Finally, we should be cautious about the use of the time-series method for finding Lyapunov exponents for periodic time series. Obviously, if the time series is periodic, the above procedure will always give $\epsilon_N = \epsilon_0$, i.e., $\lambda = 0$, regardless of the size of N . This is not what we would expect because the Lyapunov exponent in this case is supposed to tell us how fast nearby trajectories converge to the stable periodic orbit and hence must be a negative value. Thus, this method should not be used to compute Lyapunov exponents for periodic time series.
-

2.6 Laboratory Investigation

In this section we focus our attention on experimental investigation, and specifically on some essential laboratory techniques for capturing the complex behavior of switching converter circuits. We will briefly review the commonly used instruments for capturing time-domain waveforms, phase portraits and frequency spectra. Our main discussion will be focused on the various laboratory techniques for displaying Poincaré sections and bifurcation diagrams on the oscilloscope.

2.6.1 Capturing Waveforms, Phase Portraits and Frequency Spectra

The use of analog oscilloscopes for capturing periodic waveforms is common in engineering practice. However, analog oscilloscopes generally work only for periodic waveforms. Typically, we see a “shaking” waveform on the oscillo-

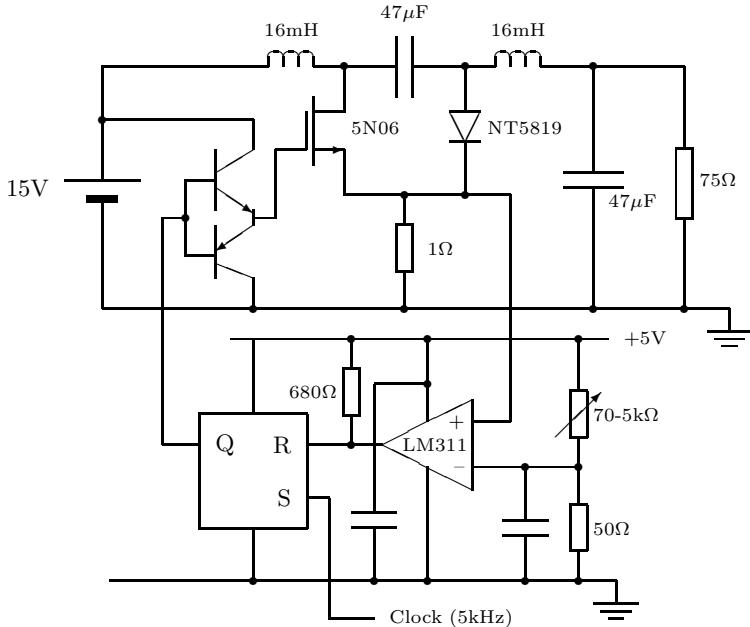


FIGURE 2.8

Ćuk converter under fixed-frequency current-mode control. The RS flip-flop block is constructed from a pair of NOR gates.

scope when a chaotic or quasi-periodic signal is probed. To display a chaotic or quasi-periodic waveform, we may use a digital storage oscilloscope (DSO) which can “memorize” the waveform for a certain time period and display it at a later time.

To capture phase portraits, the usual technique is to use the X-Y mode of the oscilloscope instead of a sweeping time base [117]. Again, analog oscilloscopes display “shaking” phase portraits for aperiodic signals. In practice, such “shaking” phase portraits can still be recorded if they clearly depict the appearance of the attractors.

Aperiodic signals can be easily distinguished from periodic signals by inspecting their frequency spectra. Spectral analyzers are commonly used for this purpose. Alternatively, we may use a DSO that can perform Fast Fourier Transform (FFT) on the signal being measured.

Example: A Ćuk Converter under Fixed-Frequency Current-Mode Control

As an example, we consider the Ćuk converter operating under fixed-frequency current-mode control [153], as shown in [Figure 2.8](#). This circuit can be easily constructed in the laboratory and its operation can be briefly described as follows. The essential control variable is the sum of the two inductor currents

which is picked up by the $1\ \Omega$ sensing resistor. The voltage across this sensing resistor is then compared with an adjustable threshold voltage which serves as a bifurcation parameter. The on-off status of the power switch (5N06) is determined by the output of the comparator (LM311). Essentially, when the power switch is on, the voltage across the sensing resistor ramps up, and as it reaches the threshold voltage, the RS flip-flop (actually a pair of NOR gates) is re-set and the power switch is turned off. Then, the control variable ramps down, until the clock pulse sets the RS flip-flop again and turns the switch back on. The cycle repeats at 5 kHz. In [Chapter 6](#), we will study this circuit in some depth. It will be shown that the qualitative behavior of this converter is dependent upon the choice of the parameter values. Here, we show in [Figures 2.9](#) and [2.10](#) some typical waveforms, phase portraits and frequency spectra obtained from this circuit.

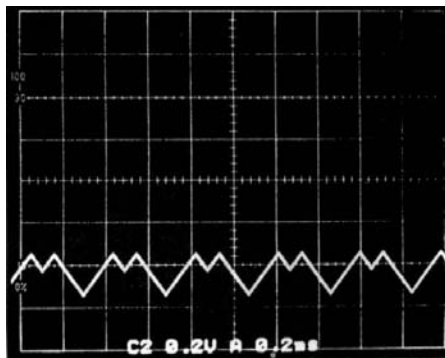
2.6.2 Capturing Poincaré Sections on Oscilloscopes

Principle of Poincaré Section Measurement

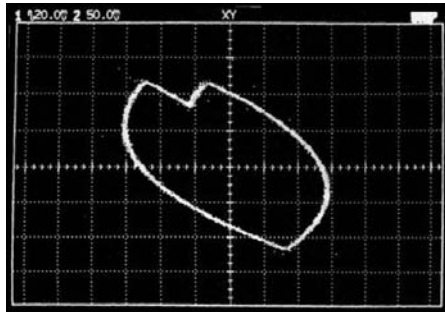
Obviously, since the oscilloscope can only display 2-dimensional phase portraits, we can at best view a projection of an attractor. Using the X-Y mode of the oscilloscope, we can display a 2-dimensional projection which in effect is a phase portrait, from any two given signals. This is adequate as long as the 2-dimensional projection clearly reflects the type of the attractor. For most cases, we are still able to tell, from a 2-dimensional projection, confidently if it is a periodic orbit. However, for a torus or chaotic attractor, we usually cannot make a definite conclusion unless we know what its Poincaré section looks like. To show a Poincaré section on the oscilloscope, what we need to do is to identify the moment when the trajectory cuts through a certain 2-dimensional plane which has been chosen as the Poincaré section.

Suppose the system's variables are x , y and z , and the oscilloscope is now plotting x against y using the X-Y mode [117]. Thus, the oscilloscope is showing the projection of the attractor on the x-y plane. We may define a Poincaré section as $z = k$, where k is a suitable constant. Imagine that the attractor is traversing in the 3-dimensional space and is cutting through the plane $z = k$ in both upward and downward directions, as shown in [Figure 2.11](#). Further suppose that we have a means to highlight the intersecting points on the projection. (We will explain how to do it later.) If the motion is periodic, such as the one shown in the figure, the projection should adequately reflect the periodicity of the motion. In this case, we see stationary points on the projection being highlighted.

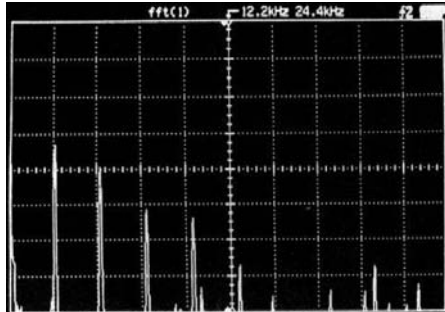
It should be noted that, by definition, the Poincaré section captures only one direction of crossing so that the period, if finite, can be correctly found. In a period-2 orbit as shown in [Figure 2.3 \(a\)](#), for example, the Poincaré section should correctly show only two crossing points, instead of four. Moreover, if the motion is quasi-periodic, we should see a closed loop on the projection, as shown in [Figure 2.3 \(b\)](#), and likewise for chaotic motion.



(a)



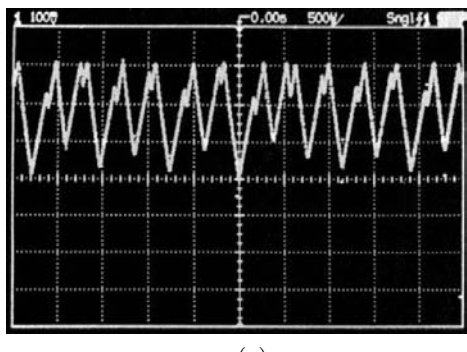
(b)



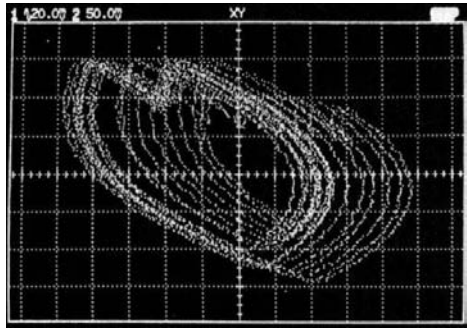
(c)

FIGURE 2.9

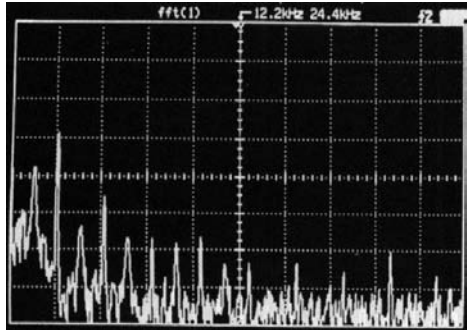
Experimental waveform, phase portrait and frequency spectrum from a Ćuk converter operating under current-mode control showing period-2 operation. Reference for $i_1 + i_2$ set at 0.49 A. (a) Inductor current (1×0.2 A/div, 0.2 ms/div, lowest horizontal grid line is 0 A); (b) phase portrait of inductor current against a capacitor voltage; (c) FFT of inductor current [153].



(a)



(b)



(c)

FIGURE 2.10

Experimental waveform, phase portrait and frequency spectrum from a Ćuk converter operating under current-mode control showing chaotic operation. Reference for i_1+i_2 set at 0.74 A. (a) Inductor current (1×1 V/div, $500 \mu\text{s}/\text{div}$, lowest horizontal grid line is 0 A); (b) phase portrait of inductor current against a capacitor voltage; (c) FFT of inductor current [153].

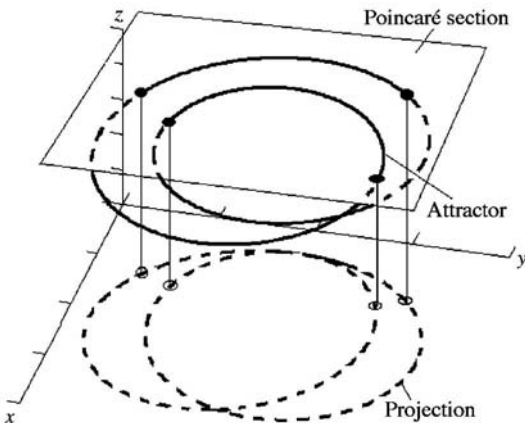


FIGURE 2.11

Poincaré section and 2-dimensional projection of an attractor.

Clearly, we need a comparator circuit to determine the instant when the attractor is hitting the plane $z = k$. This can be done easily using the circuit shown in [Figure 2.12](#). The function of this circuit is to produce a pulse whenever the signal z is equal to the value k which is set by a potentiometer. The display of the Poincaré section is then left to the oscilloscope. The idea is to make use of the Z-axis modulation function of the oscilloscope, which momentarily brightens the trace when its Z-input receives a pulse. Thus, if the output from the circuit described above is applied to the Z-input of the oscilloscope, the trace will momentarily brighten whenever the attractor intersects the plane $z = k$.

Example: An Autonomous Ćuk Converter

As an example, we consider a third-order autonomous Ćuk converter [155], as shown in [Figure 2.13](#). This circuit operates under a so-called free-running current-mode control which is effectively a bang-bang type of control. The sum of the inductor currents, sampled by a 0.1Ω sensing resistor, is compared with a reference signal which is derived continuously from the output voltage via a feedback circuit. The comparison is actually done by a Schmitt trigger circuit which also provides adjustment for the width of the hysteretic band. Referring to the circuit diagram, the feedback voltage gain is adjusted by R_μ and the inductor dc current level is adjusted by R_K . The $1 \text{ M}\Omega$ variable resistor sets the width of the hysteretic band and hence the switching frequency.

Analysis of the dynamics of this converter (see [Chapter 6](#)) reveals the possibility of a Hopf bifurcation, and computer simulation consistently reveals the characteristic sequence of changes in qualitative behavior starting from

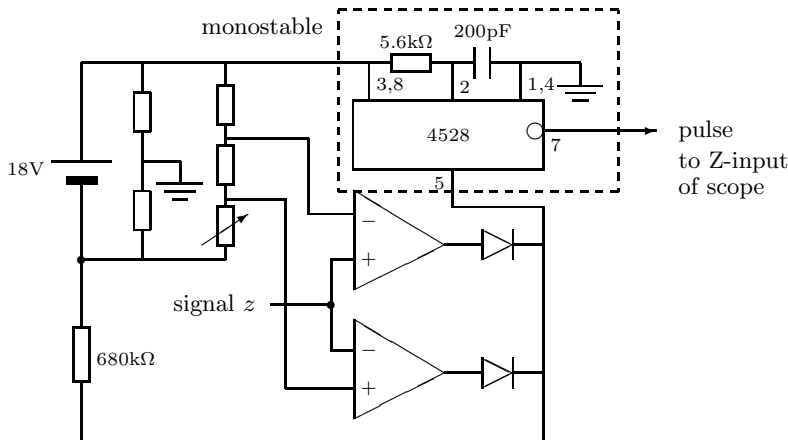


FIGURE 2.12

Circuit for detecting intersection of attractor and Poincaré section.

fixed point, via limit cycles and quasi-periodic orbits, to chaos [155]. Experimental study would inevitably require examining Poincaré sections since quasi-periodic and chaotic attractors can only be distinguished from the appearance of their Poincaré sections. Figure 2.14 shows the sequence of phase portraits starting from fixed point, through limit cycle and quasi-periodic orbit, to chaotic orbit.

Poincaré Sections for Non-Autonomous Circuits

For non-autonomous systems, Poincaré sections can be obtained in a likewise manner with the Z-axis modulation set to sample at the switching frequency of the converter under study. The resulting display contains bright dots along with the attractor, and the number of bright dots indicates the period of repetition in the case of periodic and subharmonic motion. Specifically, N bright dots means that the system is attracted to a subharmonic orbit whose period is N times the switching period. A large number of irregularly and densely located points may indicate chaos.

2.6.3 Plotting Bifurcation Diagrams on Oscilloscopes

Bifurcation diagrams are frequently used for identifying the way in which a system's qualitative behavior changes as some chosen parameters are varied. To display a bifurcation diagram, we need to construct a circuit which generates the necessary signals to the oscilloscope for displaying a bifurcation diagram. We will begin with basic operational requirements and then discuss the details of the implementation. For brevity, we will refer to the electronic circuit being studied as *system under test* (SUT).

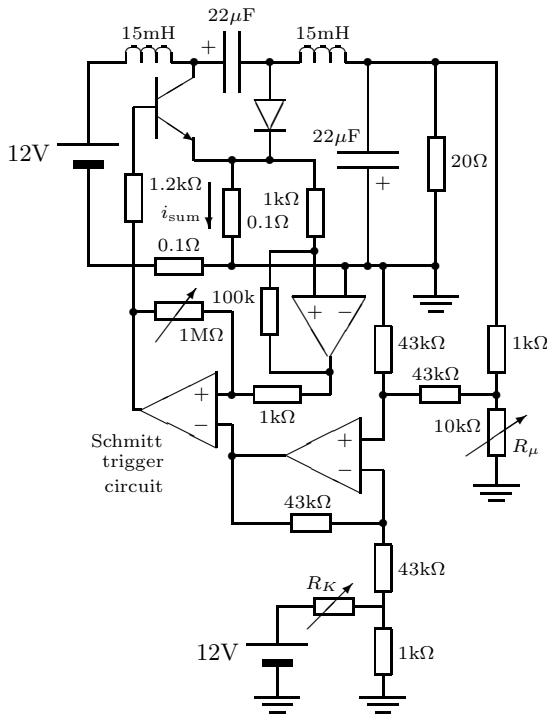


FIGURE 2.13
Experimental circuit of free-running autonomous Ćuk converter.

Basic Operating Principle

We first examine what a bifurcation diagram contains. A typical bifurcation diagram, as discussed in [Section 2.4.2](#), has its horizontal axis corresponding to variation of a bifurcation parameter and its vertical axis corresponding to the sampled steady-state value of a variable from the SUT. Obviously, we can make use of the X-Y mode of the oscilloscope to display a bifurcation parameter provided the necessary signals are applied to the X and Y input channels. In order to generate these signals, we need to perform two basic processes:

1. Vary a given parameter of the SUT according to a slowly swept sawtooth voltage which is applied to the X-input of the oscilloscope.
2. Sample a given signal from the SUT and send the sampled data to the Y-input of the oscilloscope.

Moreover, these two functions must be performed in a well coordinated manner. Firstly, the sawtooth must sweep relatively slowly, and the value of

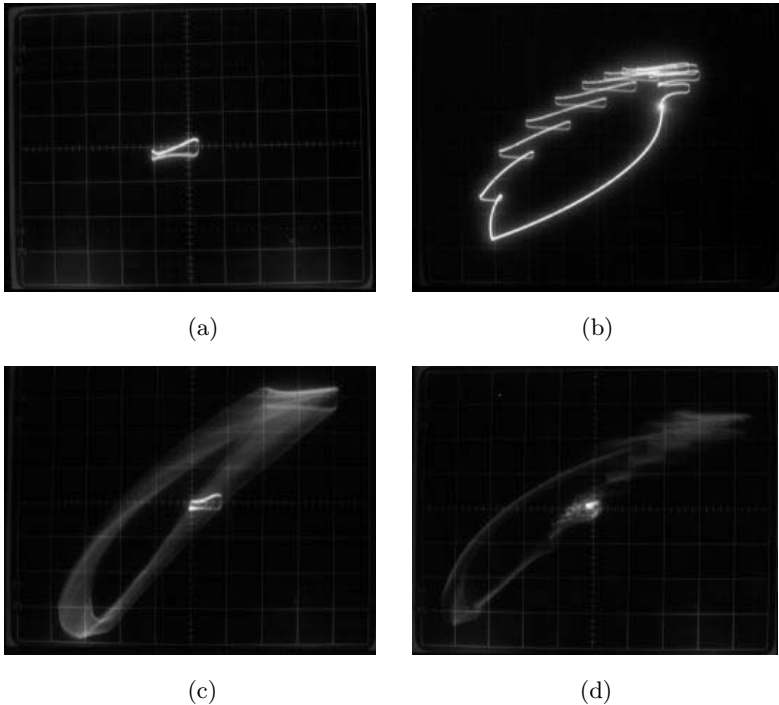


FIGURE 2.14

Phase portraits from autonomous Cuk converter showing (a) fundamental (period-1) solution; (b) limit cycle with a point on Poincaré section; (c) quasi-periodic orbit with a closed path on Poincaré section; (d) chaotic orbit with scattered points on Poincaré section [155]. The output voltage across the 20Ω load is used as input to the Poincaré section detector circuit of Figure 2.12.

the bifurcation parameter is set according to the sawtooth voltage in a step-wise manner. Then, for each value of the bifurcation parameter, the SUT is sampled to give enough data to the Y-input channel. Figure 2.15 shows the functional block diagram of the measurement system.

Digital Implementation

We now consider a digital implementation of the required measurement system. The sawtooth voltage can be generated by a D/A converter which reads the output from one or more digital counters. The horizontal resolution of the bifurcation diagram is determined by the number of bits of the D/A converter. A 12-bit D/A converter, for instance, will offer 4096 steps, and hence will give 4096 points along the horizontal axis of the bifurcation diagram to be displayed on the oscilloscope. Figure 2.16 shows the block diagram of a

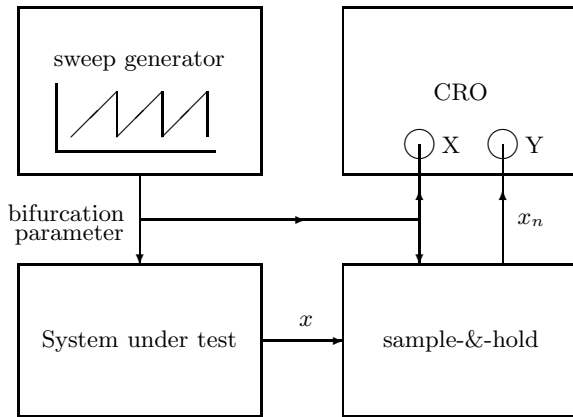


FIGURE 2.15

Block diagram of the system for displaying bifurcation diagrams. x denotes the variable to be sampled from the system under test (SUT). The CRO can be replaced by a computer which acquires the data from the sample-and-hold and the sawtooth generator, and plots/prints the bifurcation diagram.

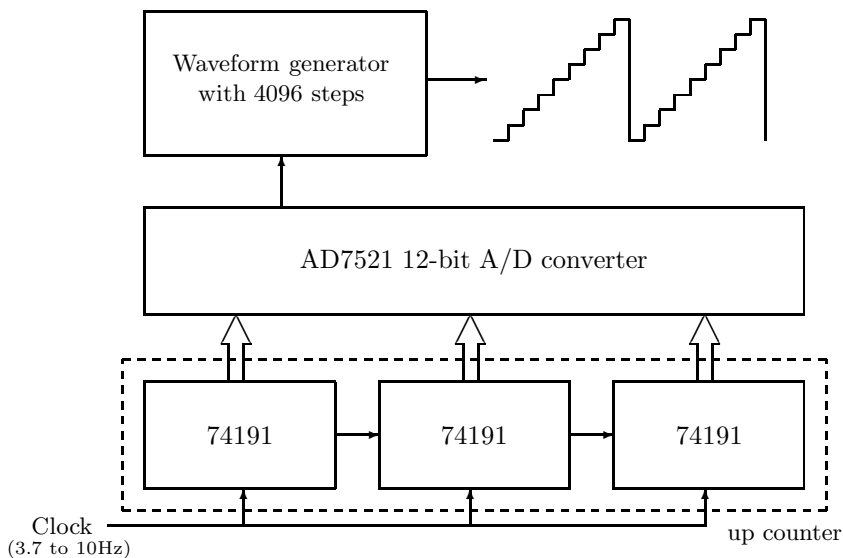


FIGURE 2.16

Block diagram of sawtooth generator. Output serves as voltage analog of bifurcation parameter to be sent to X-input channel of oscilloscope and the system under test (SUT).

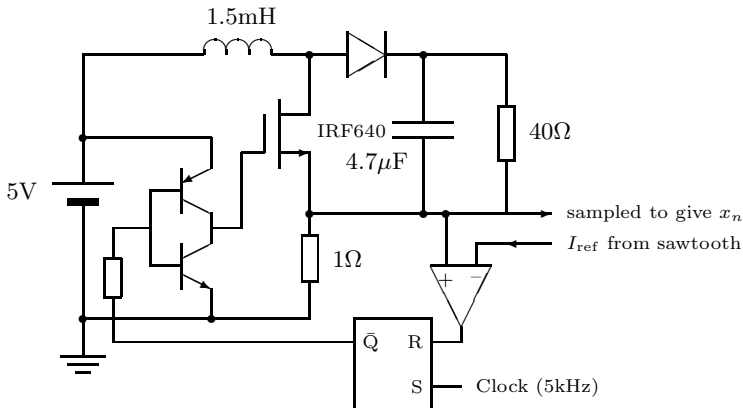


FIGURE 2.17

Schematic of experimental current-mode controlled boost converter, I_{ref} being the bifurcation parameter supplied by the sawtooth generator. The RS flip-flop block consists of a pair of NOR gates.

possible implementation of the sawtooth generator. The next question is how fast we should drive the counter, i.e., how fast should the sawtooth sweep.

The value of the sawtooth voltage controls the value of the bifurcation parameter used in the SUT. At each step of the sawtooth voltage, we have to ensure that enough time is given to sample enough data points from the SUT which are to be sent to the Y-input of the oscilloscope. If the sampling is done at a frequency f_s Hz, and N data points are to be displayed for each value of the bifurcation parameter, then the sawtooth must sweep as slowly as N/f_s second per step. Thus, if a 12-bit D/A converter is used, the sweep rate of the sawtooth should be lower than $f_s/(4096N)$ Hz.

Finally, the vertical resolution is controlled by the number of sampled data displayed during each step of the slowly swept sawtooth. Usually 500 samples are adequate. This value, denoted by N above, will affect the sweep rate of the sawtooth.

Example: A Simple Switching Converter

Suppose we wish to obtain a bifurcation diagram for the current-mode controlled boost converter shown in Figure 2.17. Our aim is to capture a bifurcation diagram on the oscilloscope, with I_{ref} as the bifurcation parameter (horizontal axis) and the inductor current as the sampled data (vertical axis).

The operation of the circuit can be described briefly as follows. A 5 kHz clock periodically turns on the power switch. While the switch is on, the inductor current climbs up linearly until its value is equal to I_{ref} which is the bifurcation parameter. When the inductor current reaches (just exceeds) I_{ref} , the comparator goes high, resetting the RS flip-flop. This turns off the power

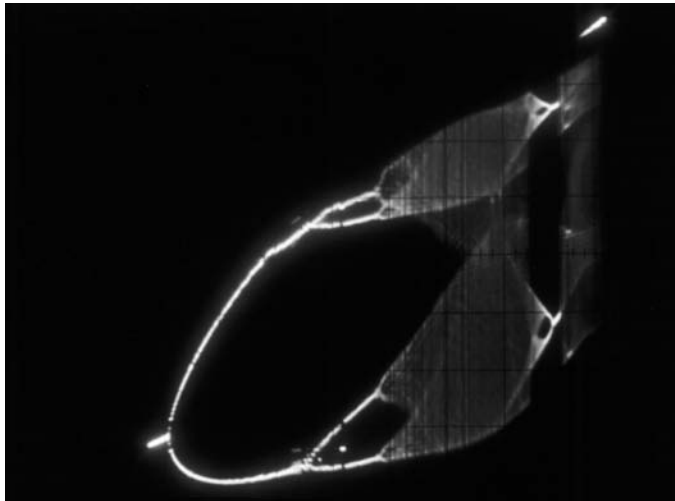


FIGURE 2.18

Bifurcation diagram from oscilloscope for the current-mode controlled boost converter, inductor current being the variable (vertical axis) and peak inductor current I_{ref} being the bifurcation parameter (horizontal axis) [146].

switch. Once the switch is turned off, the inductor current ramps down until the next clock pulse sets the RS flip-flop again and turns the switch back on. The cycle repeats periodically at 5 kHz.

The sampling is to be done at the switching frequency of the boost converter, i.e., 5 kHz. The variable to be sampled is the inductor current which is picked up by the 1Ω sensing resistor. The slowly swept sawtooth effectively defines I_{ref} , and is also sent to the X-input of the oscilloscope. 500 samples of inductor current are displayed at each step of the bifurcation parameter.

Figure 2.18 shows a photograph of the oscilloscope display as the trace sweeps horizontally from left to right, corresponding to I_{ref} swept from 0 to about 1 A. A 12-bit A/D converter is used for the sawtooth generator, i.e., a maximum of 4096 horizontal steps can be recorded. At each step 500 samples are displayed.

A Practical Note on Sampling Power Electronics Waveforms

In the above example, a problem related to the sampling of signals from switching circuits is worth noting. Specifically, there are possible ringings (fast oscillatory pulses) sandwiched between smooth segments due to the presence of parasitic inductance and capacitance. When sampling such signals (e.g., inductor current in the above example), care should be taken to avoid sampling at the ringings. We can either apply suitable filtering or deliberately

delay the sampling instant. In our example above, sampling is synchronized with the turn-on instants of the power switch, but with a small delay to avoid the ringing pulses.

2.6.4 Alternative Methods of Plotting Bifurcation Diagrams in the Laboratory

If the bifurcation parameter is a signal variable (e.g., the reference current), the sawtooth sweep method can be used. But if one intends to study the bifurcations in response to the variation of a power variable (e.g., the input voltage) or a physical parameter (e.g., the load resistance), other methods have to be used. There is a simpler way to display a bifurcation diagram on the oscilloscope. The idea is to use the Z-axis modulation to implicitly sample the required variable. This will eliminate the sample-and-hold circuit described above. If the oscillator blanking pulse of the pulse-width-modulator in the converter is available, we may simply use it to drive the Z-input of the oscilloscope and hence eliminate the need for constructing a separate driving circuit as mentioned in the previous sub-section. It is worth noting that the use of Z-axis modulation for obtaining bifurcation diagrams is simpler, but is less flexible compared to the use of an extra sample-and-hold circuit which allows the use of a computer for plotting, storing and further manipulating the data obtained from the SUT.

Furthermore, we may generate the sweeping voltage manually with a voltage supply. If we can do it steadily and slowly, we can still get a reasonably good bifurcation diagram. It should be understood that the capturing of the diagram can be done by a DSO, or by a camera using a long exposure time if an analog oscilloscope is used.

Finally, there is an important criterion for displaying a bifurcation diagram on the oscilloscope. The bifurcation parameter has to be a voltage or represented by a voltage. In the case where the bifurcation parameter is a current or value of a component (e.g., a resistance), we need to devise a way to make a voltage analog of the bifurcation parameter. This would vary from case to case. For instance, if the load resistance is the bifurcation parameter, we need to produce a voltage analog of the resistance value, sweep it through a suitable range, and feed it to the X-input of the oscilloscope. A handy way to do this is to use a two-limb rheostat with a common jockey. A portion of one limb is connected as the load, and the other limb connected to a separate voltage source. The voltage across the same portion of the second limb is fed to the X-input channel of the oscilloscope. Thus, the variation (i.e., manual sweep) of the load resistance is proportional to the voltage fed to the X-input.

2.7 Roles of Laboratory Experiments and Computer Simulations

In closing this chapter, it is worth reiterating that laboratory experiments and computer simulations serve a two-fold purpose in the investigation of complex behavior of physical systems.

1. As in traditional scientific studies, laboratory experiments and computer simulations serve to verify results which have been found on the basis of some numerical or behavioral models.
2. Many nonlinear phenomena in practical systems are often first observed during experimental measurements and routine simulations, and detailed analysis is done subsequently to provide explanations to the observed phenomena. This latter mode of investigation is particularly relevant to practical electronic systems.

As we will see in the later chapters, experimentations and simulations are used, as appropriate, for the purpose of verification as well as for providing quick clues to the choice of suitable models for analysis.

3

Modeling of Switching Power Converters for Nonlinear Dynamical Analysis

In its simplest terms, the operation of a switching converter can be described as an orderly repetition of a fixed sequence of circuit topologies. The conversion function of the converter is determined by the constituent topologies and the order in which they are repeated. Such toggling between topologies is achieved by placing switches at suitable positions and turning them on and off in such a way that the required topological sequence is produced. The usual control strategy to achieve a certain conversion function is to vary the relative time durations of the constituent topologies, which are usually not linearly related to the ultimate control objective. Thus, the overall operation is *time-varying and nonlinear*. Without appropriate models, analysis of these switching circuits would prove to be difficult.

Up to now, the modeling of switching converters has evolved around two basic approaches, namely, *discrete-time approach* and *averaging approach*. In this chapter we describe the basic principles of these modeling approaches and apply them to the boost and buck converters which have been shown to be the two *basic* types of converter topologies [91]. Our purpose here is to illustrate the key procedures for obtaining adequate models for the purpose of nonlinear dynamical analysis.

3.1 A Glimpse at Discrete-Time Modeling

The inherent piecewise switched operation of switching converters implies a multi-topological model in which one particular circuit topology describes the system for a particular interval of time. Also, the operation is *cyclic*, implying that the involving topologies repeat themselves periodically. Thus, a natural way to model such kind of operation is to split the system into several sub-systems, each being responsible for describing the system in one sub-interval of time. If we wish to find the solution at a particular future time t , we take an initial value, identify which sub-system is in charge, solve that particular sub-system, and continue to solve the appropriate sub-system as time advances. At the switching instants (at which the sub-systems toggle), a “stitching”

process has to be performed, which involves substitution of the final value of the previous sub-interval as the initial value of the present sub-interval. In the following, we test-drive this method on the simple boost converter, and our aim is to give a quick overview of the essential steps involved in the derivation of discrete-time models.

3.1.1 Ad Hoc Derivation of the Discrete-Time Iterative Map for the Boost Converter

The very first step in the analysis of a multi-topological circuit is to write down the state equations which describe the individual switched circuits. For converters operating in continuous conduction mode,* two switched circuits can be identified, one corresponding to the “switch-on” interval and the other to the “switch-off” interval. Let us consider the simple boost converter shown in [Figure 3.1](#). For the sake of simplicity in this introductory section, we set the value of the equivalent-series-resistance r_C to zero. In this case, the state equations can be written as

$$\dot{\mathbf{x}} = \mathbf{A}_1 \mathbf{x} + \mathbf{B}_1 E \quad \text{for switch-on interval } t_n \leq t < t'_n \quad (3.1)$$

$$\dot{\mathbf{x}} = \mathbf{A}_2 \mathbf{x} + \mathbf{B}_2 E \quad \text{for switch-off interval } t'_n \leq t < t_{n+1} \quad (3.2)$$

where

$$\mathbf{x} = \begin{bmatrix} v_C \\ i_L \end{bmatrix} \quad (3.3)$$

$$\mathbf{A}_1 = \begin{bmatrix} -1 \\ CR & 0 \\ 0 & 0 \end{bmatrix}, \quad \mathbf{B}_1 = \begin{bmatrix} 0 \\ 1 \\ \frac{1}{L} \end{bmatrix} \quad (3.4)$$

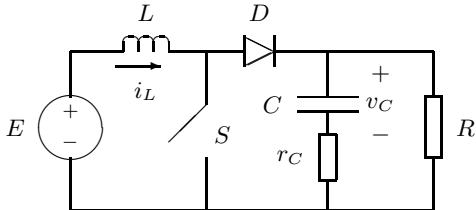
$$\mathbf{A}_2 = \begin{bmatrix} -1 & 1 \\ CR & C \\ -1 & 0 \\ \frac{1}{L} & 0 \end{bmatrix}, \quad \mathbf{B}_2 = \begin{bmatrix} 0 \\ 1 \\ \frac{1}{L} \end{bmatrix} \quad (3.5)$$

$$t_{n+1} = t_n + T; \quad T \text{ being the switching period.} \quad (3.6)$$

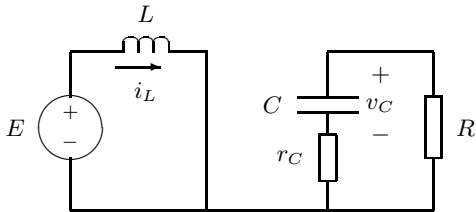
The sparseness of the matrix \mathbf{A}_1 permits the solution for the switch-on interval to be found easily by directly integrating the RHS of (3.1), i.e.,

$$\mathbf{x}(t) = \begin{bmatrix} v_C(t_n)e^{-(t-t_n)/CR} \\ i_L(t_n) + \frac{E(t-t_n)}{L} \end{bmatrix} \quad \text{for } t_n < t < t'_n. \quad (3.7)$$

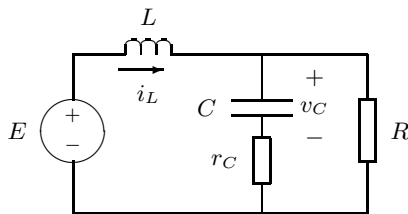
*At this point, we may simply regard the continuous conduction mode as a specific operating condition where the inductor current is always non-zero.



(a)



(b)



(c)

FIGURE 3.1

Boost converter. (a) Basic circuit; (b) circuit topology when switch S is turned on; (c) circuit topology when switch S is turned off and continuous conduction of the inductor current is maintained.

Then, putting $t = t'_n$ into the above equation gives the value of x at the end of the switch-on interval, i.e.,

$$v_C(t'_n) = v_C(t_n)e^{-dT/CR} \quad (3.8)$$

$$i_L(t'_n) = i_L(t_n) + \frac{EdT}{L} \quad (3.9)$$

where $d = t'_n/T$ and is known as *duty cycle* in much of the literature of power electronics.

To find the solution for the switch-off interval, we may apply Laplace transformation to (3.2) to yield the following equation in the s -domain. Note that

the Laplace transform of the input voltage is E/s .

$$\begin{aligned} \mathbf{X}(s) &= [s\mathbf{1} - \mathbf{A}_2]^{-1} [\mathbf{x}(t'_n) + \mathbf{B}_2 E(s)] \\ &= \frac{\begin{bmatrix} s & \frac{1}{C} \\ -\frac{1}{L} & s + \frac{1}{CR} \end{bmatrix} \begin{bmatrix} v_C(t'_n) \\ i_L(t'_n) + \frac{E}{sL} \end{bmatrix}}{s^2 + \frac{s}{CR} + \frac{1}{LC}} \end{aligned} \quad (3.10)$$

where $\mathbf{X}(s)$ denotes the Laplace transform of $\mathbf{x}(t)$. Thus, from (3.10), we may write the s -domain expressions for the capacitor voltage and the inductor current as

$$V_c(s) = \frac{E}{s} + \frac{K_1 s + K_2}{H(s)} \quad (3.11)$$

$$I_L(s) = \frac{E}{Rs} + \frac{K_3 s + K_4}{H(s)} \quad (3.12)$$

where

$$K_1 = v_C(t'_n) - E \quad (3.13)$$

$$K_2 = \frac{1}{C} i_L(t'_n) - 2\sigma E \quad (3.14)$$

$$K_3 = i_L(t'_n) - \frac{E}{R} \quad (3.15)$$

$$K_4 = \frac{1}{CR} i_L(t'_n) - \frac{1}{L} v_C(t'_n) + \left(\frac{R}{L} - 2\sigma \right) \frac{E}{R} \quad (3.16)$$

$$2\sigma = \frac{1}{CR} \quad (3.17)$$

$$H(s) = s^2 + \frac{s}{CR} + \frac{1}{LC}. \quad (3.18)$$

Then, by taking the inverse Laplace transformation of the partial fraction expansions of $V_c(s)$ and $I_L(s)$, the time-domain expressions for v_C and i_L for the interval $t'_n < t < t_{n+1}$ can be found.

$$\begin{aligned} v_C(t) &= E + K_1 e^{-\sigma(t-t'_n)} \cos \omega(t-t'_n) \\ &\quad + \frac{K_2 - K_1 \sigma}{\omega} e^{-\sigma(t-t'_n)} \sin \omega(t-t'_n) \end{aligned} \quad (3.19)$$

$$\begin{aligned} i_L(t) &= \frac{E}{R} + K_3 e^{-\sigma(t-t'_n)} \cos \omega(t-t'_n) \\ &\quad + \frac{K_4 - K_3 \sigma}{\omega} e^{-\sigma(t-t'_n)} \sin \omega(t-t'_n) \end{aligned} \quad (3.20)$$

where

$$\omega = \sqrt{\frac{1}{LC} - \sigma^2}. \quad (3.21)$$

Now, since K_1 , K_2 , K_3 and K_4 are functions of $\mathbf{x}(t'_n)$ which is in turn a function of $\mathbf{x}(t_n)$ and d , a difference equation involving $\mathbf{x}(t_{n+1})$, $\mathbf{x}(t_n)$ and d can be obtained by putting $t = t_{n+1}$ and $t_{n+1} - t'_n = (1-d)T$ into (3.19) and (3.20). The general form of this difference equation is

$$\mathbf{x}(t_{n+1}) = \mathbf{f}(\mathbf{x}(t_n), d) \quad (3.22)$$

where the function $\mathbf{f}(.)$ is given by

$$\mathbf{f}(\mathbf{x}, d) = \begin{bmatrix} f_{11} & f_{12} \\ f_{21} & f_{22} \end{bmatrix} \mathbf{x} + \begin{bmatrix} g_1 \\ g_2 \end{bmatrix} E, \quad (3.23)$$

with

$$\begin{aligned} f_{11} &= e^{-\frac{dT}{CR} - \sigma(1-d)T} \left[\cos((1-d)\omega T) - \frac{\sigma}{\omega} \sin((1-d)\omega T) \right] \\ f_{12} &= \frac{1}{\omega C} e^{-\sigma(1-d)T} \sin((1-d)\omega T) \\ f_{21} &= -\frac{1}{\omega L} e^{-\frac{dT}{CR} - \sigma(1-d)T} \sin((1-d)\omega T) \\ f_{22} &= e^{-\sigma(1-d)T} \left[\cos((1-d)\omega T) + \frac{1}{\omega} \left(\frac{1}{CR} - \sigma \right) \sin((1-d)\omega T) \right] \\ g_1 &= 1 - e^{-\sigma(1-d)T} \left[\cos((1-d)\omega T) \right. \\ &\quad \left. - \frac{1}{\omega} \left(\frac{dT}{LC} - \sigma \right) \sin((1-d)\omega T) \right] \\ g_2 &= \frac{1}{R} \left\{ 1 + e^{-\sigma(1-d)T} \left[\left(\frac{RdT}{L} - 1 \right) \cos((1-d)\omega T) \right. \right. \\ &\quad \left. \left. + \frac{1}{\omega} \left[\left(\frac{1}{CR} - \sigma \right) \frac{RdT}{L} + \frac{R}{L} - \sigma \right] \sin((1-d)\omega T) \right] \right\}. \end{aligned}$$

Equation (3.22) is the *discrete-time state equation* for the boost converter operating in continuous conduction mode. In much of the literature, the terms *iterative map*, *iterative function* and *Poincaré map* have been used synonymically with *discrete-time state equation*.

Finally, we need to define a control law to complete the model. This control law essentially relates the value of d in each switching cycle with one or more of the state variables. We will come back to this point in [Section 3.6](#).

3.1.2 Steady-State Solution

To avoid obscuring the essentials, we simply assume that a unique steady-state equilibrium point exists. The steady-state operating point can be found by enforcing periodicity, i.e., putting $\mathbf{x}(t_{n+1}) = \mathbf{x}(t_n)$ in (3.22). The result is

the following linear equation:^{*}

$$\begin{bmatrix} 1 - f_{11} & -f_{12} \\ -f_{21} & 1 - f_{22} \end{bmatrix} \begin{bmatrix} V_c \\ I_L \end{bmatrix} = \begin{bmatrix} g_1 \\ g_2 \end{bmatrix} E \quad (3.24)$$

with the f 's and g 's evaluated at $d = D$.

The steady-state values of the capacitor voltage and inductor current of the boost converter can hence be found using Cramer's rule, provided $(1 - f_{11})(1 - f_{22}) - f_{21}f_{12}$ does not vanish, i.e.,

$$V_c = \frac{[g_1(1 - f_{22}) + g_2f_{12}]E}{(1 - f_{11})(1 - f_{22}) - f_{21}f_{12}} \Big|_{d=D} \quad (3.25)$$

$$I_L = \frac{[g_2(1 - f_{11}) + g_1f_{21}]E}{(1 - f_{11})(1 - f_{22}) - f_{21}f_{12}} \Big|_{d=D} \quad (3.26)$$

At this point, we clearly recognize that the function $\mathbf{f}(.)$ in the discrete-time state equation (3.22) is far too complex to permit any systematic analysis to be conveniently performed. Simplification is needed to facilitate analysis. In the following we will introduce a simple series approximation which permits the original discrete-time state equation to be approximated to any desired degree of accuracy.

3.1.3 Approximation by Series Expansion

In most practical situations, the circuit parameters are often chosen such that the form of $\mathbf{f}(.)$ can be dramatically simplified. For example, in the case of the switching converters under study, T/CR and σT are usually small. Thus, the trigonometric and the exponential functions can be approximated as finite series expansions. The accuracy of the approximation is determined by the number of terms included in the series expansions. This issue will be discussed in more detail in [Section 3.3](#).

Applying a second-degree series approximation to the f 's in (3.23), we get the following approximate expressions for the boost converter:

$$f_{11} \approx 1 - \frac{T}{CR} + \frac{1}{2} \left(\frac{T}{CR} \right)^2 - \frac{(1-d)^2 T^2}{2LC} \quad (3.27)$$

$$f_{12} \approx \frac{(1-d)T}{C} - \frac{R}{2} \left[\frac{(1-d)T}{CR} \right]^2 \quad (3.28)$$

^{*}For a given fixed duty cycle, it is not difficult to show that the system always converges to an equilibrium point. The argument is that all elements are incrementally passive and there are no self-oscillating loops or cutsets. By the contraction principle, the system must converge to a unique equilibrium point. A rigorous proof can be found in Tse and Adams [149].

$$f_{21} \approx -\frac{(1-d)T}{L} + \frac{(1-d^2)T^2}{2LC} \quad (3.29)$$

$$f_{22} \approx 1 - \frac{(1-d)^2 T^2}{2LC} \quad (3.30)$$

$$g_1 \approx \frac{(1-d^2)T^2}{2LC} \quad (3.31)$$

$$g_2 \approx \frac{T}{L} \quad (3.32)$$

Note that as we have omitted r_C in the analysis, the above expressions do not contain any terms involving r_C . Also, putting the above approximate expressions in (3.25) and (3.26), we get the steady-state equilibrium point as

$$V_c = \frac{E}{1-D}(1+\xi) \quad (3.33)$$

$$I_L = \frac{E}{R(1-D)^2} \left[1 - \frac{RTD(1-D)^2}{2L} + \epsilon \right] \quad (3.34)$$

where ξ and ϵ are first or higher order terms and can be neglected.

3.2 General Procedure for Derivation of Discrete-Time Iterative Maps for the Basic Switching Converters

In the previous section, the discrete-time analysis method was introduced in a somewhat informal fashion, in that only the boost converter was treated and some less general properties were made use of in the derivation of the state equation, such as the sparseness of the system matrices. In this section, we describe a formal procedure for deriving discrete-time matrix state equation, which is valid for all switching converters regardless of their exact circuit topologies and topological sequences.

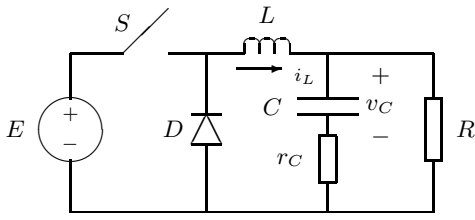
3.2.1 Continuous Conduction Mode

When the switching converter is operating in continuous conduction mode, its topological sequence consists of two linear circuits described by the following state equations:

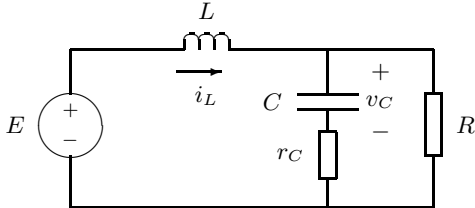
$$\dot{\mathbf{x}} = \mathbf{A}_1 \mathbf{x} + \mathbf{B}_1 e(t) \quad \text{for } t_n \leq t < t_n + dT \quad (3.35)$$

$$\dot{\mathbf{x}} = \mathbf{A}_2 \mathbf{x} + \mathbf{B}_2 e(t) \quad \text{for } t_n + dT \leq t < t_{n+1} \quad (3.36)$$

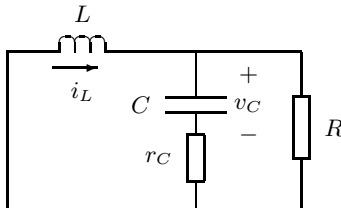
where \mathbf{x} again denotes the state vector $[v_C \ i_L]^T$, $e(t)$ the input voltage (which is varying with time in general), d the duty cycle, T the switching period, the



(a)



(b)



(c)

FIGURE 3.2

Buck converter. (a) Basic circuit; (b) circuit topology when switch S is turned on; (c) circuit topology when switch S is turned off and continuous conduction of the inductor current is maintained.

\mathbf{A} 's and \mathbf{B} 's represent system matrices, and t_n denotes nT . Figures 3.1 and 3.2 show, respectively, the topological sequence for the boost and buck converters operating in continuous conduction mode.

In a likewise fashion as illustrated in Section 3.1, the value of \mathbf{x} at the end of the first sub-interval is first expressed in terms of that at the beginning of the sub-interval. The standard form of this expression is

$$\mathbf{x}(t_n + dT) = \Phi_1(dT)\mathbf{x}(t_n) + \int_{t_n}^{t_n + dT} \Phi_1(t_n + dT - \tau) \mathbf{B}_1 e(t).d\tau \quad (3.37)$$

$$= \Phi_1(dT)\mathbf{x}(t_n) + \int_0^{dT} \Phi_1(\xi) \mathbf{B}_1 e(t).d\xi \quad (3.38)$$

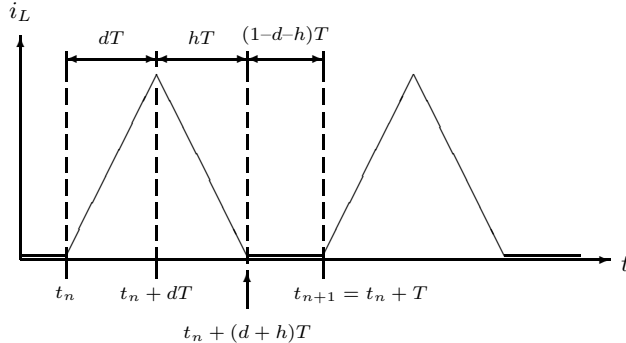


FIGURE 3.3

Inductor current waveform in discontinuous conduction mode.

where Φ_1 is the corresponding transition matrix. Similarly for the second sub-interval, the following expression is written.

$$\mathbf{x}(t_{n+1}) = \Phi_2(\bar{dT})\mathbf{x}(t_n + dT) + \int_0^{\bar{dT}} \Phi_2(\xi)\mathbf{B}_2 e(t).d\xi \quad (3.39)$$

where

$$\bar{d} = 1 - d. \quad (3.40)$$

The total increment of \mathbf{x} acquired over one switching period can be obtained by substituting (3.39) in (3.38). Furthermore, assuming that the input voltage $e(t)$ is a “slowing” varying function (in the sense that $e(t)$ remains nearly constant within a switching period), the above process of successive substitutions yields

$$\mathbf{x}_{n+1} = \Phi_t(d)\mathbf{x}_n + \Psi_t(d)e(nT) \quad (3.41)$$

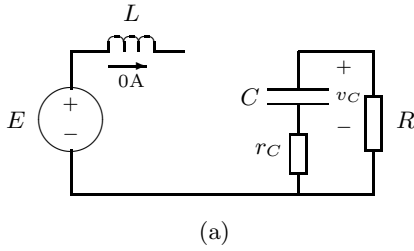
where

$$\mathbf{x}_n = \mathbf{x}(t_n), \quad (3.42)$$

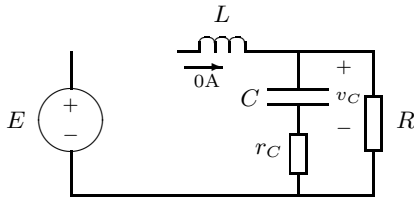
$$\Phi_t(d) = \Phi_2(\bar{dT})\Phi_1(dT), \quad (3.43)$$

$$\Psi_t(d) = \Phi_2(\bar{dT}) \int_0^{dT} \Phi_1(\xi)\mathbf{B}_1 d\xi + \int_0^{\bar{dT}} \Phi_2(\xi)\mathbf{B}_2 d\xi. \quad (3.44)$$

Equation (3.41) is the general discrete-time iterative map for the basic switching converter working in continuous conduction mode. It should be noted that from the system’s viewpoint, d is an input, and (3.41) does not possess a linear term in d . Direct application of linear methods is thus prohibited. Use of this equation in the analysis of switching converters will be discussed in the later chapters.



(a)



(b)

FIGURE 3.4

Circuit topologies for (a) boost converter and (b) buck converter when both switch and diode are turned off. These topologies take charge for the $(1 - d - h)T$ sub-interval, as shown in [Figure 3.3](#), when the converters operate in discontinuous conduction mode.

3.2.2 Discontinuous Conduction Mode

When the switching converter is operating in discontinuous conduction mode, the inductor current takes a zero value for a finite sub-interval of time, as illustrated in [Figure 3.3](#). For this case, an additional circuit topology has to be considered, corresponding to the sub-interval of time during which the inductor current is zero. [Figure 3.4](#) shows the additional circuit topologies for the boost and buck converters. The set of linear state equations, for the discontinuous-conduction-mode case, becomes

$$\dot{x} = A_1 x + B_1 e(t) \quad \text{for } t_n \leq t < t_n + dT \quad (3.45)$$

$$\dot{x} = A_2 x + B_2 e(t) \quad \text{for } t_n + dT \leq t < t_n + (d + h)T \quad (3.46)$$

$$\dot{x} = A_3 x + B_3 e(t) \quad \text{for } t_n + (d + h)T \leq t < t_{n+1} \quad (3.47)$$

where hT is the duration of the second sub-interval and $h < 1 - d$.

Applying the technique of successive substitution to the above system, we get a discrete-time iterative map similar in form to (3.41), except that the matrices Φ_t and Ψ_t are now functions of d and h , and are given by

$$\Phi_t(d, h) = \Phi_3(\bar{h}T)\Phi_2(hT)\Phi_1(dT) \quad (3.48)$$

$$\Psi_t(d, h) = \Phi_3(\bar{h}T)\Phi_2(hT) \int_0^{dT} \Phi_1(\xi)B_1 d\xi$$

$$+ \Phi_3(\bar{h}T) \int_0^{hT} \Phi_2(\xi) \mathbf{B}_2 d\xi + \int_0^{\bar{h}T} \Phi_3(\xi) \mathbf{B}_3 d\xi \quad (3.49)$$

where

$$\bar{h} = 1 - d - h. \quad (3.50)$$

At this point we note that when the switching converter is operating in discontinuous conduction mode, two additional conditions apply to reduce the order of the system by one and to eliminate the dependence of Φ_t and Ψ_t on the variable h .

1. The inductor current is zero for the sub-interval $t_n + (d+h)T \leq t \leq t_{n+1}$. Thus, $i_L(t_n) = 0$ for all n . This implies that the inductor current does not act as a state variable in this discrete-time model, and the state equation is essentially first order with the capacitor voltage as the only state variable.
2. Continuity of the inductor current guarantees that

$$\lim_{t \rightarrow t'_n +} i_L(t) = \lim_{t \rightarrow t'_n -} i_L(t) = i_{L,\text{peak}} \quad (3.51)$$

where $t'_n = t_n + dT$ and $i_{L,\text{peak}}$ is the peak inductor current. This leads effectively to an expression for h in terms of d , thus eliminating the dependence of Φ_t and Ψ_t on h . For example, if the inductance current is taken as a triangular waveform, then the expression relating h and d for the boost converter is simply

$$h = \frac{ed}{v_C - e}, \quad (3.52)$$

and that for the buck converter is

$$h = \frac{(e - v_C)d}{v_C}. \quad (3.53)$$

When these conditions are taken into account, the form of the resulting iterative map differs significantly from that of (3.41). In general, the iterative map for the basic switching converter operating in discontinuous conduction mode is given by

$$v_C(t_{n+1}) = f(v_C(t_n), d) \quad (3.54)$$

where $f(\cdot)$ is derived by enforcing the above conditions on (3.41).

3.3 Approximation of Iterative Maps by Series Expansions

In the derivation of the discrete-time iterative maps, the transition matrices Φ_1 , Φ_2 and Φ_3 are involved. In general, we can write these transition matrices

as

$$\Phi_k(\xi) = e^{\mathbf{A}_k \xi} \quad (3.55)$$

where the exponential matrix $e^{\mathbf{A}_k \xi}$ is given by the following infinite series:

$$e^{\mathbf{A}_k \xi} \doteq \mathbf{1} + \mathbf{A}_k \xi + \frac{1}{2!} \mathbf{A}_k^2 \xi^2 + \cdots + \frac{1}{n!} \mathbf{A}_k^n \xi^n + \cdots \quad (3.56)$$

Here, we note that $e^{\mathbf{A}_k \xi}$ is a square matrix of the same order as \mathbf{A}_k , whose elements are functions of ξ . Literature abounds with methods for calculating $e^{\mathbf{A}_k \xi}$ as functions of ξ in closed form [125]. However, the approach is usually quite complicated, and for most practical purposes, it suffices to approximate $e^{\mathbf{A}_k \xi}$ by the first N terms of the exponential series.

It is important, when finite series approximation is used, to ensure that the number of terms included is sufficiently large to achieve the desired accuracy. In the following we evaluate the error incurred when only a finite number of terms are included in the computation of a transition matrix. Suppose only the first N terms are used, i.e.,

$$e^{\mathbf{A}_k \xi} \approx \mathbf{1} + \mathbf{A}_k \xi + \frac{1}{2!} \mathbf{A}_k^2 \xi^2 + \cdots + \frac{1}{N!} \mathbf{A}_k^N \xi^N. \quad (3.57)$$

Then, we may write the error matrix \mathcal{E} as

$$\mathcal{E} = \frac{1}{(N+1)!} \mathbf{A}_k^{N+1} \xi^{N+1} + \frac{1}{(N+2)!} \mathbf{A}_k^{N+2} \xi^{N+2} + \cdots \quad (3.58)$$

Now let $\|\mathbf{A}\|$ be the ∞ -norm of the square matrix \mathbf{A} of order r defined by

$$\|\mathbf{A}\| \doteq \max_i \sum_j |a_{ij}|. \quad (3.59)$$

The above norm is the maximum among the r values, each of which is the sum of $|a_{ij}|$ in the same row. Obviously, $|a_{ij}| \leq \|\mathbf{A}\|$ for all i and j .

Applying the inequality $\|\mathbf{AB}\| \leq \|\mathbf{A}\| \cdot \|\mathbf{B}\|$ to (3.58), we get an upper bound for the elements of the error matrix \mathcal{E} , i.e.,

$$\begin{aligned} |\mathcal{E}_{ij}| &\leq \sum_{m=N+1}^{\infty} \frac{1}{m!} |(i, j) \text{ element of } (\mathbf{A}_k \xi)^m| \\ &\leq \sum_{m=N+1}^{\infty} \frac{1}{m!} \|\mathbf{A}_k \xi\|^m \\ &\leq \frac{\|\mathbf{A}_k \xi\|^{N+1}}{(N+1)!} [1 + \|\mathbf{A}_k \xi\| + \|\mathbf{A}_k \xi\|^2 + \cdots] \end{aligned} \quad (3.60)$$

$$= \frac{\|\mathbf{A}_k \xi\|^{N+1}}{(N+1)! (1 - \|\mathbf{A}_k \xi\|)}. \quad (3.61)$$

The last equality assumes that $\|\mathbf{A}_k\xi\| < 1$ and hence the infinite series in (3.60) converges. Thus, the upper bound \mathcal{U} of the error when (3.57) is used to approximate $e^{\mathbf{A}_k\xi}$ is

$$\mathcal{U} = \frac{\|\mathbf{A}_k\xi\|^{N+1}}{(N+1)!(1 - \|\mathbf{A}_k\xi\|)}. \quad (3.62)$$

To get an idea of the magnitude of \mathcal{U} , we substitute in (3.62) some typical values of the system matrices. First, we note that typical elements of the system matrices are $1/C(R + r_C)$, $R/C(R + r_C)$, $1/L$, and r_C/L , and ξ is always less than the switching period T . Thus, the norm $\|\mathbf{A}_k\xi\|$ is typically less than one. For example, if $T/C(R + r_C) = 0.1$, $RT/L = 5$, $R = 25 \Omega$, and $r_C \approx 0$, then $\|\mathbf{A}_k\xi\| < 0.1 + 0.2 = 0.3$. Suppose the transition matrices are approximated using (3.57) with $N = 2$, i.e.,

$$\Phi_k(\xi) = \mathbf{1} + \mathbf{A}_k\xi + \frac{1}{2}\mathbf{A}_k^2\xi^2. \quad (3.63)$$

Then, the maximum error in the elements of $\Phi_k(\xi)$ is given by

$$\mathcal{U} = \frac{0.3^3}{3!(1 - 0.3)} = 6.4285 \times 10^{-3}. \quad (3.64)$$

The above figure is quite acceptable in practice as it gives a maximum percentage error of less than 6.4% for the elements of Φ_k . Thus, (3.63) represents a reasonably close approximation for the transition matrices concerned. The answer to whether we should use a higher-order approximation lies entirely on how much we are willing to sacrifice accuracy for simplicity.

3.4 Approximate Iterative Maps for the Boost and Buck Converters

It is well known that all existing topologies of switching converter circuits can be derived from combinations of boost and/or buck converters along with some form of transformation function, which involves an ideal transformer element which is capable of transforming DC as well as AC [128]. A rigorous demonstration of this viewpoint has been provided by Liu and Lee [91]. Thus, the boost and buck converters are of fundamental importance, and their properties naturally pertain to any complex derivative converter system. In this section we summarize the approximate expressions for the various matrices and functions involved in the iterative maps of the boost and buck converters. We will postpone the detailed discussions of the use of these iterative maps for the analysis of nonlinear behavior of switching converters to the later chapters.

TABLE 3.1

Values of f_{ij} 's and g_i 's in iterative maps of boost and buck converters operating in continuous conduction mode. For brevity, we write $\tau_C = CR$ and $\tau_L = L/R$. Also, r_C has been included in the derivations of these formulas.

	Boost converter	Buck converter
f_{11}	$1 - \frac{T}{\tau_C} + \frac{T^2}{2\tau_C^2} - \frac{(1-d)^2 T^2}{2\tau_C \tau_L}$	$1 - \frac{T}{\tau_C} + \frac{T^2}{2\tau_C^2} - \frac{T^2}{2\tau_C \tau_L}$
f_{12}	$\frac{R(1-d)T}{\tau_C} - \frac{R(1-d)^2 T^2}{2\tau_C^2}$ - $\frac{r_C(1-d)^2 T^2}{2\tau_C \tau_L}$	$\frac{RT}{\tau_C} - \frac{RT^2}{2\tau_C^2} - \frac{r_C T^2}{2\tau_C \tau_L}$
f_{21}	- $\frac{(1-d)T}{R\tau_L} + \frac{(1-d^2)T^2}{2R\tau_C \tau_L}$ + $\frac{r_C(1-d)^2 T^2}{2R^2 \tau_L^2}$	- $\frac{T}{R\tau_L} + \frac{T^2}{2R\tau_C \tau_L} + \frac{r_C T^2}{2R^2 \tau_L^2}$
f_{22}	$1 - \frac{(1-d)^2 T^2}{2\tau_C \tau_L} + \frac{r_C^2(1-d)^2 T^2}{2R^2 \tau_L^2}$	$1 - \frac{r_C T}{R\tau_L} - \frac{T^2}{2\tau_C \tau_L} + \frac{r_C^2 T^2}{2R^2 \tau_L^2}$
g_1	$\frac{(1-d^2)T^2}{2\tau_C \tau_L}$	$\left(1 - \frac{d}{2}\right) \frac{dT^2}{\tau_C \tau_L}$
g_2	$\frac{T}{R\tau_L} - \frac{r_C(1-d^2)T^2}{2R^2 \tau_L^2}$	$\frac{dT}{R\tau_L} - \left(1 - \frac{d}{2}\right) \frac{r_C dT^2}{R^2 \tau_L^2}$

3.4.1 Continuous Conduction Mode

Application of second-degree approximation to the switching converter operating in continuous conduction mode leads to an approximate state equation of the form similar to (3.41), namely,

$$\mathbf{x}_{n+1} = \mathbf{F}(d)\mathbf{x}_n + \mathbf{G}(d)e(t_n) \quad (3.65)$$

where $e(t_n)$ is the value of the input voltage at $t = t_n$,

$$\mathbf{F}(d) = \begin{bmatrix} f_{11}(d) & f_{12}(d) \\ f_{21}(d) & f_{22}(d) \end{bmatrix} \quad \text{and} \quad \mathbf{G}(d) = \begin{bmatrix} g_1(d) \\ g_2(d) \end{bmatrix}. \quad (3.66)$$

Table 3.1 summarizes the approximate expressions for the f_{ij} 's and g_i 's for the boost and buck converters. For the sake of notational brevity, τ_C and τ_L are used to denote the time constants CR and L/R respectively. Also, the approximation $R + r_C \approx R$ has been applied in these expressions.

TABLE 3.2

Approximate expressions of $f(\cdot)$ for boost and buck converters operating in discontinuous conduction mode. For brevity, we write $\tau_C = CR$, $\tau_L = L/R$, $v_C = v_C(t_n)$, and $e = e(t_n)$.

	Boost converter	Buck converter
$f(\cdot)$	$\left(1 - \frac{T}{\tau_C} + \frac{T^2}{2\tau_C^2}\right) v_C + \frac{d^2 T^2 e_n^2}{2\tau_C \tau_L (v_C - e_n)}$	$\left(1 - \frac{T}{\tau_C} + \frac{T^2}{2\tau_C^2}\right) v_C + \frac{d^2 T^2 e (e - v_C)}{2\tau_C \tau_L v_C}$

3.4.2 Discontinuous Conduction Mode

As explained in [Section 3.2](#), the iterative map for the switching converter operating in discontinuous conduction mode takes the following form:

$$v_C(t_{n+1}) = f(v_C(t_n), d). \quad (3.67)$$

An approximate expression for the function $f(\cdot)$ can, in a similar fashion, be obtained via a second-degree approximation. We tabulate the results in [Table 3.2](#) for the boost and buck converters. As we can see here, the iterative maps for the case of discontinuous conduction mode differ significantly from those for continuous conduction mode. We therefore expect quite significant difference in the dynamical behavior of switching converters operating in discontinuous conduction mode from those operating in continuous conduction mode. We will cover this in detail in [Chapter 4](#).

3.5 The Method of Averaging

The averaging approach was developed by Middlebrook and Ćuk [98] in the late 1970s for modeling switching converters. The main objective of this approach is to eliminate the time-varying parameters in the original system equations. Essentially, an averaged model discards the switching details and focuses only on the envelope of the dynamical motion, and is therefore well suited for characterizing switching converters in the low-frequency domain. In engineering practice, such averaged models are often linearized to yield linear time-invariant models that can be analyzed in the standard frequency domain, facilitating design of control loops and evaluation of transient responses in ways that are familiar to engineers. In this book, however, since our objective

is to study nonlinear behavior, we will not perform any linearization but rather analyze the averaged models as they are.

3.5.1 General Procedure

Suppose the switching converter under study toggles between N circuit topologies. In one switching cycle, it spends a fraction of time in one particular topology. Again, we let \mathbf{x} be the state vector, d_j be the fraction of the period in which the circuit stays in the j th topology, and T be the period of one switching cycle. Obviously, $d_1 + d_2 + \dots + d_N = 1$. Thus, as we did before, we can write down the following state equations for the system:

$$\dot{\mathbf{x}} = \begin{cases} \mathbf{A}_1\mathbf{x} + \mathbf{B}_1E & \text{if } t_n \leq t < t_n + d_1T \\ \mathbf{A}_2\mathbf{x} + \mathbf{B}_2E & \text{if } t_n + d_1T \leq t < t_n + (d_1 + d_2)T \\ \dots \\ \mathbf{A}_N\mathbf{x} + \mathbf{B}_NE & \text{if } t_n + (1 - d_N)T \leq t < t_{n+1} \end{cases} \quad (3.68)$$

where \mathbf{A}_j and \mathbf{B}_j are the system matrices for the j th topology, and E is the input voltage.

The essential step in the modeling is to “average” out the system matrices [98], yielding the following continuous-time averaged model:

$$\dot{\mathbf{x}} = \mathbf{A}_m\mathbf{x} + \mathbf{B}_mE \quad \text{for all } t \quad (3.69)$$

where

$$\mathbf{A}_m = \sum_{j=1}^N d_j \mathbf{A}_j \quad \text{and} \quad \mathbf{B}_m = \sum_{j=1}^N d_j \mathbf{B}_j. \quad (3.70)$$

In essence, averaging retains the low-frequency properties while it ignores the detailed dynamics within a switching cycle. Usually, the validity of averaged models is only restricted to the low-frequency range up to an order of magnitude below the switching frequency. For this reason, averaged models become inadequate when the aim is to explore nonlinear phenomena that may appear across a wide spectrum of frequencies. Nevertheless, averaging techniques can be useful to analyze those bifurcation phenomena which are confined to the low-frequency range, as we will show later in this book.

We note further that the input voltage has been assumed to be fixed. However, if the input voltage is allowed to vary with time, such variation must be at least an order of magnitude slower than the fastest variation of the state variables that the averaged model is capable of characterizing. In other words, compared to the discrete-time model, the allowable input voltage variation should be much slower. Here, we simply take it as a constant, but we do bear in mind that the averaged model is still valid for very slowly varying input voltages.

3.5.2 Averaged Models for the Boost and Buck Converters

Clearly, the derivation of \mathbf{A}_m and \mathbf{B}_m is all that is needed to get the averaged model for a given switching converter. The algebra involved is simple. For the case of the simple switching converters operating in continuous conduction mode, the model takes the form of

$$\dot{\mathbf{x}} = \mathbf{A}_m(d)x + \mathbf{B}_m(d)E \quad \text{for all } t \quad (3.71)$$

where d is the duty cycle. For the boost converter, \mathbf{A}_m and \mathbf{B}_m are given, respectively, by

$$\mathbf{A}_m = \begin{bmatrix} -1 & \frac{R(1-d)}{C(R+r_C)} \\ \frac{C(R+r_C)}{-R(1-d)} & \frac{-Rr_C(1-d)}{L(R+r_C)} \end{bmatrix} \quad \text{and} \quad \mathbf{B}_m = \begin{bmatrix} 0 \\ \frac{1}{L} \end{bmatrix}, \quad (3.72)$$

and for the buck converter, they are

$$\mathbf{A}_m = \begin{bmatrix} -1 & \frac{R}{C(R+r_C)} \\ \frac{-R}{L(R+r_C)} & \frac{-Rr_C}{L(R+r_C)} \end{bmatrix} \quad \text{and} \quad \mathbf{B}_m = \begin{bmatrix} 0 \\ \frac{d}{L} \end{bmatrix}. \quad (3.73)$$

For the case of discontinuous conduction mode, the general form given in (3.69) is still valid. Moreover, as argued in [Section 3.2.2](#), the model is first-order, and we need to consider only v_C . For the boost converter, we get

$$\frac{dv_C(t)}{dt} = \frac{-1}{C(R+r_C)}v_C(t) + \frac{RdhT}{2LC(R+r_C)}E \quad (3.74)$$

where d and h are as defined in [Section 3.2.2](#) (see [Figure 3.3](#)). We also recall that h and d are related by (3.52). Thus, we may write (3.74) as

$$\frac{dv_C(t)}{dt} = \frac{-v_C(t)}{C(R+r_C)} + \frac{Rd^2T}{2LC(R+r_C)} \left[\frac{E^2}{v_C(t) - E} \right], \quad (3.75)$$

which is the averaged state equation for the boost converter operating in discontinuous conduction mode.

In a likewise manner, we get the averaged state equation for the buck converter operating in discontinuous conduction mode as

$$\frac{dv_C(t)}{dt} = \frac{-v_C(t)}{C(R+r_C)} + \frac{Rd^2T}{2LC(R+r_C)} \left[\frac{E(E - v_C(t))}{v_C(t)} \right]. \quad (3.76)$$

TABLE 3.3

Steady-state solutions for boost and buck converters by solving equation (3.77), assuming $R + r_C \approx R$.

Converter	Continuous conduction mode	Discontinuous conduction mode
Boost	$V_C = \frac{E}{1 - D}$ $I_L = \frac{E}{R(1 - D)^2}$	$V_C = \frac{E}{2} \left[1 + \sqrt{1 + \frac{2RD^2T}{L}} \right]$
Buck	$V_C = DE$ $I_L = \frac{DE}{R}$	$V_C = \frac{2E}{1 + \sqrt{1 + \frac{8L}{RD^2T}}}$

3.5.3 Steady-State Solutions

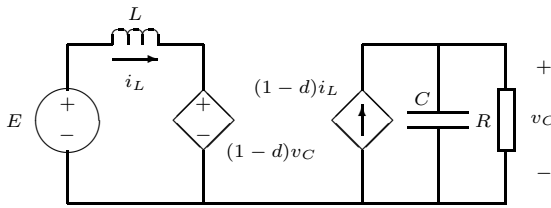
Suppose the system stabilizes to a steady state with the duty cycle equal to D . The solution of the steady-state value of \mathbf{x} (sometimes called equilibrium point) is particularly simple with the averaged models. Essentially, since $d\mathbf{x}/dt = 0$ in the steady state, the steady-state solution, \mathbf{X} , can be found by solving the algebraic equation

$$\mathbf{X} = -\mathbf{A}_m(D)^{-1}\mathbf{B}_m E \quad (3.77)$$

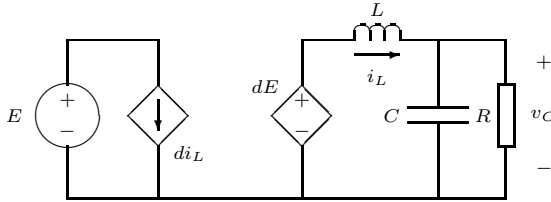
where superscript -1 denotes matrix inversion. The results for the boost and buck converters are tabulated in [Table 3.3](#).

3.5.4 Averaged Circuit Models

An obvious advantage of the averaging approach is the provision of *time-invariant* state equations in continuous time, which allow rather straightforward synthesis of equivalent circuit models that can be easily used by engineers. For instance, (3.72) and (3.73) can be translated to equivalent circuit models for the boost and buck converters by straightforward reconstruction of loops and nodes in accordance with Kirchhoff's laws. The results are shown in [Figure 3.5](#). Likewise, from (3.75) and (3.76), we get the equivalent circuit models shown in [Figure 3.6](#). At this point we take note that these circuit models can be linearized to give "linear models," and hence frequency-domain models as well. In fact, the linearization of averaged models has been widely practiced by power electronics engineers, and until now, the use of linearized averaged models has been the industry standard for feedback loop characteri-



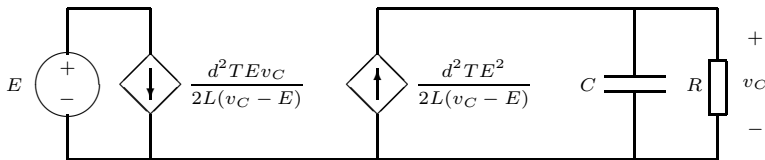
(a)



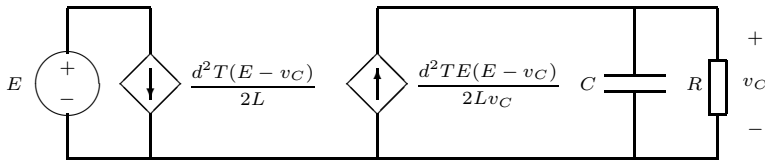
(b)

FIGURE 3.5

Averaged circuit models for (a) boost converter and (b) buck converter operating in continuous conduction mode, with r_C omitted for simplicity.



(a)



(b)

FIGURE 3.6

Averaged circuit models for (a) boost converter and (b) buck converter operating in discontinuous conduction mode, with r_C omitted for simplicity.

zation and control design of switching power supplies [33, 118]. But since our objective in this book is to examine nonlinear behavior, we will stick to the original averaged models in our analysis.

3.6 Control Law to Complete the Model

The discrete-time and averaged models described in the foregoing treat the duty cycle as an input. In practice, the duty cycle is controlled via some feedback mechanisms. Thus, to complete the model, we need to state the control law which is usually a set of equations by which the duty cycle is explicitly or implicitly defined.

For instance, in the usual pulse-width modulation control, a control signal (deriving from the state variables) and a ramp signal are compared, and their intersection defines the switching instant. Thus, the control law can be as simple as

$$V_{\text{ramp}}(dT) = v_{\text{con}}(\mathbf{x}(dT)) \quad (3.78)$$

where $V_{\text{ramp}}(t)$ is a ramp voltage and $v_{\text{con}}(\cdot)$ is a suitable control signal derived from the state variables. From this equation, we can find d for each switching period.

In general, the control equation varies from case to case, depending upon the type of feedback configuration used. In later chapters we will examine a few control laws which are commonly used in practice, e.g., current-mode control, free-running hysteretic control, etc.

3.7 Determination of the Boundary of Operating Modes

From the models derived in the foregoing for the two different operating modes, we clearly see that the dynamical behavior of switching converters is strongly affected by the operating mode they assume. It is therefore important to know the condition under which a given converter operates in a particular mode. This problem can be solved very easily by considering the inductor current waveform. In order to operate in continuous conduction mode, the inductor current must be non-zero throughout the entire switching period. This requirement can be translated to

$$I_{L,\text{average}} - \frac{\Delta I}{2} > 0 \quad (3.79)$$

where ΔI and $I_{L,\text{average}}$ are, respectively, the peak-to-peak ripple magnitude and the average value of the inductor current, as illustrated in [Figure 3.7](#).

The value of ΔI in general depends on the size of the inductance, input voltage, output voltage, duty cycle and switching period. For $I_{L,\text{average}}$, we may simply look up [Table 3.3](#). In particular, for the boost converter, we have $\Delta I = EDT/L$ and $I_{L,\text{average}} = E/R(1 - D)^2$. Thus, the condition for

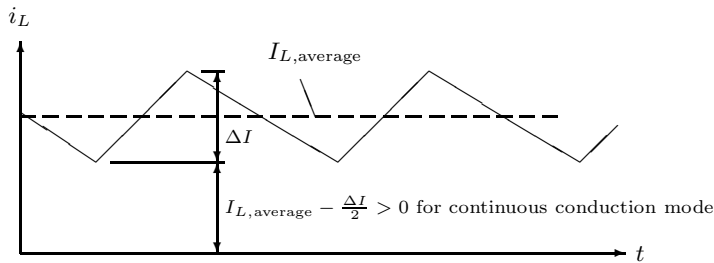


FIGURE 3.7

Condition for operation in continuous conduction mode.

operating in continuous conduction mode is

$$\frac{L}{RT} > \frac{D(1-D)^2}{2}. \quad (3.80)$$

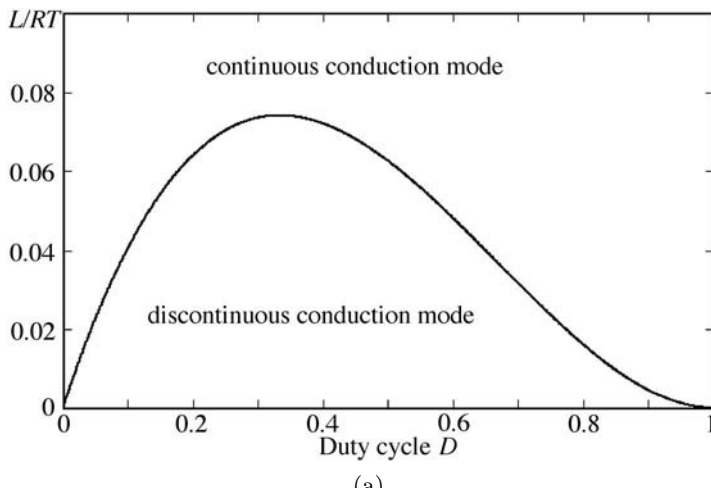
In a likewise fashion, we get the condition for the buck converter to operate in continuous conduction mode as

$$\frac{L}{RT} > \frac{1-D}{2}. \quad (3.81)$$

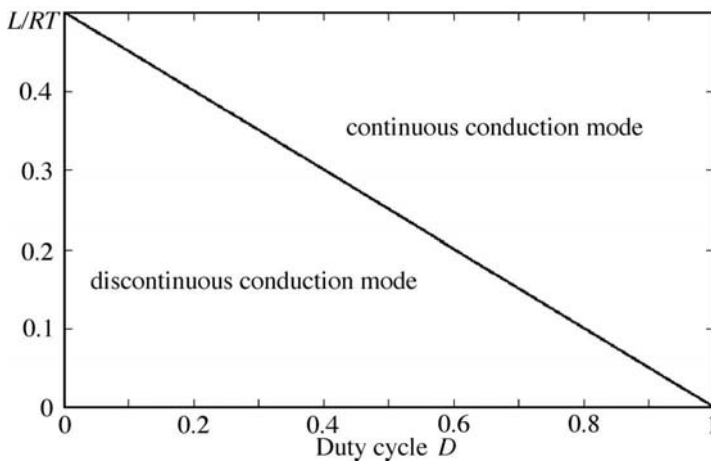
[Figure 3.8](#) shows the boundary of the two operating modes for the boost and buck converters. In both cases, if the value of L/RT is below a certain value, the converter can operate in continuous conduction mode if the duty cycle is greater than a certain value. This result agrees with our intuition because if the “switch-off” interval is too long, the inductor current would have fallen to zero. However, for the boost converter, as shown in [Figure 3.8 \(a\)](#), the converter can also operate in continuous conduction mode if the duty cycle is small enough. This is somewhat counter-intuitive, but not at all mysterious. In fact, it is not difficult to see that when the duty cycle is small, the output voltage is expected to be close to or just a little bigger than the input voltage. Thus, the inductor current goes up fast during the switch-on interval but goes down very slowly during the switch-off interval. If the duty cycle is small, the inductor current cannot reach zero during the switch-off interval, thus keeping itself in continuous conduction. For the extreme case where the duty cycle is zero, i.e., the switch remains open all the time, we immediately see from [Figure 3.1](#) that the steady-state inductor current is equal to E/R .

3.8 Border Collision: A Trivial Case

From the foregoing discussion, we immediately see that if either D , L or R is allowed to vary over a wide range, the converter can possibly change its



(a)

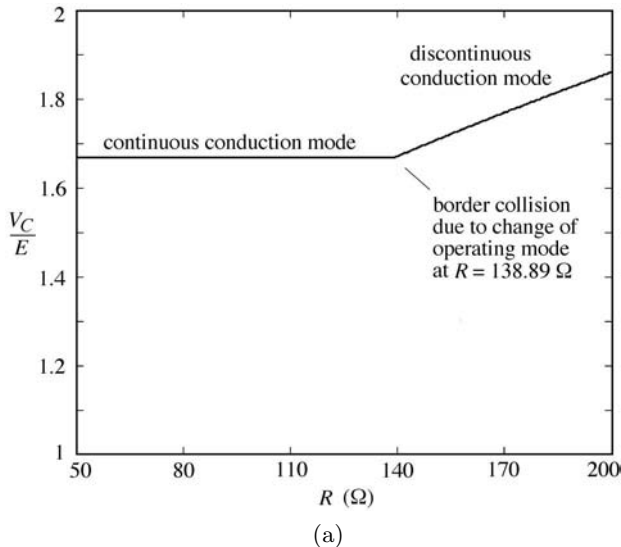


(b)

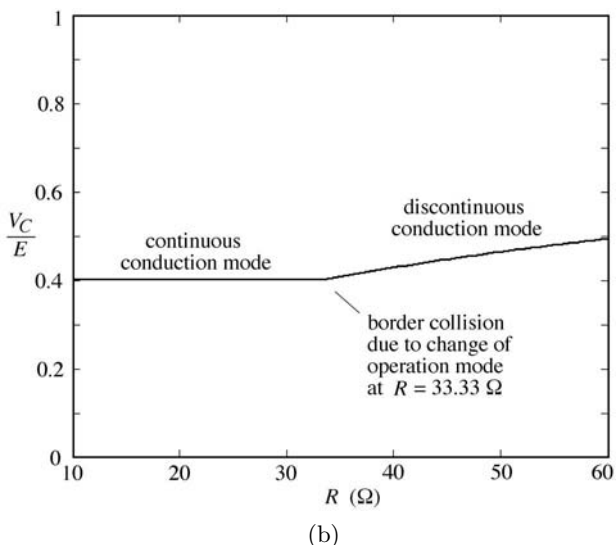
FIGURE 3.8

Boundary of operating modes for (a) boost converter, and (b) buck converter.

mode of operation. Here, we recall our discussion in [Chapter 1](#) that a special kind of bifurcation can possibly be resulted from a change of operating mode from continuous conduction to discontinuous conduction, or vice versa. In practice, it is quite common that the load resistance may vary over a wide range of values. If the design does not take into account the possible change of operating mode, the converter may fail to maintain a regulated output voltage. This phenomenon is an example of border collision, which is caused



(a)



(b)

FIGURE 3.9

Bifurcation diagrams showing border collision due to change of operating mode for (a) boost converter and (b) buck converter, with $L = 1$ mH, $T = 0.0001$ s, and $D = 0.4$.

by a *structural change* as the load resistance varies across the boundary of the operating modes. With the help of [Table 3.3](#), we may plot specific bifurcation diagrams with R serving as the bifurcation parameter, as shown in [Figure 3.9](#).

3.9 Pros and Cons of the Models

We are now able to develop discrete-time models and averaged models for switching converters. Before we use these models for analysis, it is important to understand what they are good for and what their limitations are. In fact, choosing the right model for analysis is as important as the analysis itself.

First of all, the method of averaging is simple and more likely to give tractable mathematical and circuit models; it is, however, useful only for characterizing low-frequency or slow-scale phenomena. On the contrary, the derivation of discrete-time models is more complicated but the models offer more complete information on the dynamical behavior of the systems under study. Since the discrete-time model is derived from sampling the system at discrete times, the information contained in the model is limited by the sampling rate. In the case where the sampling rate equals the switching frequency, the model is capable of describing all dynamical behavior up to the switching frequency, but is totally ignorant of the dynamics within a switching period. If we want finer details, we have to raise the sampling rate.

As we will see later in this book, each method can be used to study the bifurcation behavior of switching converters. The key question is “when to use what.” This issue is best illustrated with real situations. We will come back to it when we have to determine which model to use for studying a particular phenomenon. In brief, averaged models and discrete-time models are capable of characterizing slow-scale and fast-scale phenomena, respectively. Averaged models enjoy simplicity but contain less dynamical information, whereas discrete-time models contain fuller information but require more complex mathematics.

4

Analysis of Period-Doubling Bifurcation in Switching Converters Operating in Discontinuous Conduction Mode

The use of iterative maps for the study of dynamical properties of switching converters has a long history in power electronics. Discrete-time analytical models were first derived in the mid 1970s for the analysis of simple switching converters [111]. The purpose then was to obtain a dynamical model which allows small-signal stability analysis and feedback design to be carried out for switching converters. Linearization was always the vital step, and no nonlinear dynamics was studied.

In this chapter we re-visit the use of iterative maps. But instead of killing the nonlinear terms through the process of linearization as the engineers did, we try to preserve as much nonlinearity as possible. We will begin with switching converters operating in discontinuous conduction mode, which are first-order systems, as discussed in [Chapter 3](#). In the course of our investigation, iterative maps will be used as the main analytical tools for locating bifurcation points, with supporting evidence to be provided by computer simulations and laboratory experiments. In summary, our main objectives in this chapter are:

1. To review the procedure for deriving the describing iterative map for a given switching converter;
 2. To illustrate the key steps taken in the analysis of bifurcation behavior of switching converters using iterative maps;
 3. To identify the basic bifurcation behavior exhibited by switching converters operating in discontinuous conduction mode.
-

4.1 Review of the Derivation of Iterative Maps

In [Chapter 3](#), we have detailed the procedures for deriving iterative maps for switching converters. For the case of discontinuous conduction mode, the

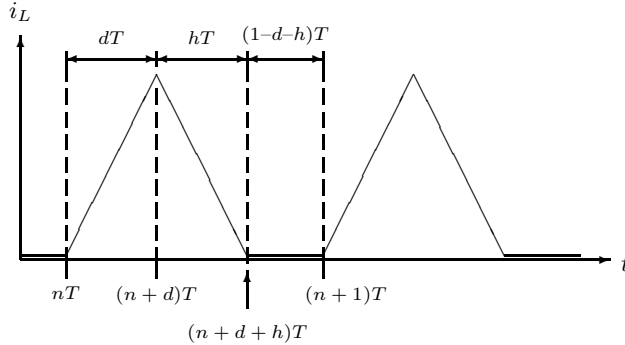


FIGURE 4.1

Inductor current waveform in discontinuous conduction mode.

iterative map is first-order. The procedure for deriving this first-order map has been discussed in [Section 3.2.2](#). We summarize the essential steps as follows:

1. Write down the state equations for all involving circuit topologies. In the case of discontinuous conduction mode, we have three such state equations, i.e.,

$$\dot{\mathbf{x}} = \begin{cases} \mathbf{A}_1\mathbf{x} + \mathbf{B}_1E & \text{for } nT \leq t < (n+d)T \\ \mathbf{A}_2\mathbf{x} + \mathbf{B}_2E & \text{for } (n+d)T \leq t < (n+d+h)T \\ \mathbf{A}_3\mathbf{x} + \mathbf{B}_3E & \text{for } (n+d+h)T \leq t < (n+1)T \end{cases} \quad (4.1)$$

where $\mathbf{x} = [v_C \ i_L]^T$, \mathbf{A} 's and \mathbf{B} 's are the system matrices, d is the duty cycle, T is the switching period, and h is the fraction of the switching period during which the switch is off and the inductor current is non-zero. See [Figure 4.1](#).

2. Express the solution to each of these state equations in terms of the respective transition matrix.
3. “Stitch” the consecutive solutions at the switching instants by putting the final value of the previous sub-interval as the initial value of the following sub-interval. The result is the following iterative equation:

$$\mathbf{x}((n+1)T) = \Phi_3(\bar{h}T)\Phi_2(hT)\Phi_1(dT) \quad (4.2)$$

$$\begin{aligned} &\times \left(\mathbf{x}(nT) + \int_{nT}^{(n+d)T} \Phi_1(nT - \tau) \mathbf{B}_1 E.d\tau \right) \\ &+ \Phi_3(\bar{h}T)\Phi_2(hT) \int_{(n+d)T}^{(n+d+h)T} \Phi_2((n+d)T - \tau) \mathbf{B}_2 E.d\tau \\ &+ \Phi_3(\bar{h}T) \int_{(n+d+h)T}^{(n+1)T} \Phi_3((n+d+h)T - \tau) \mathbf{B}_3 E.d\tau \end{aligned}$$

where $\bar{h} = 1 - d - h$ and the transition matrix $\Phi_i(\cdot)$ is given by

$$\Phi_i(\xi) = \mathbf{1} + \sum_{n=1}^{\infty} \frac{1}{n!} A_i^n \xi^n \quad \text{for } i = 1, 2 \text{ and } 3. \quad (4.3)$$

4. Enforce the conditions specific to discontinuous conduction mode. First, the inductor current is zero for all $t = nT$. Second, d and h are related by enforcing continuity of the inductor current at the switching instant, as given in (3.52) and (3.53).
5. Apply series approximation to the transition matrices to simplify the iterative map.

Upon completing the above steps, we get a first-order iterative map of the form:

$$v_{C,n+1} = f(v_{C,n}, d_n) \quad (4.4)$$

where subscript n denotes the value at $t = nT$. See [Table 3.2](#) for the forms of iterative maps for the boost and buck converters. For easy reference in later sections of this chapter, we repeat the results here.

$$v_{C,n+1} = \alpha v_{C,n} + \frac{\beta d_n^2 E (E - v_{C,n})}{v_{C,n}} \quad \text{for buck converter} \quad (4.5)$$

$$v_{C,n+1} = \alpha v_{C,n} + \frac{\beta d_n^2 E^2}{v_{C,n} - E} \quad \text{for boost converter} \quad (4.6)$$

where

$$\alpha = 1 - \frac{T}{CR} + \frac{T^2}{2C^2R^2} \quad (4.7)$$

$$\beta = \frac{T^2}{2LC}. \quad (4.8)$$

4.2 The Closed-Loop System and Control Equation

In practice, switching converters are controlled via a feedback mechanism. The usual control objective is to keep the output voltage fixed. For simplicity, we consider a proportional feedback which effectively samples the output voltage and generates an error signal from which the value of the duty cycle is derived, i.e.,

$$d_n = H(D - \kappa(v_C - V_{\text{ref}})) \quad (4.9)$$

where D is the steady-state duty cycle, κ is the small-signal feedback gain, V_{ref} is the reference (target) output voltage, and $H(\cdot)$ accounts for the limited

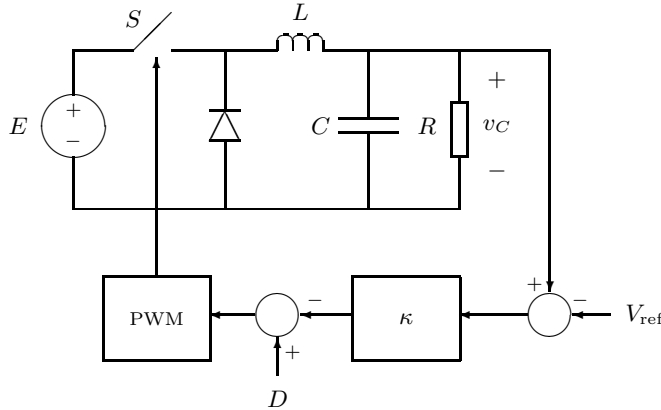


FIGURE 4.2

Schematic of the closed-loop voltage feedback buck regulator.

range of the duty cycle between 0 and 1.

$$H(x) = \begin{cases} 0 & \text{for } x < 0 \\ 1 & \text{for } x > 1 \\ x & \text{otherwise} \end{cases} \quad (4.10)$$

Figure 4.2 shows the schematic of the closed-loop system. Combining this control equation with the discrete-time map of the system, we yield a discrete-time map for the closed-loop system.

In particular, for the buck converter, we get

$$v_{C,n+1} = \alpha v_{C,n} + \frac{\beta (H(D - \kappa(v_C - V_{\text{ref}})))^2 E(E - v_{C,n})}{v_{C,n}} \quad (4.11)$$

Also, D can be found by putting $v_{C,n+1} = v_{C,n}$ in (4.11), i.e.,

$$D = \sqrt{\frac{(1 - \alpha)V_C^2}{\beta E(E - V_C)}} \quad (4.12)$$

where uppercase letters denote steady-state values as usual.

For the boost converter, the discrete-time map for the closed-loop system is

$$v_{C,n+1} = \alpha v_{C,n} + \frac{H(D - \kappa(v_{C,n} - V_{\text{ref}}))^2 \beta E^2}{v_{C,n} - E} \quad (4.13)$$

where D can be found in a likewise manner and is given by

$$D = \sqrt{\frac{(1 - \alpha)(V_C - E)V_C}{\beta E^2}}. \quad (4.14)$$

In the following we will use the discrete-time map (4.11) to study the non-linear dynamics of the buck converter operating in discontinuous conduction mode. Readers may refer to Tse [141] for a similar treatment of the boost converter.

4.3 Period-Doubling Bifurcation

The main aim of our investigation of the buck converter operating in discontinuous conduction mode is to examine the stability of its fundamental operation.* Specifically, we wish to study the way in which the system loses stability.

We consider small disturbance Δv_C around the steady-state value V_C . The usual Taylor's series expansion can be written as

$$\Delta v_{C,n+1} = \sum_{k=1}^{\infty} \frac{1}{k!} \left. \frac{\partial^k f(v_C)}{\partial v_C^k} \right|_{v_C=V_C} (\Delta v_{C,n})^k. \quad (4.15)$$

If the disturbance is small, the magnitude of $\partial f(v_C)/\partial v_C$ at $v_C = V_C$ determines the stability. This partial derivative is sometimes referred to as the *characteristic multiplier* or *eigenvalue*. For the present 1-D map, it simply corresponds to the slope of $f(x)$ at the fixed point [138].

We assume that in the neighborhood of the steady-state point the duty cycle does not saturate. Hence, we may consider the discrete-time map (4.11) without the need for applying $H(\cdot)$. Thus, the characteristic multiplier, λ , can be obtained by direct differentiation:

$$\lambda = \left. \frac{\partial f(v_C)}{\partial v_C} \right|_{v_C=V_C} = \alpha - \frac{\beta E D [2\kappa V_C (E - V_C) + DE]}{V_C^2}. \quad (4.16)$$

The system remains fundamentally stable if the magnitude of the characteristic multiplier is less than 1, i.e.,

$$|\lambda| = \left| \alpha - \frac{\beta E D [2\kappa V_C (E - V_C) + DE]}{V_C^2} \right| < 1. \quad (4.17)$$

At the boundary where the characteristic multiplier is -1 , v_C repeats itself every second period, and as the characteristic multiplier decreases below -1 , v_C may diverge in an oscillatory fashion or maintain a stable subharmonic

*In much of the system theory literature, the term *fundamental operation* refers to period-1 operation. In the case of switching converters, this refers to the usual periodic operation in which all waveforms are periodic in the switching period.

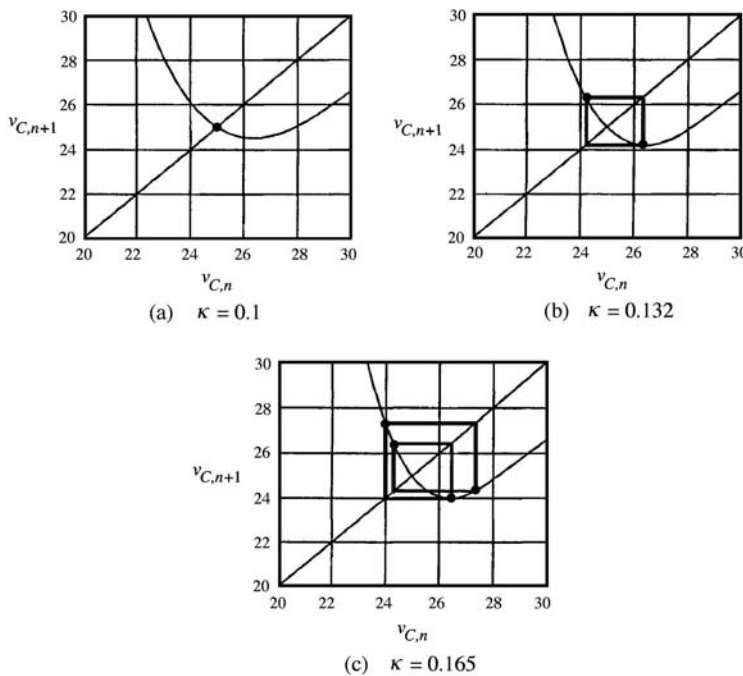


FIGURE 4.3

Iterative maps showing (a) stable fixed point; (b) period-2 subharmonic solution; and (c) period-4 subharmonic solution.

operation, depending upon the higher-order terms in (4.15). The critical value of the small-signal feedback gain can be found by setting the characteristic multiplier to -1 , i.e.,

$$\kappa_c = \frac{(1 + \alpha)V_C^2 - \beta E^2 D^2}{2\beta E D V_C(E - V_C)}. \quad (4.18)$$

Now using (4.11), we can easily arrive at some useful conclusion concerning the behavior of the system near $\kappa = \kappa_c$. As we will see, (4.11) represents a typical unimodal map [5]. A common plan of attack for such maps is as follows. Initially we set κ at a value smaller than κ_c and confirm that the system has a stable fixed point. Then, we increase κ and observe the way in which the system loses stability and bifurcates into subharmonic orbits of period 2. We further increase κ to observe a typical subharmonic cascade and eventually chaotic motion.

An example will help visualize the situation. Suppose $T/CR = 0.12$, $RT/L = 20$, $E = 33$ V, and $V_C = 25$ V. This gives $D = 0.4717$. Also it is readily verified that the value of RT/L is large enough to ensure a

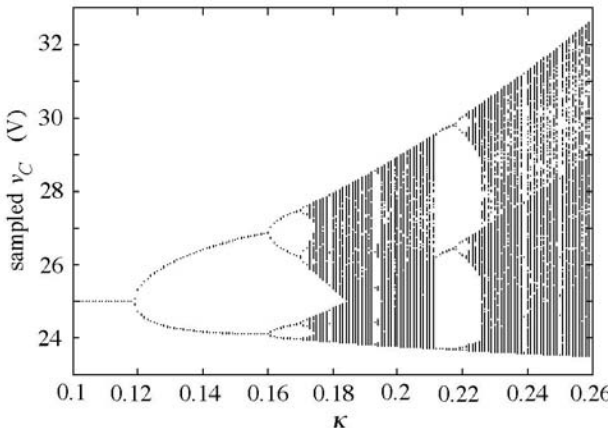


FIGURE 4.4

Bifurcation diagram from the approximate discrete-time map describing the buck converter operating in discontinuous conduction mode.

discontinuous-conduction-mode operation. Direct substitution gives

$$v_{C,n+1} = 0.8872v_{C,n} + \frac{1.2 \times 33 \times (33 - v_{C,n}) \times H(d_n)^2}{v_{C,n}} \quad (4.19)$$

where $d_n = 0.4717 - \kappa(v_{C,n} - 25)$. The characteristic multiplier, as given in (4.17), is

$$\lambda = 0.4220 - 11.9548\kappa. \quad (4.20)$$

Thus, the critical value of κ is 0.1189. Figure 4.3 shows the iterative maps corresponding to a sub-critical case ($\kappa < \kappa_c$), and two super-critical cases ($\kappa > \kappa_c$). As shown clearly, the system has a stable fixed point in the sub-critical case, and a stable subharmonic orbit in super-critical cases. Furthermore, using (4.19), a bifurcation diagram can be generated as shown in Figure 4.4. Reference to this diagram shows that the system becomes chaotic when κ is larger than about 0.17. We can confirm this by computing the average Lyapunov exponents for the same range of κ , as described in Section 2.5.1. Figure 4.5 shows the result.

4.4 Computer Simulations

In this section, we verify the period-doubling bifurcation using “exact” cycle-by-cycle simulation of the system. The simulation is based on a piecewise

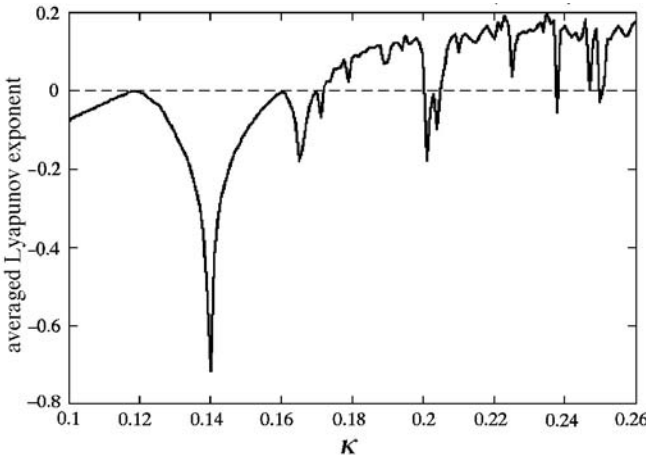


FIGURE 4.5

Average Lyapunov exponents for the buck converter operating in discontinuous conduction mode.

switched model which represents a very accurate description of the system. Essentially the model involves toggling between three linear circuits according to the duty cycle control and circuit condition. The simulation uses the following parameters: $T = 33.33 \mu\text{s}$, $E = 33 \text{ V}$, $V_C = 25 \text{ V}$, $L = 208 \mu\text{H}$, $C = 222 \mu\text{F}$, $R = 12.5 \Omega$.

We have simulated the steady-state waveforms for various values of κ . Figures 4.6 (a), 4.7 (a), 4.8 (a) and 4.9 (a) show the steady-state waveforms of the closed-loop system with $\kappa = 0.1, 0.126, 0.184$ and 0.216 respectively. The phase portraits corresponding to these four cases are shown in Figures 4.6 (b), 4.7 (b), 4.8 (b) and 4.9 (b), which demonstrate clearly the fundamental, period-2 subharmonic, period-4 subharmonic, and chaotic orbits. We have also summarized in Figure 4.10 the steady-state information in the form of a bifurcation diagram which demonstrates clearly the sequence of period-doubling subharmonics as well as the presence of a period-3 window around $\kappa = 0.245$.

The general appearance of this simulation-based bifurcation diagram resembles that of Figure 4.4. However, some noticeable differences are still observed between them, which can be attributed to the fact that Figure 4.4 is generated from an approximate iterative map whose validity relies very much on the accuracy of the truncated Taylor series. On the other hand, Figure 4.10 represents exact simulated system behavior.

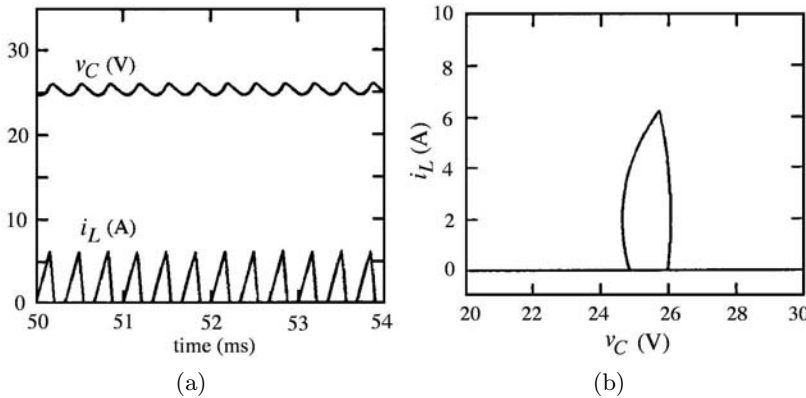


FIGURE 4.6

(a) Fundamental waveforms from simulation of the exact state equation with $\kappa = 0.1$; (b) phase portrait.

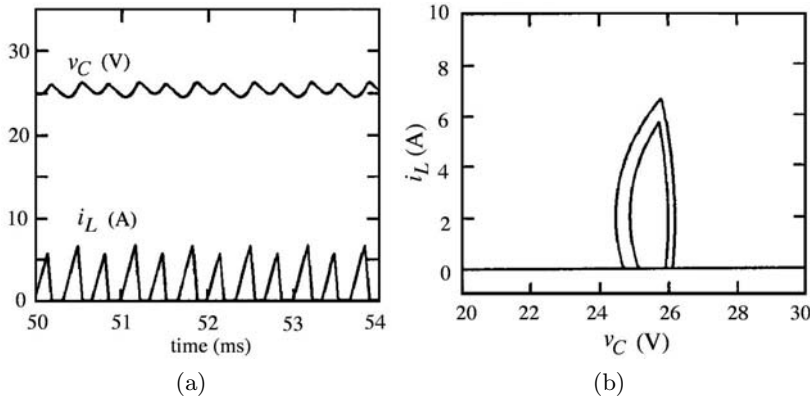


FIGURE 4.7

(a) Period-2 subharmonic waveforms from simulation of the exact state equation with $\kappa = 0.136$; (b) phase portrait.

4.5 Experimentation

Further evidence of period-doubling in switching converters operating in discontinuous conduction mode can be provided by laboratory tests. For the simple voltage feedback buck converter, a possible experimental circuit is shown in Figure 4.11.

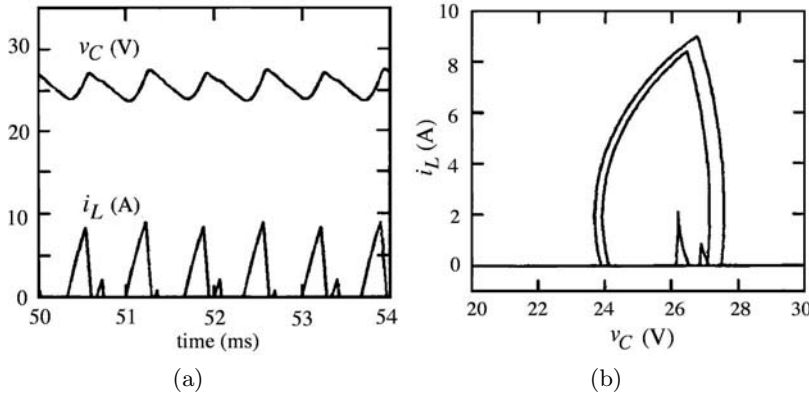


FIGURE 4.8

(a) Period-4 subharmonic waveforms from simulation of the exact state equation with $\kappa = 0.184$; (b) phase portrait.

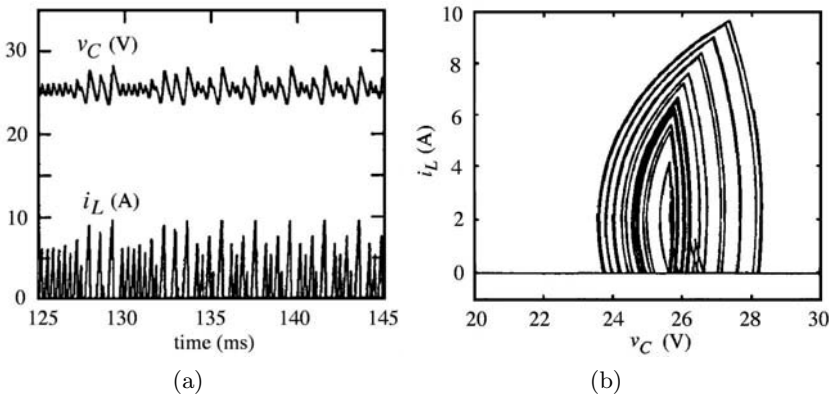


FIGURE 4.9

(a) Chaotic waveforms from simulation of the exact state equation with $\kappa = 0.216$; (b) phase portrait.

4.5.1 Circuit Operation

In the experimental circuit, the switch is implemented by a MOSFET whose on-off status is controlled by a pulse-width modulated signal. The switch is on when the positive input of the comparator is larger than the sawtooth voltage, and is off otherwise. Thus, the duty cycle is determined by the control voltage v_{con} . The small-signal relation between v_{con} and the duty cycle is given by

$$\Delta v_{\text{con}} = V_M \Delta d \quad (4.21)$$

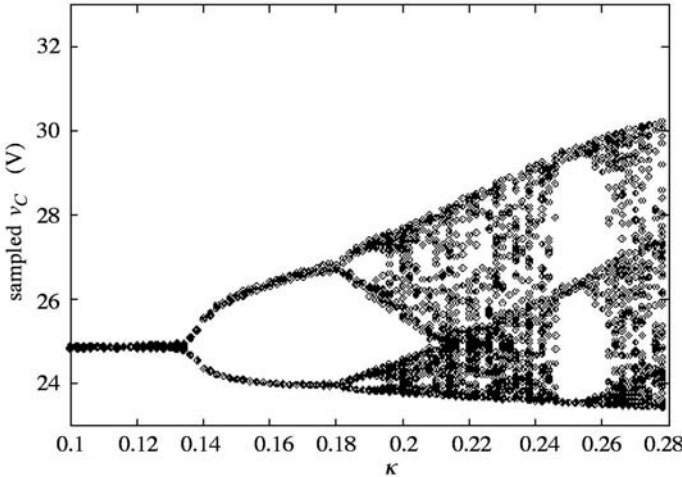


FIGURE 4.10

Bifurcation diagram from simulations; 500 consecutive points of v_C after transients are plotted for each κ .

where V_M is the height of the sawtooth voltage. Figure 4.12 shows this situation. The loop is closed by connecting the op-amp input to the converter output via a resistor ladder R_1-R_2 , as shown in Figure 4.11. Assuming an ideal op-amp characteristic, the following equation relating v_{con} and v_C is immediately clear:

$$v_{\text{con}} = \left(1 + \frac{R_f}{R_1 \parallel R_2}\right) V_Z - \frac{R_f}{R_1} v_C. \quad (4.22)$$

Separating the small-signal variation from the steady-state condition yields

$$\Delta v_{\text{con}} = -\frac{R_f}{R_1} \Delta v_C. \quad (4.23)$$

From (4.22) and (4.21), we have

$$\Delta d = -\frac{R_f}{V_M R_1} \Delta v_C. \quad (4.24)$$

Comparing (4.24) with the feedback equation, namely,

$$\Delta d = -\kappa \Delta v_C, \quad (4.25)$$

we immediately see that the feedback factor κ can be adjusted by varying R_1 and R_f since

$$\kappa = \frac{R_f}{V_M R_1}. \quad (4.26)$$

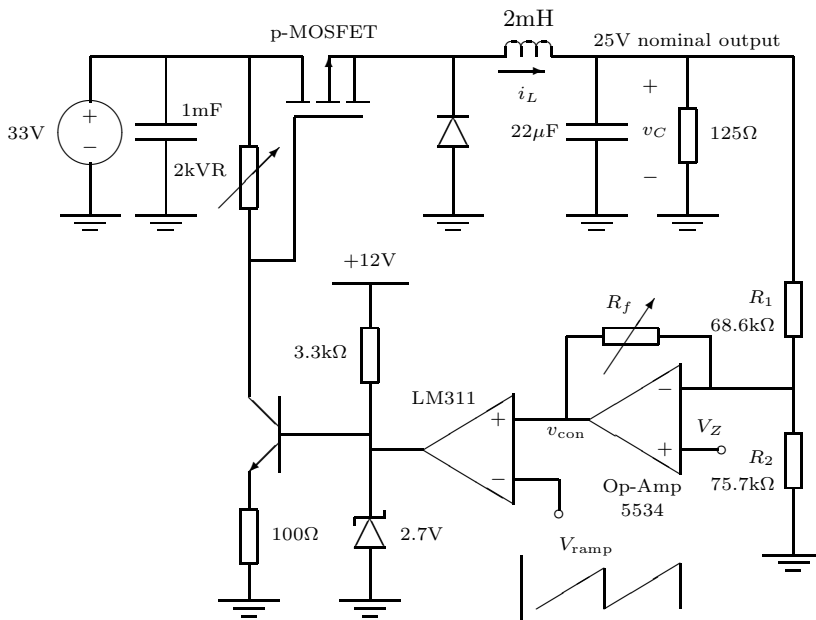


FIGURE 4.11

Experimental voltage feedback buck converter operating in discontinuous conduction mode.

Furthermore, the desired steady-state condition can be achieved by choosing a correct value for V_Z .

A few points regarding the implementation of the experimental circuit are worth noting:

1. In the earlier analytical and simulation studies, a uniform sampling scheme has been used for the feedback control. In the experiment, however, natural sampling is used for the sake of simplicity, as shown in Figure 4.12. Thus, (4.25) and (4.24) are not actually equivalent. This may introduce a subtle source of error if κ is adjusted according to (4.26). Nevertheless, such discrepancy in the sampling scheme has been shown to be of little effect on the main result concerning the period-doubling route to chaos, as will be verified in the next subsection.
2. From (4.5), we see that the system is governed by only two independent parameters, namely RT/L and T/CR . Moreover, the operating mode is determined by the parameter RT/L . The choice of component values in the experiment gives exactly the same set of parameter values as in the theoretical and simulation studies. Specifically, we reduce the power by using a resistor that is 10 times bigger than that used in the simulation. To ensure a discontinuous mode of operation, we consistently use an

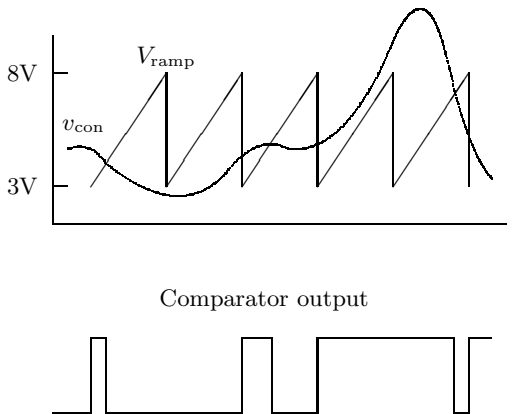


FIGURE 4.12
Pulse-width modulation.

inductor that is also 10 times bigger, thereby keeping RT/L unchanged. Similarly we use a capacitor that is 10 times smaller in order to keep T/CR unchanged. Note that T remains the same.

3. In the experiment, the power level is deliberately lowered to 5 W so as to minimize device stress. Thus, the load resistance is 125Ω . The switching frequency is 3 kHz which is low enough to ensure that the circuit is unaffected by high-frequency problems. The values of RT/L and T/CR are chosen to align with those used in our simulation studies.

4.5.2 Experimental Observations

Several representative waveforms are captured from the experimental circuit. Figures 4.13 and 4.14 show typical period-2 and period-4 subharmonic waveforms respectively. Oscilloscope pictures of the phase portraits corresponding to these two cases are shown in Figures 4.15 (a) and (b). To obtain the chaotic waveform and corresponding phase portrait, a digital storage oscilloscope is employed. Steady-state waveforms are captured over a sufficiently long interval and are shown in Figures 4.16 and 4.17.

To make things worse, *saturating nonlinearity* of the pulse-width modulator may come into play under certain conditions. As modeled by the function $H(d)$ introduced earlier in Section 4.1, saturating nonlinearity effectively confines the value of d within the range 0 to 1. In fact, it has been observed in our simulation and experimental circuit that periods with $d = 1$ as well as $d = 0$ are present when the system becomes chaotic, as exemplified in Figures 4.9 and 4.16. Detailed inspection of the circuit and waveforms reveals that, in the period preceding a period with $d = 1$, a very low output voltage occurs, caus-

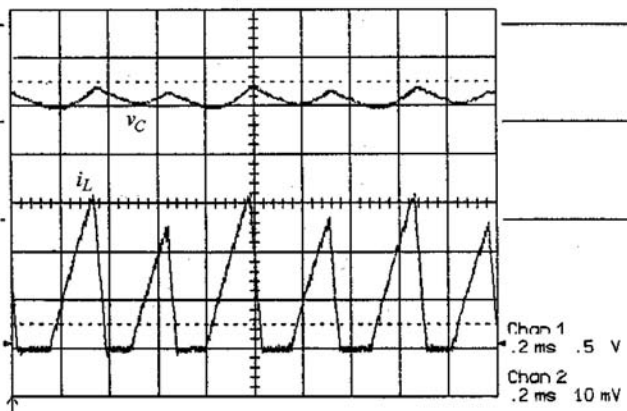


FIGURE 4.13

Period-2 waveform from experimental buck converter operating in discontinuous conduction mode [142] (upper trace: 0.5 V/div, lower trace: 10 mA/div, time base: 0.5 ms/div).

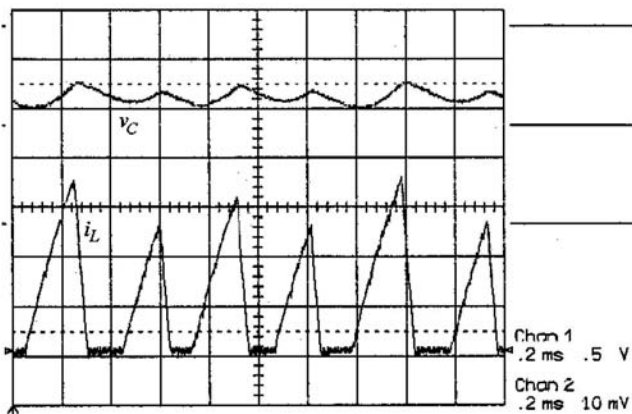


FIGURE 4.14

Period-4 waveform from experimental buck converter operating in discontinuous conduction mode [142] (upper trace: 0.5 V/div, lower trace: 10 mA/div, time base: 0.5 ms/div).

ing the value of v_{con} to rise above the upper threshold of V_{ramp} , as illustrated in Figure 4.12. The switch is thus closed for the entire period, and the inductor current increases linearly until the switch turns off in the following period. Thus, two periods appear to have been merged into one switching cycle. On the other hand, when a very high output voltage occurs, v_{con} drops below the lower threshold of V_{ramp} , causing the switch to open for the entire period.

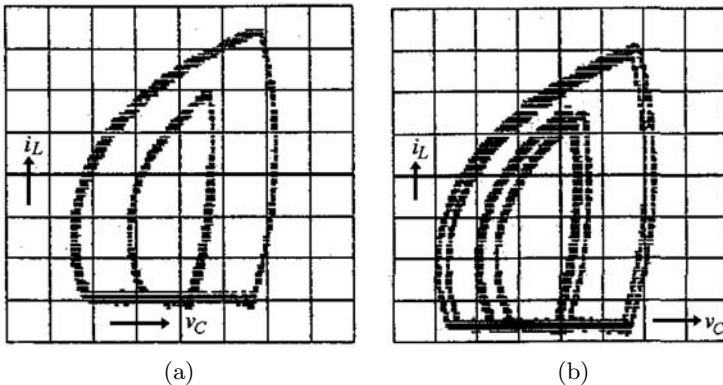


FIGURE 4.15

Phase portraits of (a) period-2 and (b) period-4 operations from experimental buck converter operating in discontinuous conduction mode [142].

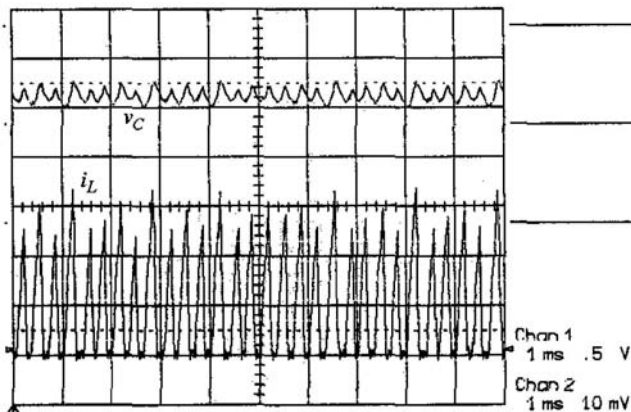


FIGURE 4.16

Chaotic waveform from experimental buck converter operating in discontinuous conduction mode [142] (upper trace: 0.5 V/div, lower trace: 10 mA/div, time base: 0.5 ms/div).

Thus, a period is “skipped.” It may be conceived that the ability to “merge” and “skip” periods, as inherited from saturating nonlinearity, constitutes a unique feature of the dynamics of switching converters. In Chapter 5, we will examine saturating nonlinearity more formally under the notion of *border collision*. Here, our experimental observation has indicated that chaos in the switching converter under study is strongly related to saturating nonlinearity. In this chapter, however, as a first investigation and to avoid beclouding, we limit ourselves to the basic phenomenon of period-doubling.

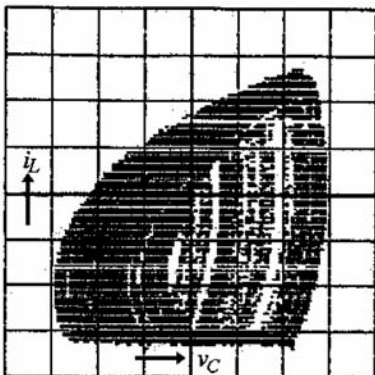


FIGURE 4.17

Phase portrait of chaotic operation from experimental buck converter operating in discontinuous conduction mode [142].

4.6 Recapitulation of Basic Phenomenology

As a remark before we close this chapter, the basic bifurcation phenomenology for switching converters operating in discontinuous conduction mode has been found to be a *flip-type* or period-doubling bifurcation [138]. At this point, there is sufficient evidence to conclude that such systems can operate chaotically if the magnitude of the small-signal feedback gain becomes too large. However, we cannot exclude the possibility of other forms of bifurcation that may occur in this class of switching converters since our study has been restricted to a particular, though representative, type of feedback control scheme. In fact, as we will see in [Chapter 6](#), the choice of the control scheme plays an important role in determining the basic phenomenology and the same converter can behave totally differently if it is controlled under a different scheme.

5

Bifurcation Behavior in Switching Power Converters: Smooth versus Non-Smooth Bifurcations

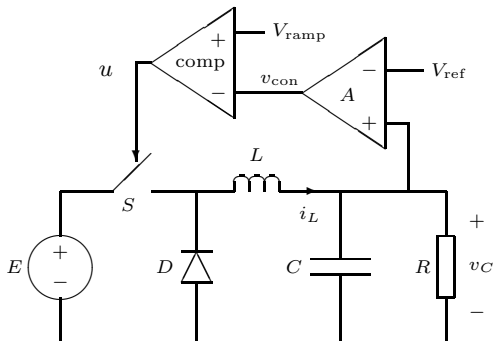
In this chapter, we continue our study of the nonlinear dynamics of switching converters on the basis of discrete-time iterative maps. In particular, we analyze a few selected second-order systems and identify their associated bifurcation phenomena. We further aim to highlight a special type of bifurcation phenomenon which is characteristic of power electronics systems in general. This phenomenon is known as *border collision*, which occurs in almost all switching power converters.

Border collision is a subject which has been studied in great depth by researchers in the physics and mathematics disciplines. Instead of presenting the theoretical aspect of border collision (which is beyond the scope of the present discussion), we try to explain the physical mechanism of border collision from a circuit operational viewpoint. Our aim is to show that border collision, as a phenomenon observed in switching converters, inherits directly from a characteristic feature of the circuit operation known as *saturating nonlinearity*.^{*} Border collision therefore forms part of the basic phenomenology for switching power converters. In the first section of this chapter, we will take a quick glimpse at the various complex phenomena, using the simple buck converter as an example. In the rest of this chapter and in later chapters, we will examine in detail the bifurcation phenomena in various types of switching converters including current-mode controlled converters, the Ćuk converter, parallel-connected converters, and power-factor-correction converters.

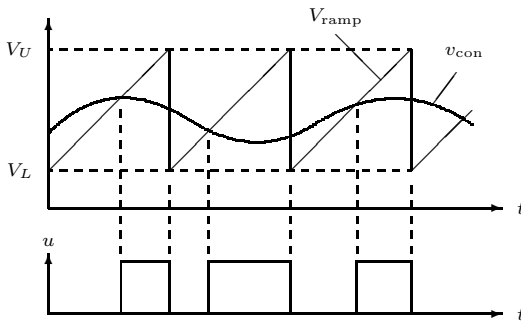
5.1 A Quick Glimpse at Complexity

Before we probe into details of the mechanisms leading to the various complex behaviors in switching power converters, it is instructive to take a quick tour

*To avoid obscuring the essentials, we ignore the case of border collision caused by a change of operating mode, e.g., from continuous to discontinuous conduction mode.



(a)



(b)

FIGURE 5.1

Voltage-mode controlled buck converter. (a) Schematic diagram; (b) operation waveform. For the purpose of illustration, details of compensator network have been omitted, and only simple proportional gain is shown.

of a typical bifurcation pattern from a simple switching converter. Without deriving any iterative function, we will study the bifurcation behavior of a buck converter through computer simulations and laboratory experiments.

5.1.1 Buck Converter Operating in Continuous Conduction Mode under Simple Voltage Feedback Control

In this section, the subject of investigation is a simple voltage feedback buck converter operating in continuous conduction mode, as shown in Figure 5.1 (a). The operation of this circuit can be briefly described as follows. When switch S turns on, the inductor current ramps up almost linearly, and when switch S turns off, the inductor current ramps down and de-energizes through the

diode to the load. In the voltage-mode control scheme, the output voltage error with respect to the reference voltage is amplified to give a control voltage v_{con} :

$$v_{\text{con}}(t) = A(v_C - V_{\text{ref}}) \quad (5.1)$$

which is then compared with a ramp signal $V_{\text{ramp}}(t)$, defined as

$$V_{\text{ramp}}(t) = V_L + (V_U - V_L) \left(\frac{t}{T} \bmod 1 \right), \quad (5.2)$$

where all symbols are explained in [Figure 5.1](#). Note that in order to keep our discussion simple, we omit details of the compensation network and retain only a simple proportional control. Nonetheless, this simplified control configuration suffices to illustrate the main features of the bifurcation behavior, as we will see shortly. The comparator output, u , gives the pulse-width-modulated signal necessary for driving the switch. Typically, the switch is turned on when $v_{\text{con}}(t) \leq V_{\text{ramp}}$, and turned off when $v_{\text{con}}(t) > V_{\text{ramp}}$, as illustrated in [Figure 5.1 \(b\)](#). The state equation can be written as

$$\dot{\mathbf{x}} = \begin{cases} \mathbf{A}_1 \mathbf{x} + \mathbf{B}_1 E & \text{switch } S \text{ on} \\ \mathbf{A}_2 \mathbf{x} + \mathbf{B}_2 E & \text{switch } S \text{ off} \end{cases} \quad (5.3)$$

where \mathbf{x} denotes the state variable, i.e., $\mathbf{x} = [v_C \ i_L]^T$, the \mathbf{A} 's and \mathbf{B} 's are the system matrices given by

$$\begin{aligned} \mathbf{A}_1 = \mathbf{A}_2 &= \begin{bmatrix} -1/RC & 1/C \\ -1/L & 0 \end{bmatrix}, \\ \mathbf{B}_1 &= \begin{bmatrix} 0 \\ 1/L \end{bmatrix}, \text{ and } \mathbf{B}_2 = \begin{bmatrix} 0 \\ 0 \end{bmatrix}. \end{aligned} \quad (5.4)$$

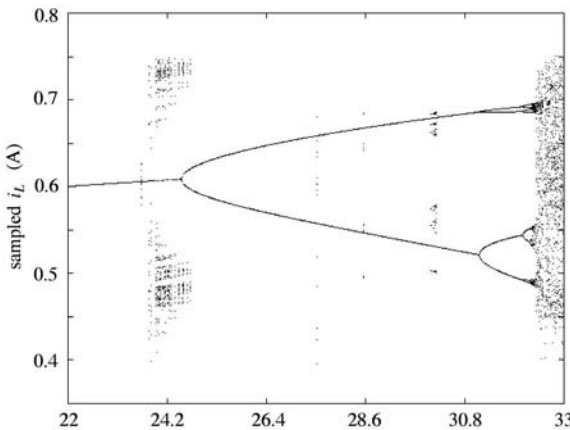
Using the above equations, exact cycle-by-cycle simulation can be performed. The parameters used in the simulations are as follows:

$$\begin{aligned} E &= 22-33 \text{ V}, L = 20 \text{ mH}, C = 47 \mu\text{F}, R = 22 \Omega, V_{\text{ref}} = 11 \text{ V}, \\ A &= 8.4, T = 400 \mu\text{s}, V_L = 3.8 \text{ V}, V_U = 8.2 \text{ V}. \end{aligned}$$

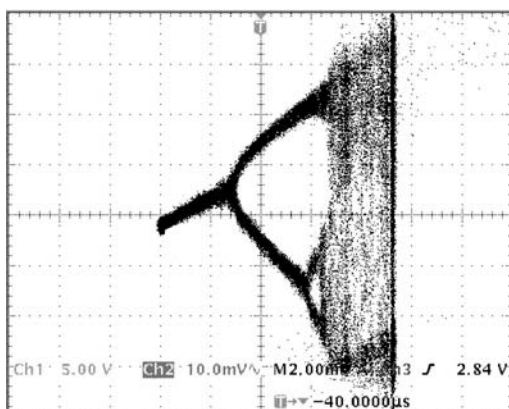
5.1.2 Bifurcation Behavior from Simulations and Measurements

The afore-described buck converter has been studied in some depth by Banerjee [6], di Bernardo et al. [16], Fossas and Olivari [48], and Hamill et al. [60]. Period-doubling bifurcation, chaos, and coexisting attractors have been observed in this converter.

In [Figure 5.2 \(a\)](#), we exemplify a typical bifurcation diagram which has been generated by computer simulations using the equations given in [Section 5.1.1](#). In this bifurcation diagram, E has been chosen as the bifurcation parameter. Also, [Figure 5.2 \(b\)](#) shows the experimentally measured bifurcation diagram.



(a)



(b)

FIGURE 5.2

Bifurcation of voltage feedback buck converter operating in continuous conduction mode. (a) Simulated bifurcation diagram, and (b) measured bifurcation diagram with inductor current versus input voltage (x-axis: 5 V/div, y-axis: 50 mA/div).

To quantify the “chaoticity” (as may be preferred by some engineers), a plot of the computed averaged largest Lyapunov exponent is shown in [Figure 5.3](#). The chaotic attractors are also captured by computer simulations and laboratory measurements. [Figures 5.4](#) and [5.5](#) show the simulated and measured phase portraits and Poincaré sections corresponding to the case where $E = 33$ V.

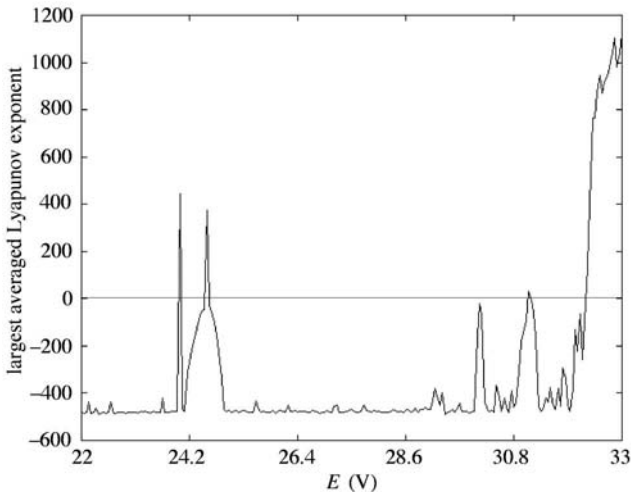


FIGURE 5.3

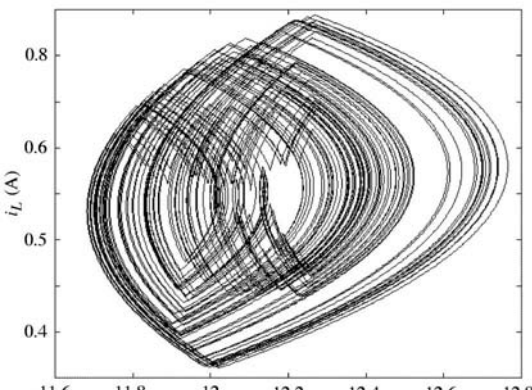
Computed largest Lyapunov exponent versus input voltage for the voltage feedback buck converter operating in continuous conduction mode.

5.1.3 A Zoo of Complex Behaviors

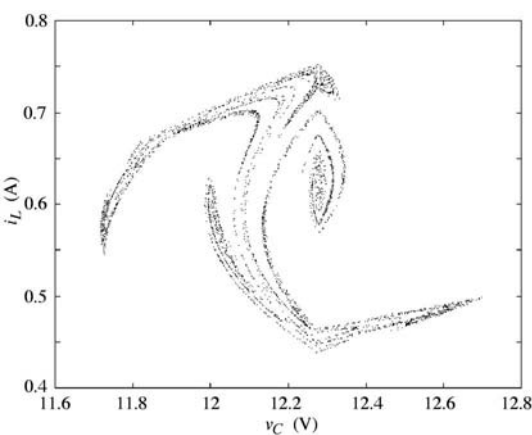
This particular buck converter exhibits an interesting bifurcation route, with the main bifurcation being period-doubling. A few features can be picked up along the bifurcation path:

1. *Expansion of chaotic attractor* — When E exceeds about 32.27 V, the converter enters a chaotic region. Beyond about 32.34 V, the chaotic attractor encounters another bifurcation, more precisely an *interior crisis*, and expands to a large chaotic attractor. The details of this transition are somewhat complicated, but we may look at it simply as a bifurcation which expands a chaotic attractor to a larger chaotic attractor.*
2. *Coexisting orbits and attractors* — In some periodic windows along the main period-doubling route, there are other orbits possibly coexisting. For example, when E is about 24 V, unstable chaotic orbits coexist with the periodic attractor, giving rise to a long transient chaotic behavior before the converter settles to the stable periodic orbit. This is manifested in the bifurcation diagram of Figure 5.2 (a) as bands of irregular

*Here, we have described the expansion of the chaotic attractor under the broad view of bifurcation. In fact, this is an example of an *interior crisis* where a chaotic attractor “collides” with a coexisting unstable chaotic orbit, leading to a sudden expansion to a large chaotic attractor which includes the original chaotic attractor as a subset [52]. See also Chapter 5 of [11].



(a)



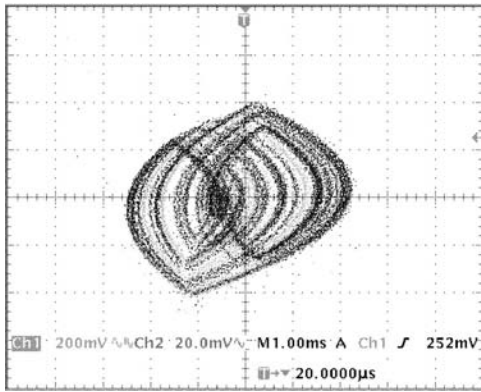
(b)

FIGURE 5.4

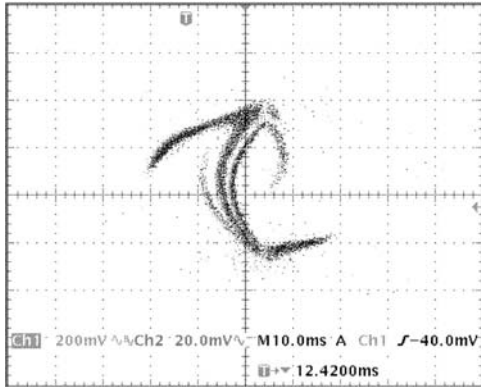
Chaotic operation of voltage mode controlled Buck converter, with $L = 20$ mH, $C = 47$ μ F, $R = 22$ Ω , $T = 400$ μ s, $E = 33$ V and $V_{\text{ref}} = 11$ V. (a) Simulated phase portrait of chaotic attractor; (b) simulated Poincaré section of chaotic attractor.

points near $E = 24$ V. In practice, engineers may occasionally see some irregular transient behavior in this input voltage range.* Furthermore, when E is near 29 V, we see similar coexisting orbits manifested as a

*Computer simulation has no noise. Thus, had the simulation been run for a much longer time and the transient iterates been discarded, these bands of irregular points would have been eliminated from the bifurcation diagram.



(a)



(b)

FIGURE 5.5

Chaotic operation of voltage mode controlled Buck converter, with $L = 20 \text{ mH}$, $C = 47 \mu\text{F}$, $R = 22 \Omega$, $T = 400 \mu\text{s}$, $E = 33 \text{ V}$ and $V_{\text{ref}} = 11 \text{ V}$. (a) Measured phase portrait of chaotic attractor plotted with inductor current (y-axis: 0.1 A/div) versus output voltage (x-axis: 0.2 V/div); (b) measured Poincaré section of chaotic attractor plotted with inductor current (y-axis: 0.1 A/div) versus output voltage (x-axis: 0.2 V/div).

small band of irregular points. But these are chaotic attractors coexisting with the main stable period-2 orbit [6].

5.1.4 “Skipped” Cycles and Border Collision

Of particular interest is the qualitative difference in the operation of the circuit before and after the crisis which occurs at around $E = 32.34 \text{ V}$. A

closer examination of the waveforms of the control signal and the pulse-width modulator output reveals that the operation of the circuit after the crisis differs significantly from that before the crisis. Specifically, we observe many “skipped” cycles, where the control signal fails to hit the ramp signal.

The presence of skipped cycles has been caused by the so-called *saturating nonlinearity*, which is usually in place to limit the ranges of values of certain control parameters. In this case, the value of v_{con} when it hits the ramp voltage, as illustrated in [Figure 5.1](#), is normally limited from above by V_U as well as from below by V_L . At the point where v_{con} just leaves the allowable range, i.e., v_{con} “grazes” at the upper or lower tip of the ramp signal, the system is said to hit a *border collision* bifurcation. Outside this range, v_{con} fails to hit the ramp signal, going either too far above or below. When v_{con} manages to hit the ramp signal every switching period, the operation is seen to be “smooth” and bifurcation develops “smoothly” according to some standard pattern, e.g., period-doubling in this case, as shown in [Figures 5.6 \(a\) to \(c\)](#). When v_{con} swings beyond the allowable range and misses the ramp signal, the system behaves completely differently. [Figure 5.6 \(d\)](#) depicts the situation after a border collision has taken place.* At this point we should stress that the expansion of the chaotic attractor at $E = 32.34$ V is a result of an interior crisis and not border collision. However, border collision as described above is a cause of the qualitative change in the circuit operation. In other words, this particular converter has actually gone through a border collision (responsible for the “skipped” cycles) as well as an interior crisis (responsible for the expansion of the chaotic attractor).

The problem of determining the kind of behavioral change that would occur at border collision is non-trivial. Essentially, the system redefines itself completely at border collision. Thus, when crossing the border, the system’s behavior can change abruptly, e.g., from one periodic orbit to another periodic orbit, from a periodic orbit to chaos, from one chaotic attractor to another chaotic attractor, etc. The analysis must necessarily require knowledge of the system descriptions both before and after border collision. In this book, we do not intend to go into details of the mathematics of border collision [8, 82, 104]. Our attention will instead be focused on the mechanisms that cause border collision in terms of circuit operations.

*In formal terms, as we mentioned in [Chapter 1](#), the necessary criterion for border collision is a *structural change* which is equivalent to an alteration of the topological sequence in the case of switching converters. Obviously, the topological sequence is altered at the saturation boundary as evidenced by the presence of “skipped” cycles.

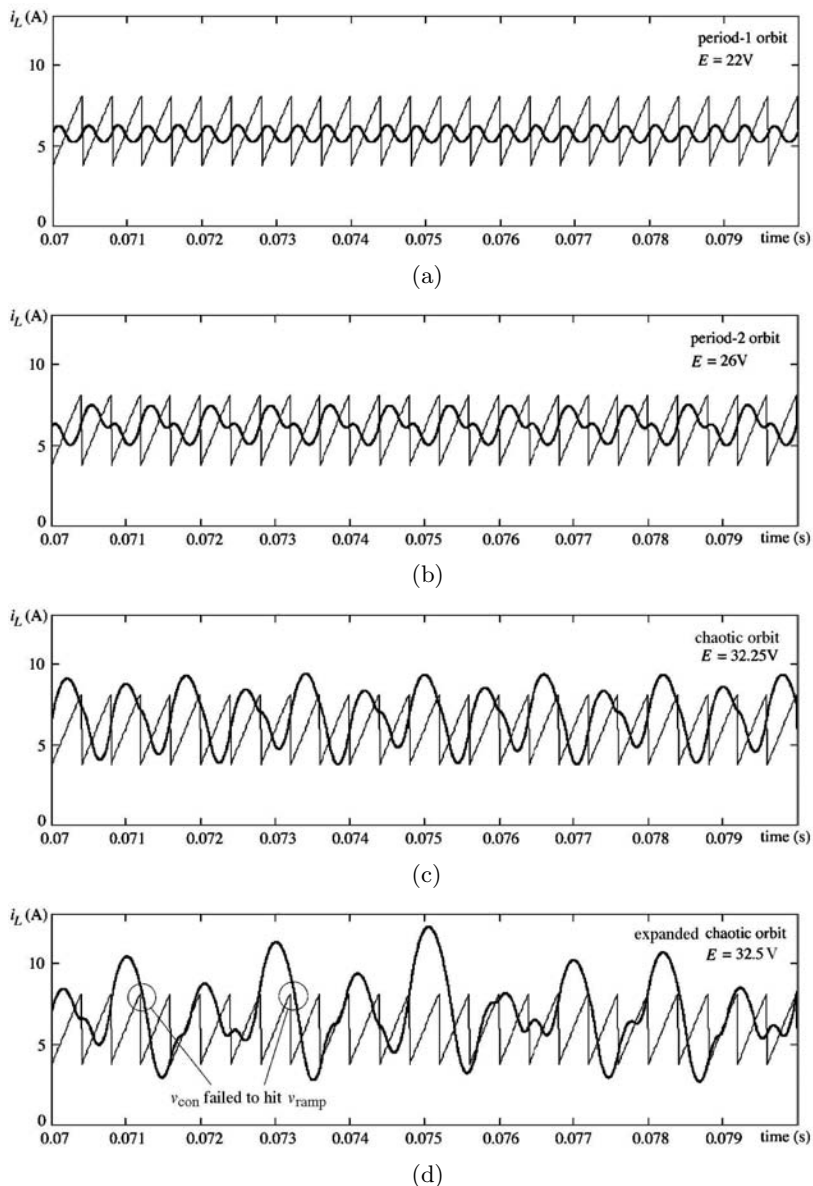


FIGURE 5.6

Control signal and ramp signal waveforms from voltage feedback buck converter. (a) Period-1 orbit; (b) period-2 orbit; (c) chaotic orbit; (d) expanded chaotic orbit featuring “skipped” cycles. Note that in (d), the control signal fails to hit the ramp signal for some cycles, as circled.

5.2 Current-Mode Controlled Switching Converters

As mentioned in [Chapter 1](#), current-mode control is one of the most popular control methods used for achieving fast output regulation in switching converters, and its basic philosophy is to “program” or force the inductor current to follow a reference value which is provided by an output feedback circuit.

In the rest of this chapter, we will study the current-mode controlled boost converter in some depth using the discrete-time modeling approach. Our initial focus is the high-frequency dynamics of the *inner current loop* which is the heart of the current-mode control. This inner loop can become unstable under certain conditions, and as we will see, the basic phenomenology associated with this inner loop is period-doubling which is not detectable by the averaged dynamical model.

5.2.1 Overview of Operation

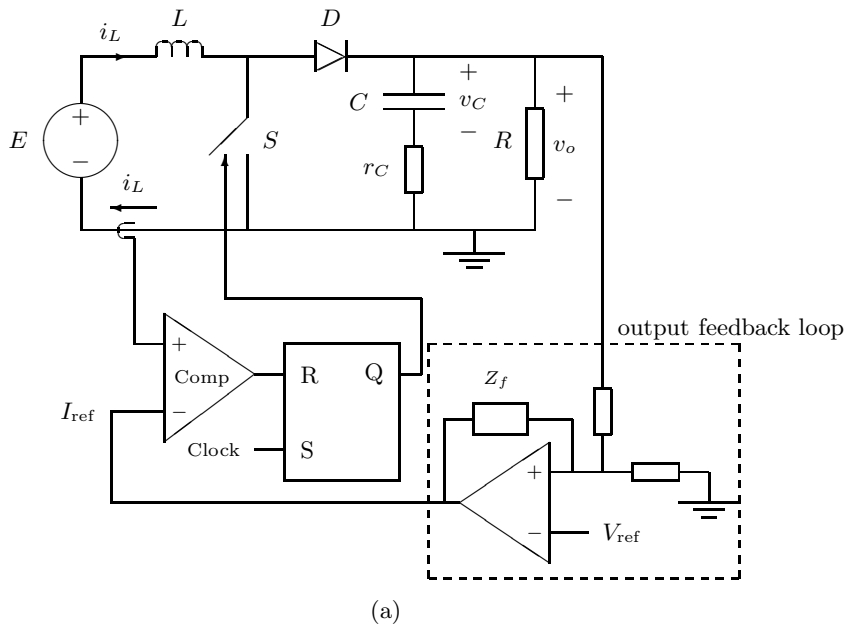
[Figure 5.7 \(a\)](#) shows the schematic diagram of a current-mode controlled boost converter. Enclosed in the dashed box is the output feedback loop, which will be omitted in our initial study. Note that as far as the dynamics of the inner current loop is concerned, it suffices to consider the system without the output feedback loop. This is because the output feedback loop is usually much slower and its purpose is to adjust the reference value I_{ref} in the event of load variation. Thus, the omission of the voltage feedback loop should not alter the high-frequency dynamics of the inner current loop. For simplicity and for consistency with the usual nomenclature, we refer to the system as an *open-loop system* if the output voltage loop is absent.

The circuit operation of the inner current loop can be briefly described as follows. First of all, the inductor current, i_L , is chosen as the programming variable which, by comparing with a reference current I_{ref} , generates the on-off driving signal for switch S . Specifically, switch S is turned on at the beginning of the cycle, i.e., at $t = nT$. The inductor current increases while switch S is on. As i_L climbs to the value of I_{ref} , switch S is turned off, and remains off until the next cycle begins. A typical waveform of the inductor current is shown in [Figure 5.7 \(b\)](#). The state equation that describes the dynamics of the boost converter can be written as

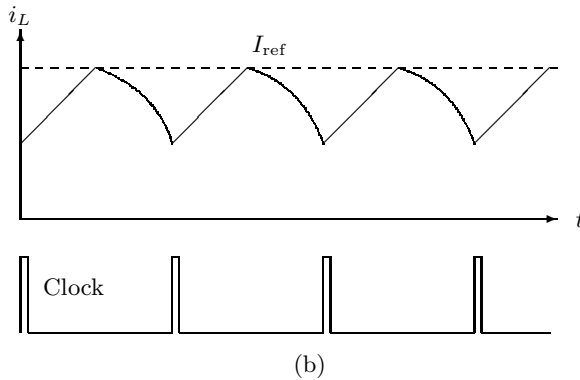
$$\dot{\mathbf{x}} = \begin{cases} \mathbf{A}_1 \mathbf{x} + \mathbf{B}_1 E & \text{for switch } S \text{ on} \\ \mathbf{A}_2 \mathbf{x} + \mathbf{B}_2 E & \text{for switch } S \text{ off} \end{cases} \quad (5.5)$$

where \mathbf{x} denotes the state variable, i.e., $\mathbf{x} = [v_C \ i_L]^T$, the \mathbf{A} 's and \mathbf{B} 's are the system matrices given by

$$\mathbf{A}_1 = \begin{bmatrix} -1/C(R + r_C) & 0 \\ 0 & 0 \end{bmatrix},$$



(a)



(b)

FIGURE 5.7

Current-mode controlled boost converter. (a) Circuit schematic; (b) inductor current waveform.

$$\begin{aligned} \mathbf{A}_2 &= \begin{bmatrix} -1/C(R+r_C) & R/C(R+r_C) \\ -R/L(R+r_C) & 0 \end{bmatrix}, \\ \mathbf{B}_1 = \mathbf{B}_2 &= \begin{bmatrix} 0 \\ 1/L \end{bmatrix}. \end{aligned} \quad (5.6)$$

With the output feedback loop closed, the system is said to be a *closed-loop* system. The additional loop allows the reference I_{ref} to be adjusted dynamically in accordance with the load variation. Typically, a proportional-

integral type of control network is incorporated to ensure fast response in the event of load fluctuation as well as to maintain the necessary steady-state condition in the event of a change in the demand of the load current.

5.2.2 Derivation of the Describing Iterative Map

Our purpose in this subsection is to derive the iterative function that describes the current-mode controlled boost converter. In the open-loop case, since the control parameter of interest is the reference current I_{ref} , an iterative function of the following form is desired:

$$\mathbf{x}_{n+1} = f(\mathbf{x}_n, I_{\text{ref}}) \quad (5.7)$$

where $\mathbf{x} = [v_C \ i_L]^T$, and subscript n denotes the value at the beginning of the n th cycle, i.e., $\mathbf{x}_n = \mathbf{x}(nT)$.

Following the same procedure as described in [Section 3.2](#), the iterative function drops out initially in the form of

$$\begin{bmatrix} v_{C,n+1} \\ i_{L,n+1} \end{bmatrix} = \begin{bmatrix} f_{11}(d_n) & f_{12}(d_n) \\ f_{21}(d_n) & f_{22}(d_n) \end{bmatrix} \begin{bmatrix} v_{C,n} \\ i_{L,n} \end{bmatrix} + \begin{bmatrix} g_1(d_n) \\ g_2(d_n) \end{bmatrix} E \quad (5.8)$$

where the f_{ij} 's and g_i 's are given in [Table 3.1](#). However, since an iterative map of the form (5.7) is desired, d_n should be expressed in terms of I_{ref} . By inspection of the circuit and the inductor current waveform, we have

$$L \frac{di_L}{dt} = L \frac{I_{\text{ref}} - i_{L,n}}{d_n T} = E \quad (5.9)$$

$$\Rightarrow d_n = \frac{I_{\text{ref}} - i_{L,n}}{(E/L)T} \quad (5.10)$$

Now, we may combine (5.8) and (5.10) to obtain the required iterative map for the open-loop current-mode controlled boost converter.

In the case of the closed-loop system, the model requires an additional equation to describe the relationship between the output voltage and the reference current. For simplicity, we consider a linear proportional feedback configuration, and the required equation is

$$\begin{aligned} I_{\text{ref}} &= I_{\text{ref}_s} - \kappa(v_o(nT + d_n T) - V_{\text{ref}}) \\ &\approx I_{\text{ref}_s} - \kappa(v_C(nT)e^{-d_n T/C(R+r_C)} - V_{\text{ref}}) \end{aligned} \quad (5.11)$$

where κ is the feedback gain which can be chosen to modify the closed-loop dynamics, V_{ref} is the reference steady-state output voltage, and I_{ref_s} is the steady-state reference current. Since $d_n T \ll CR$, we may write

$$e^{-\frac{d_n T}{CR}} \approx 1 - \frac{d_n T}{CR} + \frac{d_n^2 T^2}{2C^2 R^2}. \quad (5.12)$$

Also, by inspection of the waveform,

$$I_{\text{ref}} = \frac{E}{L} d_n T + i_{L,n}. \quad (5.13)$$

Thus, by solving d_n numerically, we are able to generate \boldsymbol{x} iteratively for any given value of κ , which is equivalent to obtaining an iterative function of the form

$$\boldsymbol{x}_{n+1} = f(\boldsymbol{x}_n, \kappa). \quad (5.14)$$

The above iterative maps describing the open-loop and closed-loop current-mode controlled boost converters will be used in later parts of this chapter to study the manner in which the system loses stability.

5.3 Initial Simulation Study of the Boost Converter under Current-Mode Control

In the study of nonlinear systems, initial simulation or experimentation often proves to be useful, and sometimes mandatory, in providing important clues to the choice of analytical approach. Since nonlinear systems can behave in many different ways, it would be hard to pinpoint what to look for in the analysis if no prior knowledge is gathered about the likely behavior of the system under study. In this section, we collect some representative time-domain waveforms from computer simulation of the current-mode controlled boost converter and make an initial evaluation of the possible behavior exhibited by the system.

The parameters used in the simulation are: $T = 100 \mu\text{s}$, $L = 1.5 \text{ mH}$, $R = 40 \Omega$, and $E = 5 \text{ V}$. To mimic the true behavior of the circuit, the exact piecewise switched model is used for simulation. Also, for consistency with usual practice, a duty cycle limiter $d \leq 0.9$ is included in the simulation. This will prevent the switch from being closed for the entire period (i.e., continuously being closed for more than one period) in the case where the reference current is large.

We begin with a relatively small value of I_{ref} . [Figure 5.8](#) shows the steady-state inductor current waveform and phase portrait, which clearly demonstrate a stable period-1 operation. This is the usual operation or the only practically acceptable operation for power converters.

When I_{ref} is increased, period-1 operation is no longer possible. Essentially, when I_{ref} reaches a certain value, the period of operation doubles itself, as shown in [Figure 5.9](#). The periodic operation is clearly seen from the phase portrait. Moreover, further increase in I_{ref} leads directly to chaotic operation, as shown in [Figure 5.10](#). It is worth noting that under chaotic operation the spectrum has a continuous and broad-band nature, as reflected by the magnitude of the fast Fourier transform (FFT) shown in [Figure 5.10 \(c\)](#).

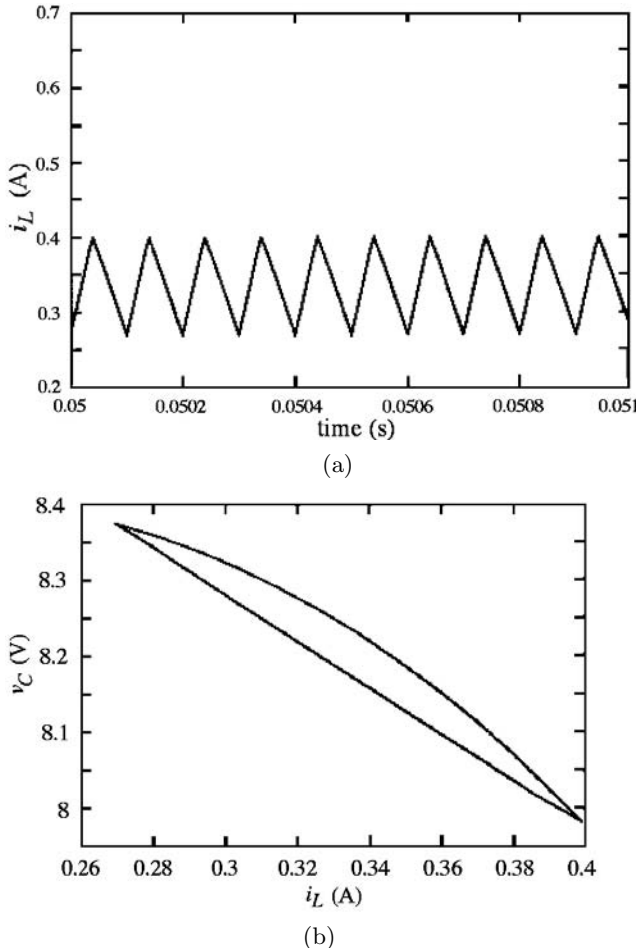
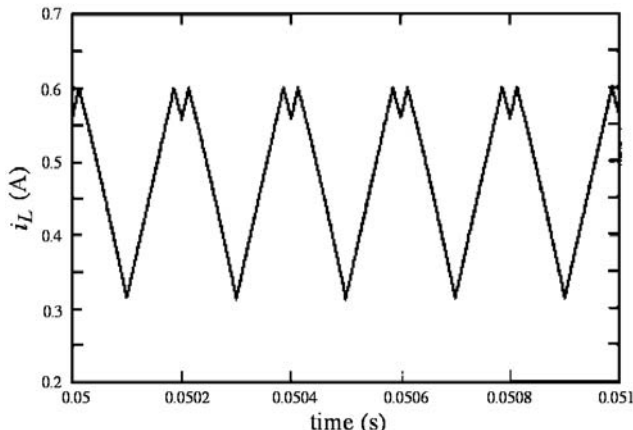


FIGURE 5.8

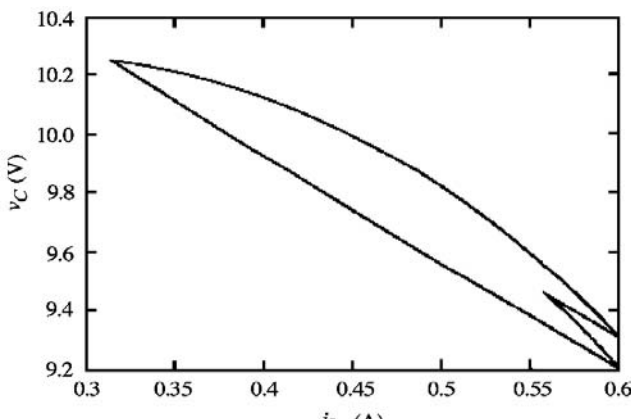
Period-1 operation. (a) Simulated inductor current waveform; (b) phase portrait [25].

Based on the above simulations, we may summarize our initial observations as follows:

1. The system loses its stability via a period-doubling bifurcation, and may (or may not) continue to double its period. This is an indication of the possible occurrence of a standard period-doubling cascade.
2. The system may go to chaos at a certain value of I_{ref} without continuing to double its period. As we have mentioned previously, the system is likely to have been struck by *border collision*. In fact, careful readers



(a)



(b)

FIGURE 5.9

Period-2 operation. (a) Simulated inductor current waveform; (b) phase portrait [25].

may have detected the occurrence of border collision from the time-domain waveform of Figure 5.10 (a). Specifically, the inductor current fails to touch the reference value for some periods due to the presence of the duty-cycle limiter in this case. This indicates that the operation has hit a “boundary” which is set by the duty-cycle limiter.*

*Note that even in the absence of the duty-cycle limiter, the duty cycle is naturally limited to a maximum of 1. The phenomenon should therefore remain qualitatively unaffected by the exact value of the duty cycle limit or its presence.

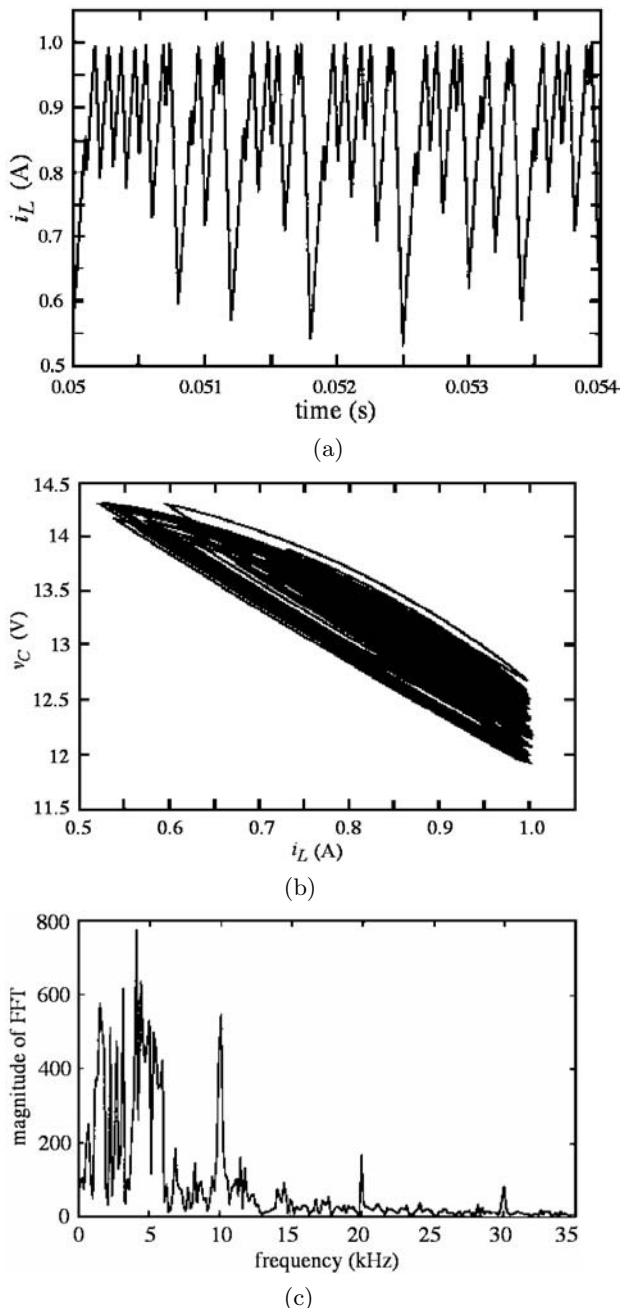


FIGURE 5.10

Chaotic operation. (a) Simulated inductor current waveform; (b) phase portrait; (c) FFT spectrum [25].

At this point, we have collected first evidence that the likely basic phenomena are period-doubling and border collision. To probe further, we may try altering some parameters and observe how period-doubling and border collision interact with each other. In varying the circuit parameters, there are several rules that we need to observe. First, we wish to keep the operation in continuous conduction mode which is a defining condition for our study. Thus, the inductance and load resistance should be kept within a certain range. The output capacitance, moreover, can be varied over a wide range without affecting the operating mode.

5.4 Bifurcation Behavior of the Open-Loop Current-Mode Controlled Boost Converter

5.4.1 Analysis via the Iterative Map

In view of the possible period-doubling bifurcation observed in the initial simulation study, we follow a traditional analysis to locate the onset of the first and subsequent period-doubling bifurcations. The main step is to examine the characteristic multipliers of the system. We begin with the iterative function $\mathbf{f}(\cdot)$ given in (5.7) and compute the characteristic multipliers corresponding to a given operating point \mathbf{X} . The first period-doubling bifurcation occurs when one of the characteristic multipliers equals -1 . Likewise, computation of the characteristic multipliers of the function $\mathbf{f}(\mathbf{f}(\cdot))$ can locate the onset of the second period-doubling bifurcation (i.e., from period-2 to period-4 orbits), if it exists.

In general, the characteristic multipliers of an iterative function $\mathbf{f}(\cdot)$ are the roots, λ , of the characteristic equation

$$\det(\lambda \mathbf{1} - J_F(\mathbf{X})) = 0 \quad (5.15)$$

where $J_F(\mathbf{X})$ is the Jacobian of $\mathbf{f}(\cdot)$ evaluated at \mathbf{X} . In the case of the current-mode controlled boost converter, $\mathbf{f}(\cdot)$ can be written as

$$\mathbf{x}_{n+1} = \mathbf{f}(\mathbf{x}_n, I_{\text{ref}}) = \begin{bmatrix} f_1(v_{C,n}, i_{L,n}, I_{\text{ref}}) \\ f_2(v_{C,n}, i_{L,n}, I_{\text{ref}}) \end{bmatrix}. \quad (5.16)$$

We recall from (5.8) that

$$f_1(\cdot) = f_{11}(d_n)v_{C,n} + f_{12}(d_n)i_{L,n} + g_1(d_n)E \quad (5.17)$$

$$f_2(\cdot) = f_{21}(d_n)v_{C,n} + f_{22}(d_n)i_{L,n} + g_2(d_n)E \quad (5.18)$$

where d_n is in turn a function of I_{ref} , as given in (5.10). Hence, the Jacobian

$J_F(\mathbf{X})$ is given by

$$J_F(\mathbf{X}) = \begin{bmatrix} \frac{\partial f_1(.)}{\partial v_{C,n}} & \frac{\partial f_1(.)}{\partial i_{L,n}} \\ \frac{\partial f_2(.)}{\partial v_{C,n}} & \frac{\partial f_2(.)}{\partial i_{L,n}} \end{bmatrix}_{x_n=\mathbf{X}} \quad (5.19)$$

where

$$\begin{aligned} \frac{\partial f_1(.)}{\partial v_{C,n}} &= f_{11}(d_n) + v_{C,n} f'_{11}(d_n) \frac{dd_n}{dv_{C,n}} \\ &\quad + i_{L,n} f'_{21}(d_n) \frac{dd_n}{dv_{C,n}} + Eg'_1(d_n) \frac{dd_n}{dv_{C,n}} \end{aligned} \quad (5.20)$$

$$\begin{aligned} \frac{\partial f_1(.)}{\partial i_{L,n}} &= v_{C,n} f'_{11}(d_n) \frac{dd_n}{di_{L,n}} + f_{12}(d_n) \\ &\quad + i_{L,n} f'_{12}(d_n) \frac{dd_n}{di_{L,n}} + Eg'_1(d_n) \frac{dd_n}{di_{L,n}} \end{aligned} \quad (5.21)$$

$$\begin{aligned} \frac{\partial f_2(.)}{\partial v_{C,n}} &= f_{21}(d_n) + v_{C,n} f'_{21}(d_n) \frac{dd_n}{dv_{C,n}} \\ &\quad + i_{L,n} f'_{22}(d_n) \frac{dd_n}{dv_{C,n}} + Eg'_2(d_n) \frac{dd_n}{dv_{C,n}} \end{aligned} \quad (5.22)$$

$$\begin{aligned} \frac{\partial f_2(.)}{\partial i_{L,n}} &= v_{C,n} f'_{21}(d_n) \frac{dd_n}{di_{L,n}} + f_{22}(d_n) \\ &\quad + i_{L,n} f'_{22}(d_n) \frac{dd_n}{di_{L,n}} + Eg'_2(d_n) \frac{dd_n}{di_{L,n}}. \end{aligned} \quad (5.23)$$

The characteristic multipliers can be computed in two steps:

1. Find the operating point corresponding to any given I_{ref} using any numerical method, e.g., Newton-Raphson method [113].
2. Solve the characteristic equation (5.15).

We are now ready to analyze the period-doubling bifurcation in this system. As mentioned earlier, one of our objectives is to investigate the effect of varying circuit parameters. For the boost converter under study (and for other simple converters as well), only two dynamical elements exist, i.e., the inductor and the output capacitor. Thus, two parameters are of interest and their dimensionless forms are (see [128])

$$\tau_L = \frac{L}{RT} \quad (5.24)$$

$$\tau_C = \frac{CR}{T}. \quad (5.25)$$

TABLE 5.1
Circuit parameters for the
open-loop current-mode
controlled boost converter.

Circuit Components	Values
Switching Period T	100 μs
Inductance L	1.5 mH
Load Resistance R	40 Ω
Input Voltage E	5 V

TABLE 5.2
Characteristic multipliers of the open-loop current-mode
controlled boost converter for $\tau_C = 8$.

I_{ref}	Characteristic multipliers	Norm	Remarks
0.4	-0.796317, 0.743175	—	Stable period-1
0.45	-0.901889, 0.748953	—	Stable period-1
0.497	-1, 0.752484	—	Period-double
0.5	0.985136, 0.575415	—	Stable period-2
0.51	0.887391, 0.636454	—	Stable period-2
0.512	0.861104, 0.655413	—	Stable period-2
0.514	0.828361, 0.680837	—	Stable period-2
0.51612	0.755725, 0.745718	—	Stable period-2
0.52	0.743632 $\pm j0.0990274$	0.750197	Stable period-2
0.53	0.7254 $\pm j0.186191$	0.748914	Stable period-2
0.54	0.707215 $\pm j0.242556$	0.747654	Stable period-2
0.55	0.689074 $\pm j0.286867$	0.746402	Stable period-2
0.56	0.670968 $\pm j0.324089$	0.745139	Stable period-2
0.57	0.652892 $\pm j0.356432$	0.743849	Stable period-2
0.58	0.634837 $\pm j0.385116$	0.742518	Stable period-2
0.59	0.6168 $\pm j0.410884$	0.741126	Stable period-2

The requirement for operating in continuous conduction mode dictates that the value of τ_L be chosen to satisfy

$$\tau_L \geq \frac{D(1 - D)^2}{2} \quad (5.26)$$

with $1 - D = E/U$ (see Section 3.7). It can be readily verified that the particular set of parameters shown in Table 5.1 satisfies (5.26). In order not to affect the operating condition, we will keep τ_L unchanged.

We may now begin to calculate the characteristic multipliers, and specifically we aim to find the condition under which a period-doubling bifurcation

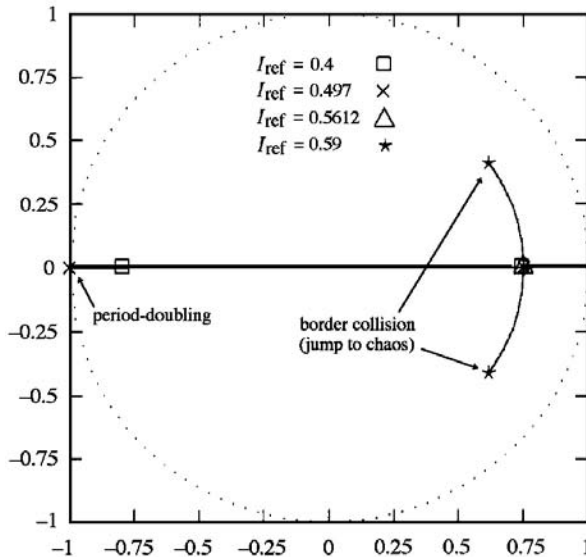


FIGURE 5.11
Loci of characteristic multipliers for $\tau_C = 8$.

occurs. We may perform the above-described calculations for different values of τ_C . Here, we exemplify the exercise with the case of $\tau_C = 8$, which represents a realistic practical situation. Since the main concern is the onset of period-doubling as I_{ref} is varied, we calculate the characteristic multipliers for a range of values of I_{ref} and follow their movements. We omit the arithmetics here and report the results tabularly in [Table 5.2](#) and also graphically in [Figure 5.11](#).

In the process of calculating the characteristic multipliers, we observe the following:

1. **Stable period-1 operation:** For $I_{\text{ref}} < 0.497$ A, the magnitudes of the characteristic multipliers are less than 1, implying stable period-1 orbits.
2. **Period-doubling bifurcation:** As I_{ref} increases, one of the characteristic multipliers moves toward -1 , and at $I_{\text{ref}} \approx 0.497$ A, the characteristic multipliers are -1 and 0.752484 , implying a period-doubling bifurcation at this point.
3. **Stable period-2 operation:** For $I_{\text{ref}} > 0.497$ A, the iterative function $f(\cdot)$ is unstable. Since the period has doubled, the function $f(f(\cdot))$ should be considered. Here, the fixed point of $f(f(\cdot))$ actually consists of two alternate fixed points of $f(\cdot)$. The characteristic multipliers can

be computed using the same procedure. In this case, right after the first period-doubling, the characteristic multipliers jump to about 1 and 0.575, and gradually move toward each other. When $I_{\text{ref}} \approx 0.516$ A, the two real characteristic multipliers collide and break off to become a complex conjugate pair.

4. **Border collision (suspected):** When I_{ref} is increased beyond 0.596 A, calculations are no longer possible since the algorithms involve determination of the steady-state operating points from the time series which has become chaotic. In fact, at the point where the period-2 orbit loses stability, the norm of the complex characteristic multipliers is about 0.74, which is far from the boundary of the unit circle. Thus, it is not possible to see the movement of the characteristic multipliers across the boundary of the unit circle, as would be expected from a standard bifurcation [65]. The system may have been struck by a border collision.*

The above analysis based on the characteristic multipliers is able to locate the onsets of period-doubling bifurcations, as long as the system has a computable operating point. However, such an analysis falls short of revealing the behavior at border collision points. It should be noted that border collision does not necessarily bring about chaos, and it may cause the system to switch to a different periodic orbit. A fuller picture regarding the bifurcation routes exhibited by the system can be quickly provided by performing numerical experiments on the iterative maps.

5.4.2 Bifurcation Diagrams Based on the Iterative Map

Based on the iterative map, i.e., (5.8) and (5.10), we can generate bifurcation diagrams handily and fast. The procedure involves straightforward generation of discrete-time values of \mathbf{x} at $t = nT$ for all n . If the iteration is allowed to proceed for a sufficiently long time, the sequence may either diverge, converge to a periodic orbit, or be attracted to a chaotic orbit. Then, for each value of the bifurcation parameter (I_{ref} in this case), we collect the discrete-time values of \mathbf{x} with the initial transient discarded. Thus, we have one set of data for each value of I_{ref} . A bifurcation diagram can then be constructed after a sufficient number of data sets are obtained.

A number of bifurcation diagrams can be constructed for different values of τ_C . [Figure 5.12](#) shows a few representative cases corresponding to $\tau_C = 1.6, 2.0, 4.0$ and 8.0 . Other circuit parameters are as listed in [Table 5.1](#). There are a few important observations we can make from these bifurcation diagrams:

*At this point, we have no strong evidence to conclude about the occurrence of border collision. We still need further confirmation, for example, from a bifurcation diagram which clearly shows a transition at the bifurcation point which does not resemble any of the standard ones, or from time-domain waveforms which show a change in the operating principle.

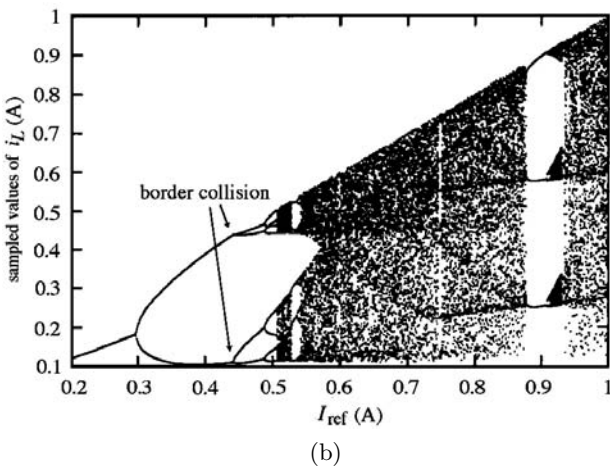
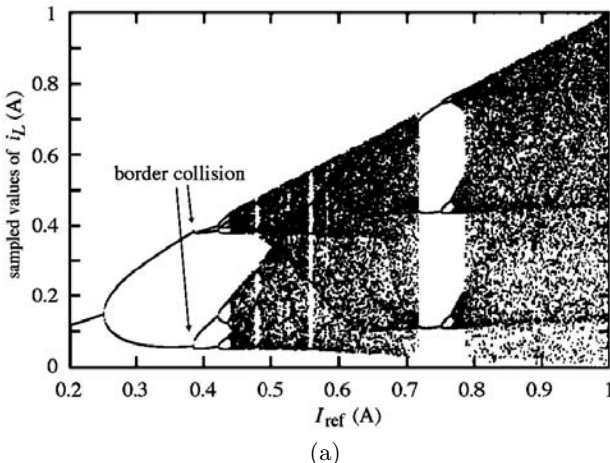
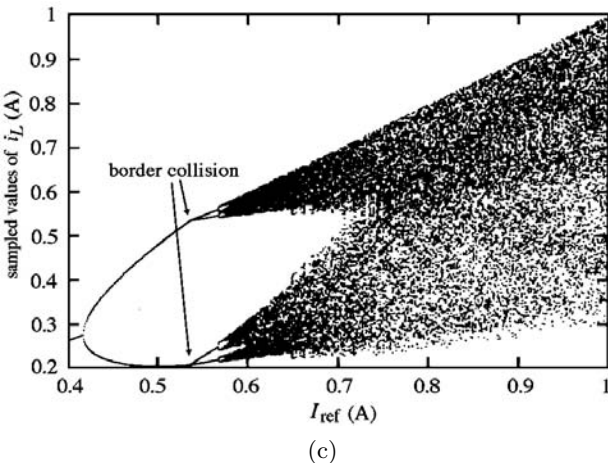


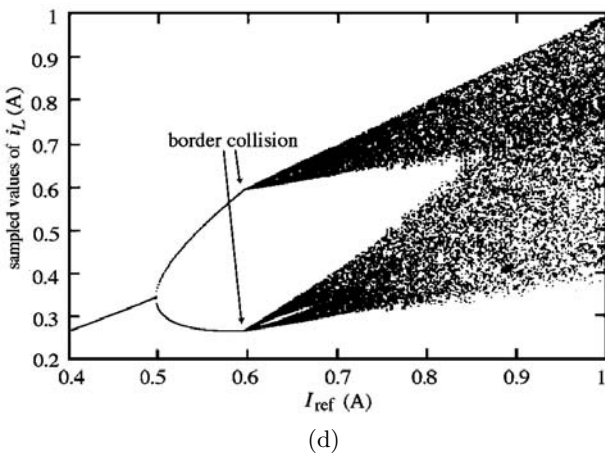
FIGURE 5.12

Bifurcation diagrams based on the iterative map. (a) $\tau_C = 1.6$; (b) $\tau_C = 2$; (c) $\tau_C = 4$; (d) $\tau_C = 8$.

1. The most notable feature of these bifurcation diagrams is the manifestation of an abrupt bifurcation that invariably occurs after one period-doubling, as marked in each diagram in [Figure 5.12](#). Such an abrupt change observed on a bifurcation diagram has been known to be caused by border collision [9, 103, 104, 172].
2. The behavioral change at the border collision is not the same for the different cases. For instance, for $\tau_C = 8$, the border collision causes a jump into “weak” chaos, which is sometimes seen as quasi-periodic behavior by the experimentalists because of its small spread. For other values of τ_C , border collision brings about a different periodic orbit.



(c)

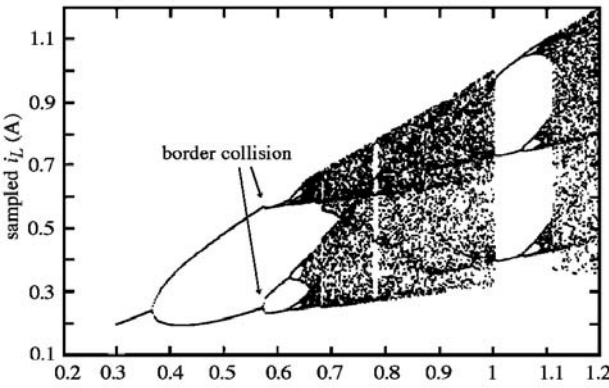


(d)

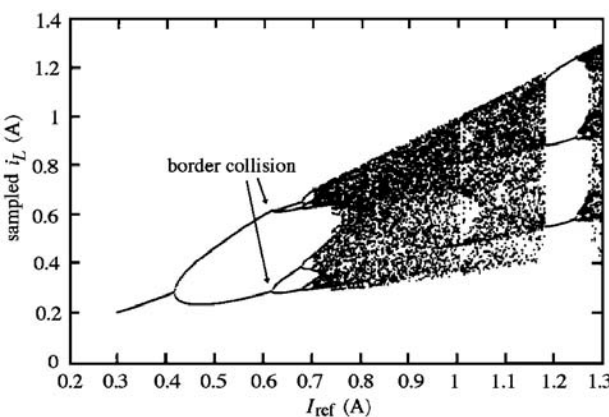
FIGURE 5.12 continued.

3. Beyond the border collision point, the bifurcation pattern continues to develop, and depending upon the value of τ_C , it runs into chaos in varying distances from the border collision point. In general, the larger the value of τ_C , the shorter the distance to chaos [25].

In summary, the bifurcation patterns are organized by period-doubling and border collision, with period-doubling being the first bifurcation adjacent to the normal period-1 operation. In the next section we will verify this basic phenomenon by performing exact simulation of the cycle-by-cycle operation of the system.



(a)



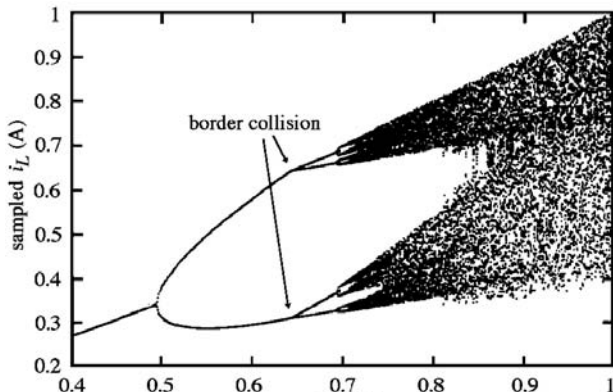
(b)

FIGURE 5.13

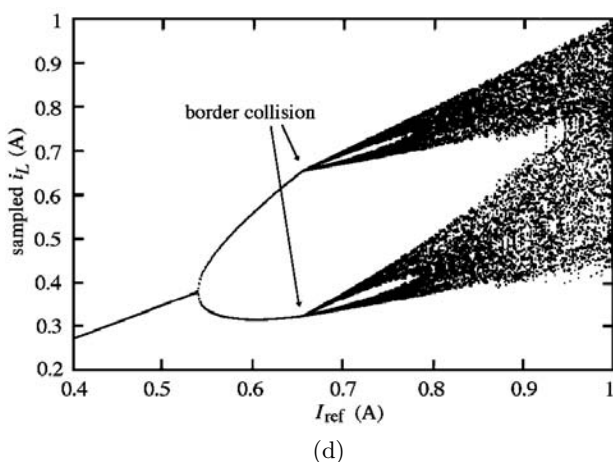
Bifurcation diagrams from exact computer simulations of circuit operation.
 (a) $\tau_C = 1.6$; (b) $\tau_C = 2$; (c) $\tau_C = 4$; (d) $\tau_C = 8$.

5.4.3 Bifurcation Diagrams Based on Circuit Simulations

As mentioned before in [Chapter 2](#), simulations based on the piecewise switched model give the true waveforms of the circuit and hence may be used to verify findings which have been obtained from discrete-time analysis. Here, we use the simulated waveforms to generate bifurcation diagrams. Specifically, a large number of the current waveforms are simulated for a range of values of I_{ref} . The values of the current at $t = nT$ are sampled from each waveform, with the initial transient discarded. A bifurcation diagram can then be constructed by plotting the sampled current values against I_{ref} . [Figure 5.13](#) shows some bifurcation diagrams constructed in this way.



(c)



(d)

FIGURE 5.13 continued.

To facilitate comparison, the same sets of parameter values are used for the bifurcation diagrams shown in [Figure 5.13](#). See [Table 5.1](#). In general, the iterative-map based bifurcation diagrams are in very good agreement with the simulated ones, except that the iterative-map based ones are shifted slightly to the right. Such discrepancy is due to the use of a truncated Taylor series in the derivation of the iterative map. Nonetheless, the basic phenomenon of the “period-doubling and border collision interplay” is clearly demonstrated by both types of computer generated bifurcation diagrams. Furthermore, if a view of the “chaoticity” is of interest (as mentioned in [Chapter 2](#)), we may compute numerically the largest average Lyapunov exponent as a function of the reference current, as exemplified in [Figure 5.14](#).

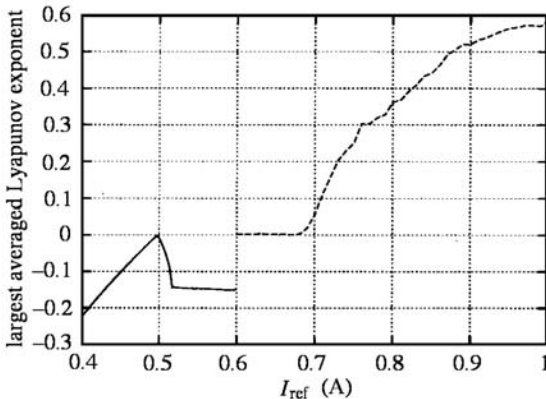


FIGURE 5.14

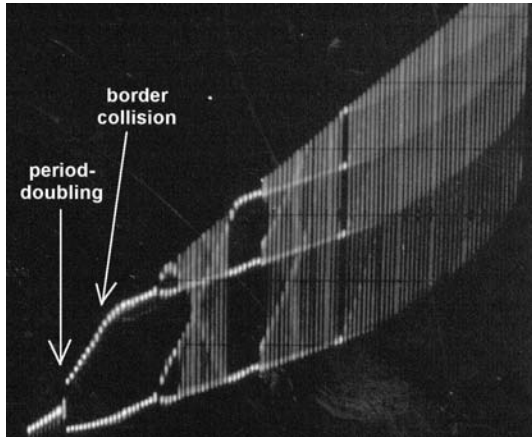
Largest average Lyapunov exponents computed from the iterative time series for $\tau_C = 8$ [25].

5.4.4 Experimental Verification

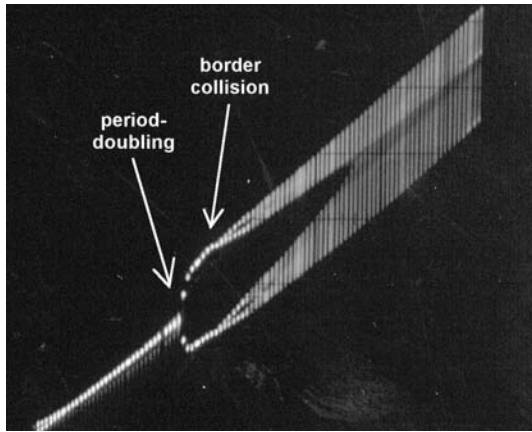
Further evidence can be obtained from laboratory experiments. In performing laboratory tests, the variation of τ_C is realized by changing the value of the output capacitance. The rest of the circuit parameters are kept unchanged so as to maintain the circuit operation in continuous conduction mode. Details of the technique for obtaining bifurcation diagrams from experimental circuits have been given in [Chapter 3](#). In [Figure 5.15](#), we collect two representative bifurcation diagrams which verify the basic phenomenon observed earlier in the computer generated bifurcation diagrams.

5.5 Theoretical Analysis of Period-Doubling Bifurcation and Border Collision

From the foregoing simulations and experiments, we have observed that border collision comes in after the first period-doubling, and brings about a sudden jump into a different periodic orbit or chaos. Of practical relevance is the question of *where these bifurcations occur*. While exact locations can be hard to find in view of the complexity of the system, analytical expressions of reasonably good approximation can be obtained if certain simplifying assumptions are made. In this section we focus on the first period-doubling and the next border collision, and derive closed-form expressions for the locations of these bifurcations.



(a)



(b)

FIGURE 5.15

Measured bifurcation diagrams from current-mode controlled boost converter. Horizontal axis: I_{ref} ; vertical axis: sampled inductor current $i_{L,n}$. From (a) to (b), the output capacitance changes from a small value to a large value corresponding to (a) $\tau_C \approx 2$; (b) $\tau_C \approx 20$ [151].

5.5.1 Analysis of Period-Doubling

In fact, the problem of locating the first period-doubling bifurcation in the current-mode controlled switching converters was solved a long time ago by power electronics engineers who interpreted this bifurcation as a fundamental stability problem [22, 66, 81, 123]. The solution is straightforward. Essentially,

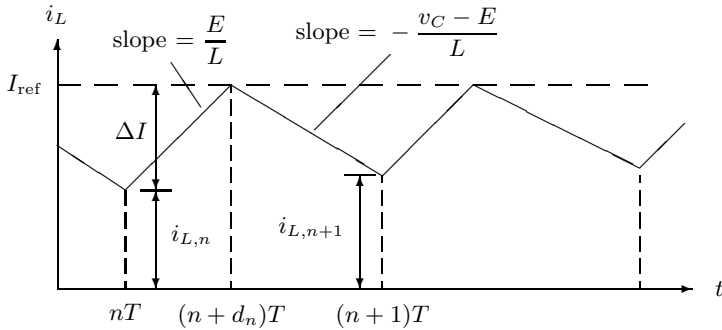


FIGURE 5.16

Inductor current waveform of the boost converter under current-mode control.

we consider the value of the inductor current at the beginning of a switching period and at the end of the period, which should be equal in the steady state. By introducing a small disturbance to the steady-state condition, the system's stability can be tested. The standard analysis proceeds as follows. We let $i_{L,n}$ and $i_{L,n+1}$ be the inductor current at $t = nT$ and $(n+1)T$ respectively, as shown in Figure 5.16. Denote the output voltage (voltage across the output capacitor) by v_C . Now, by inspecting the slopes of the inductor current in Figure 5.16, we get

$$\frac{I_{\text{ref}} - i_{L,n+1}}{(1 - d_n)T} = \frac{v_C - E}{L} \quad \text{and} \quad \frac{I_{\text{ref}} - i_{L,n}}{d_n T} = \frac{E}{L} \quad (5.27)$$

where d_n is the duty cycle of the n th switching period. Combining the above equations, we have

$$i_{L,n+1} = \left(1 - \frac{v_C}{E}\right) i_{L,n} + \frac{I_{\text{ref}} v_C}{E} - \frac{(v_C - E)T}{L}. \quad (5.28)$$

Since we are interested in the inner current loop dynamics near the steady state, we may write

$$\delta i_{L,n+1} = \left(\frac{-D}{1-D}\right) \delta i_{L,n} + O(\delta i_n^2) \quad (5.29)$$

where D is the steady-state duty cycle and δ denotes small disturbance. Clearly, the characteristic multiplier or eigenvalue, λ , is given by

$$\lambda = \frac{-D}{1 - D} \quad (5.30)$$

which must fall between -1 and 1 for stable operation. In particular, the first period-doubling occurs when $\lambda = -1$ which corresponds to

$$D = 0.5. \quad (5.31)$$

Indeed, it has been well known in power electronics that current-mode controlled converters must operate with the duty ratio set below 0.5 in order to maintain a stable period-1 operation [81]. Moreover, if the location of the period-doubling bifurcation in terms of I_{ref} is desired, we can re-express (5.31) in terms of I_{ref} by using the steady-state equation relating R , D and I_{ref} . For the boost converter, we have

$$I_{\text{ref}} = \frac{E}{R} \left[\frac{DRT}{2L} + \frac{1}{(1-D)^2} \right] \quad (5.32)$$

which can be derived from the power-balance equation

$$\left(I_{\text{ref}} - \frac{\Delta I}{2} \right) E = \frac{E^2}{(1-D)^2 R} \quad (5.33)$$

where ΔI denotes the peak-to-peak current ripple and is given by $\Delta I = DTE/L$ (see [Figure 5.16](#)). Thus, putting $D = 0.5$ in (5.32), we obtain the value of I_{ref} at the first period-doubling bifurcation, i.e.,

$$\begin{aligned} I_{\text{ref,period-doubling}} &= \frac{E}{R} \left(\frac{RT}{4L} + 4 \right) \\ &= \frac{E}{R} \left(\frac{1}{4\tau_L} + 4 \right). \end{aligned} \quad (5.34)$$

In other words, period-doubling occurs when I_{ref} exceeds the above limit. In [Chapter 9](#), we will re-visit this problem in the light of slope compensation and its effect on the location of the period-doubling bifurcation.

5.5.2 Analysis of Border Collision

As mentioned before, one of the basic causes for border collision in power electronics is *saturating nonlinearity*.* For any switching converter, the duty cycle is always bounded between 0 and 1. This is a natural saturating nonlinearity that exists in all switching converter circuits. In some practical situations, the designer may further introduce saturation boundaries to limit the operating range. In the case of the current-mode controlled boost converter studied in the foregoing, the instantaneous duty cycle is not permitted to go beyond a limit which is set by the circuit designer. In our simulations and experiments, we have set the upper limit of the duty cycle to 0.9. Even if this is not set, the maximum duty cycle is limited below 1.0 in any case. Thus, when the circuit operates within the boundary, it exhibits smooth bifurcation such as the period-doubling bifurcation at $D = 0.5$ shown earlier. Moreover, when the operation hits the boundary, it exhibits a border collision.

*The case of changing operating mode is not relevant here because if the reference current continues to increase, the converter is surely maintaining its continuous conduction mode of operation.

Suppose the upper limit of the duty cycle is D_{limit} . Our aim here is to find an expression for I_{ref} at which the duty cycle just hits this limit. Before we proceed with the analysis, we recall that border collision occurs after the first period-doubling. In other words, the system is operating with a stable period-2 orbit just before border collision. Clearly, the period-2 orbit consists of two switching periods. Suppose the duty cycle in the first period is D , and that in the following period is D' , as shown in [Figure 5.17 \(a\)](#). Let us consider the stability of this period-2 orbit. The relevant iterative equation (similar to (5.28)) is

$$i_{L,n+2} = \left(1 - \frac{v_C}{E}\right)^2 i_{L,n} + \dots \quad (5.35)$$

Assuming a large output capacitance, we have

$$v_C = \frac{E}{1 - D_{\text{average}}} = \frac{E}{\left(1 - \frac{D + D'}{2}\right)}, \quad (5.36)$$

from which we can write

$$\delta i_{L,n+2} = \left(\frac{D + D'}{2 - D - D'}\right)^2 \delta i_{L,n} + O(\delta i_{L,n}^2) \quad (5.37)$$

Thus, stability of the period-2 orbit requires that $\left|\frac{D+D'}{2-D-D'}\right| < 1$, which is equivalent to $D + D' < 1$. However, the system must deny stable period-1 orbit. Therefore, from (5.31), we require that $D_{\text{period-1}} \geq 0.5$, i.e., $\frac{1}{2}(D+D') \geq 0.5$ or $D + D' \geq 1$. Consequently, in the steady state, D' must tend toward $1 - D$, i.e.,

$$D' \rightarrow 1 - D. \quad (5.38)$$

Also, it is readily shown that m_1 and m_2 are related by

$$\frac{2m_2}{m_1 + m_2} = D + D' \quad (5.39)$$

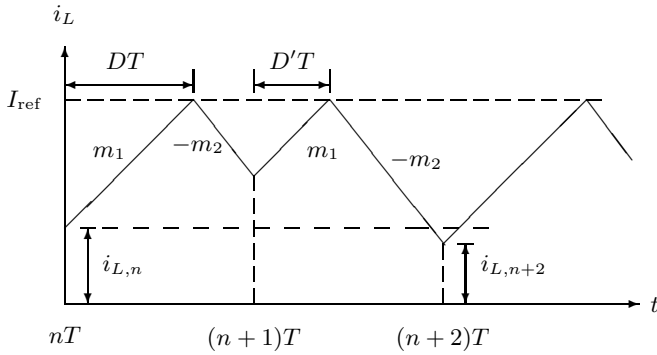
Thus, (5.38) implies

$$m_2 \rightarrow m_1 = \frac{E}{L}. \quad (5.40)$$

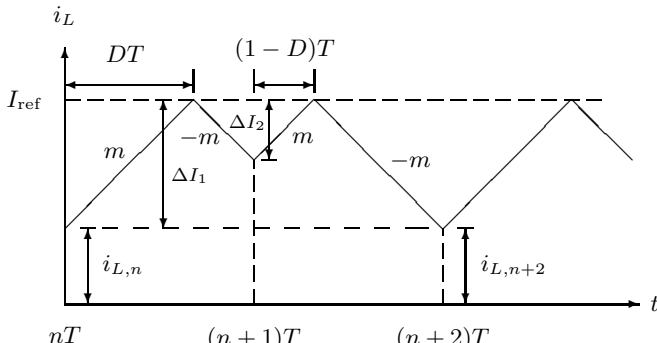
[Figure 5.17 \(b\)](#) illustrates the situation when the system is operating with a stable period-2 orbit.

Under stable period-2 operation, the duty cycles of the two constituent periods must therefore be D and $1 - D$. The average output voltage is given by

$$v_C = \frac{E}{1 - D_{\text{average}}} = \frac{E}{1 - \frac{D + (1 - D)}{2}} = 2E. \quad (5.41)$$



(a)



(b)

FIGURE 5.17

Inductor current waveform of the boost converter under period-2 operation. (a) Period-2 orbit settling to a steady state; (b) steady-state stable period-2 orbit.

Referring to Figure 5.17 (b), the average inductor current is given by

$$\begin{aligned}
 I_{L,\text{average}} &= D \left(I_{\text{ref}} - \frac{\Delta I_1}{2} \right) + (1 - D) \left(I_{\text{ref}} - \frac{\Delta I_2}{2} \right) \\
 &= D \left(I_{\text{ref}} - \frac{DTE}{2L} \right) + (1 - D) \left(I_{\text{ref}} - \frac{(1 - D)TE}{2L} \right) \\
 &= I_{\text{ref}} - \frac{ET}{2L} [1 - 2D(1 - D)]
 \end{aligned} \tag{5.42}$$

For power balance, we must have

$$I_{L,\text{average}}E = \frac{v_C^2}{R} \quad \Rightarrow \quad I_{L,\text{average}} = \frac{4E}{R}. \tag{5.43}$$

Combining (5.42) and (5.43), we have the value of I_{ref} given by

$$I_{\text{ref}} = \frac{E}{2R} \left[\frac{1 + \frac{8L}{RT} - 2D(1-D)}{\frac{L}{RT}} \right]. \quad (5.44)$$

At border collision, we simply put $D = D_{\text{limit}}$ in the above expression, giving

$$I_{\text{ref,border collision}} = \frac{E}{2R} \left[\frac{1 + 8\tau_L + 2D_{\text{limit}}(1-D_{\text{limit}})}{\tau_L} \right] \quad (5.45)$$

which is the value of I_{ref} at which border collision occurs in a current-mode controlled boost converter. In particular, if no specific duty cycle limit is set by the circuit designer, i.e., $D_{\text{limit}} = 1$, we have

$$I_{\text{ref,border collision}} = \frac{E}{2R} \left[8 + \frac{1}{\tau_L} \right]. \quad (5.46)$$

We may now apply (5.45) to locate the border collision point. For the same set of circuit parameters as in the numerical simulations, the value of $I_{\text{ref,border collision}}$ is found to be 0.667 for $D_{\text{limit}} = 1$, and 0.637 for $D_{\text{limit}} = 0.9$. [Figure 5.18](#) shows the value of $I_{\text{ref,border collision}}$ as a function of D_{limit} for the same set of circuit parameters. For other values of τ_L , a set of curves plotted in normalized values of $I_{\text{ref,border collision}}$ is shown in [Figure 5.19](#). Furthermore, [Figure 5.20](#) gives a fuller view of the main operation regions separated by the first period-doubling and border collision boundaries. In general, the theoretical formula is consistent with what we have observed in the previous computer simulations. Note that we do not expect an exact match between values found from the formula and those observed from simulations since we have assumed a very large output capacitance in the derivation of the formula, i.e., $\tau_C \gg 1$.

5.6 Bifurcation Behavior of the Closed-Loop Current-Mode Controlled Boost Converter

With the output voltage feedback loop closed, the system is made capable of regulating the output voltage. The schematic diagram of the system is shown in [Figure 5.7](#), where the dash box represents the output feedback loop in question. The operation of the circuit is basically the same as the open-loop system, except that the value of I_{ref} is no longer a constant but is being varied by the feedback loop. Usually, the transient response of the feedback loop is much slower than the switching frequency.

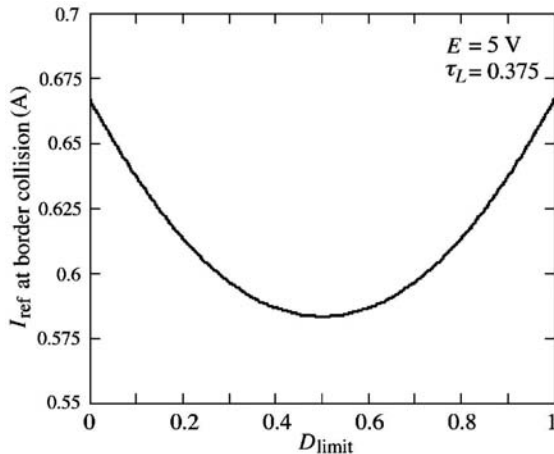


FIGURE 5.18

Theoretical I_{ref} versus D_{limit} at border collision. $E = 5 \text{ V}$, $R = 40 \Omega$, $L = 1.5 \text{ mH}$, $T = 100 \mu\text{s}$ (i.e., $\tau_L = 0.375$).

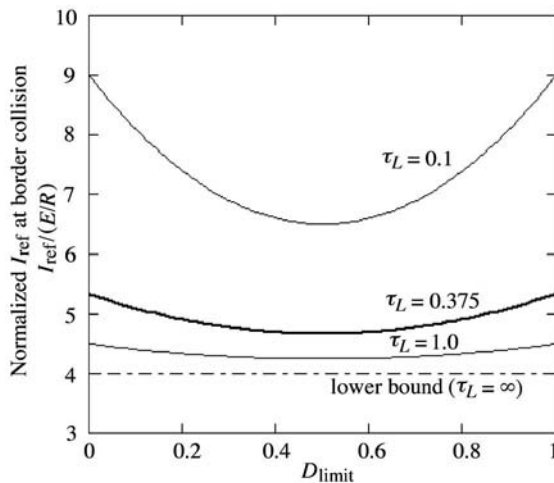


FIGURE 5.19

Normalized I_{ref} versus D_{limit} at border collision for various τ_L .

As mentioned before, the addition of the slow output feedback loop should not alter the basic bifurcation phenomena that have been found for the open-loop system. In other words, period-doubling and border collision still occur at the values of I_{ref} analyzed in the previous sections. The design problem is simply translated to the feedback loop which controls the steady-state value

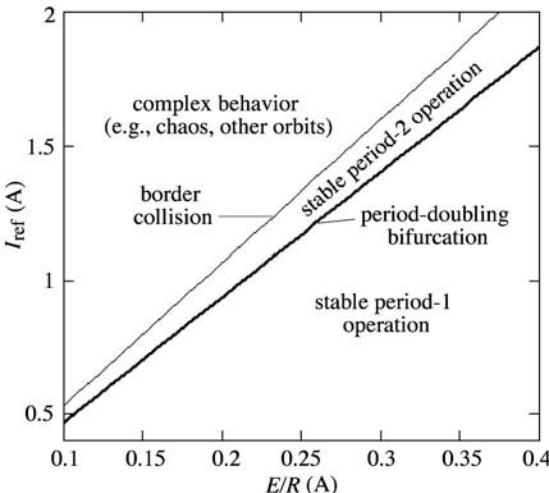


FIGURE 5.20

Theoretical operation regions and bifurcation boundaries for $R = 40 \Omega$, $L = 1.5 \text{ mH}$, $T = 100 \mu\text{s}$ (i.e., $\tau_L = 0.375$), assuming $D_{\text{limit}} = 1$.

of I_{ref} for a particular application.

In the closed-loop system, additional parameters related to the feedback loop are introduced. These new feedback parameters may also play a role in determining the bifurcation behavior of the system. Specifically, the question is whether similar or different kinds of bifurcation would occur when a particular feedback parameter is varied. It is therefore of interest to study the bifurcation behavior with some feedback parameters chosen as bifurcation parameters. In the following we focus on the proportional feedback gain, κ , which has been defined earlier in (5.11) and is repeated here for convenience:

$$I_{\text{ref}} = I_{\text{ref}_s} - \kappa(v_C(nT)e^{-d_n T/C(R+r_C)} - V_{\text{ref}}) \quad (5.47)$$

where V_{ref} is the reference steady-state output voltage, and I_{ref_s} is the steady-state reference current. In practice, the value of I_{ref_s} is controlled by the feedback loop via an integral-type of control function which adjusts I_{ref} according to the demand of the output load current.

Taking similar procedures as in Sections 5.4.2 and 5.4.3 for constructing bifurcation diagrams, we can examine the bifurcation scenarios with κ serving as the bifurcation parameter. Here, we show the computer-simulated bifurcation diagrams similar to those obtained in Section 5.4.2.

As shown in Figure 5.21, the bifurcation phenomenon is basically the same as in the open-loop case, with period-doubling and border collision interplaying to organize the bifurcation patterns. It should be noted that the abrupt bifurcation due to border collision is still visible in each bifurcation diagram

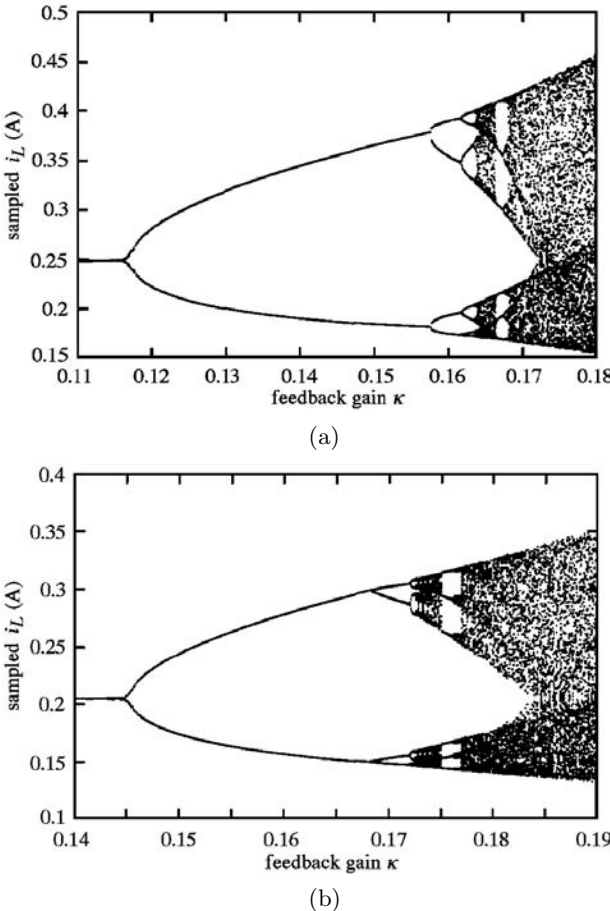
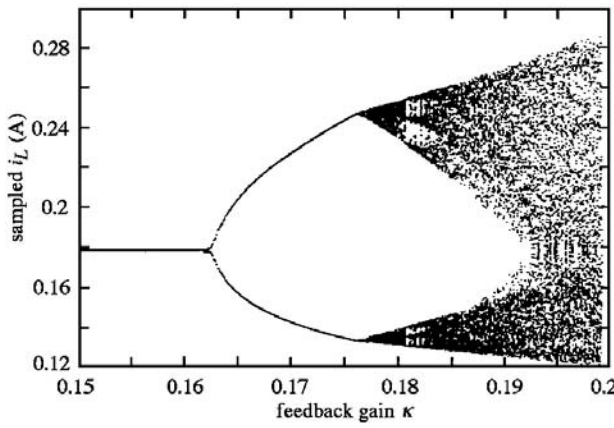


FIGURE 5.21

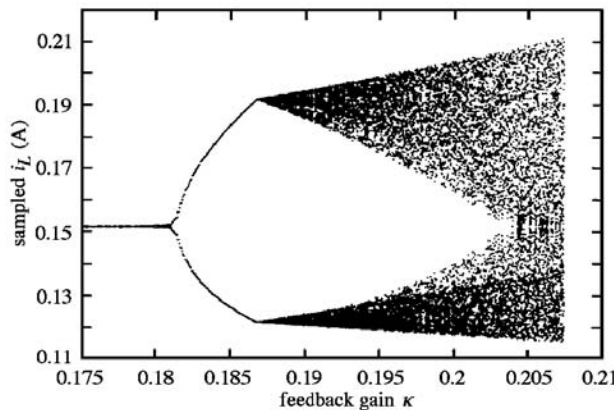
Bifurcation diagrams from computer simulations of the closed-loop current-mode controlled boost converter. (a) $I_{\text{ref}_s} = 0.3528$; (b) $I_{\text{ref}_s} = 0.2918$; (c) $I_{\text{ref}_s} = 0.25$; (d) $I_{\text{ref}_s} = 0.2$.

although it appears less obvious in some cases. We note further that for all cases shown in Figure 5.21, the value of I_{ref_s} has been kept within the stable operation range in order to focus on the effect of the feedback loop. The period-doublings and border collisions observed in these cases are due to variation of the feedback gain.

Finally, an interesting universal feature is worth noting in the current-mode controlled boost converter studied above. Specifically, comparing the open-loop and closed-loop cases, we observe a very similar transition in the appearance of the bifurcation diagram. For the open-loop case, as τ_C is increased, we



(c)



(d)

FIGURE 5.21 continued.

see that the distance to chaos along the I_{ref} axis is progressively shortened, with less number of period-doubling bifurcations after the border collision. This same transition can be observed in the closed-loop system. This corresponds to the progressive shortening of the distance to chaos along the κ axis as we decrease I_{ref_s} . In fact, the same bifurcation patterns, organized by two independent parameters (e.g., τ_C and I_{ref} in the open-loop case, and I_{ref_s} and κ in the closed-loop case), have been observed in other types of switching converters under current-mode control [23, 26, 150].

5.7 Border Collision: Is It Important?

Border collision as inherited from the built-in saturating nonlinearity of the circuit operation is a characteristic type of bifurcation which is universally observed in all power electronics circuits as well as in many other types of switching systems. From a theoretical viewpoint, this signature bifurcation is unarguably an important subject of investigation. In recent years, a lot of research efforts have been put into studying border collision in the physics and mathematics research communities [9, 14, 15, 103, 104, 172].

For engineers, however, the ultimate objective is *design*, for which stability is one of the most important criteria. For most engineering purposes, stability can be interpreted as “operation under the expected regime,” and for the case of switching converters, stable period-1 operation is the prime objective. A bifurcation phenomenon is therefore practically relevant and important if it describes the way in which the expected operating regime loses stability. For switching converters, border collision has been shown, in most cases, not the immediate bifurcation through which the system loses its stability. Thus, it is often argued that for the purpose of practical design, border collision may be a process too remote to consider. However, if border collision may lead to catastrophic consequences, the efforts spent in understanding its mechanism should be well justified, even for the mere purpose of avoiding it. Moreover, there are practical occasions where border collision is the immediate bifurcation that destabilizes the operation of a switching converter, as we will see in [Chapter 7](#).

6

Nonlinear Dynamics of the Ćuk Converter

The discrete-time modeling approach described in the previous chapters yields very effective models for describing the dynamics of nonlinear systems. Essentially, the system being modeled is sampled at a certain sampling rate and an iterative function is written to relate the state of the system at one sampling instant with that at the previous sampling instant. Clearly, the resulting model characterizes the system accurately up to the sampling frequency. If the system is of low order, e.g., one or two, the analysis is usually quite manageable. However, for higher-order systems, the derivation of the iterative function and the subsequent analysis are necessarily complicated.

In the first part of this chapter we illustrate the application of discrete-time modeling to a system of moderately high order. Specifically, we study the Ćuk converter under fixed-frequency current-mode control, which is a fourth-order system. As we will see from the results of the analysis, the system exhibits period-doubling bifurcation which is well captured by the discrete-time model.

In the second part of the chapter, the Ćuk converter is analyzed using the *averaging approach*. As we mentioned in [Chapter 3](#), the averaging approach is capable only of characterizing low-frequency behavior. Period-doubling is therefore not detectable with an averaged model. However, when the Ćuk converter is under a self-oscillating or so-called free-running current-mode control, the basic phenomenology is a Hopf-type bifurcation which is a *low-frequency bifurcation*. Here, we refer to low-frequency bifurcation as the bifurcation of dynamical behavior from a stable period-1 orbit to an orbit of much longer period. Thus, characterized by the birth of a low-frequency orbit, this type of bifurcation is well within the capability of the averaging approach for modeling its behavior.

Before we begin our study of the Ćuk converter, an important theoretical point is worth clarifying. Autonomous systems of order below three can have only fixed points or limit cycles, and no chaos [2, 162].* For any switching converter running on a fixed-frequency clock, the overall system is non-autonomous and even first-order systems can operate chaotically, as we have seen in the study of simple discontinuous-conduction-mode converters. However, no chaos should be found in self-oscillating or free-running buck, boost

*For switching converters, the term “fixed point” refers to period-1 operation and “limit cycle” refers to periodic operation with period equal to an integer multiple of the switching period.

or buck-boost converters which are autonomous systems of order below three. If we ever encounter chaos in a free-running switching converter, it must be of third order or higher.

6.1 Review of the Ćuk Converter and Its Operation

With only one smoothing inductor, simple switching converters cannot provide non-pulsating current for both input and output. The Ćuk converter [37] was proposed originally to overcome this problem by using two inductors. [Figure 6.1 \(a\)](#) shows the basic Ćuk converter. For simplicity we will focus on operation in continuous conduction mode, for which only two complementary switch states are involved, i.e., the switch is closed while the diode is open, and vice versa, as shown in [Figures 6.1 \(b\)](#) and [\(c\)](#). Provided the sum of the inductor currents remains positive, the diode conducts current for the whole sub-interval during which the switch is off, and the Ćuk converter maintains in continuous conduction mode. Thus, the situations illustrated in [Figures 6.2 \(a\)](#) and [\(b\)](#) both belong to continuous conduction mode. However, we should stress that, unlike other simple switching converters, the Ćuk converter can operate in a number of discontinuous conduction modes [46].

The Ćuk converter, being a fourth-order system, does not lend itself to any simple analysis. The complexity lies mainly in the modeling of the circuit. If the same iterative map approach can be taken, as for the case of a simple switching converter, we will end up with a fourth-order iterative map. Analysis and simulations become rather complicated. At the time of writing, however, the dynamics of the Ćuk converter remains relatively unexplored, even for the simplest mode of operation in continuous conduction.

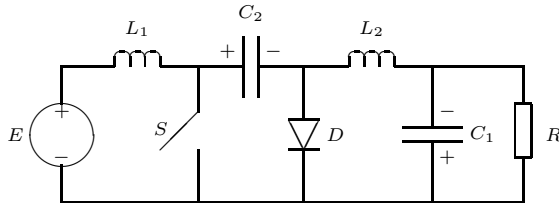
6.2 Bifurcation Behavior for Fixed-Frequency Operation

As mentioned above, the iterative map approach is applicable to the analysis of the Ćuk converter if one can bear the algebraic tedium. We start with defining a suitable state vector \mathbf{x} , e.g.,

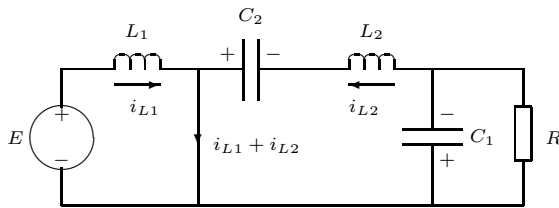
$$\mathbf{x} = [v_{C1} \ v_{C2} \ i_{L1} \ i_{L2}]^T \quad (6.1)$$

For each switch state, we can write down a state equation in the following form:

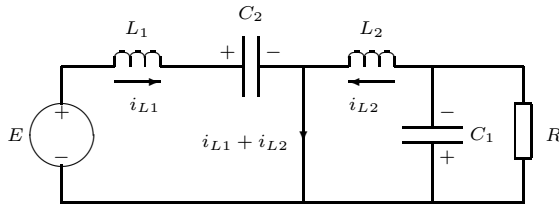
$$\frac{d\mathbf{x}}{dt} = \mathbf{A}_i \mathbf{x} + \mathbf{B}_i E \quad \text{for } i = 1, 2 \quad (6.2)$$



(a)



(b)



(c)

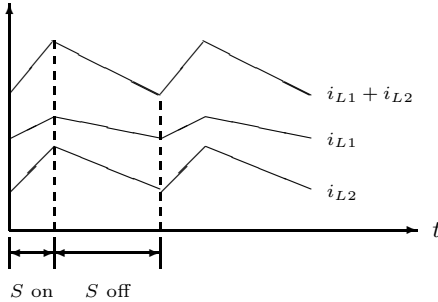
FIGURE 6.1

(a) The Cuk converter; (b) equivalent circuit when switch is on and diode is off; (c) equivalent circuit when switch is off and diode is on.

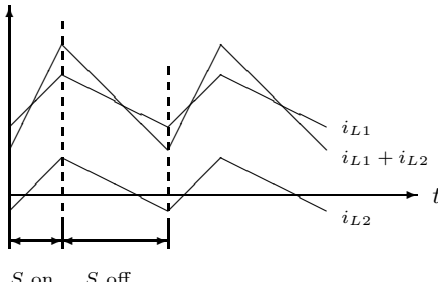
where $i = 1$ corresponds to switch being closed and diode being opened, and $i = 2$ corresponds to the complementary state. In particular, if we let $C_1 = C_2 = C$ and $L_1 = L_2 = L$, we have

$$\mathbf{A}_1 = \begin{bmatrix} -1/RC_2 & 0 & 1/C_2 & 0 \\ 0 & 0 & -1/C_1 & 0 \\ -1/L_2 & 1/L_2 & 0 & 0 \\ 0 & 0 & 0 & 0 \end{bmatrix}, \quad \mathbf{B}_1 = \begin{bmatrix} 0 \\ 0 \\ 0 \\ 1/L_1 \end{bmatrix}, \quad (6.3)$$

$$\mathbf{A}_2 = \begin{bmatrix} -1/RC_2 & 0 & 1/C_2 & 0 \\ 0 & 0 & 0 & 1/C_1 \\ -1/L_2 & 0 & 0 & 0 \\ 0 & -1/L_1 & 0 & 0 \end{bmatrix}, \quad \mathbf{B}_2 = \begin{bmatrix} 0 \\ 0 \\ 0 \\ 1/L_1 \end{bmatrix}. \quad (6.4)$$



(a)



(b)

FIGURE 6.2

(a) Inductor current waveforms in continuous mode; (b) inductor current waveforms also in continuous mode.

Following the same procedure as outlined in [Section 3.2](#), the value of \mathbf{x}_{n+1} can be expressed in terms of \mathbf{x}_n and the duty cycle d_n , i.e.,

$$\begin{bmatrix} v_{C1,n+1} \\ v_{C2,n+1} \\ i_{L1,n+1} \\ i_{L2,n+1} \end{bmatrix} = \begin{bmatrix} f_{11}(d_n) & f_{12}(d_n) & f_{13}(d_n) & f_{14}(d_n) \\ f_{21}(d_n) & f_{22}(d_n) & f_{23}(d_n) & f_{24}(d_n) \\ f_{31}(d_n) & f_{32}(d_n) & f_{33}(d_n) & f_{34}(d_n) \\ f_{41}(d_n) & f_{42}(d_n) & f_{43}(d_n) & f_{44}(d_n) \end{bmatrix} \begin{bmatrix} v_{C1,n} \\ v_{C2,n} \\ i_{L1,n} \\ i_{L2,n} \end{bmatrix} + \begin{bmatrix} g_1(d_n) \\ g_2(d_n) \\ g_3(d_n) \\ g_4(d_n) \end{bmatrix} E \quad (6.5)$$

where the $f_{ij}(\cdot)$'s and $g_i(\cdot)$'s can be found by direct substitution. If we assume $L_1 = L_2 = L$ and $C_1 = C_2 = C$ for algebraic simplicity, and define $t_c = d_n T$ and $t_d = (1 - d)T$ for notational brevity, we have

$$f_{11} = \left[1 - \frac{t_d}{CR} + \frac{t_d^2}{2} \left(\frac{1}{C^2 R^2} - \frac{1}{LC} \right) \right] \left[1 - \frac{t_c}{CR} + \frac{t_c^2}{2} \left(\frac{1}{C^2 R^2} + \frac{1}{LC} \right) \right]$$

$$+ \left(\frac{t_d}{C} - \frac{t_d^2}{2C^2R} \right) \left(-\frac{t_c}{C} + \frac{t_c^2}{2LCR} \right) \quad (6.6)$$

$$f_{12} = \left[1 - \frac{t_d}{CR} + \frac{t_d^2}{2} \left(\frac{1}{C^2R^2} - \frac{1}{LC} \right) \right] \frac{t_c^2}{2LC} + \left(\frac{t_d}{C} - \frac{t_d^2}{2C^2R} \right) \frac{t_c}{L} \quad (6.7)$$

$$\begin{aligned} f_{13} &= \left[1 - \frac{t_d}{CR} + \frac{t_d^2}{2} \left(\frac{1}{C^2R^2} - \frac{1}{LC} \right) \right] \left(\frac{t_c}{C} - \frac{t_c^2}{2C^2R} \right) \\ &\quad + \left(\frac{t_d}{C} - \frac{t_d^2}{2C^2R} \right) \left(1 - \frac{t_c^2}{LC} \right) \end{aligned} \quad (6.8)$$

$$f_{14} = 0 \quad (6.9)$$

$$f_{21} = \left(1 - \frac{t_d^2}{2LC} \right) \frac{t_c^2}{2LC} \quad (6.10)$$

$$f_{22} = \left(1 - \frac{t_d^2}{2LC} \right) \left(1 - \frac{t_c^2}{2LC} \right) \quad (6.11)$$

$$f_{23} = \left(1 - \frac{t_d^2}{2LC} \right) \left(-\frac{t_c}{C} \right) \quad (6.12)$$

$$f_{24} = \frac{t_d}{C} \quad (6.13)$$

$$\begin{aligned} f_{31} &= \left(-\frac{t_d}{L} + \frac{t_d^2}{2LCR} \right) \left[1 - \frac{t_c}{CR} + \frac{t_c^2}{2} \left(\frac{1}{C^2R^2} + \frac{1}{LC} \right) \right] \\ &\quad + \left(1 - \frac{t_d^2}{LC} \right) \left(-\frac{t_c}{C} + \frac{t_c^2}{2LCR} \right) \end{aligned} \quad (6.14)$$

$$f_{32} = \left(-\frac{t_d}{L} + \frac{t_d^2}{2LCR} \right) \frac{t_c^2}{2LC} + \left(1 - \frac{t_d^2}{LC} \right) \left(1 - \frac{t_c^2}{LC} \right) \quad (6.15)$$

$$f_{33} = \left(-\frac{t_d}{L} + \frac{t_d^2}{2LCR} \right) \left(\frac{t_c}{C} - \frac{t_c^2}{2C^2R} \right) + \left(1 - \frac{t_d^2}{LC} \right) \left(1 - \frac{t_c^2}{LC} \right) \quad (6.16)$$

$$f_{34} = 0 \quad (6.17)$$

$$f_{41} = \left(\frac{-t_d}{L} \right) \left(\frac{t_c^2}{2LC} \right) \quad (6.18)$$

$$f_{42} = \left(\frac{-t_d}{L} \right) \left(1 - \frac{t_c^2}{2LC} \right) \quad (6.19)$$

$$f_{43} = \left(\frac{-t_d}{L} \right) \left(\frac{-t_c}{C} \right) \quad (6.20)$$

$$f_{44} = 1 - \frac{t_d^2}{2LC} \quad (6.21)$$

$$g_1 = 0 \quad (6.22)$$

$$g_2 = \left(1 - \frac{t_d^2}{2LC} \right) \left(\frac{-t_d^2}{2LC} \right) + \frac{t_d^2}{LC} \left(1 - \frac{t_c^2}{2LC} \right) \quad (6.23)$$

$$g_3 = 0 \quad (6.24)$$

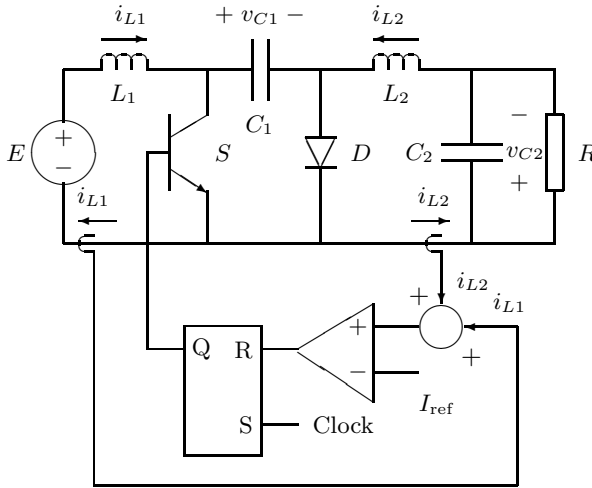


FIGURE 6.3
Schematic of current-mode controlled Ćuk converter.

$$g_4 = \frac{-t_d}{L} \left(1 - \frac{t_d^2}{2LC} \right) - \frac{t_d}{L} \left(\frac{-t_d^2}{2LC} \right) + \frac{t_c}{L} \left(1 - \frac{t_d^2}{2LC} \right). \quad (6.25)$$

6.2.1 Fixed-Frequency Current-Mode Control

Like other switching converters, the Ćuk converter can be controlled in various different ways. For instance, in a particular current-mode control scheme, we may choose the sum of the inductor currents, $i_{L1} + i_{L2}$, as the programming variable which, by comparing with a reference current I_{ref} , generates the on-off driving signal for the switch. Figure 6.3 shows the schematic of this control scheme. Essentially, the switch is turned on at the beginning of the cycle, i.e., at $t = nT$. The inductor currents increase while the switch is on. As $i_{L1} + i_{L2}$ climbs to the value of I_{ref} , the switch is turned off, and remains off until the next cycle begins. Typical waveforms are shown in Figure 6.4. We can derive the following control equation almost by inspection:

$$I_{\text{ref}} - (i_{L1} + i_{L2})_n = \left[\frac{E}{L_1} + \frac{v_{C2,n} - v_{C1,n}}{L_2} \right] d_n T \quad (6.26)$$

where subscript n denotes values at $t = nT$. Hence, we can write

$$d_n = \frac{I_{\text{ref}} - (i_{L1} + i_{L2})_n}{\left(\frac{E}{L_1} + \frac{v_{C2,n} - v_{C1,n}}{L_2} \right) T} \quad (6.27)$$

which combines with (6.5) to give the discrete-time map required.

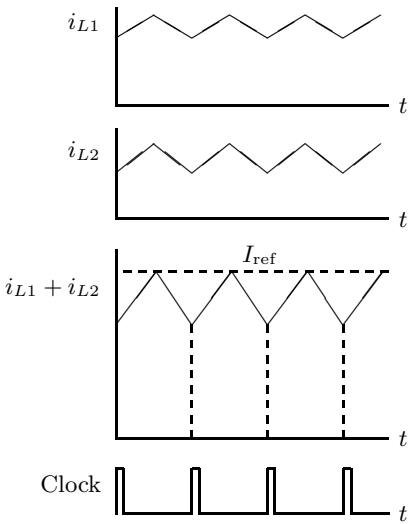


FIGURE 6.4
Waveforms of current-mode controlled Cuk converter.

In fact, we can make use of (6.5) and (6.27) to study the bifurcation phenomena of the Cuk converter under the above specific current-mode control. Moreover, if a different form of control is used, we need to derive another control equation, in lieu of (6.27), for analyzing the the system. In any case, (6.5) remains applicable.

6.2.2 Analysis of Bifurcation Behavior

To analyze the bifurcation behavior, we may repeat the same procedure used in [Chapter 5](#) for studying the current-mode boost converter. In brief, we first obtain the period- n equilibrium orbit by setting $\mathbf{x}(0) = \mathbf{x}(nT)$. For instance, for period-1 orbit, we simply have $\mathbf{x}(0) = \mathbf{x}(T)$. Then, we investigate the stability of this orbit by evaluating the magnitudes of the characteristic multipliers at the equilibrium orbit. This can be done by differentiating (6.5) to get $\Delta\mathbf{x}_{n+1} = \partial\mathbf{f}(\cdot)/\partial\mathbf{x}|_{\mathbf{x}=\mathbf{X}} \Delta\mathbf{x}_n$, where \mathbf{X} is the equilibrium point or steady-state operating point. Stability can then be determined by checking whether the magnitudes of all characteristic multipliers are less than 1.

Alternatively, we may perform quick numerical analyses to identify the bifurcation phenomena in this type of converter. Essentially, based on (6.5) and (6.27), we can obtain the discrete-time values of \mathbf{x} at $t = nT$ for all n . Typically, if we allow the iteration to proceed for a sufficiently long time, the sequence may either diverge, converge to a periodic orbit, or be attracted to a chaotic orbit. Our aim is to record behavioral changes as I_{ref} is varied.

TABLE 6.1

Circuit parameters for numerical and simulation studies of the fixed-frequency current-mode controlled Ćuk converter.

Circuit Components and Parameters	Values
Switching Period T	200 μs
Inductances L_1 and L_2	16 mH
Capacitances C_1 and C_2	47 μF
Load Resistance R	75 Ω
Input Voltage E	15 V

In our numerical experiments, the values of the components are chosen to ensure that the circuit operates in the continuous mode, as listed in [Table 6.1](#). A typical bifurcation diagram is shown in [Figure 6.5](#). From this diagram we observe that when I_{ref} is below 0.49 A, the system is attracted to a period-1 orbit. As we increase I_{ref} the period-1 orbit loses stability and gives way to a period-2 orbit. When I_{ref} is further increased beyond about 0.58 A, the system “collides” with the border where the waveform of the sum of the inductor currents just touches I_{ref} right at the clock pulse. Beyond this point, chaotic motion is observed. It is worth noting that since I_{ref} corresponds to the power that the converter delivers, a given converter can operate in the usual periodic fashion provided that the power level is limited to a certain value. In other words, with a given set of component values and input voltage, although the converter is capable of supplying both step-up and step-down output voltage, the power level must be restricted to ensure proper operation.

6.2.3 Verification by Computer Simulations

To verify the foregoing findings regarding the bifurcation behavior of the fixed-frequency current-mode controlled Ćuk converter, we perform exact cycle-by-cycle simulation of the system. All four possible switch states are considered in the simulating model. Essentially, the simulation program toggles among the four possible configurations according to the states of switches, and solves the appropriate describing equation with a sufficiently small time step. Note that unlike the iterative map derived earlier, the simulation program does not only deal with continuous-conduction-mode operation, but also emulates appropriately the circuit operation in various discontinuous conduction modes [46]. Thus, the simulation gives the true waveforms of the circuit.

[Figures 6.6, 6.7](#) and [6.8](#) show the period-1, period-2 and chaotic waveforms, corresponding to $I_{\text{ref}} = 0.4$ A, 0.5 A and 0.7 A, respectively. Also, by performing a large number of simulations for a range of values of I_{ref} , and discarding waveforms of the first 1000 periods, we obtain the steady-state orbits for dif-

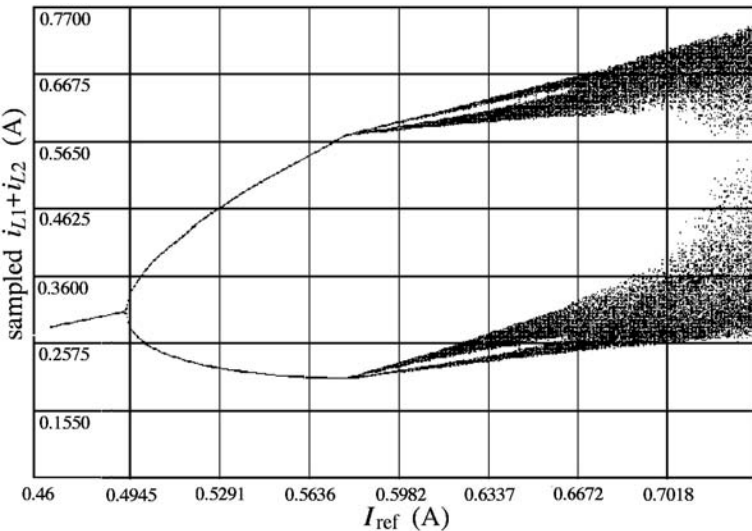


FIGURE 6.5

Bifurcation diagram from the iterative map for the fixed-frequency current-mode controlled Čuk converter. Y-axis is the sum of the inductor currents sampled at $t = nT$ and x-axis is the reference current I_{ref} serving as the bifurcation parameter.

ferent values of I_{ref} in the range $0.46 < I_{\text{ref}} < 0.74$. Results are collected in the form of a bifurcation diagram, as shown in [Figure 6.9](#).

The above findings have also been confirmed by laboratory measurements. Readers may refer to [Section 2.6.1](#) for experimental results.

6.2.4 Interim Conclusion on the Basic Phenomenology

At this point, we may make an interim conclusion regarding the basic phenomenology of the fixed-frequency current-mode Čuk converter. Essentially, the system loses stability via period-doubling bifurcation, similar to the cases of the current-mode controlled boost and buck converters. This observation remains true regardless of the presence of an output voltage feedback loop which may be needed in practice for regulation purposes. This is because period-doubling bifurcation is a high-frequency phenomenon which should be unaffected by the relatively slow output feedback loop. Thus, we may conclude that converters under fixed-frequency current-mode control generally lose stability via a period-doubling type of bifurcation. Moreover, border collision as a result of saturating the duty cycle will always occur, and the mechanism is exactly as described in [Section 5.5.2](#).

At this stage, no definite conclusion may be drawn regarding the occurrence

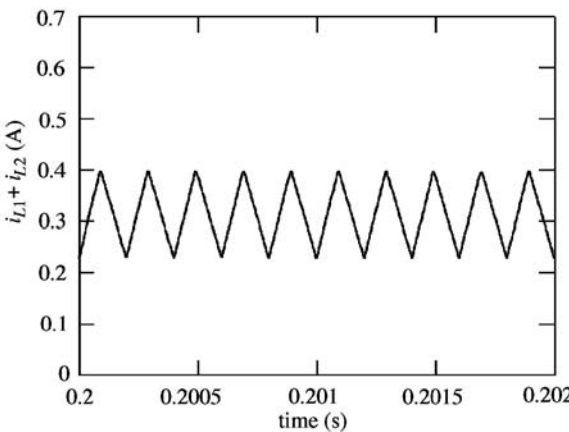


FIGURE 6.6

Computer simulation of period-1 waveform with $I_{\text{ref}} = 0.4 \text{ A}$.

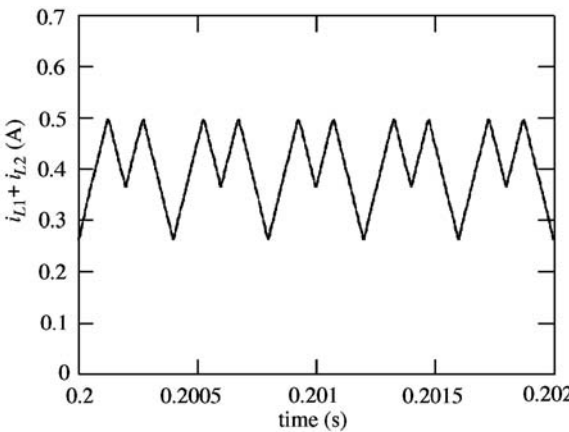


FIGURE 6.7

Computer simulation of period-2 waveform with $I_{\text{ref}} = 0.5 \text{ A}$.

of other kinds of phenomena in this type of converter system. In fact, as is typical in the analysis of nonlinear problems, the only way to find out about the behavior of a given nonlinear system is to analyze it all from scratch since subtle differences in the system configuration can give totally different behavior.

In the rest of this chapter, we continue to study the current-mode controlled Cuk converter. However, instead of applying a fixed-frequency clock to drive the switch, we will employ a self-oscillating loop for generating the on-off driving signal for the switch. As will be shown later, the basic phenomenol-

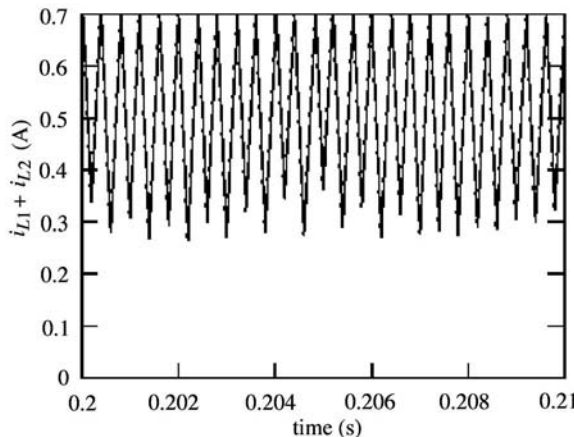


FIGURE 6.8

Computer simulation of chaotic waveform with $I_{\text{ref}} = 0.7 \text{ A}$.

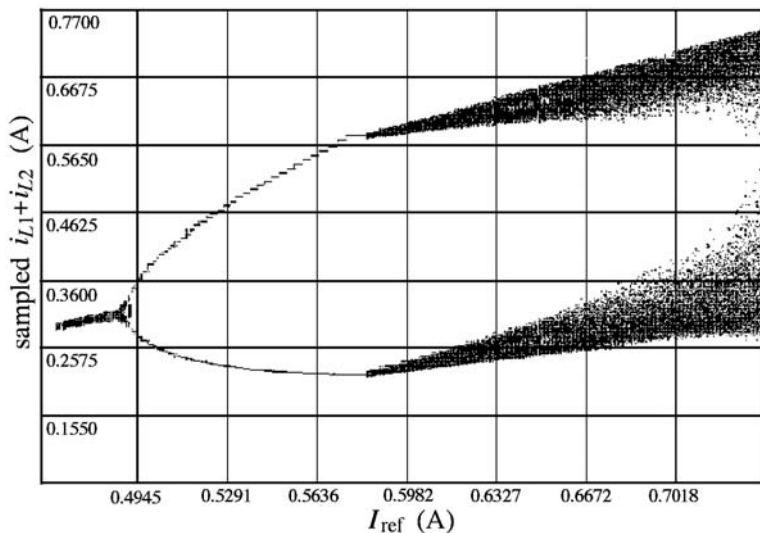


FIGURE 6.9

Bifurcation diagram from computer simulations of the fixed-frequency current-mode controlled Ćuk converter. Y-axis is the sum of the inductor currents sampled at $t = nT$ and x-axis is the reference current I_{ref} serving as the bifurcation parameter [150].

ogy is completely different, and in that case the analysis can be carried out effectively and simply by means of an averaged model.

6.3 Bifurcation Behavior for Free-Running Operation

Self-oscillating or free-running current-controlled switching converters are often used in low-cost switching power supplies, since they require no external clocks and their constructions are relatively simple. In contrast to their non-autonomous counterparts for which chaos is observed even for the simplest first-order discontinuous-mode converters, free-running converters of order below three cannot exhibit chaos. The essential feature of an autonomous switching converter is the absence of any external driving signal, which is mandatory in the non-autonomous case for periodic switching of the power switch. In this section we study the Ćuk converter operating in free-running (autonomous) mode. In particular, we will present the following aspects of investigation: (i) derivation of describing state equation; (ii) stability of the equilibrium state and identification of Hopf bifurcation based on the describing state equation; (iii) computer simulations of the circuits revealing the bifurcation from fixed point, through limit cycles and quasi-periodic orbits, and eventually to chaos.

6.3.1 Autonomous System Modeling

In the free-running Ćuk converter under study, the switch is turned on and off, in a hysteretic fashion, when the sum of the inductor currents falls below or rises above a certain pre-set hysteretic or tolerance band [168]. The average value and width of this pre-set band are adjusted by a feedback Schmitt trigger circuit. Also, the output voltage is fed back to set the average value of the hysteretic band, forcing the control variable to be related by the following control equation.

$$i_{L1} + i_{L2} = g(v_{C1}) \quad (6.28)$$

where $g(\cdot)$ is the control function. For example, a simple proportional control takes the form of

$$\Delta(i_{L1} + i_{L2}) = -\mu\Delta v_{C1} \quad (6.29)$$

where μ is the gain factor. This equation has the following equivalent form, assuming regulated output.

$$i_{L1} + i_{L2} = K - \mu v_{C1} \quad (6.30)$$

where K and μ are the control parameters. [Figure 6.10](#) shows a simplified schematic of the system.

The system can be represented by the following state equations where $s = 1$

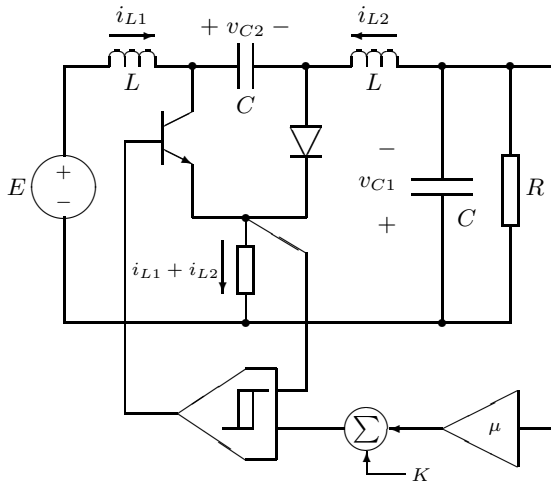


FIGURE 6.10
Cuk converter under free-running current-mode control.

when the switch is turned on, and $s = 0$ when the switch is off.

$$\left\{ \begin{array}{l} \frac{di_{L1}}{dt} = -\frac{(1-s)v_{C2}}{L} + \frac{E}{L} \\ \frac{di_{L2}}{dt} = \frac{v_{C2}s}{L} - \frac{v_{C1}}{L} \\ \frac{dv_{C1}}{dt} = \frac{i_{L2}}{C} - \frac{v_{C1}}{CR} \\ \frac{dv_{C2}}{dt} = \frac{(1-s)i_{L1}}{C} - \frac{i_{L2}s}{C} \end{array} \right. \quad (6.31)$$

The averaged model has the same form as above, with s replaced by the duty cycle d which is the fraction of the switching period for which the switch is turned on.

Since $i_{L1} + i_{L2}$ is related to v_{C1} by a linear algebraic equation, the system reduces its order by one. Specifically, when the control equation (6.30) is taken into account, the system can be reduced to the following third-order system.

$$\left\{ \begin{array}{l} \frac{di_{L2}}{dt} = \frac{v_{C2}d}{L} - \frac{v_{C1}}{L} \\ \frac{dv_{C1}}{dt} = \frac{i_{L2}}{C} - \frac{v_{C1}}{CR} \\ \frac{dv_{C2}}{dt} = \frac{(1-d)(K - \mu v_{C1})}{C} - \frac{i_{L2}}{C} \end{array} \right. \quad (6.32)$$

where d is the duty cycle. Also, from (6.30),

$$\frac{d(i_{L1} + i_{L2})}{dt} = -\frac{\mu dv_{C1}}{dt}. \quad (6.33)$$

Substitution of the involving derivatives gives

$$d = \frac{1}{2} - \frac{\frac{\mu L}{C} i_{L2} - \left(1 + \frac{\mu L}{CR}\right) v_{C1} + E}{2v_{C2}}, \quad (6.34)$$

which must satisfy $0 < d < 1$. Finally, putting (6.34) into (6.32) results in the following state equations that describe the dynamics of the autonomous system.

$$\begin{cases} \frac{di_{L2}}{dt} = -\frac{\mu i_{L2}}{2C} - \left(1 - \frac{\mu L}{CR}\right) \frac{v_{C1}}{2L} + \frac{v_{C2}}{2L} - \frac{E}{2L} \\ \frac{dv_{C1}}{dt} = \frac{i_{L2}}{C} - \frac{v_{C1}}{CR} \\ \frac{dv_{C2}}{dt} = -\frac{i_{L2}}{C} + \left(\frac{K - \mu v_{C1}}{2C}\right) \left(1 + \frac{\frac{\mu L}{C} i_{L2} - \left(1 + \frac{\mu L}{CR}\right) v_{C1} + E}{v_{C2}}\right) \end{cases} \quad (6.35)$$

Note that this representation is valid only if $0 < d < 1$. Thus, when analyzing the system numerically we must implement a saturating function such that the value of d is clipped at 0 or 1, as appropriate.

6.3.2 Dimensionless Equations

The afore-derived state equations can be put in a dimensionless form. Define the dimensionless state variables as follows:

$$x_1 = \frac{Ri_{L2}}{E}, \quad x_2 = \frac{v_{C1}}{E}, \quad x_3 = \frac{v_{C2}}{E}. \quad (6.36)$$

Also define the dimensionless time and parameters as follows:

$$\tau = \frac{Rt}{2L}, \quad \xi = \frac{L/R}{CR}, \quad \kappa_1 = \mu R, \quad \kappa_o = \frac{KR}{E}. \quad (6.37)$$

Direct substitution of these new dimensionless variables, time and parameters in the autonomous equations (6.35) yields the following dimensionless autonomous equations:

$$\begin{cases} \frac{dx_1}{d\tau} = -\xi \kappa_1 x_1 - (1 - \kappa_1 \xi) x_2 + x_3 - 1 \\ \frac{dx_2}{d\tau} = 2\xi(x_1 - x_2) \\ \frac{dx_3}{d\tau} = -2\xi x_1 + \xi(\kappa_o - \kappa_1 x_2) \left(1 + \frac{\kappa_1 \xi x_1 - (1 + \kappa_1 \xi) x_2 + 1}{x_3}\right) \end{cases} \quad (6.38)$$

To complete the model, saturation must be included. Now, d may be written as

$$d = 0.5 - \frac{\kappa_1 \xi x_1 - (1 + \kappa_1 \xi) x_2 + 1}{2x_3}. \quad (6.39)$$

The condition for saturation is

$$d > 1 \Leftrightarrow \kappa_1 \xi x_1 - (1 + \kappa_1 \xi) x_2 + x_3 + 1 < 0 \quad (6.40)$$

$$\text{or} \quad d < 0 \Leftrightarrow \kappa_1 \xi x_1 - (1 + \kappa_1 \xi) x_2 - x_3 + 1 > 0. \quad (6.41)$$

By putting $d = 1$ or 0 in (6.32) and performing dimensionless substitution, the state equations for saturation are

$$\begin{cases} \frac{dx_1}{d\tau} = 2(x_3 - x_2) \\ \frac{dx_2}{d\tau} = 2\xi(x_1 - x_2) \\ \frac{dx_3}{d\tau} = -2\xi x_1 \end{cases} \quad \text{for } d > 1, \quad (6.42)$$

$$\text{and} \quad \begin{cases} \frac{dx_1}{d\tau} = -2x_2 \\ \frac{dx_2}{d\tau} = 2\xi(x_1 - x_2) \\ \frac{dx_3}{d\tau} = -2\xi x_1 + 2\xi(\kappa_0 - \kappa_1 x_2) \end{cases} \quad \text{for } d < 0. \quad (6.43)$$

The equilibrium point can be calculated by putting $dx_1/d\tau = dx_2/d\tau = dx_3/d\tau = 0$ in (6.38) and considering the restricted sign of X_2 . This gives

$$\mathbf{X} = \begin{bmatrix} X_1 \\ X_2 \\ X_3 \end{bmatrix} = \begin{bmatrix} X_s \\ X_s \\ X_s + 1 \end{bmatrix} \quad (6.44)$$

where

$$X_s = \frac{-(1 + \kappa_1) + \sqrt{(1 + \kappa_1)^2 + 4\kappa_o}}{2}. \quad (6.45)$$

6.3.3 Stability of Equilibrium Point and Hopf Bifurcation

The Jacobian, $J(\mathbf{X})$, for the dimensionless system evaluated at the equilibrium point is given by

$$J(\mathbf{X}) = \begin{bmatrix} -\kappa_1 \xi - (1 - \kappa_1 \xi) & 1 & 0 \\ 2\xi & -2\xi & 0 \\ J_{31} & J_{32} & J_{33} \end{bmatrix}$$

where

$$J_{31} = -2\xi + \frac{\kappa_1 \xi^2 (\kappa_o - \kappa_1 X_s)}{1 + X_s} \quad (6.46)$$

$$J_{32} = \frac{-2\kappa_1 \xi - \xi(1 + \kappa_1 \xi)(\kappa_o - \kappa_1 X_s)}{1 + X_s} \quad (6.47)$$

$$J_{33} = \frac{\xi(\kappa_o - \kappa_1 X_s)(X_s - 1)}{(1 + X_s)^2}. \quad (6.48)$$

From (6.45), $X_s(X_s + 1) = \kappa_o - \kappa_1 X_s$. The Jacobian can hence be simplified to

$$J(\mathbf{X}) = \begin{bmatrix} -\kappa_1 \xi & -(1 - \kappa_1 \xi) & 1 \\ 2\xi & -2\xi & 0 \\ -2\xi + \kappa_1 \xi^2 X_s & \frac{-2\kappa_1 \xi}{1 + X_s} - \xi(1 + \kappa_1 \xi) X_s & \frac{-\xi X_s(1 - X_s)}{1 + X_s} \end{bmatrix}. \quad (6.49)$$

We will now examine the stability of the equilibrium point and the trajectory around the equilibrium point by deriving the eigenvalues of the system at the equilibrium point. The usual procedure is to solve the following equation for λ :

$$\det[\lambda \mathbf{I} - J(\mathbf{X})] = 0 \quad (6.50)$$

Upon expanding, we get

$$\begin{aligned} \lambda^3 + & \frac{\xi[(\kappa_1 + 2) + (\kappa_1 + 3)X_s - X_s^2]}{1 + X_s} \lambda^2 \\ & + \frac{2\xi[2 + (\xi + 2)X_s - \xi(\kappa_1 + 1)X_s^2]}{1 + X_s} \lambda \\ & + \frac{4\xi[\kappa_1 + \xi(1 + 2X_s)]}{1 + X_s} = 0. \end{aligned} \quad (6.51)$$

Using this equation, the following conditions are easily verified:

$$\lim_{\lambda \rightarrow -\infty} \det[\lambda \mathbf{I} - J(\mathbf{X})] \rightarrow -\infty \quad (6.52)$$

$$\text{and } \det[-J(\mathbf{X})] > 0. \quad (6.53)$$

Hence, there exists at least one $\lambda \in (-\infty, 0)$ such that $\det[\lambda \mathbf{I} - J(\mathbf{X})] = 0$, i.e., the system has at least one negative real eigenvalue. Also, numerical calculations of eigenvalues for the practical range of parameters $0 < \kappa_0 < 100$, $0 < \kappa_1 < 10$ and $0.01 < \xi < 10$ reveal that the other two eigenvalues are a complex conjugate pair which have either a positive or negative real part depending upon values of κ_0 and κ_1 . In particular the following observations are made:

1. For small values of κ_0 , the pair of complex eigenvalues has a negative real part.

TABLE 6.2Eigenvalues at $\xi = 0.0136$ showing dependence on κ_0 .

	$\kappa_1 = 1$	Remarks
$\kappa_0 = 1$	$-0.0078725 \pm j0.232363,$ -0.0274423	Stable equilibrium point
$\kappa_0 = 3$	$-0.00666899 \pm j0.232102,$ -0.0275472	Stable equilibrium point
$\kappa_0 = 5$	$-0.00482465 \pm j0.231866,$ -0.0275798	Stable equilibrium point
$\kappa_0 = 7$	$-0.0029592 \pm j0.231535,$ -0.0276402	Stable equilibrium point
$\kappa_0 = 9$	$-0.0011668 \pm j0.231428,$ -0.0276955	Stable equilibrium point
$\kappa_0 = 11$	$0.000538546 \pm j0.231217,$ -0.0277466	Unstable equilibrium point

2. As κ_0 increases, the real part of the complex eigenvalues gets less negative, and at a critical value of κ_0 , the real part changes from negative to positive. [Table 6.2](#) shows a typical scenario of the variation of the eigenvalues.
3. The critical value of κ_0 depends on the values of κ_1 and ξ . [Figure 6.11](#) shows the boundary curves where the sign of the real part of the complex eigenvalues changes. On these curves, the system loses stability via a *Hopf bifurcation* [56, 135].

To establish a Hopf bifurcation formally, one needs to show that, for given ξ and κ_1 , there exists κ_0 for which the following conditions are satisfied by the complex eigenvalue pair [2]:

$$\text{Re}(\lambda)|_{\kappa_0=\kappa_{0c}} = 0 \quad (6.54)$$

$$\text{Im}(\lambda)|_{\kappa_0=\kappa_{0c}} \neq 0 \quad (6.55)$$

$$\frac{d}{d\kappa_0} \text{Re}(\lambda) \Big|_{\kappa_0=\kappa_{0c}} \neq 0 \quad (6.56)$$

where κ_{0c} is the critical value of κ_0 at which a Hopf bifurcation occurs. Note that the last condition is necessary to ensure that the complex eigenvalue pair moves from the left side to the right side of the complex plane “transversally,” i.e., without “locusing” along the imaginary axis. In fact, all the above conditions can be numerically established using (6.51).

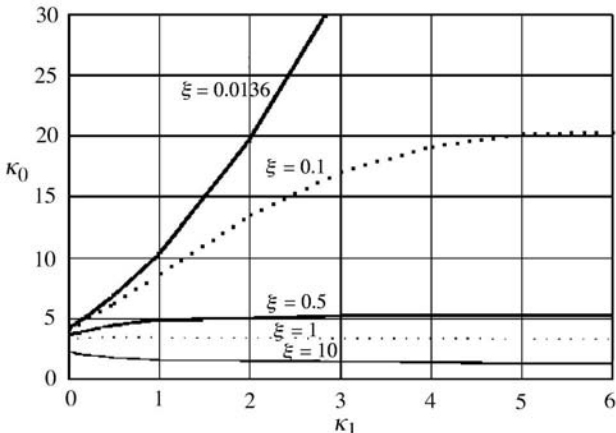


FIGURE 6.11

Boundary of stability. Area below the curve corresponds to stable equilibrium points, and that above to unstable equilibrium points.

6.3.4 Local Trajectories from Describing Equation

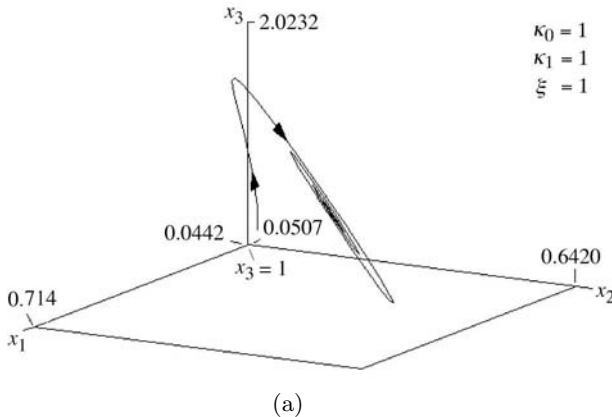
We now re-examine the stability in terms of the local trajectories near the equilibrium point. Our aim is to observe, by plotting the local trajectories, the behavior of the system as it goes from a stable region to an unstable region. The trajectory of the system near the equilibrium point can be easily derived from the corresponding eigenvalues and eigenvectors. Suppose the eigenvalues and corresponding eigenvectors are

$$\lambda_r, \sigma \pm j\omega \quad \text{and} \quad \bar{v}_r, \bar{v}_1 \pm j\bar{v}_2. \quad (6.57)$$

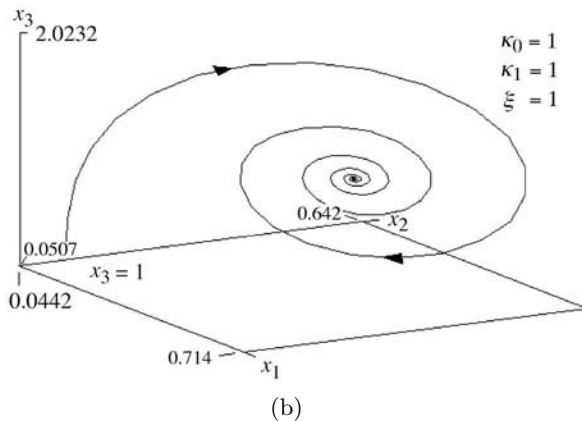
The solution in general is given by

$$\mathbf{x}(t) = c_r e^{\lambda_r t} \bar{v}_r + 2c_c e^{\sigma t} [\cos(\omega t + \phi_c) \bar{v}_1 - \sin(\omega t + \phi_c) \bar{v}_2] \quad (6.58)$$

where c_r , c_c and ϕ_c are determined by initial conditions. The geometry of the trajectory is best described in terms of the eigenline L_r which is parallel to \bar{v}_r , and the eigenplane E_c which is spanned by \bar{v}_1 and \bar{v}_2 , the intersection of L_r and E_c being the equilibrium point. Essentially, since the real eigenvalue is negative, the system moves initially in the direction of L_r , going toward E_c . At the same time it moves in a helical motion converging toward or diverging away from L_r , depending upon the sign of the real part of the complex eigenvalues. As it lands on E_c , it keeps spiraling along E_c toward or away from the equilibrium point. The following examples illustrate two typical local trajectories, corresponding to a stable and an unstable equilibrium point.



(a)



(b)

FIGURE 6.12

Two views of the stable local trajectory for $\xi = \kappa_0 = \kappa_1 = 1$ (based on averaged model).

We first examine the stable system with $\xi = \kappa_0 = \kappa_1 = 1$. The Jacobian matrix evaluated at the equilibrium point is

$$J(X) = \begin{pmatrix} -1 & 0 & 1 \\ 2 & -2 & 0 \\ -1.58579 & -2.24264 & -0.171573 \end{pmatrix}. \quad (6.59)$$

The eigenvalues, λ , and their corresponding eigenvectors, \bar{v} , are found as

$$\lambda = -2.74051, -0.215533 \pm j1.69491$$

$$\bar{v} = \begin{pmatrix} -0.297167 \\ 0.802604 \\ 0.517222 \end{pmatrix}, \begin{pmatrix} 0.185114 \mp j0.399955 \\ -0.114761 \mp j0.339261 \\ 0.823104 \end{pmatrix}$$

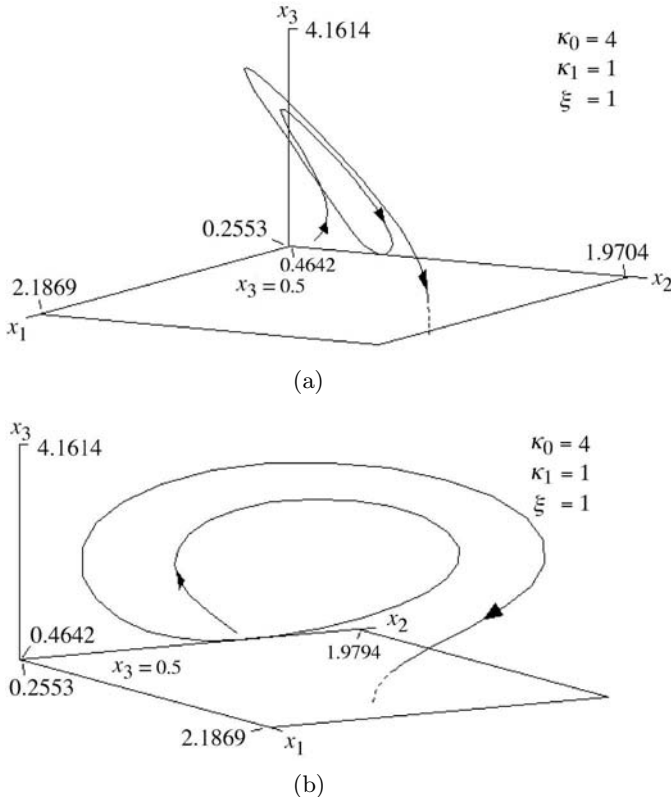


FIGURE 6.13

Two views of the unstable local trajectory for $\xi = \kappa_1 = 1$, $\kappa_0 = 4$ (based on averaged model).

Since the trajectory moves in the 3-dimensional space, it is best viewed using a 3-d plot which is available in most plotting softwares. Two plots of the trajectory from different perspectives are shown in Figure 6.12.

We next examine the unstable system with $\xi = \kappa_1 = 1$ and $\kappa_0 = 4$. As shown in Figure 6.11, the system just loses stability. The Jacobian matrix evaluated at the equilibrium point is

$$J(X) = \begin{pmatrix} -1 & 0 & 1 \\ 2 & -2 & 0 \\ -0.763932 & -3.36656 & 0.130495 \end{pmatrix}. \quad (6.60)$$

The eigenvalues, λ , and their corresponding eigenvectors, \bar{v} , are found as

$$\lambda = -2.9757, 0.0530965 \pm j1.63879$$

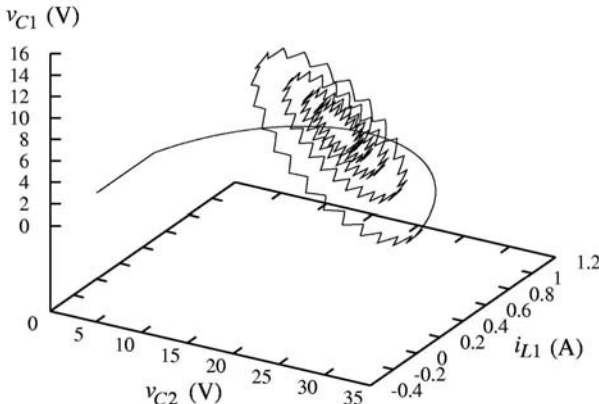


FIGURE 6.14

Trajectory spiraling into stable period-1 orbit ($K = 0.4$) from exact cycle-by-cycle simulation.

$$\bar{v} = \begin{pmatrix} -0.331404 \\ 0.679316 \\ 0.654753 \end{pmatrix}, \begin{pmatrix} 0.233197 \mp j0.362892 \\ -0.033598 \mp j0.326689 \\ 0.840282 \end{pmatrix}.$$

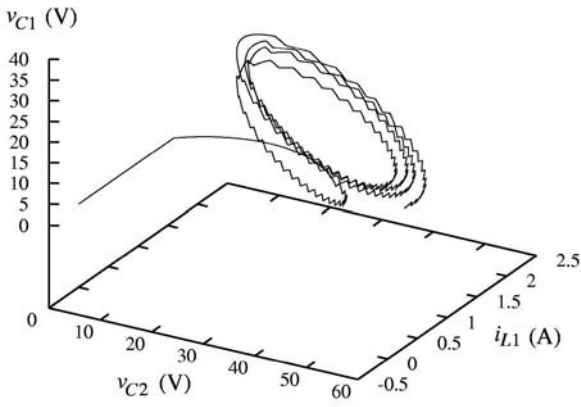
Two 3-d plots of the local trajectory from different perspectives are shown in Figure 6.13.

From the above examples, we clearly observe that the system loses stability via Hopf bifurcation as a stable spiral develops into an unstable spiral in the locality of the equilibrium point. In the next section we re-examine the system using exact computer simulations of the actual switching circuit. As we will see, the system develops into a limit cycle as it loses stability, and further develops into quasi-periodic and chaotic orbits.

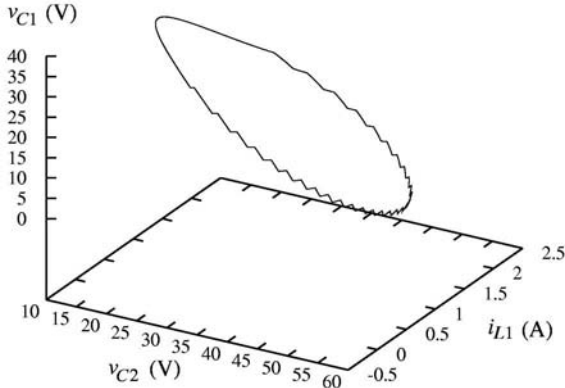
6.3.5 Computer Simulations

Since the foregoing analysis is based on a nonlinear state equation which is derived from an approximate (averaged) continuous model, it falls short of predicting the details of the bifurcation sequence. Instead of refining the model, we will examine the system using computer simulation which employs an exact piecewise switched model. Essentially the computer simulation program generates the cycle-by-cycle waveforms of all capacitor voltages and inductor currents by toggling between a set of state equations that describe the constituent linear circuits for all possible switch states. The program also incorporates the free-running current-control algorithm for determining the switch state during simulation.

In the simulation study of the free-running Cuk converter, we set the input



(a)



(b)

FIGURE 6.15

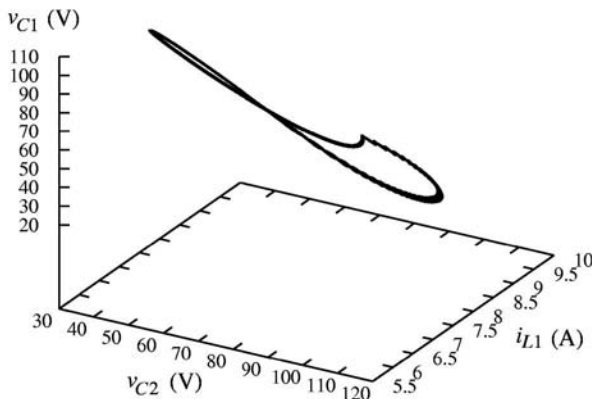
(a) Trajectory spiraling away from the unstable period-1 orbit; (b) limit cycle ($K = 1.5$), both from exact cycle-by-cycle simulation.

voltage at 15 V and the values of the components as follows.

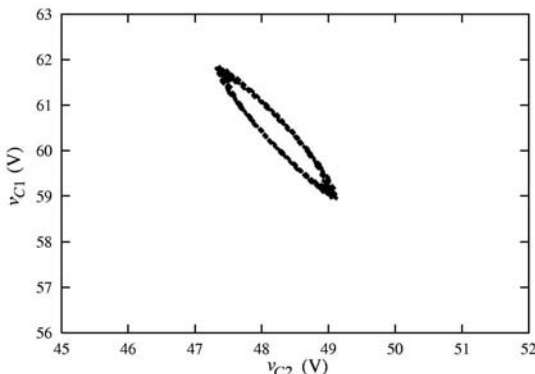
$$L_1 = L_2 = 10 \text{ mH}, \quad C_1 = C_2 = 47 \mu\text{F}, \quad R = 40 \Omega.$$

Note that since we are simulating the actual circuit, the parameters used will be μ and K instead of the dimensionless ones used for analysis. In particular we will focus on the qualitative change of dynamics as the parameters are varied, as hinted from the result of Section 6.3.3.

To see the trend, it suffices to keep μ constant and vary K . A summary of the observed behavior is as follows. A complete view of the effect of ξ , μ



(a)



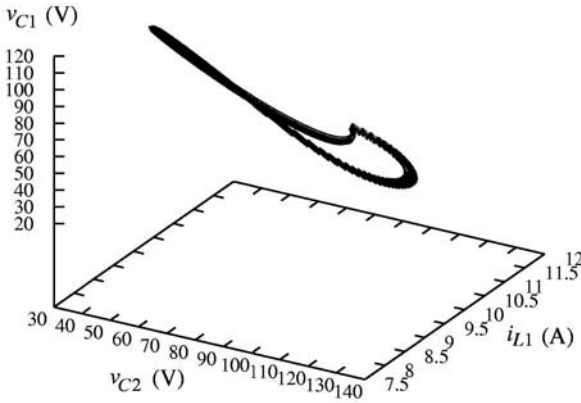
(b)

FIGURE 6.16

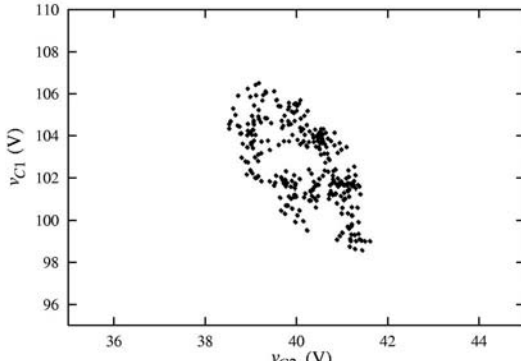
(a) Quasi-periodic orbit from exact cycle-by-cycle simulation; (b) blow-up of a Poincaré section taken at $i_1 = 8.2$ ($K = 10.5$).

and K on the stability of the fundamental equilibrium state will be provided shortly.

1. When K is small, the trajectory spirals into a fixed period-1 orbit, corresponding to a fixed point in the averaged system. [Figure 6.14](#) shows the simulated trajectory.
2. For a larger K , the period-1 orbit becomes unstable, and the trajectory spirals outward as shown in [Figure 6.15 \(a\)](#), and settles into a limit cycle, as shown in [Figure 6.15 \(b\)](#).
3. For yet a larger K , a quasi-periodic orbit can be observed, as shown in



(a)



(b)

FIGURE 6.17

(a) Chaotic orbit from exact cycle-by-cycle simulation; (b) blow-up of a Poincaré section taken at $i_1 = 9.5$ ($K = 13$).

[Figure 6.16 \(a\)](#). A Poincaré section is shown in [Figure 6.16 \(b\)](#) which essentially contains the points of the intersection of the trajectory and the vertical plane $i_1 = 8.2$.

4. Finally, chaos occurs when K is further increased. [Figures 6.17 \(a\)](#) and [\(b\)](#) show the trajectory and a Poincaré section.

Furthermore, based on a number of simulation runs, we can obtain the boundary of stability similar to [Figure 6.11](#), for different values of ξ . More precisely, the boundary curves define the values of parameters for which a trajectory changes its qualitative behavior from one that spirals into a fixed

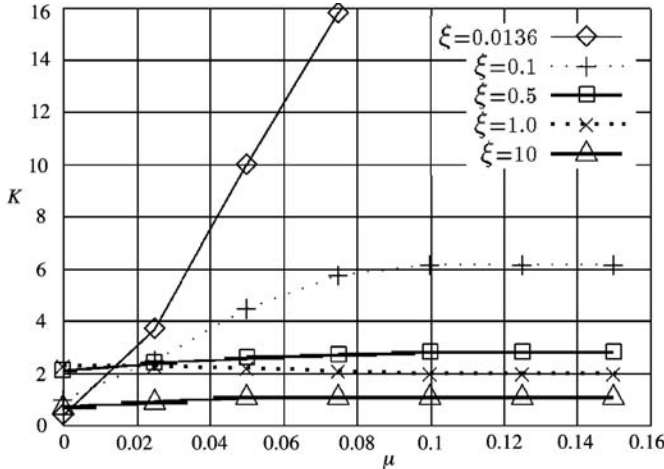


FIGURE 6.18

Boundary of stability from exact simulation. Area below the curve corresponds to stable fundamental operation, and that above to operations other than stable fundamental operation. These curves agree with the analytical curves shown earlier.

period-1 orbit (i.e., fixed point corresponding to the case of averaged model) to one that spirals away from it. As shown in [Figure 6.18](#), the stability boundary curves obtained from exact circuit simulations agree with those of [Figure 6.11](#) obtained from the averaged model.

At this point we have collected evidence from both analysis and computer simulation suggesting that the Hopf-type bifurcation is a basic bifurcation behavior for the Ćuk converter operating under a free-running current-mode control. Laboratory experiments would provide complementary evidence for the analytical and computer generated behavior. For details of an experimental circuit and results, we refer the readers to [Chapter 2](#). In particular, see [Figure 2.13](#) for the circuit schematic and [Figure 2.14](#) for a series of phase portraits and Poincaré sections showing the transition from a stable period-1 orbit to chaos, through limit cycles and quasi-periodic orbits.

6.4 Recapitulation

In concluding this chapter, it is worth mentioning that the Ćuk converter, despite being a popular type of switching converter, is still rarely studied in the literature. Much work has been reported on its steady-state operation

and practical implementation, but very little has been known about its non-linear dynamics. In this chapter we have studied this converter when it is operated under two particular current-mode control configurations. Under fixed-frequency current-mode control, the basic phenomenon is still period-doubling, which seems to be universal across all current-mode controlled converters so far studied. Here, we make no mention of border collision but assume that the readers are aware of its presence when the concerned bifurcation parameter continues to vary. When a free-running hysteretic control takes charge of the operation, however, a completely different bifurcation behavior is observed. In this case, a slow-scale Hopf-type bifurcation is the major player. Because the phenomenon is a slow-scale or low-frequency one, we are able to analyze it with a simple averaged model. This also disproves the commonly held belief that averaged models are not useful for nonlinear dynamical analysis. The real gist of the problem is whether the model is adequate for studying the particular behavior concerned. The next two chapters will provide further supporting evidence of this viewpoint.

Bifurcation Behavior of Parallel-Connected Buck Converters via Discrete-Time Models

In this and the next chapters, we examine parallel-connected systems of switching converters which have become a popular design choice for high current applications [112, 116, 139]. We first examine the case of connecting buck converters in parallel in this chapter, and move on to the case of connecting boost converters in parallel in the next chapter. Our focus is bifurcation behavior and how it is affected by the choice of parameter values. As we will see, initial simulation and experimentation play an important role in guiding the choice of analytical models. Specifically, knowing the basic phenomenology of the system can greatly facilitate the choice between the use of discrete-time models and that of averaged models. This point will be illustrated in this and the next chapters.

7.1 Parallel-Connected Switching Converters

7.1.1 The Basic Issue of Current Sharing

Paralleling power converters allows high current to be delivered to loads without the need to employ devices of high power ratings. The main design issue in parallel converters is the control of the sharing of current among the constituent converters. If a switching converter is regarded as a voltage regulator that provides very stiff voltage to a load, then it is theoretically impossible to put two such converters in parallel feeding the same load and sharing equal current, unless the two converters are perfectly identical. In practice, mandatory control is needed to ensure proper current sharing, and many effective control schemes have been proposed in the past [50, 90, 112, 116, 131, 139, 140]. One common approach is to employ an active control scheme to force the current in one converter to follow that of the other. The essence of this control approach is to monitor the difference of the output currents in two constituent converters (i.e., *current error*) and incorporate this information in the main voltage control loop. Specifically, for the case of two converters connected in parallel, one converter simply has a voltage feedback control while the other has an additional inner current loop

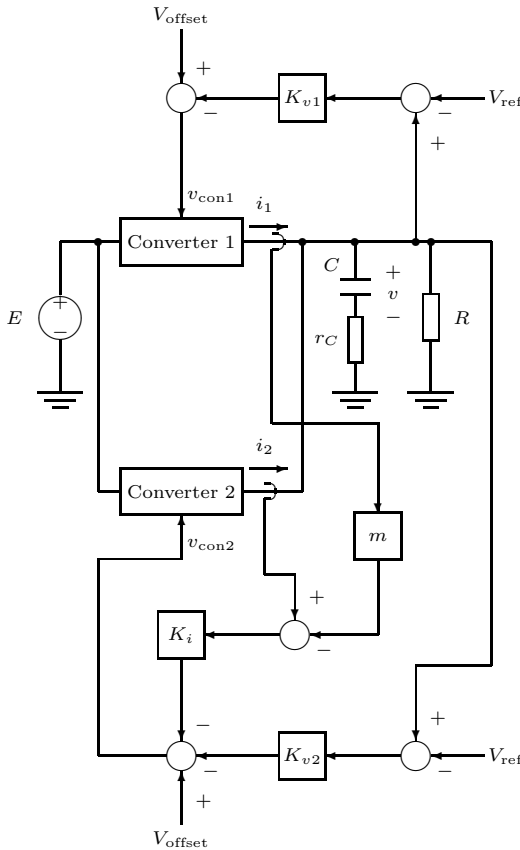


FIGURE 7.1

Block diagram of parallel-connected switching converters under a master-slave control.

that provides the current error information which is used in turn to “adjust” the voltage feedback loop to ensure equal sharing of current. Such a scheme is commonly known as the *master-slave* current-sharing scheme [112, 131].

7.1.2 The Master-Slave Scheme for Current Sharing

The system under study consists of two switching converters which are connected in parallel feeding a common load. The current drawn by the load is shared properly between the two buck converters by the action of a master-slave control scheme, as mentioned briefly in the preceding section. [Figure 7.1](#) shows the block diagram of this master-slave configuration.

Denoting the two converters as Converter 1 and Converter 2 as shown in

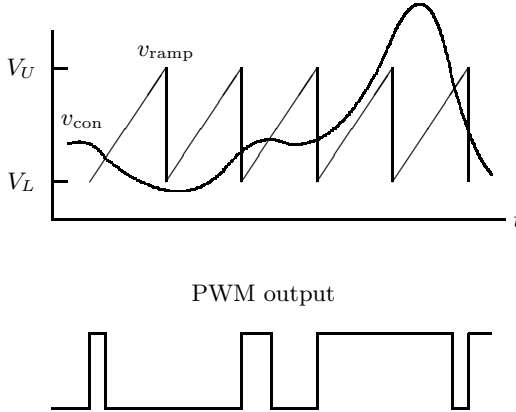


FIGURE 7.2

Pulse-width modulation (PWM) showing relationship between the control voltage and the PWM output.

Figure 7.1, the operation of the system can be described as follows. Both converters are controlled via a simple pulse-width modulation (PWM) scheme, in which a control voltage v_{con} is compared with a sawtooth signal to generate a pulse-width modulated signal that drives the switch, as shown in Figure 7.2. The sawtooth signal of the PWM generator is given by

$$v_{\text{ramp}} = V_L + (V_U - V_L) \frac{t \bmod T}{T}, \quad (7.1)$$

where V_L and V_U are the lower and upper voltage limits of the ramp, and T is the switching period. The PWM output is “high” when the control voltage is greater than V_{ramp} , and is “low” otherwise.

For Converter 1, the control voltage is derived from a voltage feedback loop, i.e.,

$$v_{\text{con}1} = V_{\text{offset}} - K_{v1}(v - V_{\text{ref}}), \quad (7.2)$$

where V_{offset} is a dc offset voltage that gives the steady-state duty cycle, V_{ref} is the reference voltage, and K_{v1} is the voltage feedback gain for Converter 1.

For Converter 2, an additional current error signal, which is proportional to the weighted difference of the output currents of the two converters, determines the control voltage. Specifically we write the control voltage for Converter 2 as

$$v_{\text{con}2} = V_{\text{offset}} - K_{v2}(v - V_{\text{ref}}) - K_i(i_2 - mi_1), \quad (7.3)$$

where K_{v2} is the voltage feedback gain of Converter 2, K_i is the current feedback gain, and m is a current weighting factor. Under this scheme, the output current of Converter 2 will follow that of Converter 1 at a ratio of m to 1,

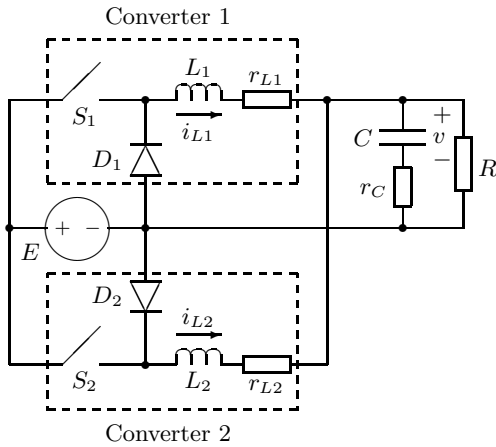


FIGURE 7.3

Two parallel-connected buck converters.

where $m > 0$. When $m = 1$, we expect equal current sharing. In much of the literature, Converter 1 is referred to as the “master” which operates independently, and Converter 2 the “slave” which imitates the master’s current value.

7.2 State Equations for Two Parallel Buck Converters

The foregoing section defines the essential control scheme that provides current sharing and output voltage regulation. In this section we complete the system description by specifying the type of converter for Converters 1 and 2. Specifically, both Converters 1 and 2 are a simple buck converter. Figure 7.3 shows the circuit diagram of the parallel-connected buck converters.

When the converters are operating in continuous conduction mode, diode D_i is always in complementary state to switch S_i , for $i = 1, 2$. That is, when S_i is on, D_i is off, and vice versa. Hence, only four switch states are possible during a switching cycle, namely

- (i) S_1 and S_2 are on;
- (ii) S_1 is on and S_2 is off;
- (iii) S_1 is off and S_2 is on;
- (iv) S_1 and S_2 are off.

The state equations corresponding to these switch states are generally given by

$$\begin{aligned}\dot{\mathbf{x}} &= \mathbf{A}_1\mathbf{x} + \mathbf{B}_1E && \text{for } S_1 \text{ and } S_2 \text{ on} \\ \dot{\mathbf{x}} &= \mathbf{A}_2\mathbf{x} + \mathbf{B}_2E && \text{for } S_1 \text{ on and } S_2 \text{ off} \\ \dot{\mathbf{x}} &= \mathbf{A}_3\mathbf{x} + \mathbf{B}_3E && \text{for } S_1 \text{ off and } S_2 \text{ on} \\ \dot{\mathbf{x}} &= \mathbf{A}_4\mathbf{x} + \mathbf{B}_4E && \text{for } S_1 \text{ and } S_2 \text{ off},\end{aligned}\tag{7.4}$$

where E is the input voltage, \mathbf{x} is the state vector defined as

$$\mathbf{x} = [v \ i_1 \ i_2]^T,\tag{7.5}$$

and the \mathbf{A} 's and \mathbf{B} 's for the case of two buck converters are given by

$$\mathbf{A}_1 = \mathbf{A}_2 = \mathbf{A}_3 = \mathbf{A}_4$$

$$= \begin{bmatrix} -\frac{1}{C(R+r_C)} & \frac{R}{C(R+r_C)} & \frac{R}{C(R+r_C)} \\ -\frac{R}{L_1(R+r_C)} - \frac{1}{L_1} \left(\frac{r_C R}{R+r_C} + r_{L1} \right) & -\frac{1}{L_1} \left(\frac{r_C R}{R+r_C} \right) \\ -\frac{R}{L_2(R+r_C)} & -\frac{1}{L_2} \left(\frac{r_C R}{R+r_C} \right) & -\frac{1}{L_2} \left(\frac{r_C R}{R+r_C} + r_{L2} \right) \end{bmatrix},\tag{7.6}$$

$$\mathbf{B}_1 = \begin{bmatrix} 0 \\ \frac{1}{L_1} \\ \frac{1}{L_2} \end{bmatrix}, \quad \mathbf{B}_2 = \begin{bmatrix} 0 \\ \frac{1}{L_1} \\ 0 \end{bmatrix}, \quad \mathbf{B}_3 = \begin{bmatrix} 0 \\ 0 \\ \frac{1}{L_2} \end{bmatrix}, \quad \mathbf{B}_4 = \begin{bmatrix} 0 \\ 0 \\ 0 \end{bmatrix}.\tag{7.7}$$

It is worth noting that the sequence of switch states, in general, takes the order as written in (7.4), i.e., starting with “ S_1 and S_2 on” and ending with “ S_1 and S_2 off” in a switching cycle. However, either “ S_1 on S_2 off” or “ S_1 off S_2 on” (not both) goes in the middle, depending upon the duty cycles of S_1 and S_2 . In the case where S_1 has a larger duty cycle, we should omit the third equation in (7.4), and likewise for the case where S_2 has a larger duty cycle. This should be taken care of in the simulation and analysis.

7.3 Initial Simulation Study

We now begin our investigation with computer simulations. Since we are primarily concerned with system stability in conjunction with the feedback design, we will focus our attention on the effects of varying the various gains on the bifurcation behavior of the system. In particular, the gains K_{v1} , K_{v2} , K_i and m present themselves as design parameters that can be changed at will. We will henceforth focus on variation of these parameters.

TABLE 7.1

Component values and steady-state voltages used in simulation. ESR stands for equivalent series resistance.

Circuit Components	Values
Switching Period T	$40 \mu\text{s}$
Input Voltage E	40 V
Output Voltage v	20 V
Offset Voltage V_{offset}	3 V
Inductance L_1 , ESR r_{L1}	1.5 mH, 0.05 Ω
Inductance L_2 , ESR r_{L2}	3.0 mH, 0.2 Ω
Capacitance C , ESR r_C	4.7 μF , 0.01 Ω
Load Resistance R	10 Ω

The simulation is based on the exact state equations derived in [Section 7.2](#). Essentially, for each set of parameter values, time-domain cycle-by-cycle waveforms are generated by solving the appropriate linear equation in any sub-interval of time, according to the states of the switches which are determined from values of the control voltages $v_{\text{con}1}$ and $v_{\text{con}2}$. Sampled data are then collected at $t = nT$ in the steady state. With a sufficient number of sets of steady-state data, we can construct the bifurcation diagrams as required. The circuit parameters used in the simulations are shown in [Table 7.1](#).

Voltage Feedback Gains as Bifurcation Parameters

We first keep K_{v2} constant and vary K_{v1} . The bifurcation diagram, as shown in [Figure 7.4](#), shows period-doubling bifurcation and chaos. In addition, we see sudden expansion of the chaotic attractor at around $K_{v1} = 7.5$. This phenomenon is similar to the interior crisis we mentioned earlier in [Section 5.1](#) when we discussed the voltage feedback buck converter. Next, we keep K_{v1} constant and vary K_{v2} . The bifurcation diagram, as shown in [Figure 7.5](#), again manifests period-doubling bifurcation, chaos and sudden expansion of the attractor. Finally, we vary K_{v1} and K_{v2} simultaneously, and the corresponding bifurcation diagram is shown in [Figure 7.6](#). Similar bifurcation scenarios are observed.

Current Gain as Bifurcation Parameter

In studying the bifurcation behavior in respect of current gain variation, we keep m , K_{v1} and K_{v2} constant, and vary K_i . It is found that the system remains in stable period-1 operation irrespective of the choice of K_i . Basically K_i only determines how close the slave follows the master. The larger K_i is, the closer the slave's output current is to the master's.

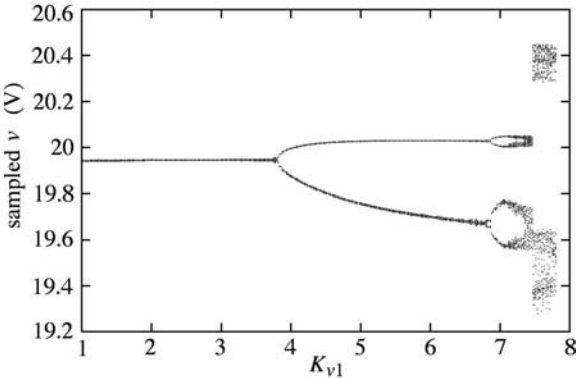


FIGURE 7.4

Bifurcation diagram with K_{v1} as bifurcation parameter ($K_{v2} = 3.5$, $K_i = 5$ and $m = 1$). First period-doubling occurs when $K_{v1} = 3.85$.

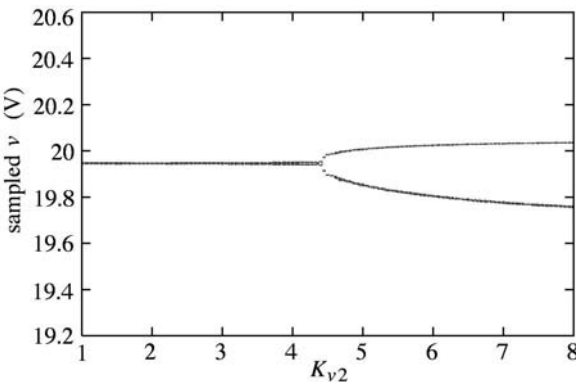


FIGURE 7.5

Bifurcation diagram with K_{v2} as bifurcation parameter ($K_{v1} = 3.5$, $K_i = 5$ and $m = 1$). First period-doubling occurs when $K_{v2} = 4.10$.

Current Sharing Ratio as Bifurcation Parameter

The final computer investigation is performed for variation of the current sharing ratio m . This time, we fix K_{v1} , K_{v2} and K_i at suitable values such that the system is in stable operation. We vary m and collect bifurcation diagrams which look typically like the one shown in [Figure 7.7](#).

In this case, we find no trace of any standard types of bifurcation. The stable period-1 operation suddenly gives way to chaos. Note that the chaotic attractor seems to spread over only a narrow range of values, as shown in [Figure 7.7](#). This is sometimes called one-piece chaos, as the bifurcation diagram

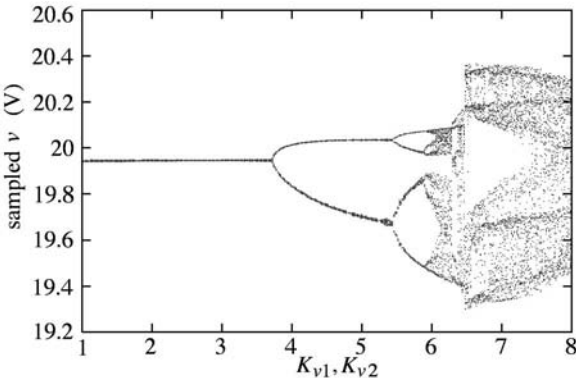


FIGURE 7.6

Bifurcation diagram with K_{v1} and K_{v2} as bifurcation parameters varying simultaneously ($K_i = 5$, $m = 1$).

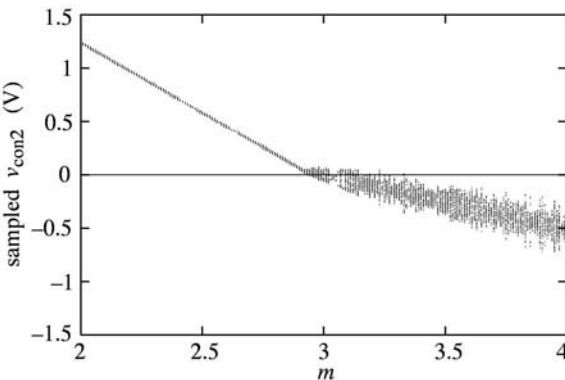
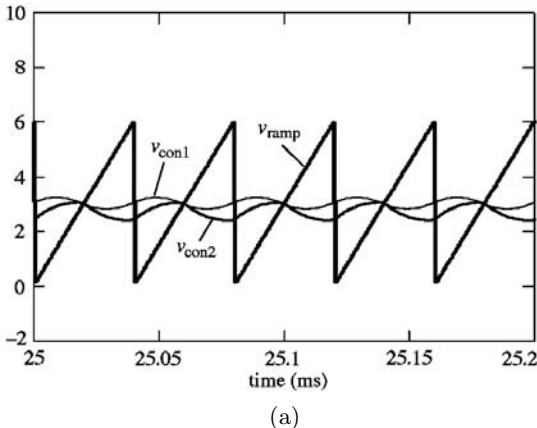


FIGURE 7.7

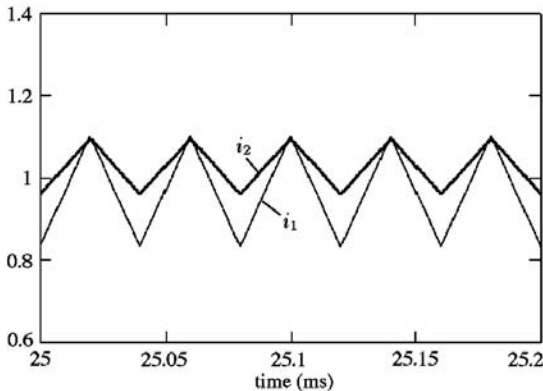
Bifurcation diagram with current sharing ratio m as bifurcation parameter ($K_{v1} = 3.0$, $K_{v2} = 3.0$, $K_i = 5$).

shows a single wedge-like pattern. This type of bifurcation has been observed in piecewise smooth maps and identified as *border collision* by Nusse, Ott and Yorke [104]. In the following, we will investigate this bifurcation in terms of the circuit operation, and we will apply the viewpoint of saturating nonlinearity to analyze this phenomenon. Specifically, we consider the time-domain waveforms of the control voltages v_{con1} and v_{con2} and examine the way in which these signals cross the ramp in the process of generating the PWM signals.

In normal operation, v_{con1} and v_{con2} hit the ramp once per switching cycle as shown in Figure 7.8 (a), and the corresponding inductor waveforms are



(a)



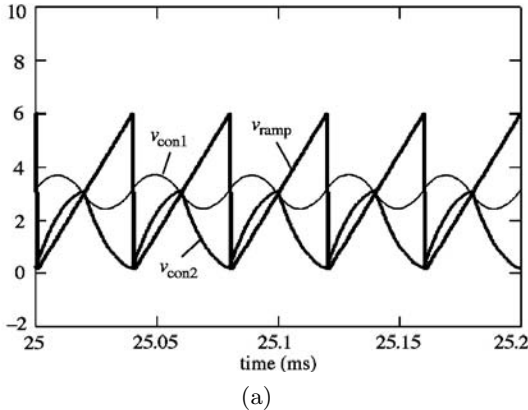
(b)

FIGURE 7.8

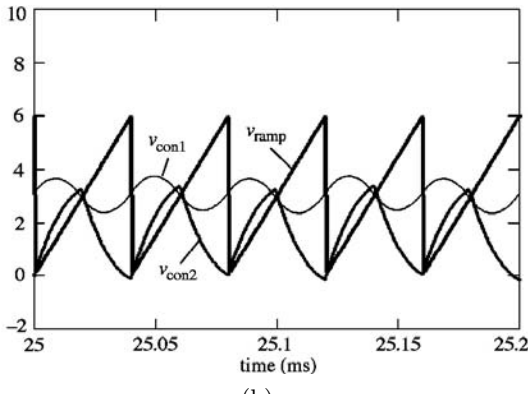
Stable period-1 operation. (a) Control voltages and ramp; (b) inductor currents.

shown in [Figure 7.8 \(b\)](#). Now, if we increase m and examine the waveform, we observe the following qualitative change near the point of border collision.

- Before border collision — Control signal $v_{\text{con}2}$ is above the lower tip of the ramp. Normal operation is maintained, as shown in [Figure 7.9 \(a\)](#).
- After border collision — Control signal $v_{\text{con}2}$ goes slightly underneath the lower tip of the ramp, and then moves upward to hit the ramp from below. Thus, Converter 2 does not turn on its switch at the usual turn-on instant. Instead, it does so at an instant shortly after the vertical edge of v_{ramp} . The duty cycle is disturbed, and chaos begins. [Figure 7.9 \(b\)](#) shows the waveforms shortly after the bifurcation. It may



(a)



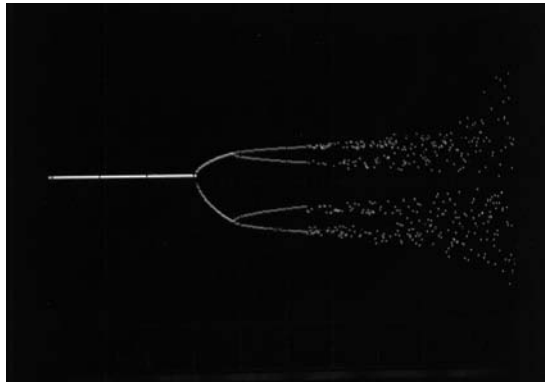
(b)

FIGURE 7.9

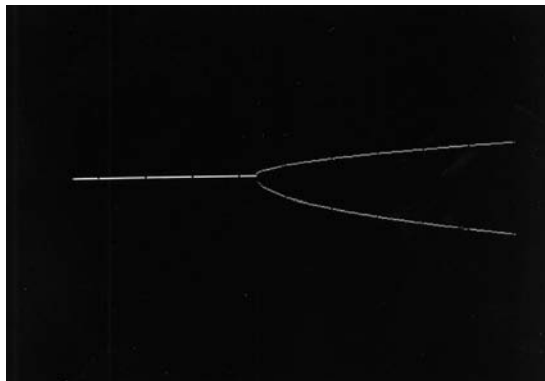
Control voltage waveforms (a) just before border collision ($m = 2.8$); and (b) just after border collision ($m = 3.0$).

appear counter-intuitive that $v_{\text{con}2}$ rises up and hits the ramp from below while the switch of Converter 2 is still off. In fact, this is possible because $v_{\text{con}2}$ is an image of the output voltage which is governed by the entire parallel-connected system. Near the point of border collision, Converter 1 shares most of the load current. Thus, if Converter 1 turns on as usual at the vertical edge of the ramp, the output voltage (and $v_{\text{con}2}$) rises as usual.

We may conclude that the system fails to operate in the expected period-1 regime when m increases to a certain value. This suggests that stable period-1 operation of this system requires keeping m below a certain threshold. In Section 7.6, we will analyze the condition under which this bifurcation occurs.



(a)



(b)

FIGURE 7.10

Bifurcation diagrams with (a) K_{v1} as the bifurcation parameter; (b) K_{v2} as the bifurcation parameter (vertical scale: 0.2 V/div).

7.4 Experimentation

The computer simulations described in the foregoing have essentially provided an initial indication of the possible bifurcation behavior exhibited by the parallel converter system under study. In summary, what these simulations suggest is that

1. the system loses stability via period-doubling if the voltage feedback gains are too large;
2. the behavior of the system is relatively unaffected by variation of the current gain;

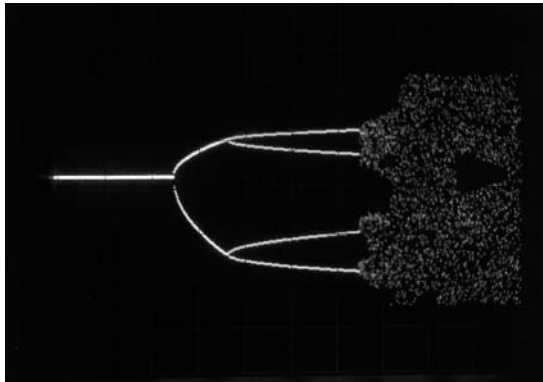


FIGURE 7.11

Bifurcation diagram with both K_{v1} and K_{v2} varied simultaneously (vertical scale: 0.2 V/div).

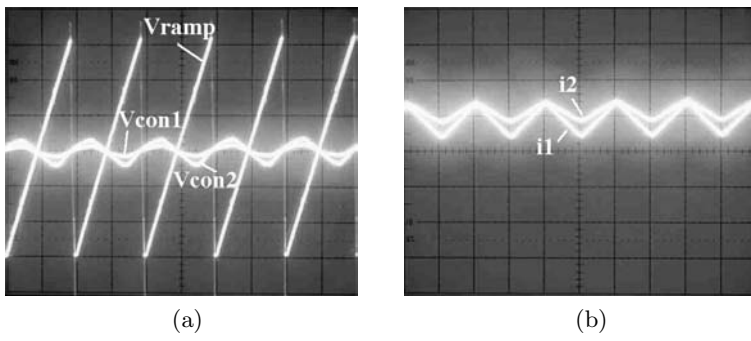


FIGURE 7.12

(a) Control voltage waveforms under stable period-1 operation (vertical scale: 1 V/div, horizontal scale: 20 μ s/div); (b) inductor current waveforms under stable period-1 operation (vertical scale: 0.2 A/div, horizontal scale: 20 μ s/div).

3. the system jumps into chaos when the current sharing ratio m reaches a certain threshold.

Although simulations have been performed using the original piecewise switched model and hence should provide realistic observations, we may still be uncertain about the actual system's behavior which may be different from the simulated behavior due to the presence of device parasitics and switching delays which have not been taken into account in the simulations. Laboratory experiments would be helpful to verify the simulated behavior. In this case, an experimental system of parallel buck converters can be easily constructed

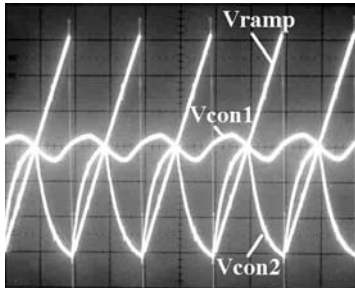


FIGURE 7.13

Control voltage waveforms at the boundary of border collision (vertical scale: 1 V/div, horizontal scale: 20 μ s/div).

according to the circuit shown in Figure 7.1. For ease of comparison, the parameter values used in the experiments are the same as those used in the simulations.

Bifurcation diagrams are captured with K_{v1} and K_{v2} serving as bifurcation parameters. In particular, Figure 7.10 shows the bifurcation diagrams when K_{v1} and K_{v2} are varied individually, and Figure 7.11 shows the bifurcation diagram when K_{v1} and K_{v2} are varied simultaneously. It has been found that the corresponding values of K_{v1} and K_{v2} at the first onset of period-doubling are about 4.0, consistent with our simulation results.

The time-domain waveforms under stable period-1 operation and at the boundary of border collision are also captured. In particular, Figures 7.12 (a) and (b) show the control voltage waveforms and inductor current waveforms under stable period-1 operation. Figure 7.13 shows the control voltage waveforms at the boundary of border collision, which corresponds to current sharing ratio m of about 2.8.

7.5 Analysis of Period-Doubling Bifurcation

From the foregoing simulation and experimental studies, we have identified period-doubling bifurcation in a system of parallel buck converters when the voltage feedback gains are varied. We have also seen how a stable operation suddenly gives way to chaos when the current sharing ratio is increased. In this and the next sections we analyze these bifurcations in terms of a suitable discrete-time model. We will first derive the model, and examine the Jacobian and the way the system loses stability.

7.5.1 Derivation of the Discrete-Time Map

Our purpose in this section is to derive a discrete-time map that describes the dynamics of a system of two buck converters connected in parallel, as defined earlier in [Section 7.2](#) (see [Figure 7.3](#)), in the neighborhood of the period-1 steady state. We let \mathbf{x} be the state vector as defined previously, and further let d_1 and d_2 be the duty cycle of Converter 1 (master) and Converter 2 (slave), respectively. The discrete-time map that we aim to find takes the following form:

$$\mathbf{x}_{n+1} = \mathbf{f}(\mathbf{x}_n, d_{1,n}, d_{2,n}) \quad (7.8)$$

where subscript n denotes the value at the beginning of the n th cycle, i.e., $\mathbf{x}_n = \mathbf{x}(nT)$. For the closed-loop system, we also need to find the feedback equations that relate $d_{1,n}$ and $d_{2,n}$ to \mathbf{x}_n .

The state equations are given in (7.4) for different switch states. The order in which the system toggles between the switch states depends on d_1 and d_2 . We will study periodic orbits for which $d_{2,n} > d_{1,n}$ for all n as this allows a convenient derivation of the discrete-time model. In particular the assumption $d_2 > d_1$ is consistent with our simulation study since r_{L1} has a lower value than r_{L2} . Note that such an assumption loses no generality.

Recall that if $d_2 > d_1$, the state “ S_1 on and S_2 off” should be omitted. Hence, we have three switch states:

1. For $nT < t \leq nT + d_{1,n}T$, both S_1 and S_2 are turned on.
2. For $nT + d_{1,n}T < t \leq nT + d_{2,n}T$, S_1 is turned off and S_2 remains on.
3. For $nT + d_{2,n}T < t \leq (n+1)T$, both S_1 and S_2 are off.

In each switch state, the describing state equation is $\dot{\mathbf{x}} = \mathbf{A}_j \mathbf{x} + \mathbf{B}_j E$, where $j = 1, 3, 4$. (Note that $j = 2$ does not appear here.) For each state equation we can derive the solution, and by stacking up the solutions, \mathbf{x}_{n+1} can be expressed in terms of \mathbf{x}_n , $d_{1,n}$ and $d_{2,n}$, i.e.,

$$\begin{aligned} \mathbf{x}_{n+1} = & \Phi_4((1 - d_{2,n})T)\Phi_3((d_{2,n} - d_{1,n})T)\Phi_1(d_{1,n}T)\mathbf{x}_n \\ & + \Phi_4((1 - d_{2,n})T)\Phi_3((d_{2,n} - d_{1,n})T)(\Phi_1(d_{1,n}T) - \mathbf{1})\mathbf{A}_1^{-1}\mathbf{B}_1E \\ & + \Phi_4((1 - d_{2,n})T)(\Phi_3((d_{2,n} - d_{1,n})T) - \mathbf{1})\mathbf{A}_3^{-1}\mathbf{B}_3E \\ & + (\Phi_4((1 - d_{2,n})T) - \mathbf{1})\mathbf{A}_4^{-1}\mathbf{B}_4E, \end{aligned} \quad (7.9)$$

where $\mathbf{1}$ is the unit matrix, and $\Phi_j(\xi)$ is the transition matrix corresponding to \mathbf{A}_j and is given by

$$\Phi_j(\xi) = e^{\mathbf{A}_j \xi} = \mathbf{1} + \sum_{k=1}^{\infty} \frac{1}{k!} \mathbf{A}_j^k \xi^k, \quad \text{for } j = 1, 2, 3, 4. \quad (7.10)$$

For the parallel-connected buck converters, we let $\mathbf{A} = \mathbf{A}_1 = \mathbf{A}_2 = \mathbf{A}_3 = \mathbf{A}_4$ and $\Phi(\xi) = \Phi_1(\xi) = \Phi_2(\xi) = \Phi_3(\xi) = \Phi_4(\xi)$. Hence, (7.9) can be written as

$$\begin{aligned} \mathbf{x}_{n+1} = & \Phi(T)\mathbf{x}_n + \Phi(T)\mathbf{A}^{-1}\mathbf{B}_1E + \Phi((1 - d_{1,n})T)\mathbf{A}^{-1}(\mathbf{B}_3 - \mathbf{B}_1)E \\ & + \Phi((1 - d_{2,n})T)\mathbf{A}^{-1}(\mathbf{B}_4 - \mathbf{B}_3)E - \mathbf{A}^{-1}\mathbf{B}_4E. \end{aligned} \quad (7.11)$$

Our next step is to find the feedback relations that connect the duty cycles and the state variables. The control voltages $v_{\text{con}1}$ and $v_{\text{con}2}$, as given before by (7.2) and (7.3), can be rewritten as

$$v_{\text{con}1} = U_1 + \kappa_1^T \mathbf{x} \quad (7.12)$$

$$v_{\text{con}2} = U_2 + \kappa_2^T \mathbf{x} \quad (7.13)$$

where U_1 and U_2 are constants, and the gain vectors κ_1 and κ_2 are

$$\kappa_1^T = [-K_{v1} \ 0 \ 0] \quad \text{and} \quad \kappa_2^T = [-K_{v2} \ K_im \ -K_i]. \quad (7.14)$$

The ramp function can also be rewritten simply as

$$v_{\text{ramp}} = \alpha + \beta(t \bmod T), \quad (7.15)$$

where α and β are constants. To find the defining equations for the duty cycles, we first note that the switches are turned off when $v_{\text{con}1} = v_{\text{ramp}}$ and $v_{\text{con}2} = v_{\text{ramp}}$. Now, define $s_1(\mathbf{x}_n, d_{1,n})$ and $s_2(\mathbf{x}_n, d_{1,n}, d_{2,n})$ as

$$\begin{aligned} s_1(\mathbf{x}_n, d_{1,n}) &\stackrel{\text{def}}{=} v_{\text{con}1} - v_{\text{ramp}} \\ &= U_1 + \kappa_1^T \mathbf{x}(d_{1,n}T) - (\alpha + \beta d_{1,n}T) \\ &= U_1 + \kappa_1^T [\Phi(d_{1,n}T) \mathbf{x}_n + (\Phi(d_{1,n}T) - \mathbf{1}) \mathbf{A}^{-1} \mathbf{B}_1 E] \\ &\quad - (\alpha + \beta d_{1,n}T) \end{aligned} \quad (7.16)$$

$$\begin{aligned} s_2(\mathbf{x}_n, d_{1,n}, d_{2,n}) &\stackrel{\text{def}}{=} v_{\text{con}2} - v_{\text{ramp}} \\ &= U_2 + \kappa_2^T \mathbf{x}(d_{2,n}T) - (\alpha + \beta d_{2,n}T) \\ &= U_2 + \kappa_2^T [\Phi(d_{2,n}T) \mathbf{x}_n + \Phi(d_{2,n}T) \mathbf{A}^{-1} \mathbf{B}_1 E \\ &\quad + \Phi((d_{2,n} - d_{1,n})T) \mathbf{A}^{-1} (\mathbf{B}_3 - \mathbf{B}_1) E - \mathbf{A}^{-1} \mathbf{B}_3 E] \\ &\quad - (\alpha + \beta d_{2,n}T). \end{aligned} \quad (7.17)$$

Thus, S_1 and S_2 are turned off, respectively, when

$$s_1(\mathbf{x}_n, d_{1,n}) = 0 \quad (7.18)$$

and

$$s_2(\mathbf{x}_n, d_{1,n}, d_{2,n}) = 0. \quad (7.19)$$

Solving (7.18) and (7.19), $d_{1,n}$ and $d_{2,n}$ can be obtained. Combining with (7.11), we have the discrete-time iterative map for the closed-loop system.

7.5.2 Derivation of the Jacobian

The Jacobian plays an important role in the study of dynamical systems [2, 162]. The essence of using a Jacobian in the analysis of dynamical systems lies in the capture of the dynamics in the small neighborhood of an equilibrium

point or orbit (stable or unstable). We will make use of this conventional method to examine the bifurcation phenomena observed in [Section 7.5.3](#). But before we move on, we need to find the necessary expressions that enable the Jacobian to be computed.

Suppose the equilibrium point is given by $\mathbf{x}(nT) = \mathbf{X}$. The Jacobian of the discrete-time map evaluated at the equilibrium point can be written as follows:

$$\begin{aligned} J(\mathbf{X}) &= \frac{\partial \mathbf{f}}{\partial \mathbf{x}_n} - \frac{\partial \mathbf{f}}{\partial d_{1,n}} \left(\frac{\partial s_1}{\partial d_{1,n}} \right)^{-1} \left(\frac{\partial s_1}{\partial \mathbf{x}_n} \right) \\ &\quad - \frac{\partial \mathbf{f}}{\partial d_{2,n}} \left(\frac{\partial s_2}{\partial d_{2,n}} \right)^{-1} \left[\left(\frac{\partial s_2}{\partial \mathbf{x}_n} \right) \right. \\ &\quad \left. + \frac{\partial s_2}{\partial d_{1,n}} \left(\frac{\partial s_1}{\partial d_{1,n}} \right)^{-1} \left(\frac{\partial s_1}{\partial \mathbf{x}_n} \right) \right] \Big|_{\mathbf{x}_n=\mathbf{X}}, \end{aligned} \quad (7.20)$$

where

$$\frac{\partial \mathbf{f}}{\partial \mathbf{x}_n} = \begin{bmatrix} \frac{\partial f_1}{\partial v_n} & \frac{\partial f_1}{\partial i_{1,n}} & \frac{\partial f_1}{\partial i_{2,n}} \\ \frac{\partial f_2}{\partial v_n} & \frac{\partial f_2}{\partial i_{1,n}} & \frac{\partial f_2}{\partial i_{2,n}} \\ \frac{\partial f_3}{\partial v_n} & \frac{\partial f_3}{\partial i_{1,n}} & \frac{\partial f_3}{\partial i_{2,n}} \end{bmatrix} \quad (7.21)$$

$$\frac{\partial \mathbf{f}}{\partial d_{1,n}} = \left[\frac{\partial f_1}{\partial d_{1,n}} \quad \frac{\partial f_2}{\partial d_{1,n}} \quad \frac{\partial f_3}{\partial d_{1,n}} \right]^T \quad (7.22)$$

$$\frac{\partial s_1}{\partial \mathbf{x}_n} = \begin{bmatrix} \frac{\partial s_1}{\partial v_n} & \frac{\partial s_1}{\partial i_{1,n}} & \frac{\partial s_1}{\partial i_{2,n}} \end{bmatrix} \quad (7.23)$$

$$\frac{\partial \mathbf{f}}{\partial d_{2,n}} = \left[\frac{\partial f_1}{\partial d_{2,n}} \quad \frac{\partial f_2}{\partial d_{2,n}} \quad \frac{\partial f_3}{\partial d_{2,n}} \right]^T \quad (7.24)$$

$$\frac{\partial s_2}{\partial \mathbf{x}_n} = \begin{bmatrix} \frac{\partial s_2}{\partial v_n} & \frac{\partial s_2}{\partial i_{1,n}} & \frac{\partial s_2}{\partial i_{2,n}} \end{bmatrix}. \quad (7.25)$$

Using (7.11), (7.16) and (7.17), we can find all the derivatives in (7.20). First, $\partial \mathbf{f} / \partial \mathbf{x}_n$ can be found from (7.11), i.e.,

$$\frac{\partial \mathbf{f}}{\partial \mathbf{x}_n} = \Phi(T). \quad (7.26)$$

Also, direct differentiation gives $\partial \mathbf{f} / \partial d_{1,n}$ as

$$\frac{\partial \mathbf{f}}{\partial d_{1,n}} = -T\Phi((1 - d_{1,n})T)(\mathbf{B}_3 - \mathbf{B}_1)\mathbf{E}. \quad (7.27)$$

Likewise, we get $\partial \mathbf{f} / \partial d_{2,n}$ as

$$\frac{\partial \mathbf{f}}{\partial d_{2,n}} = -T\Phi((1-d_{2,n})T)(\mathbf{B}_4 - \mathbf{B}_3)E. \quad (7.28)$$

From (7.16), we obtain $\partial s_1 / \partial x_n$ readily as

$$\frac{\partial s_1}{\partial \mathbf{x}_n} = \kappa_1^T \Phi(d_{1,n}T). \quad (7.29)$$

Again by direct differentiation, we get

$$\begin{aligned} \frac{\partial s_1}{\partial d_{1,n}} &= \kappa_1^T \frac{\partial \Phi(d_{1,n}T)}{\partial d_{1,n}} \mathbf{x}_n + \kappa_1^T \frac{\partial(\Phi(d_{1,n}T) - \mathbf{1}) \mathbf{A}^{-1} \mathbf{B}_1}{\partial d_{1,n}} E - \beta T \\ &= \kappa_1^T (\mathbf{A}T\Phi(d_{1,n}T)) \mathbf{x}_n + \kappa_1^T (\Phi(d_{1,n}T) \mathbf{B}_1 T) E - \beta T \\ &= T\kappa_1^T \Phi(d_{1,n}T) (\mathbf{A}\mathbf{x}_n + \mathbf{B}_1 E) - \beta T. \end{aligned} \quad (7.30)$$

And from (7.17), we get

$$\frac{\partial s_2}{\partial \mathbf{x}_n} = \kappa_2^T \Phi(d_{2,n}T). \quad (7.31)$$

Finally, we need to get $\partial s_2 / \partial d_{2,n}$ and $\partial s_2 / \partial d_{1,n}$. From (7.17) we have

$$\begin{aligned} \frac{\partial s_2}{\partial d_{2,n}} &= \kappa_2^T \frac{\partial \Phi(d_{2,n}T)}{\partial d_{2,n}} \mathbf{x}_n + \kappa_2^T \frac{\partial \Phi(d_{2,n}T) \mathbf{A}^{-1} \mathbf{B}_1}{\partial d_{2,n}} E \\ &\quad + \kappa_2^T \frac{\partial \Phi((d_{2,n} - d_{1,n})T) \mathbf{A}^{-1} (\mathbf{B}_3 - \mathbf{B}_1)}{\partial d_{2,n}} E - \beta T \\ &= \kappa_2^T (\mathbf{A}T\Phi(d_{2,n}T)) \mathbf{x}_n + \kappa_2^T (\Phi(d_{2,n}T) \mathbf{B}_1 T) E \\ &\quad + \kappa_2^T \Phi((d_{2,n} - d_{1,n})T) (\mathbf{B}_3 - \mathbf{B}_1) TE - \beta T \\ &= T\kappa_2^T \Phi(d_{2,n}T) (\mathbf{A}\mathbf{x}_n + \mathbf{B}_1 E) \\ &\quad + T\kappa_2^T \Phi((d_{2,n} - d_{1,n})T) (\mathbf{B}_3 - \mathbf{B}_1) E - \beta T, \end{aligned} \quad (7.32)$$

and

$$\begin{aligned} \frac{\partial s_2}{\partial d_{1,n}} &= \kappa_2^T \frac{\partial \Phi((d_{2,n} - d_{1,n})T) \mathbf{A}^{-1} (\mathbf{B}_3 - \mathbf{B}_1) E}{\partial d_{1,n}} \\ &= -T\kappa_2^T \Phi((d_{2,n} - d_{1,n})T) (\mathbf{B}_3 - \mathbf{B}_1) E. \end{aligned} \quad (7.33)$$

Now, putting all the derivatives into (7.20) gives

$$\begin{aligned} J(\mathbf{X}) &= \Phi(T) + \frac{\Phi((1-d_{1,n})T) (\mathbf{B}_3 - \mathbf{B}_1) E \kappa_1^T \Phi(d_{1,n}T)}{\kappa_1^T \Phi(d_{1,n}T) (\mathbf{A}\mathbf{x}_n + \mathbf{B}_1 E) - \beta} \\ &\quad + \frac{\Phi((1-d_{2,n})T) (\mathbf{B}_4 - \mathbf{B}_3) E [\kappa_2^T \Phi(d_{2,n}T) + W]}{Z} \end{aligned} \quad (7.34)$$

where

$$W = \frac{-\kappa_2^T \Phi((d_{2,n} - d_{1,n})T)(\mathbf{B}_3 - \mathbf{B}_1)E\kappa_1^T \Phi(d_{1,n}T)}{\kappa_1^T \Phi(d_{1,n}T)(\mathbf{A}\mathbf{x}_n + \mathbf{B}_1E) - \beta}, \quad (7.35)$$

$$\begin{aligned} Z = & \kappa_2^T \Phi(d_{2,n}T)(\mathbf{A}\mathbf{x}_n + \mathbf{B}_1E) \\ & + \kappa_2^T \Phi((d_{2,n} - d_{1,n})T)(\mathbf{B}_3 - \mathbf{B}_1)E - \beta. \end{aligned} \quad (7.36)$$

Numerical algorithms can now be developed for computing $J(\mathbf{X})$ and hence the characteristic multipliers, as will be shown shortly.

7.5.3 Characteristic Multipliers and Period-Doubling Bifurcation

The Jacobian derived in the foregoing subsection provides a means to evaluate the dynamics of the system. Here, we study in particular the loci of the characteristic multipliers (also called eigenvalues), the aim being to identify possible bifurcation scenarios as the voltage feedback gains are varied. To find the characteristic multipliers, we solve the following polynomial equation in λ , whose roots actually give the characteristic multipliers.

$$\det[\lambda \mathbf{1} - J(\mathbf{X})] = 0 \quad (7.37)$$

where $J(\mathbf{X})$ is the Jacobian found previously. We will pay attention to the movement of the characteristic multipliers as K_{v1} and K_{v2} are varied. Any crossing from the interior of the unit circle to the exterior indicates a bifurcation. In particular, if a real characteristic multiplier goes through -1 as it moves out of the unit circle, a period-doubling occurs [85, 162].

Using (7.34), we can generate loci of characteristic multipliers numerically. Since we are interested here in varying K_{v1} and K_{v2} , we keep $m = 1$, thereby ensuring that the system is remote from any border collision due possibly to large m , as we have seen previously in the simulations and experiments. Other parameter values are the same as those used in the simulations. Now, we can proceed with the numerical calculations of the eigenvalues. Typical loci are tabulated in [Tables 7.2](#) and [7.3](#), which are graphically illustrated in [Figures 7.14](#) and [7.15](#). Both loci indicate a period-doubling bifurcation as K_{v1} and K_{v2} vary. This agrees with the simulation and experimental results in [Sections 7.3](#) and [7.4](#).

7.6 Analysis of Border Collision

As observed in the simulation, a border collision occurs when m increases beyond a certain limit. In this section, we attempt to analyze this border collision and specifically to find the limit of m below which the system maintains

TABLE 7.2Characteristic multipliers for different values of K_{v1} .

K_{v1}	Characteristic multipliers	Remarks
2.60	$-0.576 \pm j0.394, 0.997$	Stable 1T
3.00	$-0.628 \pm j0.273, 0.997$	Stable 1T
3.20	$-0.651 \pm j0.189, 0.997$	Stable 1T
3.38	$-0.668, -0.668, 0.997$	Stable 1T
3.45	$-0.784, -0.574, 0.997$	Stable 1T
3.60	$-0.890, -0.499, 0.997$	Stable 1T
3.80	$-0.986, -0.444, 0.997$	Stable 1T
3.85	$-1.000, -0.433, 0.997$	Period-doubling

TABLE 7.3Characteristic multipliers for different values of K_{v2} .

K_{v2}	Characteristic multipliers	Remarks
2.40	$-0.565 \pm j0.300, 0.997$	Stable 1T
2.60	$-0.590 \pm j0.263, 0.997$	Stable 1T
3.00	$-0.636 \pm j0.168, 0.997$	Stable 1T
3.28	$-0.664, -0.664, 0.997$	Stable 1T
3.40	$-0.779, -0.572, 0.997$	Stable 1T
3.60	$-0.865, -0.522, 0.997$	Stable 1T
4.00	$-0.982, -0.470, 0.997$	Stable 1T
4.10	$-1.000, -0.462, 0.997$	Period-doubling

stable operation. In the following study, we assume that K_{v1} and K_{v2} are kept within the stable range so that the system is remote from any period-doubling bifurcation due possibly to large K_{v1} and K_{v2} .

Inspection of the loci of the characteristic multipliers reveals that a sudden “jump” occurs as m increases, which is typical of border collision [104, 172]. Such a bifurcation arises when $v_{\text{con}1}$ or $v_{\text{con}2}$ begins to pass over or under the ramp without hitting it during the whole switching period. This situation is illustrated in [Figure 7.16](#). As m increases, the system traverses from one situation where $v_{\text{con}1}$ and $v_{\text{con}2}$ both hit the ramp, to another where $v_{\text{con}1}$ or $v_{\text{con}2}$ misses the ramp. Such a transition, as we have explained before in [Chapter 5](#), is a consequence of saturating nonlinearity.

By studying the expressions of $v_{\text{con}1}$, $v_{\text{con}2}$ and v_{ramp} , we can estimate the critical value of m , at which border collision takes place. Ignoring the ripple, we have $v \approx V_{\text{ref}}$ in the steady state. Thus, (7.2) and (7.3) can be approximated by

$$v_{\text{con}1}(t) \approx V_{\text{offset}}, \quad (7.38)$$

$$v_{\text{con}2}(t) \approx V_{\text{offset}} - K_i[i_2(t) - mi_1(t)]. \quad (7.39)$$

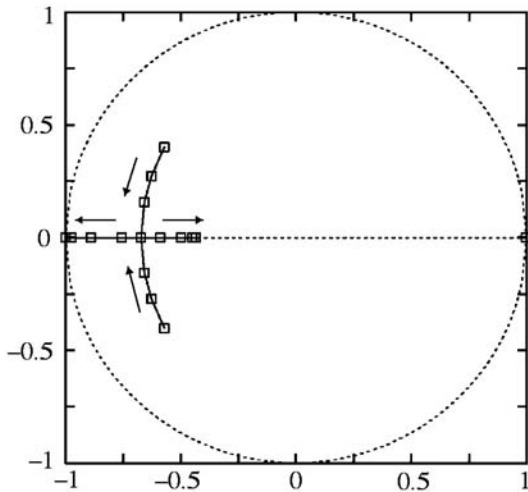


FIGURE 7.14

Locus of characteristic multipliers as K_{v1} varies. Arrows indicate increasing K_{v1} .

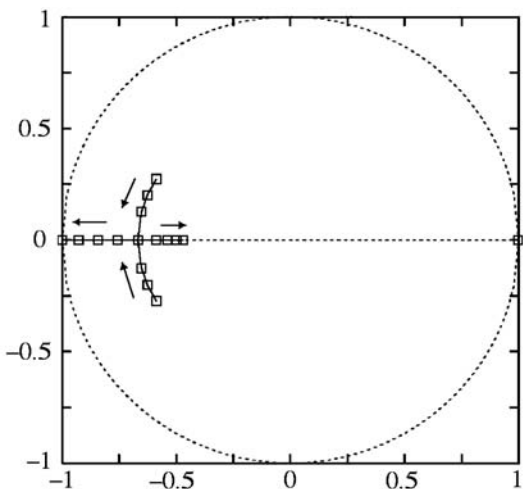
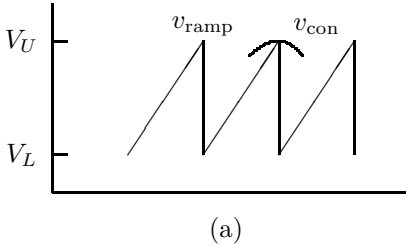


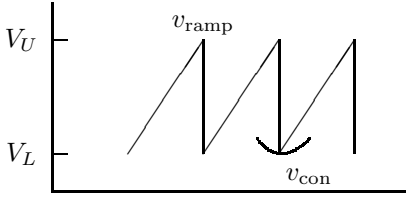
FIGURE 7.15

Locus of characteristic multipliers as K_{v2} varies. Arrows indicate increasing K_{v2} .

Since V_{offset} is always set between V_L and V_U , $v_{\text{con}1}$ will always hit the ramp during a switching cycle. We therefore need only to focus on $v_{\text{con}2}(nT)$. As mentioned before, we assume that $d_2 > d_1$ in the neighborhood of the period-



(a)



(b)

FIGURE 7.16

The two possible border collision scenarios.

1 orbit. Also, neglecting the middle period $(d_{2,n} - d_{1,n})T$ in the period-1 orbit and assuming $i_2(d_{1,n}T) \approx mi_1(d_{1,n}T)$, and neglecting the ESRs of the inductors, we may express $i_1(nT)$ and $i_2(nT)$ as

$$i_1(nT) = i_1(d_{1,n}T) - \frac{v}{L_1}(1 - d_{1,n})T, \quad (7.40)$$

$$i_2(nT) = i_2(d_{1,n}T) - \frac{v}{L_2}(1 - d_{1,n})T. \quad (7.41)$$

Putting (7.40) and (7.41) in (7.39), we get

$$v_{\text{con}2}(nT) = V_{\text{offset}} - K_i v(1 - d_{1,n})T \left(\frac{m}{L_1} - \frac{1}{L_2} \right). \quad (7.42)$$

Now, we may substitute either $v_{\text{con}2}(nT) = V_L$ or $v_{\text{con}2}(nT) = V_U$ in (7.42) to obtain the critical value of m . In particular, putting $v_{\text{con}2}(nT) = V_L$ in (7.42) gives

$$m_{\text{crit}} = \left(\frac{V_{\text{offset}} - V_L}{K_i v(1 - d_{1,n})T} + \frac{1}{L_2} \right) L_1, \quad (7.43)$$

where m_{crit} is the critical value of m at which $v_{\text{con}2}$ just hits V_L at $t = nT$. Furthermore, $v_{\text{con}2}(nT) = V_U$ gives a negative value for m , which is not possible, thus ruling out the possibility of a border collision with $v_{\text{con}2}$ hitting V_U .

Using the same set of parameter values and voltages as in [Section 7.3](#), we find that $m_{\text{crit}} = 2.75$ which agrees very well with the bifurcation diagram shown in [Figure 7.7](#).

The above result clearly illustrates that the current-sharing ratio m in a master-slave controlled parallel converter system must be kept below a certain value in order to ensure a stable period-1 operation.

7.7 A Remark on Modeling: Can It Be Simpler?

As a final remark before closing this chapter, the analysis here has followed a discrete-time approach, involving the derivation of an iterative map and the analysis of the Jacobian evaluated at the equilibrium point. We have shown that the bifurcation phenomena are well captured by the iterative map, although the complicated and implicit form of the map admits only numerical studies. Moreover, we stress that this choice of analytical approach is unavoidable because the basic phenomenology is period-doubling which necessitates a model that characterizes the system at least as frequently as one switching period. In the next chapter we will study a system of parallel boost converters which apparently does not require such frequent characterization. As we will see shortly, similar to the case of the free-running Ćuk converter, averaged models are found to be adequate since the basic phenomenology is a low-frequency Hopf-type bifurcation.

Slow-Scale Bifurcation Behavior of Parallel-Connected Boost Converters via Averaged Models

In this chapter we continue our study of parallel converter systems. In particular, our choice of the constituent converters is the boost-type converter. Because of the fundamental difference in the phenomenology between the boost converter and the buck converter, the analysis adopted here differs from that used in the previous chapter. Precisely, in the previous chapter, we have applied the discrete-time modeling approach to analyze period-doubling bifurcation in a system of buck converters connected in parallel, which is essentially a high-frequency bifurcation phenomenon. For the case of connecting boost converters in parallel, however, initial experimentation shows that it exhibits a kind of low-frequency bifurcation. As explained before in [Chapter 6](#), this type of bifurcation should be well within the capability of the averaging approach for modeling its behavior. In the rest of this chapter, we will describe the details of this system and how the averaged model reveals its bifurcation behavior.

8.1 The System of Parallel-Connected Boost Converters

The system under study here is structurally the same as the one described in [Section 7.1.2](#). Thus, the basic control equations are as given before in (7.1) to (7.3). However, instead of the buck converter, the boost converter is employed for both Converters 1 and 2. [Figure 8.1](#) shows two boost converters connected in parallel. As in the case of the parallel buck converters, the presence of four switches (S_1 , S_2 , D_1 and D_2) allows a total of sixteen possible switch states, and in each switch state the circuit is a linear third-order circuit.

Similar to the case of the parallel buck converters, when the converters are operating in continuous conduction mode, diode D_i is always in complementary state to switch S_i , for $i = 1, 2$. That is, when S_i is on, D_i is off, and vice versa. Hence, only four switch states are possible during a switching cycle, namely

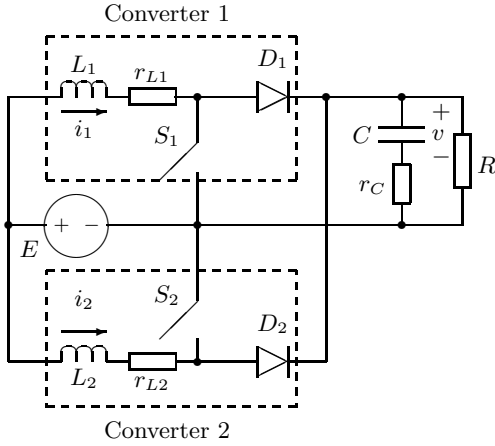


FIGURE 8.1
Two parallel-connected boost converters.

- (i) S_1 and S_2 are on;
- (ii) S_1 is on and S_2 is off;
- (iii) S_1 is off and S_2 is on;
- (iv) S_1 and S_2 are off.

The state equations corresponding to these switch states are likewise given by (7.4), with the \mathbf{A} 's and \mathbf{B} 's given by

$$\mathbf{A}_1 = \begin{bmatrix} -\frac{r_{L1}}{L_1} & 0 & 0 \\ 0 & -\frac{r_{L2}}{L_2} & 0 \\ 0 & 0 & -\frac{1}{C(R+r_C)} \end{bmatrix}, \quad (8.1)$$

$$\mathbf{A}_2 = \begin{bmatrix} -\frac{r_{L1}}{L_1} & 0 & 0 \\ 0 & -\frac{1}{L_2}(\frac{r_C R}{R+r_C} + r_{L2}) - \frac{R}{L_2(R+r_C)} & \frac{1}{C(R+r_C)} \\ 0 & \frac{R}{C(R+r_C)} & -\frac{1}{C(R+r_C)} \end{bmatrix}, \quad (8.2)$$

$$\mathbf{A}_3 = \begin{bmatrix} -\frac{1}{L_1}(\frac{r_C R}{R+r_C} + r_{L1}) & 0 & -\frac{R}{L_1(R+r_C)} \\ 0 & -\frac{r_{L2}}{L_2} & 0 \\ \frac{R}{C(R+r_C)} & 0 & -\frac{1}{C(R+r_C)} \end{bmatrix}, \quad (8.3)$$

$$\mathbf{A}_4 = \begin{bmatrix} -\frac{1}{L_1} \left(\frac{r_C R}{R+r_C} + r_{L1} \right) & 0 & -\frac{R}{L_1(R+r_C)} \\ 0 & -\frac{1}{L_2} \left(\frac{r_C R}{R+r_C} + r_{L2} \right) - \frac{R}{L_2(R+r_C)} & 1 \\ \frac{R}{C(R+r_C)} & \frac{R}{C(R+r_C)} & -\frac{1}{C(R+r_C)} \end{bmatrix}, \quad (8.4)$$

$$\mathbf{B}_1 = \mathbf{B}_2 = \mathbf{B}_3 = \mathbf{B}_4 = \begin{bmatrix} \frac{1}{L_1} \\ \frac{1}{L_2} \\ 0 \end{bmatrix}. \quad (8.5)$$

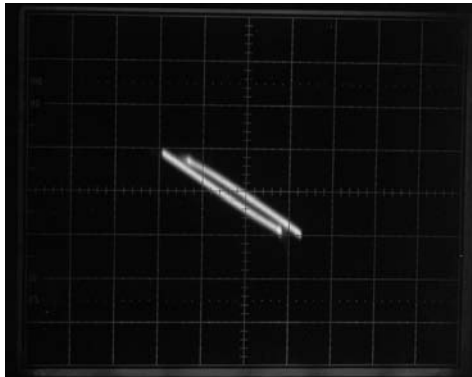
As in the case of the buck system studied in [Chapter 7](#), the sequence of switch states, in general, takes the order as written in (7.4), i.e., starting with “ S_1 and S_2 on” and ending with “ S_1 and S_2 off” in a switching cycle. However, either “ S_1 on S_2 off” or “ S_1 off S_2 on” (not both) goes in the middle, depending upon the duty cycles of S_1 and S_2 . In the case where S_1 has a larger duty cycle, we should omit the third equation in (7.4), and likewise for the case where S_2 has a larger duty cycle. This should be taken care of in the simulation and analysis.

8.2 Initial Experimentation

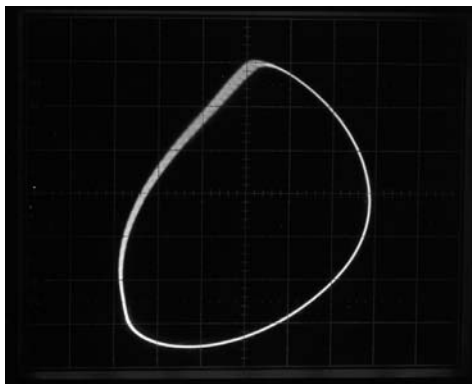
We begin our investigation with an experimental system which is constructed according to the circuit shown in [Figure 7.1](#), with Converters 1 and 2 both realized by the boost converter. Our purpose is to get some initial idea of the possible kind of behavior exhibited by this system. The circuit parameters are shown in [Table 8.1](#).

TABLE 8.1
Circuit parameters used in initial experimentation.

Circuit Components	Values
Switching Period T	$40 \mu\text{s}$
Input Voltage E	12 V
Output Voltage v	24 V
Reference Voltage V_{ref}	24 V
Inductance L_1	0.004 H
Inductance L_2	0.004 H
Capacitance C	$10 \mu\text{F}$
Load Resistance R	10Ω



(a)

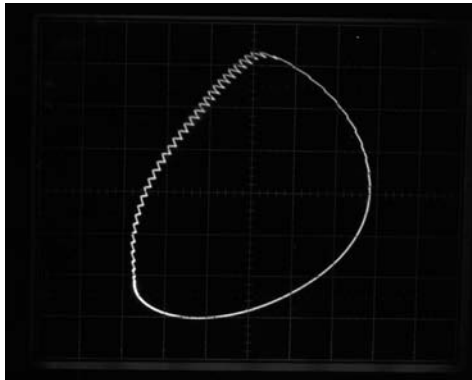


(b)

FIGURE 8.2

Sequence of changes observed experimentally when feedback gain K_{v2} is increased. (a) Stable period-1 orbit (horizontal scale: 5 V/div, vertical scale: 0.04 A/div); (b) quasi-periodic orbit; (c) limit cycle (horizontal scale: 10 V/div, vertical scale: 0.4 A/div) [72].

Of particular interest is the way the system changes its qualitative behavior when some parameters are varied. In the experiment, we try varying the feedback gains K_{v1} , K_{v2} and K_i , and observe the changes. The main observation is that the system loses stability as K_{v1} or K_{v2} is increased, while its qualitative behavior is unaffected by the variation of K_i . The way it loses stability is via a typical Hopf-type bifurcation in which the period-1 operation bifurcates into quasi-periodic orbits and limit cycles. To exemplify the situation, we show in Figure 8.2 the sequence of changes when we increase K_{v2} . In all the oscilloscope pictures, y -axis corresponds to i_1 and x -axis corresponds to v . Here, we see a stable period-1 orbit in Figure 8.2 (a), a quasi-periodic



(c)

FIGURE 8.2 continued.

orbit in [Figure 8.2 \(b\)](#), and a limit cycle in [Figure 8.2 \(c\)](#). To confirm the quasi-periodicity and the periodicity of the limit cycle observed in [Figures 8.2 \(b\)](#) and [\(c\)](#), we show the corresponding stroboscopic maps in [Figure 8.3](#).

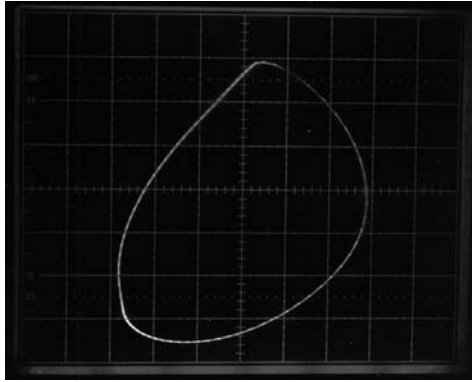
8.3 Averaged Model for Two Parallel Boost Converters

From the initial experimentation, we have learned that the system exhibits a Hopf-type bifurcation which is essentially a low-frequency phenomenon since the quasi-periodic orbits or limit cycles formed after the bifurcation point are low-frequency orbits. Averaged models are therefore adequate in describing this behavior. In the following we will derive an averaged model for the system of parallel boost converters and use it to predict the onset of Hopf bifurcation.

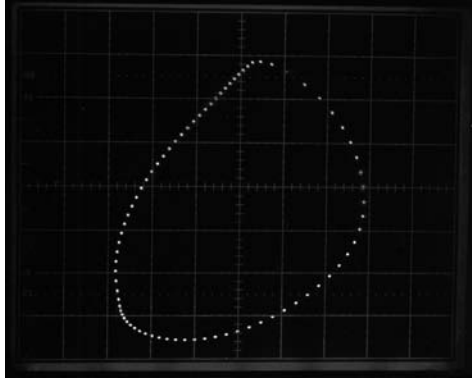
8.3.1 Derivation of State Equations

The averaged model for the parallel-connected boost converters is shown in [Figure 8.4](#). We assume that r_{L1} , r_{L2} and r_C are zero in order to simplify the subsequent analysis. The system can be represented by the averaged equations:

$$\begin{aligned}\frac{di_1}{dt} &= \frac{-(1-d_1)v}{L_1} + \frac{E}{L_1} \\ \frac{di_2}{dt} &= \frac{-(1-d_2)v}{L_2} + \frac{E}{L_2}\end{aligned}\tag{8.6}$$



(a)



(b)

FIGURE 8.3

(a) Stroboscopic map of Figure 8.2 (b) showing quasi-periodic orbit; (b) stroboscopic map of Figure 8.2 (c) showing limit cycle [72]. Horizontal scale: 10 V/div, vertical scale: 0.4 A/div.

$$\frac{dv}{dt} = \frac{(1 - d_1)i_1}{C} + \frac{(1 - d_2)i_2}{C} - \frac{v}{RC},$$

where d_1 and d_2 are the duty cycles of Converter 1 and Converter 2. Also, the particular control method dictates that the duty cycles be given by:

$$d_1 = D - k_{v1}(v - V_{\text{ref}}) \quad (8.7)$$

and

$$d_2 = D - k_{v2}(v - V_{\text{ref}}) - k_i(i_2 - i_1), \quad (8.8)$$

where D is the steady-state duty cycle, $k_{v1} = K_{v1}/(V_U - V_L)$, $k_{v2} = K_{v2}/(V_U - V_L)$ and $k_i = K_i/(V_U - V_L)$. Furthermore, $0 < d_1 < 1$ and $0 < d_2 < 1$ should

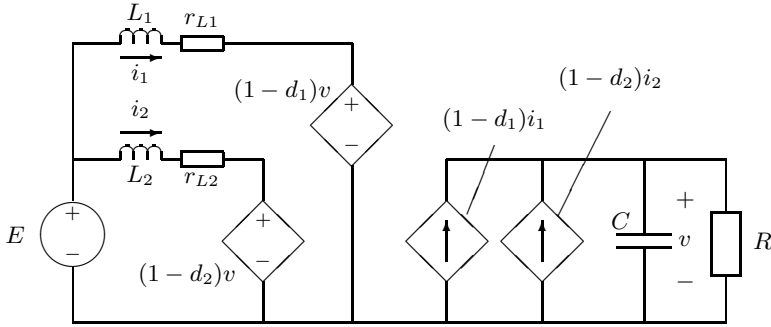


FIGURE 8.4

Averaged model of parallel-connected boost converters.

be satisfied. Putting (8.7) and (8.8) into (8.6), we get the following state equations that describe the dynamics of the system:

$$\begin{aligned}\frac{di_1}{dt} &= \frac{-(1 - D + k_{v1}(v - V_{\text{ref}}))v}{L_1} + \frac{E}{L_1} \\ \frac{di_2}{dt} &= \frac{-(1 - D + k_{v2}(v - V_{\text{ref}}) + k_i(i_2 - i_1))v}{L_2} + \frac{E}{L_2} \\ \frac{dv}{dt} &= \frac{(1 - D + k_{v1}(v - V_{\text{ref}}))i_1}{C} \\ &\quad + \frac{(1 - D + k_{v2}(v - V_{\text{ref}}) + k_i(i_2 - i_1))i_2}{C} - \frac{v}{RC}. \end{aligned} \quad (8.9)$$

The state equations are valid only when $0 < d_1 < 1$ and $0 < d_2 < 1$. Such conditions are satisfied when the system is operating in the neighborhood of the stable equilibrium state.

8.3.2 Dimensionless Equations

The afore-derived state equations can be put in a dimensionless form. We define the dimensionless state variables as follows:

$$x_1 = \frac{i_1 R}{V_{\text{ref}}}, x_2 = \frac{i_2 R}{V_{\text{ref}}}, x_3 = \frac{v}{V_{\text{ref}}}. \quad (8.10)$$

We also define the dimensionless time and parameters as follows:

$$\tau = \frac{t}{T}, \xi_1 = \frac{L_1}{RT}, \xi_2 = \frac{L_2}{RT}, \zeta = \frac{CR}{T}, \quad (8.11)$$

$$\kappa_{v1} = k_{v1} V_{\text{ref}}, \kappa_{v2} = k_{v2} V_{\text{ref}}, \kappa_i = \frac{k_i V_{\text{ref}}}{R}, e = \frac{E}{V_{\text{ref}}}. \quad (8.12)$$

Direct substitution of these new dimensionless variables, time and parameters in the state equations (8.9) yields the following dimensionless state equations:

$$\begin{aligned}\frac{dx_1}{d\tau} &= \frac{e - (1 - D + \kappa_{v1}(x_3 - 1))x_3}{\xi_1} \\ \frac{dx_2}{d\tau} &= \frac{e - (1 - D + \kappa_{v2}(x_3 - 1) + \kappa_i(x_2 - x_1))x_3}{\xi_2} \\ \frac{dx_3}{d\tau} &= \frac{(1 - D + \kappa_{v1}(x_3 - 1))x_1}{\zeta} \\ &\quad + \frac{(1 - D + \kappa_{v2}(x_3 - 1) + \kappa_i(x_2 - x_1))x_2 - x_3}{\zeta}.\end{aligned}\tag{8.13}$$

Now, (8.7) and (8.8) can be written as

$$d_1 = D - \kappa_{v1}(x_3 - 1)\tag{8.14}$$

$$\text{and } d_2 = D - \kappa_{v2}(x_3 - 1) - \kappa_i(x_2 - x_1).\tag{8.15}$$

To complete the model, saturation must be included. When $d_1 < 0$ and/or $d_2 < 0$, we put $d_1 = 0$ and/or $d_2 = 0$ in (8.6) and perform dimensionless substitution. Similarly, when $d_1 > d_{\max}$ and/or $d_2 > d_{\max}$, we put $d_1 = d_{\max}$ and/or $d_2 = d_{\max}$ in (8.6) and perform dimensionless substitution.

8.3.3 Equilibrium Point Calculation

The equilibrium point can be calculated by setting all time-derivatives in (8.13) to zero and solving for x_1 , x_2 and x_3 . This gives $e = 1 - D$ and

$$\mathbf{X} = \begin{bmatrix} X_1 \\ X_2 \\ X_3 \end{bmatrix} = \begin{bmatrix} \frac{1}{2(1-D)} \\ \frac{1}{2(1-D)} \\ 1 \end{bmatrix}.\tag{8.16}$$

8.4 Stability of Equilibrium Point and Hopf Bifurcation

The Jacobian, $J(\mathbf{X})$, for the dimensionless system evaluated at the equilibrium point is given by

$$J(\mathbf{X}) = \begin{bmatrix} 0 & 0 & \frac{-(\kappa_{v1} + 1 - D)}{\xi_1} \\ \frac{\kappa_i}{\xi_2} & \frac{-\kappa_i}{\xi_2} & \frac{-(\kappa_{v2} + 1 - D)}{\xi_2} \\ \frac{2e(1 - D) - \kappa_i}{2e\xi} & \frac{2e(1 - D) + \kappa_i}{2e\xi} & \frac{\kappa_{v1} + \kappa_{v2} - 2e}{2e\xi} \end{bmatrix}.\tag{8.17}$$

We now study the stability of the equilibrium point and the trajectory in the neighborhood of the equilibrium point by deriving the eigenvalues of the system at the equilibrium point. The usual procedure is to solve the following equation for λ :

$$\det[\lambda \mathbf{1} - J(\mathbf{X})] = 0. \quad (8.18)$$

Expanding (8.18) gives

$$\begin{aligned} & \lambda^3 + \left(\frac{\kappa_i}{\xi_2} - \frac{\kappa_{v1} + \kappa_{v2} - 2e}{2e\zeta} \right) \lambda^2 \\ & + \left[\left(\frac{\kappa_{v2} + 1 - D}{\xi_2} \right) \left(\frac{2e(1 - D) + \kappa_i}{2e\zeta} \right) \right. \\ & + \left(\frac{2e(1 - D) - \kappa_i}{2e\zeta} \right) \left(\frac{\kappa_{v1} + 1 - D}{\xi_1} \right) \\ & - \left. \left(\frac{\kappa_i}{\xi_2} \right) \left(\frac{\kappa_{v1} + \kappa_{v2} - 2e}{2e\zeta} \right) \right] \lambda \\ & + \left[\left(\frac{\kappa_i}{\xi_2} \right) \left(\frac{\kappa_{v1} + 1 - D}{\xi_1} \right) \left(\frac{2(1 - D)}{\zeta} \right) \right] = 0. \end{aligned} \quad (8.19)$$

From the above equation, we can easily verify the following conditions:

$$\lim_{\lambda \rightarrow -\infty} \det[\lambda \mathbf{1} - J(\mathbf{X})] \rightarrow -\infty \quad (8.20)$$

and

$$\det[-J(\mathbf{X})] > 0. \quad (8.21)$$

Hence, there exists at least one negative real λ such that $\det[\lambda \mathbf{1} - J(\mathbf{X})] = 0$. Also, numerical calculations of eigenvalues for the practical range of parameters ($\xi_1 = \xi_2 = 10$, $\zeta = 2.5$, $e = 0.5$ and $D = 0.5$) reveal that the other two eigenvalues are a complex conjugate pair which have either a positive or negative real part depending upon values of κ_{v1} and κ_{v2} . In particular, the following observations are made.

1. For small values of κ_{v1} and κ_{v2} , the pair of eigenvalues have a negative real part.
2. As κ_{v1} and/or κ_{v2} increases, the real part of the complex eigenvalues gets less negative, and at a critical value of κ_{v1} and/or κ_{v2} , the real part changes from negative to positive. [Table 8.2](#) shows a typical scenario of the variation of the eigenvalues. The loci are plotted in [Figure 8.5](#) for ease of reference.
3. The critical value of κ_{v1} and/or κ_{v2} depends on the values of ξ_1 , ξ_2 , ζ , e , D and κ_i . As we increase κ_{v1} and/or κ_{v2} , the sign of the real part of the complex eigenvalues changes, and the system loses stability via a *Hopf bifurcation* [2, 162].

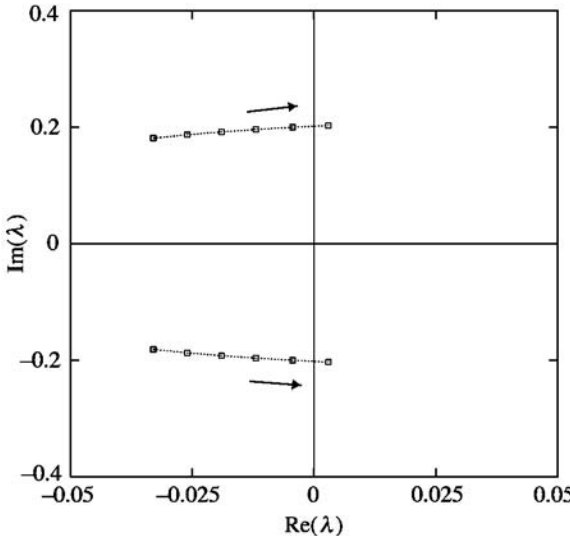


FIGURE 8.5

Loci of the complex eigenvalue pair moving from left to right as κ_{v2} increases.

TABLE 8.2

Eigenvalues for increasing value of κ_{v2} ($\kappa_{v1} = 0.48$ and $\kappa_i = 0.40$).

κ_{v2}	Eigenvalues	Remarks
0.340	$-0.0330 \pm j0.1810, -0.0460$	Stable equilibrium point
0.380	$-0.0260 \pm j0.1870, -0.0440$	Stable equilibrium point
0.420	$-0.0190 \pm j0.1920, -0.0420$	Stable equilibrium point
0.460	$-0.0120 \pm j0.1960, -0.0410$	Stable equilibrium point
0.500	$-0.0044 \pm j0.2000, -0.0390$	Stable equilibrium point
0.540	$0.0030 \pm j0.2030, -0.0380$	Unstable equilibrium point

The situation is very similar to the case of the Ćuk converter under free-running hysteretic control. As explained in [Section 6.3.3](#), in order to show Hopf bifurcation as κ_{v2} is varied (likewise for any other parameters), we need to establish the following conditions:

$$\text{Re}(\lambda)|_{\kappa_{v2}=\kappa_{v2c}} = 0 \quad (8.22)$$

$$\text{Im}(\lambda)|_{\kappa_{v2}=\kappa_{v2c}} \neq 0 \quad (8.23)$$

$$\frac{d}{d\kappa_{v2}} \text{Re}(\lambda) \Big|_{\kappa_{v2}=\kappa_{v2c}} \neq 0 \quad (8.24)$$

where κ_{v2c} is the critical value of κ_{v2} at which a Hopf bifurcation occurs. We also recall that the last condition is necessary to ensure that the movement of

the complex eigenvalue pair does not slide along the imaginary axis. In fact, all the above conditions can be numerically established using (8.19).

8.5 Local Trajectories from the Averaged Equations

In this section, we re-examine the stability in terms of the local trajectories near the equilibrium point. Since the use of an averaged model for predicting nonlinear phenomena will become inadequate when stability is lost, our aim in this section is to observe, by plotting the local trajectories, the behavior of the system as it goes from a stable region to an unstable region. For further investigation beyond the bifurcation point predicted by the averaged model, we have to resort to the exact piecewise switched model, as will be discussed in [Section 8.6](#).*

We begin with the stable system. From [Table 8.2](#), we may choose $\kappa_{v1} = 0.48$, $\kappa_{v2} = 0.45$ and $\kappa_i = 0.40$. The Jacobian evaluated at the equilibrium point is

$$J(\mathbf{X}) = \begin{bmatrix} 0 & 0 & -0.098 \\ 0.04 & -0.04 & -0.095 \\ 0.04 & 0.36 & -0.028 \end{bmatrix}. \quad (8.25)$$

The eigenvalues, λ , and their corresponding eigenvectors, \bar{v} , are found as

$$\lambda = -0.041, -0.013 \pm j0.195 \quad (8.26)$$

$$\bar{v} = \begin{bmatrix} 0.916 \\ -0.116 \\ 0.384 \end{bmatrix}, \begin{bmatrix} 0.028 \pm j0.410 \\ 0.030 \pm j0.398 \\ 0.820 \end{bmatrix}. \quad (8.27)$$

The local trajectory is shown in [Figure 8.6](#).

Next, we examine the unstable system with $\kappa_{v1} = 0.48$, $\kappa_{v2} = 0.55$ and $\kappa_i = 0.40$. The system loses stability. The Jacobian evaluated at the equilibrium point is

$$J(\mathbf{X}) = \begin{bmatrix} 0 & 0 & -0.098 \\ 0.04 & -0.04 & -0.105 \\ 0.04 & 0.36 & 0.012 \end{bmatrix}. \quad (8.28)$$

The eigenvalues, λ , and their corresponding eigenvectors, \bar{v} , are found as

$$\lambda = -0.038, 0.00484 \pm j0.204 \quad (8.29)$$

*The trajectory in the neighborhood of the equilibrium point can be described analytically in terms of the eigenvalues and eigenvectors of the system near the equilibrium point. The local dynamics of this third-order system is coincidentally the same as that of the free-running Cuk converter. See [Section 6.3.4](#) for a general description.

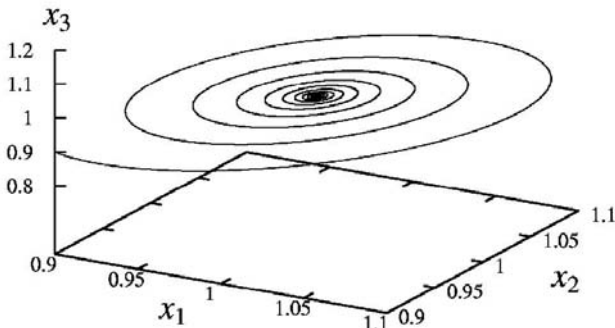


FIGURE 8.6

A view of the stable (spiraling inward) local trajectory generated from the averaged model ($\kappa_{v1} = 0.48$, $\kappa_{v2} = 0.45$ and $\kappa_i = 0.40$).

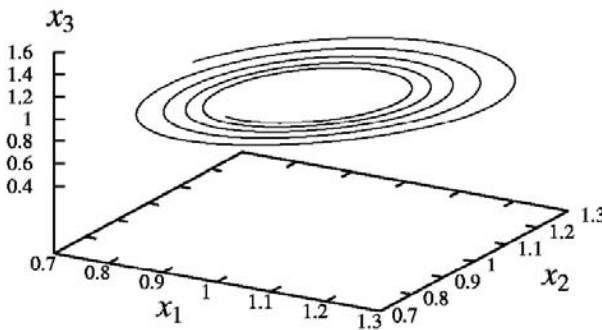


FIGURE 8.7

A view of the unstable (spiraling outward) local trajectory generated from the averaged model ($\kappa_{v1} = 0.48$, $\kappa_{v2} = 0.55$ and $\kappa_i = 0.40$).

$$\bar{v} = \begin{bmatrix} 0.923 \\ -0.151 \\ 0.355 \end{bmatrix}, \begin{bmatrix} 0.00933 \pm j0.393 \\ 0.015 \pm j0.420 \\ 0.818 \end{bmatrix}. \quad (8.30)$$

A view of the local trajectory is shown in Figure 8.7. Also, in Figure 8.8, we observe how the trajectory settles into a limit cycle after the initial transient period.

From the above examples, we clearly observe that the system loses stability via a Hopf bifurcation. Before the bifurcation, the local trajectory spirals into the equilibrium point. After the bifurcation, the local trajectory spirals away from the equilibrium point and settles down into a limit cycle. In the following section, we will re-examine the system using cycle-by-cycle computer simulations of the actual circuit operation.

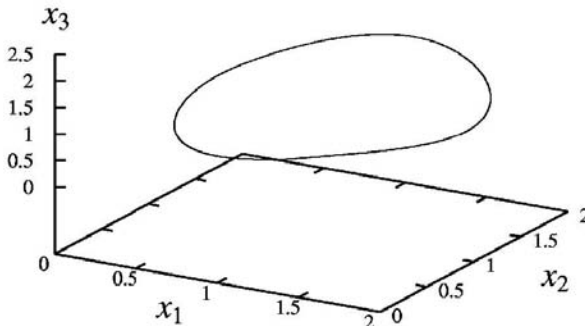


FIGURE 8.8

Limit cycle generated from the averaged model ($\kappa_{v1} = 0.48$, $\kappa_{v2} = 0.55$ and $\kappa_i = 0.40$).

8.6 Computer Simulation Study

Since the foregoing analysis is based on a set of nonlinear state equations which is derived from an averaged continuous model, it falls short of revealing further details beyond the bifurcation point. In this section, we examine the system using computer simulation which employs an exact piecewise switched model. Essentially, using the state equations in [Section 8.1](#) and incorporating suitable algorithms that take into account the possible operation of the circuit in discontinuous conduction mode, we can emulate the exact cycle-by-cycle operation of the system. Thus, the simulation results represent viable

TABLE 8.3

Component values and steady-state voltages used in simulation. (ESR stands for equivalent series resistance.)

Circuit Components	Values
Switching Period T	$40 \mu\text{s}$
Input Voltage E	12 V
Output Voltage v	24 V
Reference Voltage V_{ref}	24 V
Inductance L_1 , ESR r_{L1}	0.004 H, 0.05 Ω
Inductance L_2 , ESR r_{L2}	0.004 H, 0.2 Ω
Capacitance C , ESR r_C	$10 \mu\text{F}$, 0.01 Ω
Load Resistance R	10 Ω

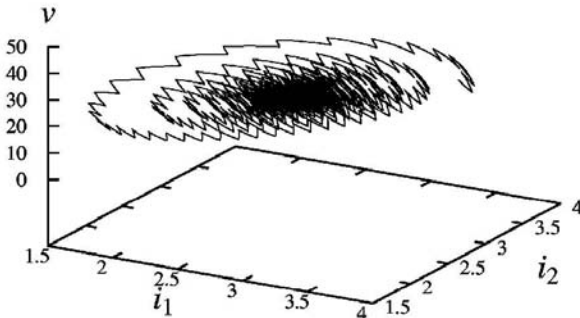


FIGURE 8.9

A view of the stable (spiraling inward) local trajectory generated from the exact piecewise switched model.

verification of the behavior of the real circuit.

Since we are primarily concerned with system stability in conjunction with the feedback design, we will focus our attention on the effects of varying the various gains on the bifurcation behavior of the system. In particular, the gains K_{v1} , K_{v2} and K_i present themselves as design parameters that can be changed at will.

The simulation is based on the exact state equations given in [Section 8.1](#). For each set of parameter values, time-domain cycle-by-cycle waveforms can be generated by solving the appropriate linear equation in any sub-interval of time, according to the states of the switches which are determined from values of the control voltages $v_{\text{con}1}$ and $v_{\text{con}2}$. Sampled data are then collected at $t = nT$ in the steady state. With a sufficient number of sets of steady-state data, we can construct bifurcation diagrams. The circuit parameters used in our simulations are shown in [Table 8.3](#).

Since we are simulating the actual circuit, the original circuit parameters will be used instead of the dimensionless ones. In particular we will focus on the qualitative change of dynamical behavior as K_{v1} and/or K_{v2} is varied. To observe the trend, we keep K_{v1} constant and vary K_{v2} . Similarly, we may keep K_{v2} constant and vary K_{v1} . A summary of the observed behavior is as follows.

- When K_{v2} is small, the trajectory spirals into a fixed period-1 orbit, corresponding to a fixed point in the averaged system. [Figure 8.9](#) shows the simulated trajectory.
- When K_{v2} is increased beyond a critical value, the period-1 orbit becomes unstable, and the trajectory spirals outward, as shown in [Figure 8.10](#), and settles into a quasi-periodic orbit, as shown in [Figure 8.11](#).

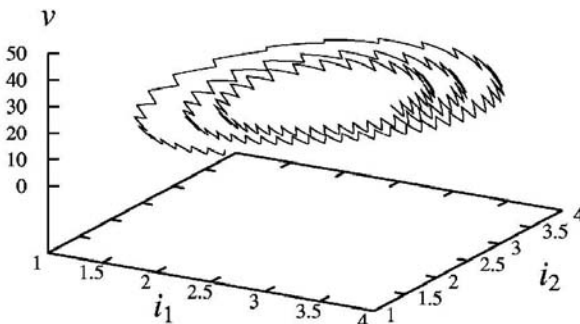


FIGURE 8.10

A view of the unstable (spiraling outward) local trajectory generated from the exact piecewise switched model.

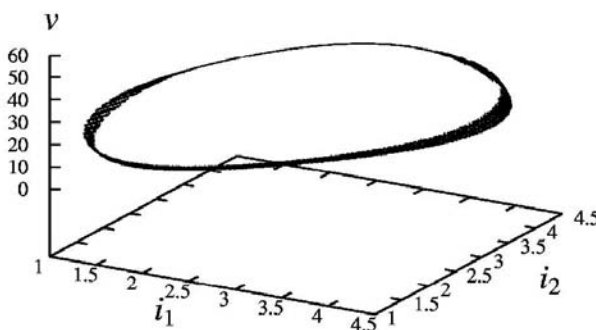


FIGURE 8.11

Quasi-periodic orbit generated from the exact piecewise switched model.

The above observations confirm the prediction we made in [Section 8.5](#) based on the averaged equations.

In order to give a fuller picture of the dynamics of the system beyond the Hopf bifurcation point, we need to generate a large number of trajectories and bifurcation diagrams. In the following, we show a few representative bifurcation diagrams and some typical sequences of trajectories as some selected parameters are varied.

We first keep K_{v1} and K_i constant and vary K_{v2} . A bifurcation diagram is shown in [Figure 8.12](#). The sequence of simulated trajectories shown in [Figure 8.13](#) reveals a typical Hopf bifurcation, in which a stable equilibrium state breaks down to quasi-periodic orbits and limit cycles. The corresponding stroboscopic maps confirming quasi-periodicity and periodicity are shown in [Figure 8.14](#). In fact, if we keep K_{v2} and K_i constant and vary K_{v1} , we observe similar bifurcation behavior.

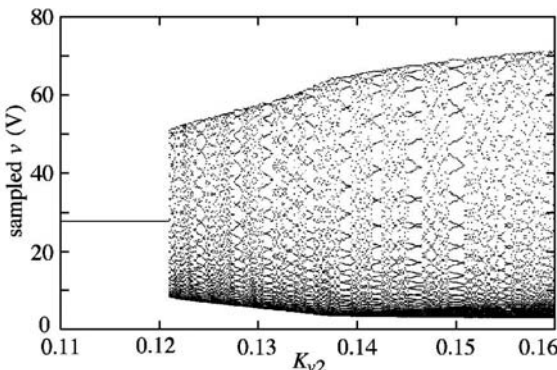
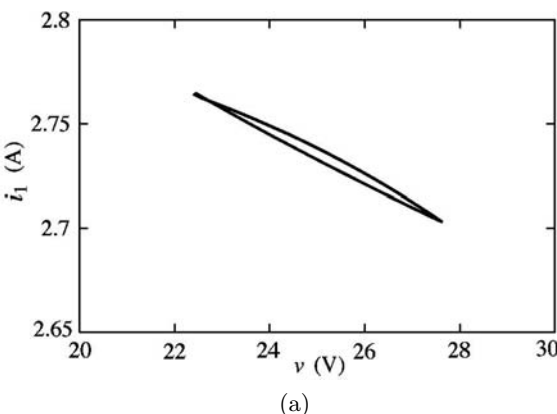


FIGURE 8.12

Bifurcation diagram with K_{v2} as bifurcation parameter ($K_{v1} = 0.11$ and $K_i = 1$).



(a)

FIGURE 8.13

Sequence of change of qualitative behavior. (a) Stable period-1 orbit ($K_{v1} = 0.11$, $K_{v2} = 0.11$ and $K_i = 1$); (b) quasi-periodic orbit ($K_{v1} = 0.11$, $K_{v2} = 0.13$ and $K_i = 1$); (c) limit cycle ($K_{v1} = 0.11$, $K_{v2} = 0.15$ and $K_i = 1$).

Finally, to study the bifurcation behavior in respect of current gain variation, we keep K_{v1} and K_{v2} constant, and vary K_i . It is found that the system remains in stable period-1 operation irrespective of the choice of K_i . Basically K_i only determines how close the slave follows the master. The larger K_i is, the closer the slave's output current is to the master's.

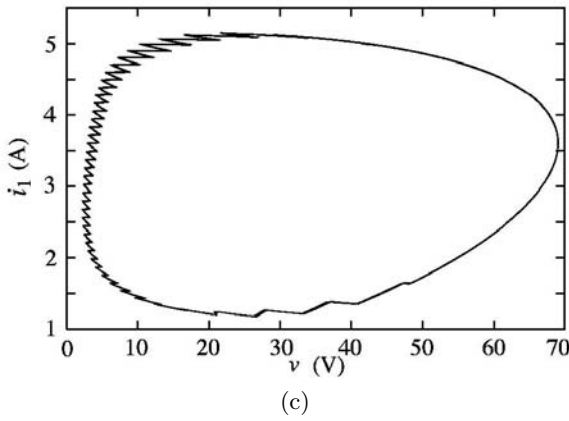
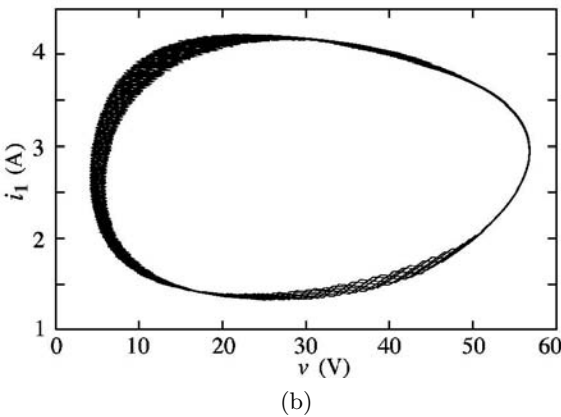
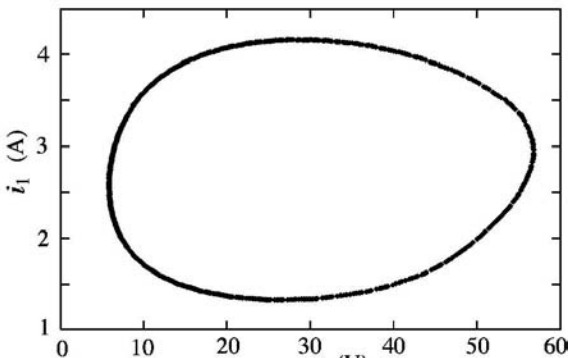


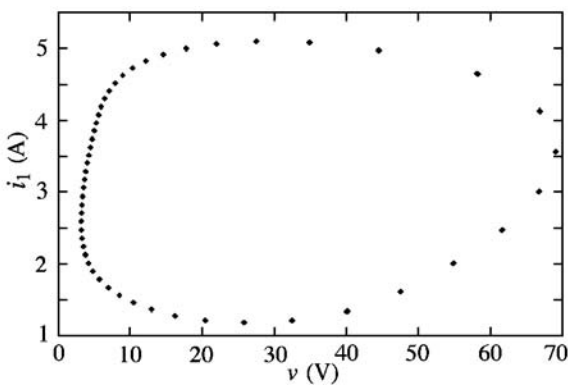
FIGURE 8.13 continued.

8.7 Usefulness of Averaged Models

In concluding this chapter, we reiterate that despite the usual belief that averaged models are generally not applicable for the study of bifurcation behavior, their use can yield simple and effective analytical solutions when dealing with low-frequency bifurcation phenomena. In this chapter we have shown how an averaged model can be used to explain some low-frequency nonlinear phenomena in a parallel system of two boost converters under a master-slave control scheme. It has been found that Hopf bifurcation can occur when the voltage feedback gains are too large. In engineering design, stable period-1 operation is the only acceptable operation. Thus, in practice, instability often refers to failure of the circuit in maintaining its operation in the expected stable



(a)



(b)

FIGURE 8.14

(a) Stroboscopic map of Figure 8.13 (b) showing quasi-periodic orbit; (b) stroboscopic map of Figure 8.13 (c) showing limit cycle.

period-1 regime. Here, we have identified the parameters whose variations cause “instability” and analyzed the detailed bifurcation behavior via simple averaged models.

Fast-Scale Bifurcation Analysis of Power-Factor-Correction Boost Converters

In engineering, stability is often interpreted as a behavioral condition in which the system being examined is operating in the expected regime. For instance, in power electronics, we refer to a stable operation as a specific periodic operation. When a switching converter fails to maintain its operation in this expected manner, it is considered unstable. In conventional power electronics, all those subharmonic, quasi-periodic and chaotic operations are regarded as being undesirable and should be avoided. Thus, the traditional design objective must include the prevention of any bifurcation within the intended operating range. In other words, any effective design must automatically avoid the occurrence of bifurcation for the range of variation of the parameters [75]. Thus, for systems that have been shown to bifurcate when a certain parameter is changed, the design problem is, in a sense, addressing the “control of bifurcation.” Such a design problem can therefore be solved on the basis of bifurcation analysis. In this chapter we will examine the traditional stability problem from a bifurcation analysis perspective. We will re-visit the boost converter under current-mode control [22, 81], and show that the widely known *ramp compensation* technique is effectively a means of controlling bifurcation. Furthermore, we apply the result of this bifurcation analysis to investigate the “fast-scale” instability problem of a power-factor-correction boost converter. Such instability may take the form of chaos or high-frequency subharmonics at certain phase angles of the mains period, and may present a subtle source of harmonic distortion that degrades the otherwise high power factor of the converter.

9.1 Bifurcation Analysis of Boost Converters under Current-Mode Control with Ramp Compensation

9.1.1 Review of Basic Operation

The boost converter under current-mode control has been analyzed thoroughly in [Chapter 5](#). Here, we extend the analysis to include the application of ramp

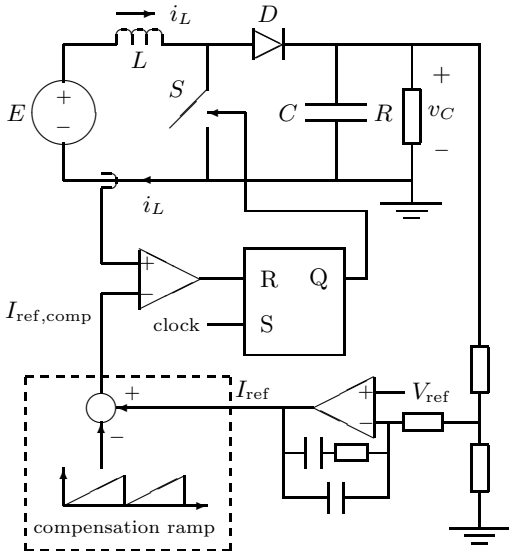


FIGURE 9.1

Boost converter under current-mode control with ramp compensation.

compensation for suppressing period-doubling bifurcation. In the following we give a quick review of its operation when ramp compensation is introduced.

The boost converter with ramp compensation is shown in Figure 9.1. Here, we notice that the reference current is first subtracted by a periodic ramp signal before it is presented to the comparator. Thus, the resulting reference current that is used to compare with the inductor current becomes

$$I_{\text{ref,comp}} = I_{\text{ref}} - m_c(t \bmod T) \quad (9.1)$$

where m_c is the slope of the compensation ramp. The operation is exactly the same as in the normal current-mode controlled converter. Specifically, the switch is turned on periodically, and off according to the output of a comparator that compares the inductor current with $I_{\text{ref,comp}}$. While the switch is on, the inductor current i_L climbs up, and as it reaches $I_{\text{ref,comp}}$, the switch is turned off, thereby causing the inductor current to ramp down until the next periodic turn-on instant. In the closed-loop system, I_{ref} is controlled via a feedback loop which attempts to keep the output voltage fixed by adjusting I_{ref} .

An important feature of the current-mode control is the presence of an inner current loop. It has been shown in Chapter 5 that, without ramp compensation, this inner loop becomes unstable when the duty ratio (designed steady-state value) exceeds 0.5. We have also seen that the system loses stability via a period-doubling bifurcation. The introduction of the compensation

ramp has been proven effective in solving this stability problem [81, 123], and the use of compensation ramp has become an industry standard for almost all current-mode control applications. In the following we attempt to uncover the magic of ramp compensation from a bifurcation control viewpoint.

9.1.2 Review of Period-Doubling Bifurcation

Before we examine the effect of ramp compensation, let us recall a few important expressions related to the period-doubling bifurcation of the current-mode controlled boost converter. We have shown in [Chapter 5](#) that the inner current loop dynamics, without ramp compensation, is described by

$$i_{L,n+1} = \left(1 - \frac{v_C}{E}\right) i_{L,n} + \frac{I_{\text{ref}} v_C}{E} - \frac{(v_C - E)T}{L}. \quad (9.2)$$

Introducing a small disturbance $\delta i_{L,n}$ to $i_{L,n}$, we have

$$\delta i_{L,n+1} = \left(\frac{-D}{1-D}\right) \delta i_{L,n} + O(\delta i_n^2), \quad (9.3)$$

from which we get the characteristic multiplier or eigenvalue, λ , as

$$\lambda = \frac{-D}{1-D}. \quad (9.4)$$

Thus, the first period-doubling occurs when $\lambda = -1$ which corresponds to $D = 0.5$. The equivalent condition for period-doubling can also be expressed in terms of I_{ref} . First, we recognize from the requirement of power balance that (see [Section 5.5.1](#))

$$\left(I_{\text{ref}} - \frac{DTE}{2L}\right) E = \frac{E^2}{(1-D)^2 R}. \quad (9.5)$$

Hence, the critical value of I_{ref} for period-doubling, without ramp compensation, is

$$I_{\text{ref,c}} = \frac{E}{R} \left[\frac{DRT}{2L} + \frac{1}{(1-D)^2} \right]_{D=0.5} \quad (9.6)$$

$$= \frac{E}{R} \left(\frac{RT}{4L} + 4 \right). \quad (9.7)$$

We will see later that the use of ramp compensation is to raise the value of $I_{\text{ref,c}}$, thereby widening the operating range.

9.1.3 Ramp Compensation from a Bifurcation Control Viewpoint

We now study the system with the ramp compensation included. [Figure 9.2](#) shows the inductor current waveform and its relationship with the reference

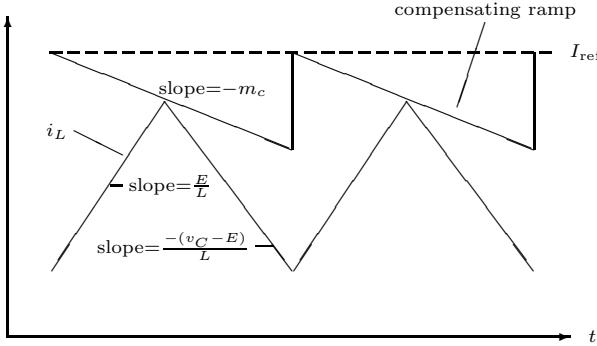


FIGURE 9.2

Illustration of current-programming control showing inductor current with ramp compensation

current. By inspecting the inductor current waveform, we get the modified iterative map for the inner loop dynamics as

$$\delta i_{n+1} = \left(\frac{M_c}{1 + M_c} - \frac{D}{(1 - D)(1 + M_c)} \right) \delta i_n + O(\delta i_n^2) \quad (9.8)$$

where $M_c = m_c L / E$ is the normalized compensating slope. Now, using (9.8), we get the eigenvalue or characteristic multiplier, λ , for the ramp-compensated inner loop dynamics as

$$\lambda = \frac{M_c}{1 + M_c} - \frac{D}{(1 - D)(1 + M_c)}. \quad (9.9)$$

Hence, by putting $\lambda = -1$, the critical duty ratio, at which the first period-doubling occurs, is

$$D_c = \frac{M_c + 0.5}{M_c + 1}. \quad (9.10)$$

From (9.6) and (9.10), we get the critical value of I_{ref} for the ramp-compensated system as

$$\begin{aligned} I_{\text{ref},c} &= \frac{E}{R} \left[\frac{DRT}{2L} + \frac{1}{(1 - D)^2} \right]_{D=D_c} \\ &= \frac{E}{R} \left[\frac{RT}{2L} \frac{M_c + 0.5}{M_c + 1} + 4(M_c + 1)^2 \right]. \end{aligned} \quad (9.11)$$

Note that $I_{\text{ref},c}$ increases monotonically as the compensating slope increases. Hence, it is obvious that ramp compensation effectively provides more margin for the system to operate without running into period-doubling bifurcation. As shown in [Figure 9.3](#), the onset of the first period-doubling has been “delayed” to a larger value of I_{ref} by the introduction of the compensation ramp.

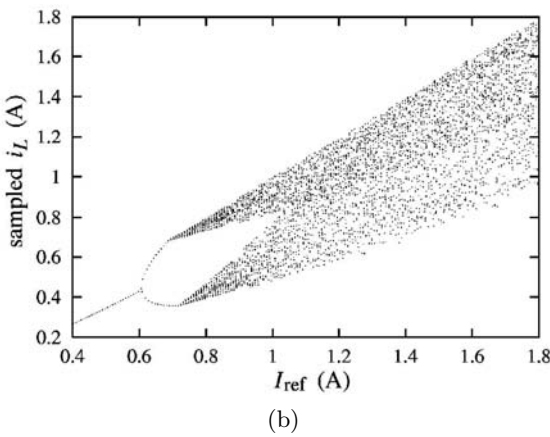
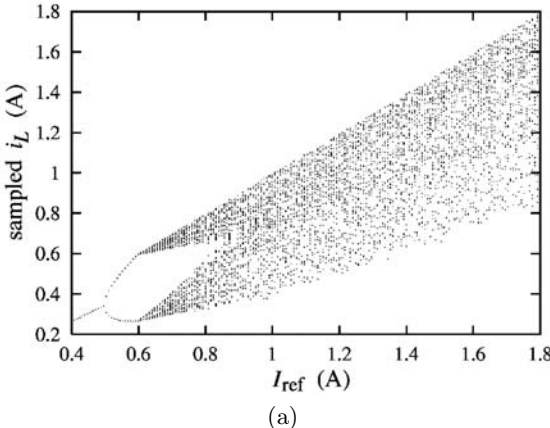


FIGURE 9.3

Bifurcation diagrams obtained numerically for the boost converter under current-programming control, showing the “delaying” of the onset of bifurcation by ramp compensation. (a) No ramp compensation; (b) with compensating ramp $m_c = 0.1E/L$; (c) $m_c = 0.3E/L$; (d) $m_c = 0.8E/L$. For all cases, $C = 20 \mu\text{F}$, $L = 1.5 \text{ mH}$, $R = 40 \Omega$, $E = 5 \text{ V}$ and $T = 100 \mu\text{s}$.

The above result can also be used for design. For example, we may plot the critical value of I_{ref} against R , as shown in Figure 9.4. The magnitude of the slope of the compensating ramp can then be chosen to provide a sufficient margin for avoiding period-doubling bifurcation. Likewise, we may consider the input voltage variation and produce a similar set of design curves that provide information on the choice of the compensating slope for ensuring a “bifurcation-free” operation, as shown in Figure 9.5. Also, we may plot the boundary curves in terms of normalized parameters, as shown in Figure 9.6.

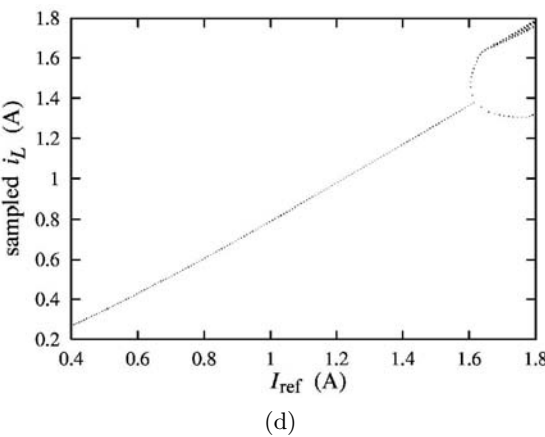
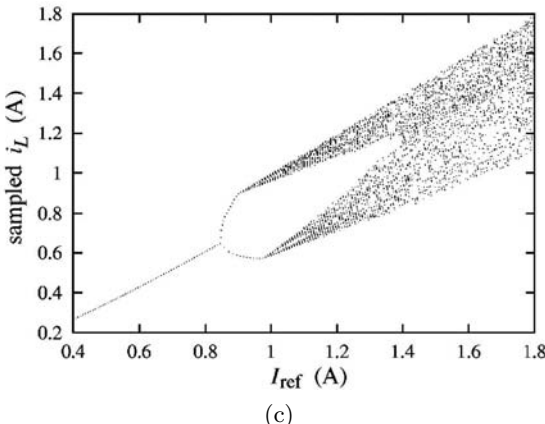


FIGURE 9.3 continued.

9.2 Application to Power-Factor-Correction Boost Converter

In the foregoing, we have described the application of ramp compensation in controlling bifurcation in a boost converter under current-mode control. In practice, the current-mode controlled converter also finds application in shaping the input current. In fact, the so-called boost rectifier or power-factor-correction converter is effectively a current-mode controlled boost converter [42, 122]. The circuit schematic is shown in [Figure 9.7](#). In this case, instead of setting I_{ref} constant for a fixed load, we let I_{ref} vary according to the input voltage waveform. Thus, the input current is being directly programmed to

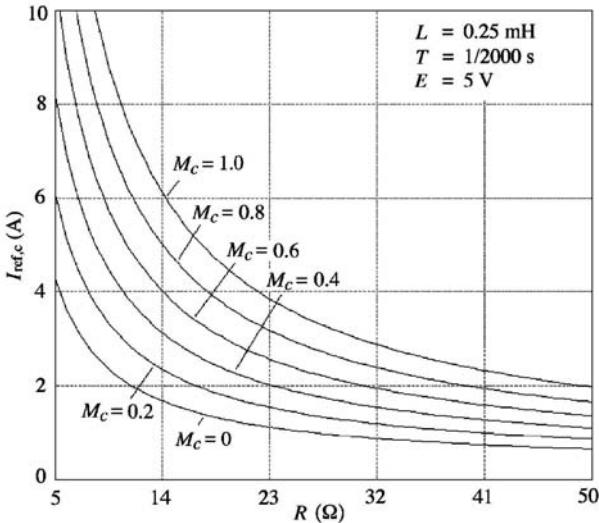


FIGURE 9.4

Specific boundary curves $I_{ref,c}$ versus R for current-programmed boost converter without compensation and with normalized compensating slope $M_c = 0.2, 0.4, 0.6, 0.8$ and 1 .

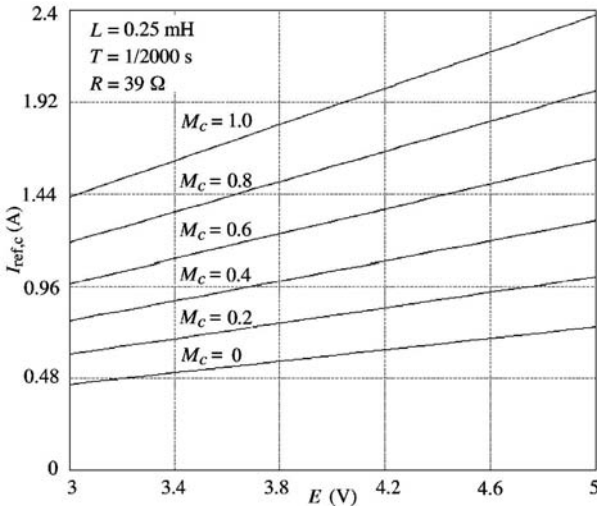


FIGURE 9.5

Specific boundary curves $I_{ref,c}$ versus E for current-programmed boost converter without compensation and with compensation slope $M_c = 0.2, 0.4, 0.6, 0.8$ and 1 .

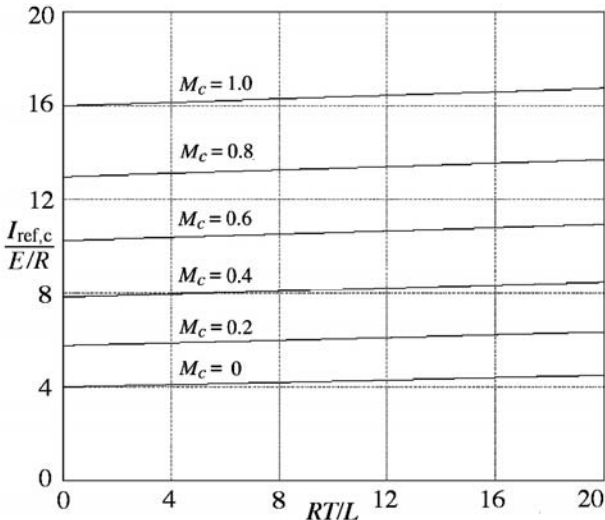


FIGURE 9.6

Specific boundary curves plotted with normalized parameters.

follow the waveform of the input voltage. The result is a nearly unity power factor.

9.2.1 Bifurcation Analysis

The bifurcation analysis described earlier is directly applicable to the case of the power-factor-correction boost converter. Effectively, since I_{ref} follows the input voltage, its waveform is a rectified sine wave whose frequency is much lower than the switching frequency. Typically, the frequency of this sine wave is 50 or 60 Hz. Thus, the situation is analogous to the case of applying a *time-varying ramp compensation* to a current-mode controlled boost converter. Suppose the input voltage is given by

$$e(t) = \hat{E} |\sin \omega_m t| \quad (9.12)$$

where ω_m is the mains angular frequency. For algebraic brevity, we express the input voltage in terms of the phase angle θ , i.e., $e(\theta) = \hat{E} |\sin \theta|$.

As shown in Figure 9.8, when the input voltage is in its first quarter cycle (i.e., $0 \leq \theta < \pi/2$), the value of I_{ref} increases, which is equivalent to applying a negative compensating ramp to I_{ref} (i.e., $M_c < 0$). Moreover, when the input voltage is in its second quarter cycle (i.e., $\pi/2 < \theta \leq \pi$), the value of I_{ref} decreases, which is equivalent to applying a positive compensating ramp to I_{ref} (i.e., $M_c > 0$). At $\theta = \pi/2$, there is no ramp compensation. Therefore,

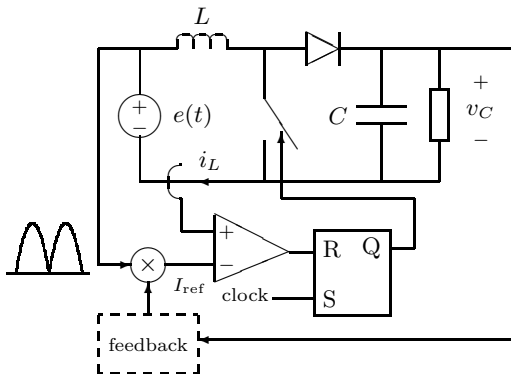


FIGURE 9.7

Schematic of the power-factor-correction boost converter showing direct programming of the input current. I_{ref} is a rectified sine wave whose amplitude is adjusted by the “feedback” network to match the power level.

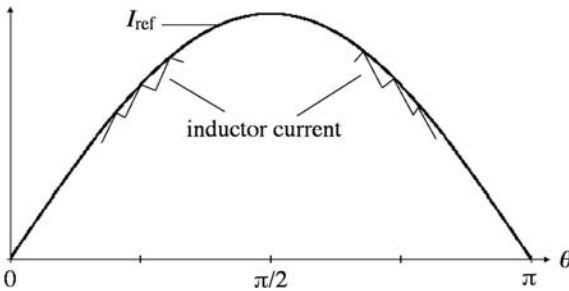


FIGURE 9.8

Programming of input current waveform in power-factor-correction boost converter. For $0 \leq \theta < \pi/2$, an effective negative ramp compensation is applied (i.e., $M_c < 0$), whereas for $\pi/2 < \theta \leq \pi$, an effective positive ramp compensation is applied (i.e., $M_c > 0$).

based on the earlier analysis, we can conclude that the system has asymmetric regions of stability for the two quarter mains cycles.

Specifically, the second quarter cycle (i.e., $\pi/2 \leq \theta < \pi$) should be more remote from period-doubling* because of the presence of ramp compensation. To be precise, we need to find the critical phase angle, θ_c , at which period-doubling occurs. Since the duty ratio is equal to $1 - e/v_C$ and M_c is

*The term period-doubling here refers to the switching period being doubled. This phenomenon is considered as a kind of *fast-scale instability* [96], to distinguish it from the average slow-scale power-factor-correction operation at the mains frequency.

$-(dI_{\text{ref}}/dt)L/\hat{E}|\sin \theta|$, we have, from (9.10),

$$|\sin \theta_c| = \frac{v_C + 2L \frac{dI_{\text{ref}}}{dt}}{2\hat{E}}. \quad (9.13)$$

Moreover, if the power factor approaches one, we have

$$I_{\text{ref}} \approx \hat{I}_{\text{in}} |\sin \theta| \quad \text{for } 0 \leq \theta \leq \pi \quad (9.14)$$

where \hat{I}_{in} is the peak input current. For brevity we restrict the analysis to the range $[0, \pi]$, understanding that the waveform repeats for every interval $[k\pi, (k+1)\pi]$, for all integers k . Thus, we have

$$\frac{dI_{\text{ref}}}{dt} \approx \omega_m \hat{I}_{\text{in}} \cos \theta \quad \text{for } 0 \leq \theta \leq \pi. \quad (9.15)$$

Hence, from (9.13), we have

$$\theta_c = 2 \arctan \left(\frac{2\hat{E} \pm \sqrt{4\hat{E}^2 - v_C^2 + 4\omega_m^2 \hat{I}_{\text{in}}^2 L^2}}{v_C - 2\omega_m \hat{I}_{\text{in}} L} \right). \quad (9.16)$$

Furthermore, incorporating the power equality, i.e., $\hat{E}\hat{I}_{\text{in}}/2 = v_C^2/R$ (assuming 100% efficiency), and defining two parameters r_v and τ_L as

$$r_v = \frac{v_C}{\hat{E}} \quad (9.17)$$

$$\tau_L = \frac{L}{R}, \quad (9.18)$$

the critical phase angle given in (9.16) can be written in the following compact form:

$$\theta_c = 2 \arctan \left(\frac{2 \pm \sqrt{4 - r_v^2 + 16\omega_m^2 \tau_L^2 r_v^4}}{r_v - 4\omega_m \tau_L r_v^2} \right). \quad (9.19)$$

By inspecting (9.19), we clearly see that the voltage ratio $r_v = v_C/\hat{E}$ and the parameter $\tau_L = L/R$ control the bifurcation behavior. For clarity, we denote the two real solutions (if they exist) by θ_{c1} and θ_{c2} . Specifically, we can identify three regions in the parameter space (see [Figure 9.9](#)):

- **Region 1 (bifurcation-free region or fast-scale stable region):**
We can readily show that if

$$\tau_L > \frac{1}{4\omega_m r_v}, \quad (9.20)$$

the solutions given by (9.19) are essentially outside of the range of interest. In fact, at the boundary $\tau_L = 1/4\omega_m r_v$, we simply have $\theta_{c1} = 0$ and $\theta_{c2} = \pi$. The operation in this region is free from period-doubling bifurcation for all time and hence is *fast-scale stable* [96].

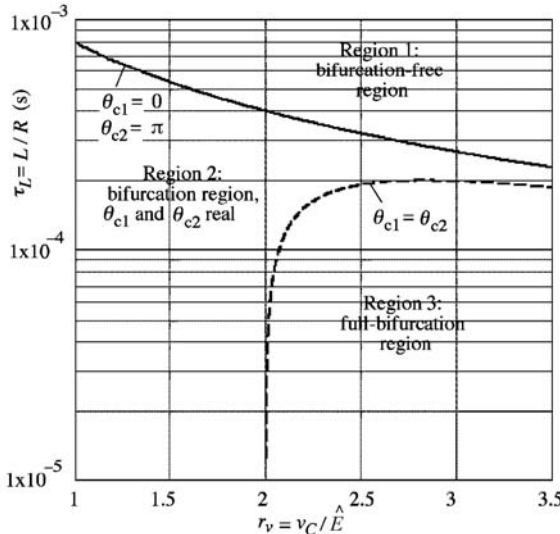


FIGURE 9.9

Bifurcation regions in parameter space (mains frequency is 50 Hz). Upper boundary curve is $\tau_L = 1/4\omega_m r_v$ and lower curve is $\tau_L = \sqrt{(r_v^2 - 4)/16\omega_m^2 r_v^4}$.

- **Region 2 (bifurcation region or partial fast-scale unstable region):** We also observe from (9.19) that if $4 - r_v^2 + 16\omega_m^2 \tau_L^2 r_v^4$ is non-negative in addition to satisfying (9.20), i.e.,

$$\sqrt{\frac{r_v^2 - 4}{16\omega_m^2 r_v^4}} \leq \tau_L < \frac{1}{4\omega_m r_v}, \quad (9.21)$$

then there are two real solutions for θ_c . Under this condition, period-doubling or fast-scale instability occurs for intervals $[0, \theta_{c1}]$ and $[\theta_{c2}, \pi]$. Moreover, as θ_{c1} and θ_{c2} get closer to each other, the stable interval diminishes. At the lower boundary $\tau_L = \sqrt{r_v^2 - 4}/16\omega_m^2 r_v^4$, the two real solutions merge together, i.e., $\theta_{c1} = \theta_{c2}$, and period-doubling bifurcation cannot be avoided.

- **Region 3 (full-bifurcation region or fast-scale unstable region):** If τ_L is below the boundary of Region 2, i.e.,

$$\tau_L \leq \sqrt{\frac{r_v^2 - 4}{16\omega_m^2 r_v^4}}, \quad (9.22)$$

the fast-scale stable interval has disappeared altogether.

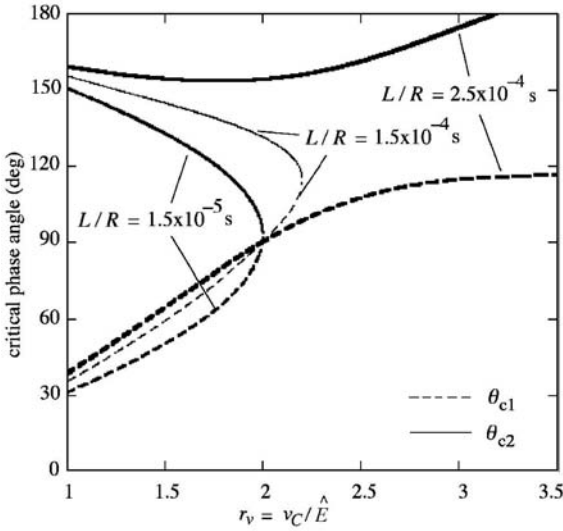


FIGURE 9.10

Critical phase angles versus v_C/\hat{E} for the power-factor-correction boost converter.

In Figure 9.10, we plot the critical phase angle as a function of r_v (i.e., v_C/\hat{E}). We summarize as follows some important observations regarding the occurrence of period-doubling in the input current waveform during the half mains cycle, i.e., $0 \leq \theta \leq \pi$.

1. To guarantee operation in the bifurcation-free regime (Region 1 in Figure 9.9), we need a sufficiently large τ_L , i.e., either a sufficiently large L or small R . This is actually the preferred operation in practice.
2. For values of v_C/\hat{E} where real solutions of θ_c exist, the converter fails to maintain the expected bifurcation-free operation for intervals of time corresponding to $\theta < \theta_{c1}$ and $\theta > \theta_{c2}$.
3. If θ_{c1} is greater than 90° , the converter would have gone into period-doubling for the whole first quarter cycle. Likewise, if θ_{c2} is less than 90° , the converter would have gone into period-doubling for the whole second quarter cycle.
4. Referring to Figure 9.9, if τ_L is smaller than a certain value (about 0.0001 for a mains frequency of 50 Hz), period-doubling is unavoidable and will occur for all values of $v_C/\hat{E} > 2$.

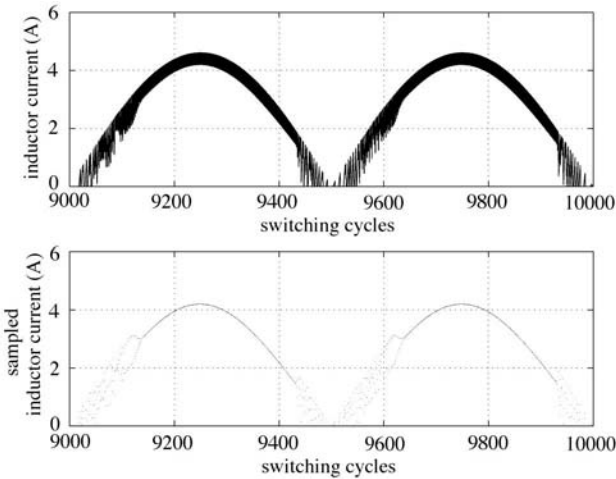


FIGURE 9.11

Simulated inductor current time-domain waveform (upper) and same waveform sampled at the switching frequency (lower) for Region 2 at $v_C/\hat{E} = \sqrt{2}$.

9.2.2 Fast-Scale Instability by Computer Simulations

In this section we verify the above findings by computer simulations. Consistent with the assumption of unity power factor used in the foregoing theoretical analysis, the reference current waveform I_{ref} is generated according to the waveform template defined in (9.14), where the peak input current \hat{I}_{in} is determined by the power equality condition, i.e., $\hat{E}\hat{I}_{\text{in}}/2 = v_C^2/R$.

The circuit component values used in the simulations are:

$$L = 2 \text{ mH}, C = 470 \mu\text{F} \text{ and } R = 135 \Omega.$$

The switching frequency and mains frequency are 50 kHz and 50Hz, respectively. This choice of component values leads to the theoretical curves of the critical phase angles corresponding to $\tau_L = 0.000015 \text{ s}$ in Figure 9.10.

Figure 9.11 shows the simulated inductor current waveform for an operation in Region 2 (bifurcation region), where real solutions of θ_c exist. The peak input voltage is $110\sqrt{2} \text{ V}$, and the reference output voltage is 220 V, which correspond to $v/\hat{E} = \sqrt{2}$ in Figure 9.10. Indeed, period-doubling bifurcation can be observed during a half mains cycle in the inductor current waveform, as shown in Figure 9.11 (upper). In order to see the period-doubling and fast-scale instability more clearly, we sample the waveform at a rate equal to the switching frequency, as shown in Figure 9.11 (lower), where the two critical phase angles and the corresponding bifurcations can be clearly identified. Between these two points the sampled values of the current follow accurately the sinusoidal shape of the reference current. A close-up view of the waveform

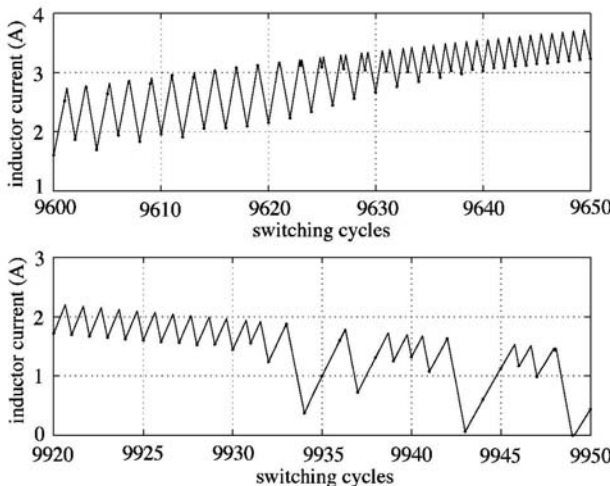


FIGURE 9.12

Close-up view of simulated inductor current waveform near the critical points for Region 2 at $v_C/\hat{E} = \sqrt{2}$.

around the critical points is shown in Figure 9.12. Furthermore, Figure 9.13 compares the values of the critical phase angles found by simulations and those obtained analytically. They are in very good agreement.

The bifurcation region characterized by the presence of a critical point in each quarter mains cycle persists until the left-hand side critical phase angle θ_{c1} reaches its maximum, i.e., 90° , corresponding to the peak current value. As mentioned in the preceding section, when θ_{c1} becomes greater than 90° , the whole first quarter cycle should have been fast-scale unstable with possible chaos for some intervals. This result is indeed confirmed by the simulated inductor current waveform shown in Figure 9.14, obtained for $v/\hat{E} = 2$.

Finally, in order to confirm the theoretical conclusion regarding the occurrence of full-bifurcation or fast-scale instability in Region 3, we present the simulation results for parameters satisfying (9.22). As shown in Figure 9.15, the system operates in full-bifurcation with the stable interval replaced completely by period-doublings and chaos.

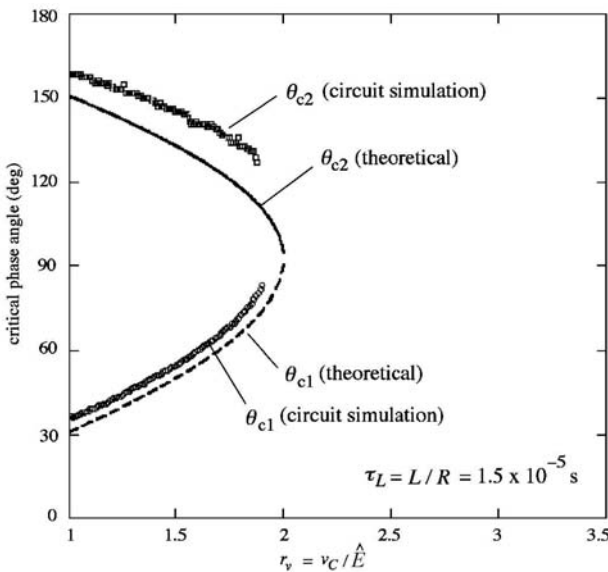


FIGURE 9.13

Critical phase angles obtained by simulations and analysis for $\tau_L = 0.000015 \text{ s}$.

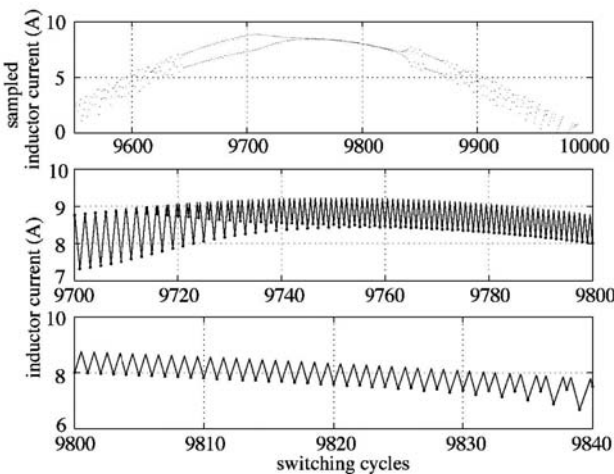


FIGURE 9.14

Simulated sampled inductor current when one critical phase angle reaches 90° for $v_C / \hat{E} = 2$ (upper) and close-up views of simulated waveform near critical points (middle and lower).

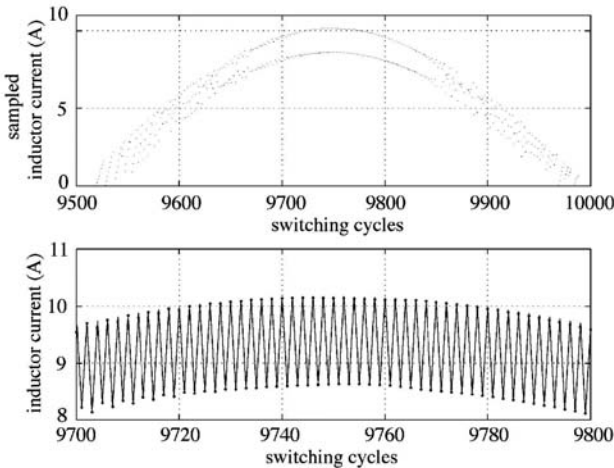


FIGURE 9.15

Simulated sampled inductor current for Region 3 at $v_C/\hat{E} = 2.5$ (upper) and close-up view of the inductor current waveform (lower).

9.3 A Note on Fast-Scale and Slow-Scale Instabilities

In the afore-described analysis, we focus on the fast-scale instability of the power-factor-correction boost converter. We have shown the possibility of fast-scale period-doubling at certain phase angles of the mains cycle. Such an instability may add to the total harmonic distortion in the input current, degrading the input power factor. Moreover, the same converter may also suffer from slow-scale instability. To study slow-scale phenomena, averaged models can be employed. Here, we stress that the appropriate averaged models should be derived by averaging over the switching period (not the mains period). In fact, period-doubling at the mains frequency has been shown possible in the power-factor-correction boost converter [107].

10

Intermittent Chaotic Operation in Switching Power Converters

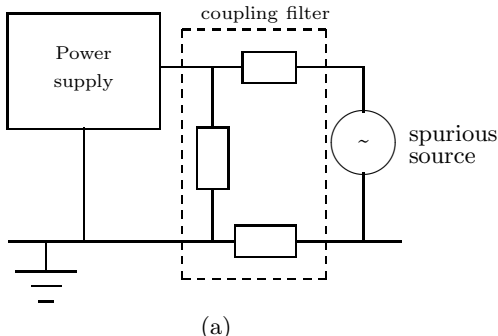
It is not uncommon in the design of switching power supplies that the rather puzzling irregular (chaotic) behavior is observed intermittently between long periods of regular behavior. Noise or bad construction is the usual blame. In this chapter we explain the “intermittent” chaos observed in switching converters in terms of coupling of spurious signals.

As we have seen in previous chapters, varying a crucial parameter can cause a bifurcation to occur. It is therefore not surprising to see that if a crucial parameter is being modulated by some external driving source, for example through an unintentional coupling, the system can be driven out of the regular operating regime intermittently. The situation is analogous to a time-varying parameter applied to the system in such a way that bifurcations occur causing the system’s behavior to change from time to time. Thus, if a spurious signal is coupled unintentionally into a crucial parameter causing it to vary over a range that covers some bifurcation points, the system may operate intermittently between the regular regime and other unwanted regimes.

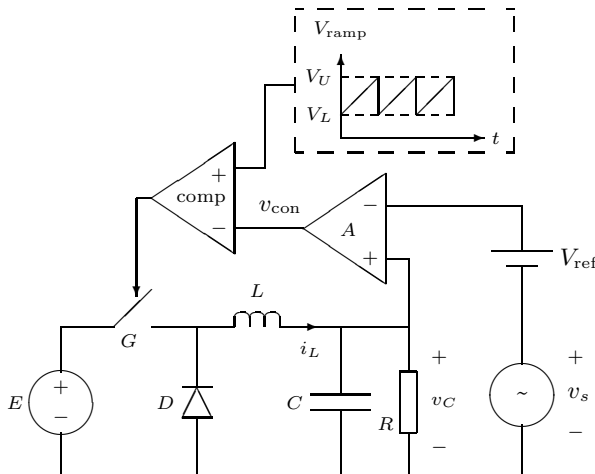
The circuit model used to study the phenomenon should naturally incorporate a weak signal which is coupled to the converter via unintended paths (e.g., conducted or radiated EMI). We show that for the case of a simple voltage-mode controlled buck converter, coupling of spurious signals into the reference voltage can cause intermittent chaotic or subharmonic operations. Similar analysis can be applied to current-mode controlled converters, with an appropriate coupling mechanism (e.g., modulation of the compensation slope by a spurious signal), to identify possible intermittent chaotic operations.

10.1 Simplified Model of Spurious Signal Intrusion

We begin with the crude but practically valid assumption that the power converter under study is not perfectly protected from intrusion of signals which are generated outside the power supply [47, 163]. The intrusion can take the form of coupling via conducted or radiated paths. Sometimes, the intruders can live on the same circuit board or be present at a very close proximity.



(a)



(b)

FIGURE 10.1

A power supply coupled with spurious source. (a) Crude model; (b) circuit model showing a buck converter with an additive intruding signal v_s acted upon the reference voltage.

Figure 10.1 (a) shows a crude model which illustrates the situation, where v_s denotes the effective additive intruding source.

In order to study the effects of coupling of spurious (intruding) signals, we need a circuit model that describes the way in which the power supply is connected to the spurious signal source. One simple approach is to model the coupling as an additive process which injects the spurious signal directly to some crucial parameters such as the reference voltage of the power supply, as shown in **Figure 10.1 (b)**.

Suppose the effective additive source is v_s , which may be due to some oscillators or PWM generators present in the proximity. For convenience we

denote the strength of the spurious source by α which is the ratio of the amplitude of v_s to V_{ref} , i.e.,

$$\alpha = \frac{\hat{v}_s}{V_{\text{ref}}} \quad (10.1)$$

where \hat{v}_s is the amplitude of the effective intruding source appearing behind the reference voltage of the power supply. We will investigate the effect of coupling the intruding source to the power supply for various levels of strengths of the intruding source as well as for different types of intruding sources (e.g., sinusoids and square pulses).

10.2 Quick Glimpse at “Intermittent” Chaos

When v_s is a sinusoidal signal of frequency f_s , the reference voltage is being modulated as

$$V_{\text{ref}} \mapsto V_{\text{ref}}(1 + \alpha \sin 2\pi f_s t). \quad (10.2)$$

Such spurious coupling can occur in power supplies that operate in an RF environment. Suppose the switching frequency is f_o , and $f_o \neq f_s$. Obviously, we would expect the effect of the intruding source on the power supply to be periodic in $1/|f_o - f_s|$.

To get a quick glimpse of the phenomenon, let us consider the buck converter shown in [Figure 10.1 \(b\)](#) for two particular effective signal strengths. The circuit parameters are as follows:

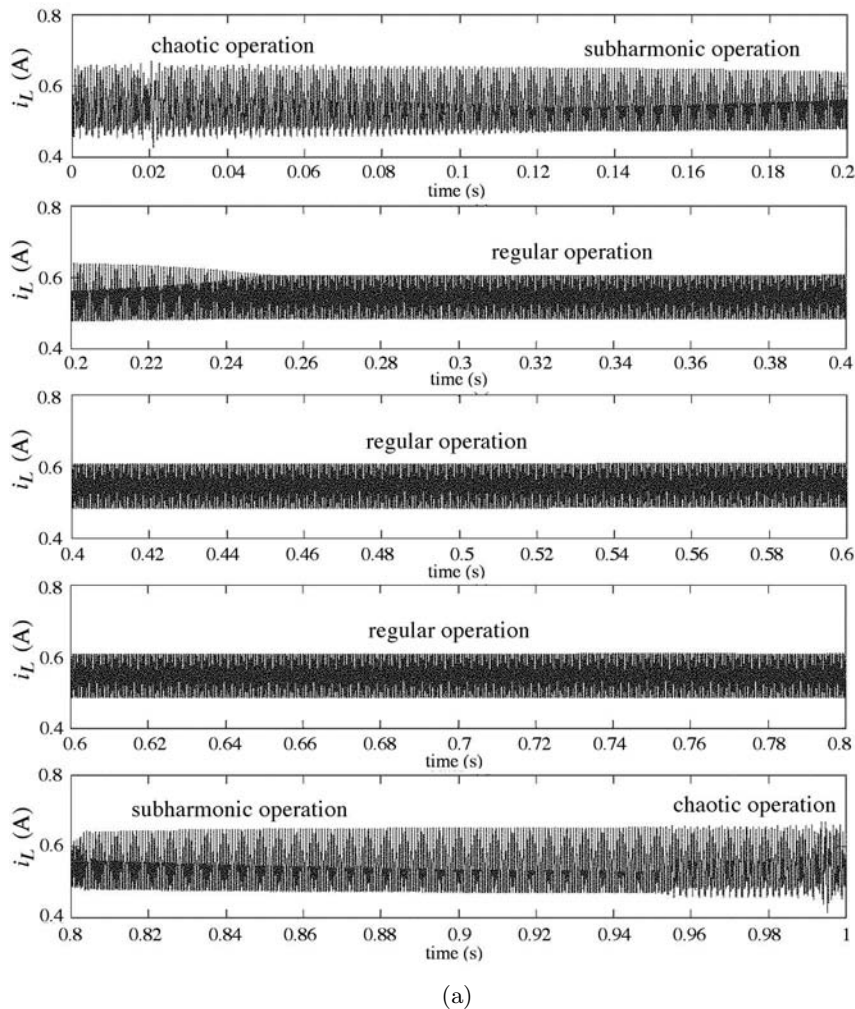
$$\begin{aligned} L &= 20 \text{ mH}, C = 47 \mu\text{F}, R = 22 \Omega, f_o = 2500 \text{ Hz}, \\ E &= 24 \text{ V}, V_{\text{ref}} = 11 \text{ V}, V_L = 3.8 \text{ V} \text{ and } V_U = 8.2 \text{ V}. \end{aligned}$$

The spurious signal frequency f_s is 2501 Hz. Time-domain cycle-by-cycle simulations are performed and the inductor current waveform is shown in [Figure 10.2](#). Here, we observe “intermittent” chaos and “intermittent” subharmonics for relatively strong and weak coupling, respectively.*

These kinds of phenomena are commonly observed by practicing power supply engineers in their design workbenches. Here, we show that the phenomena can be explained in terms of coupling of a spurious signal through unintended paths to the power supply.

The intermittent period is related to the difference between the intruding signal frequency and the power supply’s switching frequency. In this case, the intermittent period is 1 s.

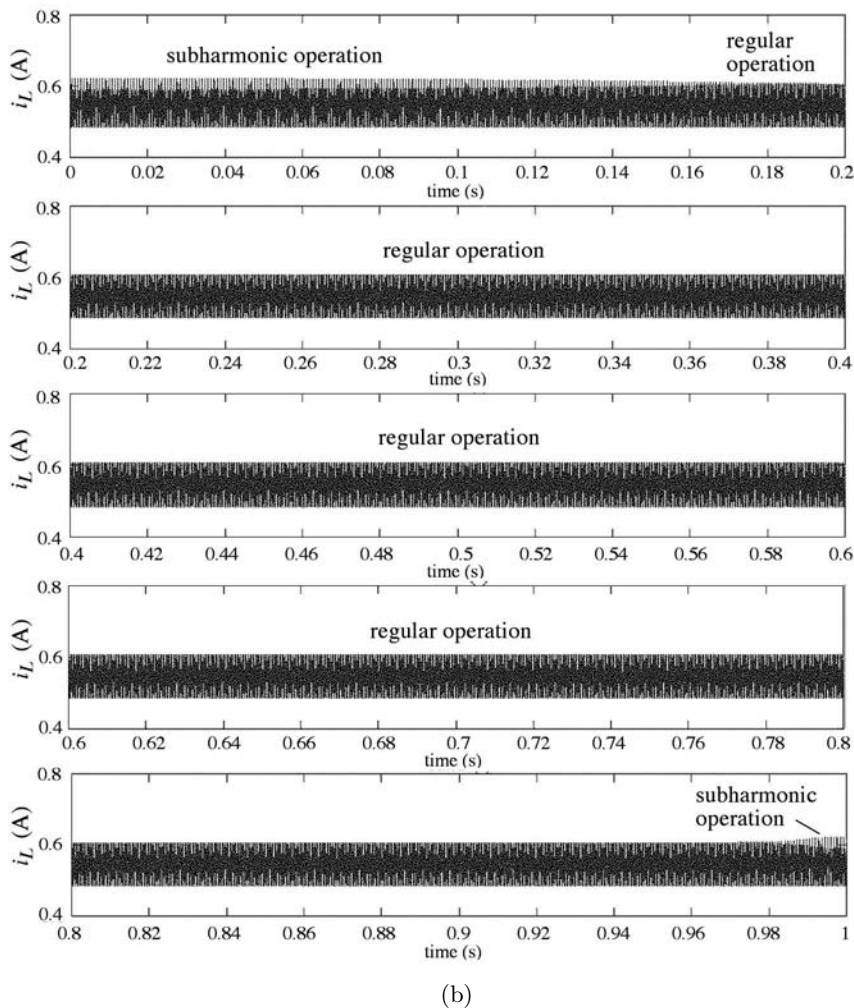
*The term *intermittent chaos* has been used in the mathematics literature to describe a few special types of chaotic behavior [109]. Here, we use the term to describe a particular operation where chaos shows up periodically between regular operations. Such intermittent chaotic operation is sometimes called *breathing* in the physics literature [119].



(a)

FIGURE 10.2

Inductor current waveform for buck converter with unintended coupling of sinusoidal intruding source for (a) $\alpha = 0.0034$ showing “intermittent” chaos, and (b) $\alpha = 0.0003$ showing “intermittent” subharmonics.



(b)

FIGURE 10.2 continued.

10.3 Time-Bifurcation Diagrams – A Closer Look

For a clear exposition of the phenomenon, it is customary in the systems theory literature to examine the “sampled waveforms,” which effectively ignore the detailed switching ripples but focus on the movement of the waveforms at periodic switching instants. Specifically we sample the waveforms at $t = nT$,

where T is the switching period, i.e., $T = 1/f_o$, and the resulting plots are called *time-bifurcation diagrams* since they reflect the change of qualitative behavior as time elapses.

10.3.1 Sinusoidal Intruding Source

We begin with the case of sinusoidal intruding signals as described in the previous section, i.e.,

$$v_s = \alpha V_{\text{ref}} \sin 2\pi f_s t. \quad (10.3)$$

Some typical time-bifurcation diagrams are shown in [Figure 10.3](#), from which we observe the following.

- When the intruding signal strength is very weak, the power supply can still maintain its regular operation, though the average operating point fluctuates. The effect is not significant.
- As the intruding signal strength increases, the power supply experiences subharmonic operation intermittently with regular operation. For a relatively low intruding signal strength, period-2 subharmonic operation is observed intermittently with regular operation. Further increase in intruding signal strength causes period-4 subharmonic operation to occur intermittently with period-2 subharmonic and regular operations.
- When the intruding signal strength is strong, the power supply experiences chaotic operation intermittently with subharmonic and regular operations.
- The intermittent period is equal to the $1/|f_o - f_s|$. Thus, if the intruding signal frequency is very close to the switching frequency of the power supply, the intermittency is long.

10.3.2 Rectangular Pulse Intruding Source

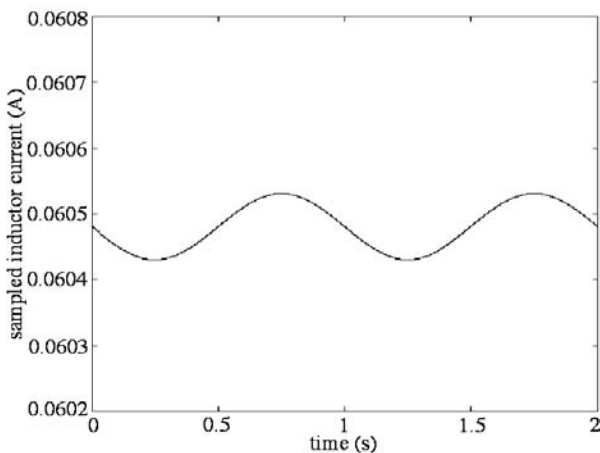
We now consider another type of spurious signal which is likely to be generated from a PWM generator of another power supply and coupled to the power supply under study through unintended paths. This situation can arise in modular power supplies with individual PWM generators. For the purpose of analysis, we assume that the intruding source v_s is given by

$$v_s = \alpha V_{\text{ref}} \text{rect}(f_s t) \quad (10.4)$$

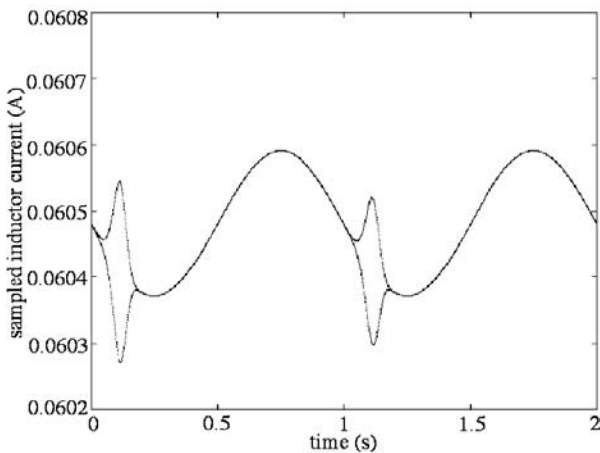
where

$$\text{rect}(x) = \begin{cases} +1 & \text{if } 0 \leq x < 0.5 \\ -1 & \text{if } 0.5 \leq x < 1 \\ \text{rect}(x-1) & \text{if } x \geq 1. \end{cases} \quad (10.5)$$

Effects similar to the case of sinusoidal intruding signals have been found from simulations. Some time-bifurcation diagrams are shown in [Figure 10.4](#).



(a) $\alpha = 0.0001$



(b) $\alpha = 0.00022$

FIGURE 10.3

Sampled inductor current waveforms (time-bifurcation diagrams) for buck converter with unintended coupling of sinusoidal intruding source for different coupling strengths. (a) Regular operation with fluctuation of average value; (b)–(d) “intermittent” subharmonics; (e)–(f) “intermittent” chaos.

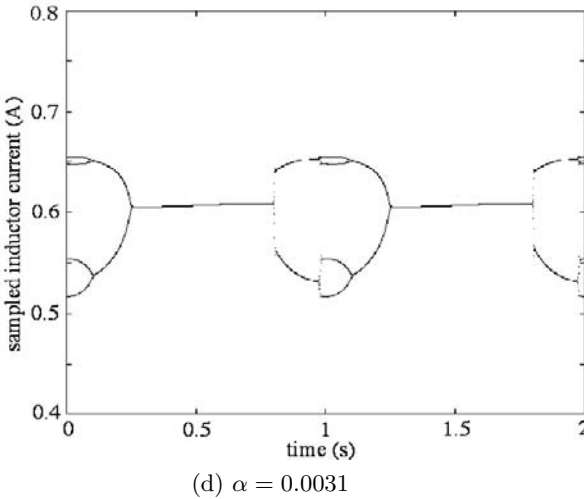
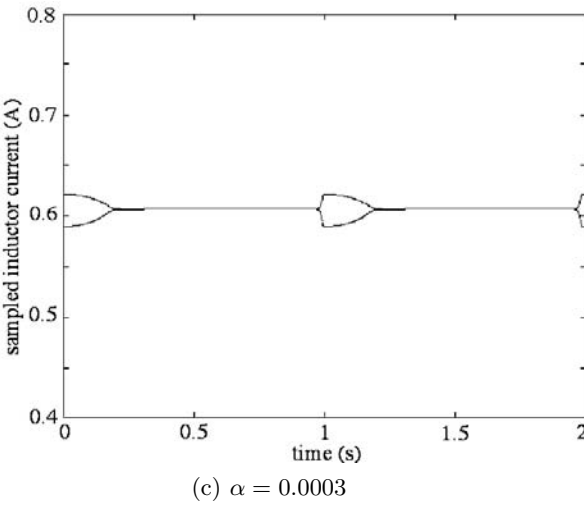
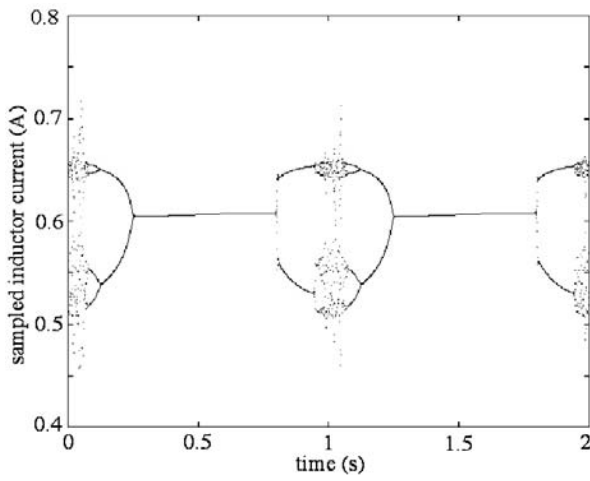


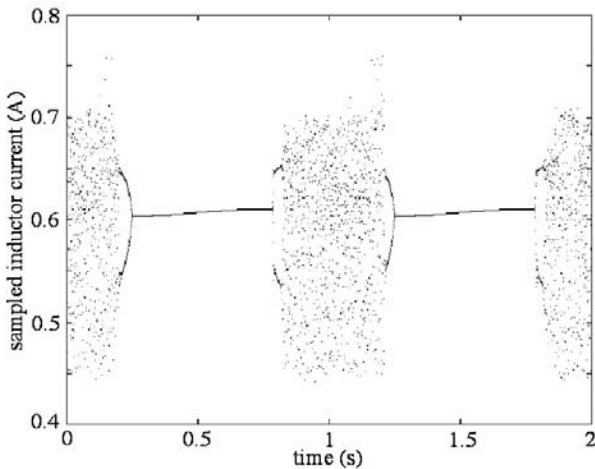
FIGURE 10.3 continued.

10.4 Experimental Observations

A circuit prototype can be constructed to verify the possibility of intermittent operation as suggested by the afore-described circuit model. To avoid obscuring the essentials, the experimental study does not include the actual coupling process which has been assumed to take place by any possible means. For the



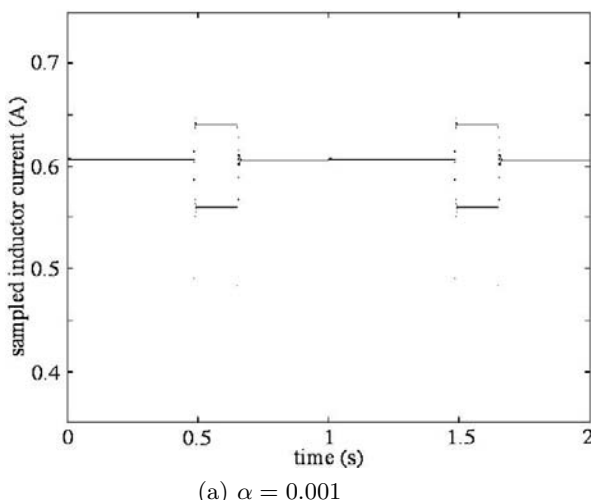
(e) $\alpha = 0.0034$



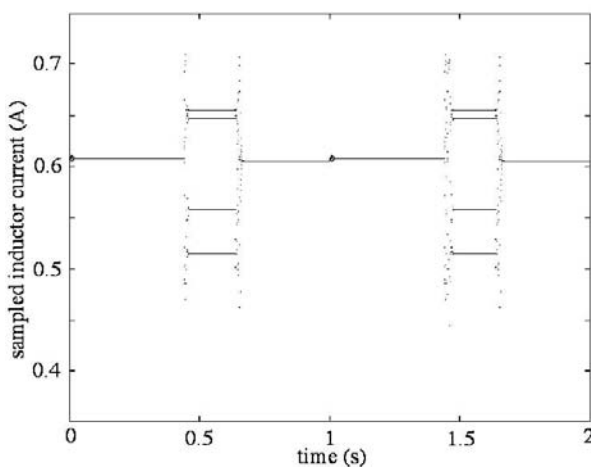
(f) $\alpha = 0.007$

FIGURE 10.3 continued.

purpose of verifying the phenomena observed from simulations, it suffices to “add” the intruding signal directly to the reference voltage. The circuit parameters are the same as those used in the simulations. Sinusoidal as well as rectangular intruding signals have been applied in the experiment. By varying the intruding signal strength, we observe “intermittent” subharmonics and chaos similar to those observed from simulations. [Figure 10.5](#) shows a few time-bifurcation diagrams obtained experimentally.



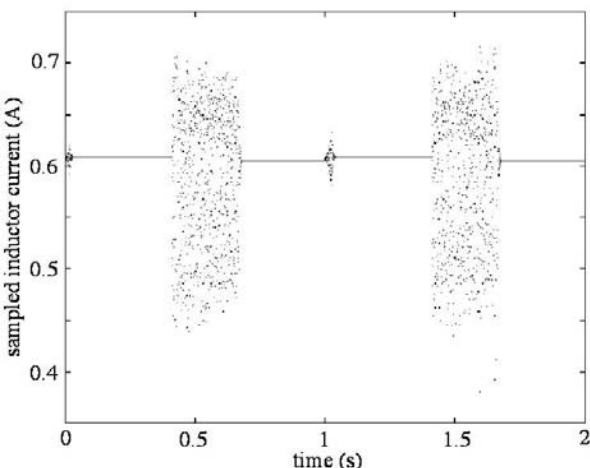
(a) $\alpha = 0.001$



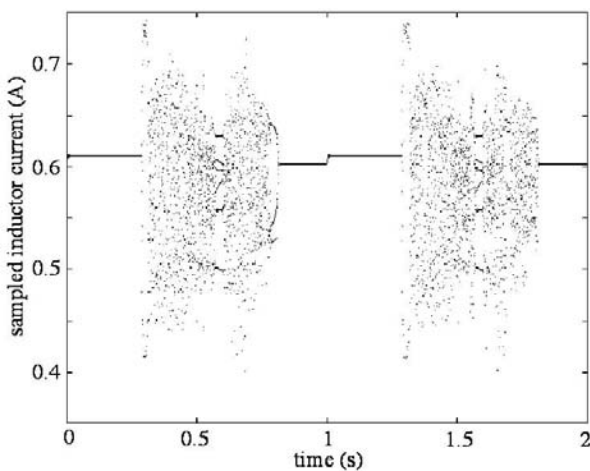
(b) $\alpha = 0.003$

FIGURE 10.4

Sampled inductor current waveforms (time-bifurcation diagrams) for buck converter with unintended coupling of rectangular intruding source for different coupling strengths. (a)–(b) “intermittent” subharmonics; (c)–(d) “intermittent” chaos.



(c) $\alpha = 0.004$

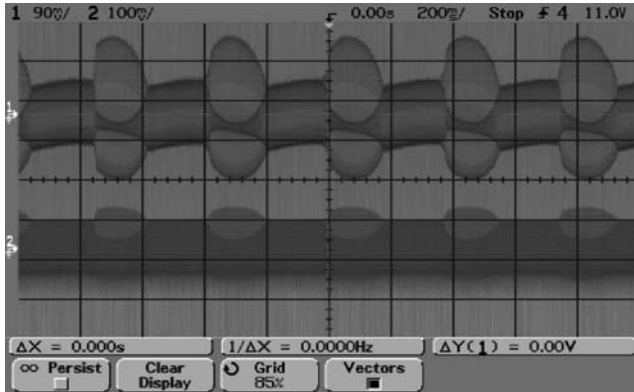


(d) $\alpha = 0.008$

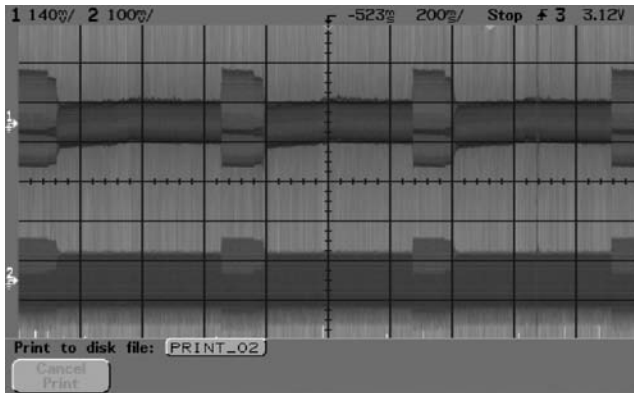
FIGURE 10.4 continued.

10.5 Parameters Affecting the Occurrence of “Intermittent” Chaos

So far, we have only considered a particular set of parameters and the general phenomena of “intermittent” subharmonics and chaos in a switching con-



(a) sinewave intruder $\alpha = 0.0012$



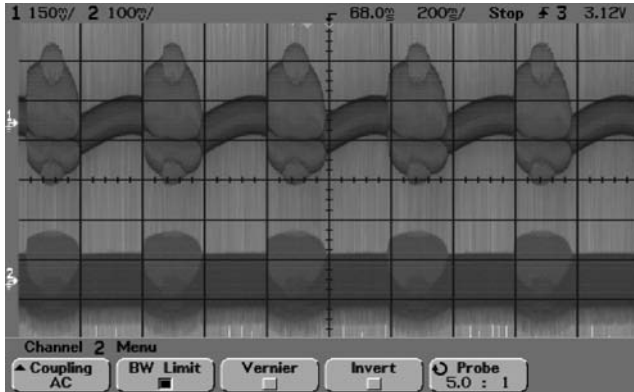
(b) rectangular wave intruder $\alpha = 0.0007$

FIGURE 10.5

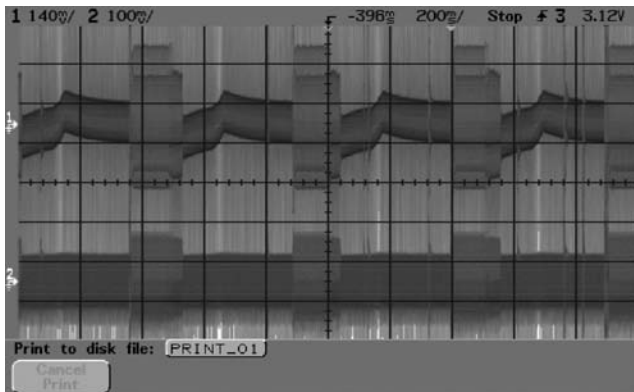
Measured time-bifurcation diagrams for buck converter with coupling of intruding source for different coupling strengths. (a)–(b) Intermittent period-2 subharmonics (upper trace: output voltage, 90 mV/div for (a) and 140 mV/div for (b); lower trace: inductor current, 100 mA/div); (c)–(d) intermittent period-2 and period-4 subharmonics (upper trace: output voltage, 150 mV/div for (c) and 140 mV/div for (d); lower trace: inductor current, 100 mA/div); (e)–(f) “intermittent” chaos (upper trace: output voltage, 250 mV/div; lower trace: inductor current, 200 mA/div).

verter. Further simulations with different sets of parameters are needed to determine whether α can be smaller or bigger in order to drive the converter into “intermittent” chaos.

The thresholds of the coupling signal strength for intermittent subharmon-



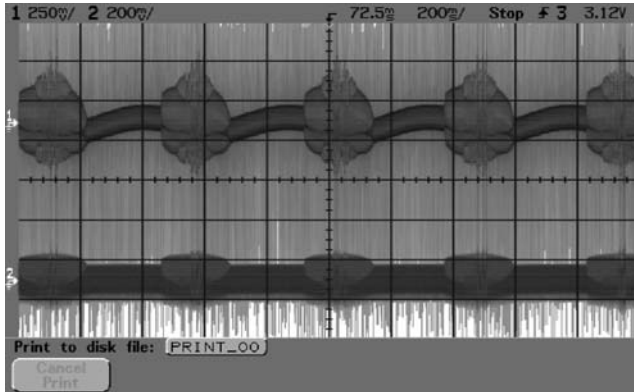
(c) sinewave intruder $\alpha = 0.0036$



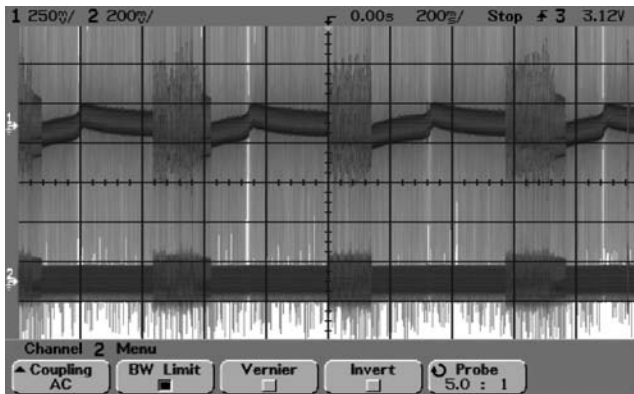
(d) rectangular wave intruder $\alpha = 0.0036$

FIGURE 10.5 continued.

ics and chaos are summarized in [Tables 10.1](#) and [10.2](#). Graphical presentations are also shown in [Figure 10.6](#), where the upper surface gives the thresholds for “intermittent” chaos and the lower surface gives the thresholds for “intermittent” subharmonics. It should be noted that these data are obtained for a particular converter operating with a specific set of circuit parameters, and they are useful for inspecting the general trend rather than providing absolute design data. Nonetheless, from these data, it is clear that if the feedback gain is higher (relatively) or the input voltage is higher (for the same output voltage), the converter is more vulnerable to attack by spurious signal coupling, i.e., a smaller α suffices to cause “intermittent” subharmonics and chaos. This observation can be easily understood because the converter concerned is closer to the operating boundary with a higher feedback gain or a



(e) sinewave intruder $\alpha = 0.004$



(f) rectangular wave intruder $\alpha = 0.0044$

FIGURE 10.5 continued.

higher input voltage, and a relatively smaller α will push it to subharmonics and chaos.

If an analytical expression for the threshold of α is desired, we may follow the standard procedure for finding the bifurcation point. The general procedure involves deriving the Jacobian and evaluating its eigenvalues, as explained previously in [Chapters 5](#) and [7](#). We omit the details here. In summary, we first derive the iterative map for the buck converter, as described in [Chapter 3](#). The desirable form of the iterative map for this study is

$$\mathbf{x}_n = f(\mathbf{x}_{n-1}, E, A, V_{\text{ref}}) \quad (10.6)$$

where \mathbf{x} is the usual state vector, E is the input voltage, A is the feedback gain, and V_{ref} is the reference voltage to which spurious signal is added. The next

TABLE 10.1Threshold values of α at which “intermittent” subharmonics occur.

Gain A	$E = 19 \text{ V}$	$E = 20 \text{ V}$	$E = 21 \text{ V}$	$E = 22 \text{ V}$	$E = 23 \text{ V}$	$E = 24 \text{ V}$
6.0	0.0045	0.0043	0.0041	0.0039	0.0036	0.0033
6.4	0.0038	0.0037	0.0035	0.0032	0.0030	0.0027
6.8	0.0033	0.0031	0.0029	0.0025	0.0024	0.0021
7.2	0.0028	0.0026	0.0024	0.0021	0.0019	0.0016
7.6	0.0023	0.0021	0.0019	0.0017	0.0014	0.0011
8.0	0.0019	0.0017	0.0015	0.0013	0.0010	0.0007
8.4	0.0015	0.0014	0.0011	0.0009	0.0005	0.0003

TABLE 10.2Threshold values of α at which “intermittent” chaos occur.

Gain A	$E = 19 \text{ V}$	$E = 20 \text{ V}$	$E = 21 \text{ V}$	$E = 22 \text{ V}$	$E = 23 \text{ V}$	$E = 24 \text{ V}$
6.0	0.0076	0.0076	0.0075	0.0074	0.0072	0.0070
6.4	0.0068	0.0068	0.0067	0.0066	0.0065	0.0063
6.8	0.0062	0.0062	0.0061	0.0060	0.0058	0.0056
7.2	0.0056	0.0056	0.0055	0.0053	0.0051	0.0049
7.6	0.0050	0.0050	0.0049	0.0048	0.0046	0.0043
8.0	0.0045	0.0045	0.0044	0.0043	0.0041	0.0038
8.4	0.0041	0.0041	0.0040	0.0039	0.0036	0.0034

step is to derive the Jacobian, as illustrated in previous chapters. Suppose the system is operating in a stable period-1 regime when no spurious signal is added to V_{ref} . Let \mathbf{X} be the steady-state value of \mathbf{x} . Then, we aim to find αV_{ref} such that period-doubling occurs when V_{ref} becomes $(1 + \alpha)V_{\text{ref}}$. Precisely at the bifurcation point, one of the eigenvalues of the Jacobian of $f(\cdot)$ is -1 , i.e.,

$$\text{eig} [J_f(\mathbf{X}, E, A, (1 + \alpha)V_{\text{ref}})] = -1 \quad (10.7)$$

where $J_f(\cdot)$ is the Jacobian of $f(\cdot)$ evaluated at the given steady-state condition with αV_{ref} added to V_{ref} . Thus, by solving (10.7), the threshold amplitude α can be found.

10.6 Summary of the Basic Phenomenon

In the foregoing, we have made an attempt to rationalize a commonly observed but rarely explained phenomenon in power supply design. By using an appropriate circuit model, “intermittent” chaos and subharmonics can be explained in terms of coupling of spurious signals. Several points are worth noting here. First, our study in this chapter has focused on a simple voltage-feedback buck

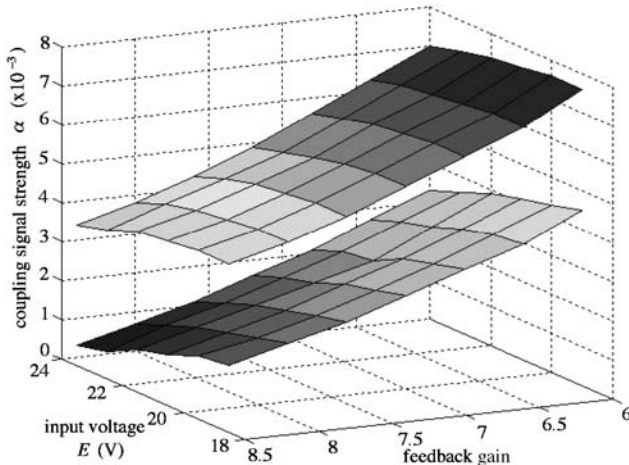


FIGURE 10.6

Graphical representation of the thresholds of coupling signal strength for “intermittent” chaos (upper surface) and “intermittent” subharmonics (lower surface).

converter. Since the purpose is to illustrate the effect of the spurious signal coupling, we retain only the essential part of the feedback circuit and the main power stage. The key phenomenon is the modulation of a crucial parameter which leads to operation in the vicinity of the stability boundary. Second, we have shown in particular that the signal strength and frequency of the intruding signal are vital parameters that affect the type of intermittent behavior and the period of intermittency. Finally, we should stress that the same analysis can be used to study the intermittent chaotic and subharmonic operations in other types of converters. For instance, current-mode controlled converters are equally vulnerable to attacks by spurious signal coupling. It should be obvious that if the compensation slope is modulated to the extent that the converter is driven out of the usual stability region, we may observe intermittent chaos or subharmonics in a current-mode controlled switching converter.

Bibliography

- [1] R. H. Abraham and C. D. Shaw, *Dynamics—The Geometry of Behavior*, Reading MA: Addison-Wesley, 1992.
- [2] K. T. Alligood, T. D. Sauer and J. A. Yorke, *Chaos: An Introduction to Dynamical Systems*, New York: Springer-Verlag, 1996.
- [3] J. Argyris, G. Faust and M. Haase, *An Exploration of Chaos*, Amsterdam: Elsevier Science BV, 1994.
- [4] D. K. Arrowsmith and C. M. Place, *An Introduction to Dynamical Systems*, Cambridge: Cambridge University Press, 1990.
- [5] A. El Aroudi, Hopf bifurcation and chaos from torus breakdown in a pwm voltage-controlled dc/dc boost converters, *IEEE Transactions on Circuits and Systems Part I*, vol. 46, no. 11, pp. 1374–1382, 1999.
- [6] S. Banerjee, Coexisting attractors, chaotic saddles, and fractal basins in a power electronic circuit, *IEEE Transactions on Circuits and Systems Part I*, vol. 44, no. 9, pp. 847–849, 1997.
- [7] S. Banerjee and K. Chakrabarty, Nonlinear modeling and bifurcations in the boost converter, *IEEE Transactions on Power Electronics*, vol. 13, no. 2, pp. 252–260, 1998.
- [8] S. Banerjee, M. S. Karthik, G. H. Yuan and J. A. Yorke, Bifurcations in one-dimensional piecewise smooth maps—theory and applications in switching circuits, *IEEE Transactions on Circuits and Systems Part I*, vol. 47, no. 3, pp. 389–394, 2000.
- [9] S. Banerjee, P. Ranjan and C. Grebogi, Bifurcation in two-dimensional piecewise smooth maps — theory and applications in switching circuits, *IEEE Transactions on Circuits and Systems Part I*, vol. 47, no. 5, pp. 633–643, 2000.
- [10] S. Banerjee, E. Ott, J. A. Yorke and G. H. Yuan, Anomalous bifurcations in dc-dc converters: borderline collisions in piecewise smooth maps, *IEEE Power Electronics Specialists Conference Record*, pp. 1337–1344, 1997.
- [11] S. Banerjee and G. Verghese (Editors), *Nonlinear Phenomena in Power Electronics: Attractors, Bifurcations, Chaos, and Nonlinear Control*, New York: IEEE Press, 2001.

- [12] A. L. Baranovski, A. Mögel, W. Schwarz and O. Woywode, Statistical analysis of a dc-dc converter, *Proceedings of International Workshop on Nonlinear Dynamics of Electronic Systems*, pp. 15–18, 1999.
- [13] R. M. Bass, B. S. Heck and R. A. Khan, Average modeling of current-controlled converters: instability prediction, *International Journal of Electronics*, vol. 77, no. 5, pp. 613–628, 1994.
- [14] M. di Bernardo, C. J. Budd and A. R. Champneys, Grazing and border-collision in piecewise-smooth systems: a unified analytical framework, *Physics Review Letters*, vol. 86, no. 12, pp. 2553–2556, 2000.
- [15] M. di Bernardo, C. J. Budd and A. R. Champneys, Corner collision implies border collision, *Physica D*, vol. 154, pp. 171–194, 2001.
- [16] M. di Bernardo, E. Fossas, G. Olivar and F. Vasca, Secondary bifurcations and high-periodic orbits in voltage controlled buck converter, *International Journal of Bifurcation and Chaos*, vol. 12, No. 7, pp. 2755–2771, 1997.
- [17] M. di Bernardo, F. Garofalo, L. Glielmo and F. Vasca, Quasi-periodic behaviours in dc-dc converters, *IEEE Power Electronics Specialists Conference Record*, pp. 1376–1381, 1996.
- [18] M. di Bernardo, L. Glielmo, F. Garofalo and F. Vasca, Switching, bifurcations and chaos in dc/dc converters, *IEEE Transactions on Circuits and Systems Part I*, vol. 45, no. 2, pp. 133–141, 1998.
- [19] M. di Bernardo and F. Vasca, Discrete-time maps for the analysis of bifurcations and chaos in dc/dc converters, *IEEE Transactions on Circuits and Systems Part I*, vol. 47, no. 2, pp. 130–143, 2000.
- [20] B. K. Bose, *Modern Power Electronics: Evolution, Technology and Applications*, New York: IEEE Press, 1992.
- [21] R. W. Brockett and J. R. Wood, Understanding power converter chaotic behavior in protective and abnormal modes, *Proceedings of Powercon II*, 1984.
- [22] A. Capel, G. Ferrante, D. O'Sullivan and A. Weinberg, Application of the injected-current control model for the dynamic analysis of switching regulators with a new concept of LC³ modulator, *IEEE Power Electronics Specialists Conference Record*, pp. 135–147, 1978.
- [23] W. C. Y. Chan and C. K. Tse, A universal bifurcation path conjectured from current-programmed switching converters, *Proceedings of International Symposium on Nonlinear Theory and Its Applications*, (NOLTA'96), Japan, pp. 121–124, 1996.
- [24] W. C. Y. Chan and C. K. Tse, On the form of feedback function that can lead to chaos in discontinuous-mode dc/dc converters, *IEEE Power Electronics Specialists Conference Record*, pp. 1317–1322, 1997.

- [25] W. C. Y. Chan and C. K. Tse, Study of bifurcation in current-programmed dc/dc boost converters: from quasiperiodicity to period-doubling, *IEEE Transactions on Circuits and Systems Part I*, vol. 44, no. 12, pp. 1129–1142, 1997.
- [26] W. C. Y. Chan and C. K. Tse, Bifurcations in current-programmed dc/dc buck switching regulators—conjecturing a universal bifurcation path, *International Journal of Circuit Theory and Applications*, vol. 26, no. 2, pp. 127–145, 1998.
- [27] K. Chakrabarty, G. Podder and S. Banerjee, Bifurcation behavior of buck converter, *IEEE Transactions on Power Electronics*, vol. 11, no. 3, pp. 439–447, 1995.
- [28] G. Chen (Editor), *Controlling Chaos and Bifurcations in Engineering Systems*, Boca Raton: CRC Press, 2000.
- [29] G. Chen and X. Dong, *From Chaos to Order: Methodologies, Perspectives and Applications*, Singapore: World Scientific, 1998.
- [30] G. Chen and T. Ueta (Editors), *Chaos in Circuits and Systems*, Singapore: World Scientific, 2002.
- [31] W. K. Chen (Editor), *The Circuits and Filters Handbook*, Boca Raton: CRC Press, 1995.
- [32] Y. Chen and A. Y. T. Leung, *Bifurcation and Chaos in Engineering*, New York: Springer-Verlag, 1998.
- [33] G. C. Chryssis, *High-Frequency Switching Power Supplies: Theory and Design*, New York: McGraw Hill, 1989.
- [34] L. O. Chua, M. Hasler, J. Neirynck and P. Verburgh, Dynamics of a piecewise linear resonant circuit, *IEEE Transactions on Circuits and Systems Part I*, vol. 29, no. 8, pp. 535–547, 1982.
- [35] L. O. Chua, C. W. Wu, A. Huang and G. Q. Zhong, A universal circuit for studying and generating chaos—Part I: routes to chaos, *IEEE Transactions on Circuits and Systems Part I*, vol. 40, no. 10, pp. 732–744, 1993.
- [36] L. O. Chua, C. W. Wu, A. Huang and G. Q. Zhong, A universal circuit for studying and generating chaos—Part II: strange attractors, *IEEE Transactions on Circuits and Systems Part I*, vol. 40, no. 10, pp. 745–761, 1993.
- [37] S. Ćuk and R. D. Middlebrook, A new optimum topology switching dc-to-dc converter, *IEEE Power Electronics Specialists Conference Record*, pp. 160–179, 1977.

- [38] J. H. B. Deane, Chaos in a current-mode controlled boost converter, *IEEE Transactions on Circuits and Systems Part I*, vol. 39, no. 8, pp. 680–683, 1992.
- [39] J. H. B. Deane and D. C. Hamill, Instability, subharmonics, and chaos in power electronic circuits, *IEEE Transactions on Power Electronics*, vol. 5, no. 3, pp. 260–268, 1990.
- [40] J. H. B. Deane and D. C. Hamill, Improvement of power supply EMC by chaos, *IEE Electronics Letters*, vol. 32, p. 1045, 1996.
- [41] R. L. Devaney, *Introduction to Chaotic Dynamical Systems*, New York: Addison-Wesley, 1989.
- [42] L. H. Dixon Jr., High power factor preregulator for off-line power supplies, *Unitrode Switching Regulated Power Supply Design Manual*, Paper 12, SEM-700, 1990.
- [43] I. Dobson, Stability of ideal thyristor and diode switching circuits, *IEEE Transactions on Circuits and Systems Part I*, vol. 42, no. 9, pp. 517–529, 1995.
- [44] P. G. Drazin, *Nonlinear Systems*, Cambridge UK: Cambridge University Press, 1992.
- [45] C. C. Fang and E. H. Abed, Saddle-node and Neimark bifurcations in pwm converters, in *Nonlinear Phenomena in Power Electronics: Attractors, Bifurcations, Chaos and Nonlinear Control*, Edited by S. Banerjee and G. Verghese, Section 5.4, pp. 229–240, New York: IEEE Press, 2001.
- [46] N. Femia, G. Spagnuolo and V. Tucci, State-space models and order reduction for dc-dc switching converters in discontinuous mode, *IEEE Transactions on Power Electronics*, vol. 10, no. 6, pp. 640–650, 1995.
- [47] J. A. Ferreira, P. R. Willcock and S. R. Holm, Sources, paths and traps of conducted EMI in switch mode circuits, *Proceedings of IEEE Industry Applications Conference*, pp. 1584–1591, 1997.
- [48] E. Fossas and G. Olivari, Study of chaos in the buck converter, *IEEE Transactions on Circuits and Systems Part I*, vol. 43, no. 1, pp. 13–25, 1996.
- [49] D. S. Garabandic and T. B. Petrovic, Modeling parallel operating PWM DC/DC power supplies, *IEEE Transactions on Industrial Electronics*, vol. 42, no. 5, pp. 545–550, 1995.
- [50] R. Giral, L. Martinez-Salamero and S. Singer, Interleaved converters operation based on CMC, *IEEE Transactions on Power Electronics*, vol. 14, no. 4, pp. 643–652, 1999.
- [51] J. Gleick, *Chaos: Making a New Science*, New York: Viking, 1987.

- [52] C. Grebogi, E. Ott and J. A. Yorke, Crisis, sudden changes in chaotic attractors, and transient chaos, *Physica D*, vol. 7D, pp. 181–200, 1983.
- [53] J. Guckenheimer and P. Holmes, *Nonlinear Oscillations, Dynamical Systems and Bifurcations of Vector Fields*, New York: Springer-Verlag, 1983.
- [54] D. Gulick, *Encounters with Chaos*, New York: McGraw Hill, 1992.
- [55] J. Hale, *Ordinary Differential Equations*, New York: Wiley, 1969.
- [56] J. Hale and H. Kocak, *Dynamics and Bifurcations*, New York: Springer-Verlag, 1991.
- [57] N. Hall (Editor), *Exploring Chaos: A Guide to the New Science of Disorder*, New York: Norton, 1991.
- [58] D. C. Hamill, Power electronics: a field rich in nonlinear dynamics, *Proceedings of International Specialists' Workshop on Nonlinear Dynamics of Electronic Systems*, pp. 165–177, 1995.
- [59] D. C. Hamill, S. Banerjee and G. C. Verghese, Chapter 1: Introduction, in *Nonlinear Phenomena in Power Electronics*, S. Banerjee and G.C. Verghese (Eds.), New York: IEEE Press, 2001.
- [60] D. C. Hamill, J. H. B. Deane and D. J. Jefferies, Modeling of chaotic dc/dc converters by iterative nonlinear mappings, *IEEE Transactions on Power Electronics*, vol. 7, no. 1, pp. 25–36, 1992.
- [61] D. C. Hamill and D. J. Jefferies, Subharmonics and chaos in a controlled switched-mode power converter, *IEEE Transactions on Circuits and Systems Part I*, vol. 35, no. 8, pp. 1059–1061, 1988.
- [62] M. Hasler, Electrical circuits with chaotic behavior, *Proceedings of IEEE*, vol. 75, no. 8, pp. 1009–1021, August 1987.
- [63] C. Hayashi, *Nonlinear Oscillations in Physical Systems*, New York: Mc-Graw Hill, 1964.
- [64] C. Hayashi, Y. Ueda and H. Kawakami, Solutions of Duffing's equation using mapping concepts, *Proceedings of International Conference on Nonlinear Oscillations*, Prague, pp. 25–40, 1968.
- [65] R. C. Hilborn, *Chaos and Nonlinear Dynamics: An Introduction for Scientists and Engineers*, New York: Oxford University Press, 2000.
- [66] B. Holland, Modelling, analysis and compensation of the current-mode converter, *Proceedings of Powercon 11*, pp. I-2-1–I-2-6, 1984.
- [67] H. H. C. Iu and C. K. Tse, A study of synchronization in chaotic autonomous Ćuk dc/dc converters, *IEEE Transactions on Circuits and Systems Part I*, vol. 47, no. 6, pp. 913–918, June 2000.

- [68] H. H. C. Iu and C. K. Tse, Bifurcation in parallel-connected boost dc/dc converters, *Proceedings of IEEE International Symposium on Circuits and Systems*, pp. II473–II476, 2000.
- [69] H. H. C. Iu and C. K. Tse, Bifurcation behaviour in parallel-connected buck converters, *IEEE Transactions on Circuits and Systems Part I*, vol. 48, no. 2, pp. 233–240, 2001.
- [70] H. H. C. Iu and C. K. Tse, Bifurcation in parallel-connected boost converters under democratic current sharing, *Proceedings of IEEE International Symposium on Industrial Electronics*, pp. 2118–2123, 2001.
- [71] H. H. C. Iu, C. K. Tse and Y. M. Lai, Effects of interleaving on the bifurcation behaviour of parallel-connected buck converters, *Proceedings of IEEE International Conference on Industrial Technology*, Bangkok, Thailand, pp. 1072–1077, December 2002.
- [72] H. H. C. Iu, C. K. Tse, V. Pjevalica and Y. M. Lai, Analysis of Hopf bifurcation in parallel-connected boost converters via averaged models, *Proceedings of IEEE International Symposium on Circuits and Systems*, Arizona USA, pp. V-305–308, 2002.
- [73] S. Jalali, I. Dobson, R. H. Lasseter and G. Venkataramanan, Switching time bifurcation in a thyristor controlled reactor, *IEEE Transactions on Circuits and Systems Part I*, vol. 43, no. 3, pp. 209–218, 1996.
- [74] M. M. Jovanović, D. E. Crow and F. Y. Lieu, A novel, low-cost implementation of democratic load-current sharing of paralleled converter modules, *IEEE Transactions on Power Electronics*, vol. 11, no. 4, pp. 604–611, 1996.
- [75] T. Kapitaniak, *Controlling Chaos*, London: Academic Press, 1996.
- [76] T. Kapitaniak, *Chaos for Engineers: Theory, Applications and Control*, Heidelberg: Springer-Verlag, 2000.
- [77] T. Kapitaniak and S. R. Bishop, *The Illustrated Dictionary of Nonlinear Dynamics and Chaos*, Chichester: Wiley, 1999.
- [78] J. G. Kassakian, M. F. Schlecht and G. C. Verghese, *Principles of Power Electronics*, Reading: Addison-Wesley, 1991.
- [79] H. Kawakami, *Theory of Nonlinear Phenomena and Dynamical Systems*, Research Institute for Mathematical Sciences, Kyoto University, Japan, No. 506, 1983.
- [80] J. H. Kim and J. Stringer (Editors), *Applied Chaos*, New York: Wiley, 1992.
- [81] A. S. Kislovski, R. Redl and N. O. Sokal, *Dynamical Analysis of Switching Mode DC/DC Converters*, New York: Van Nostrand Reinhold, 1996.

- [82] T. Kousaka, T. Ueta and H. Kawakami, Bifurcation in switched nonlinear dynamical systems, *IEEE Transactions on Circuits and Systems Part II*, vol. 46, no. 7, pp. 878–885, 1999.
- [83] P. T. Krein, *Elements of Power Electronics*, New York: Oxford University Press, 1998.
- [84] Y. Kuroe and S. Hagashi, Analysis of bifurcation in power electronic induction motor drive systems, *IEEE Power Electronics Specialists Conference Record*, pp. 923–930, 1989.
- [85] Y. A. Kuznetsov, *Elements of Applied Bifurcation Theory*, New York: Springer-Verlag, 1996.
- [86] Y. C. Lai, C. Grebogi and J. A. Lai, Sudden change in the size of chaotic attractors: how does it occur? *Applications of Chaos*, pp. 411–456, New York: Wiley Interscience, 1992.
- [87] Y. M. Lai, Power supplies, in *The Power Electronics Handbook: Devices, Circuits and Applications*, Edited by M. H. Rashid, Chapter 20, pp. 487–506, New York: Academic Press, 2001.
- [88] Y. S. Lee, *Computer Aided Analysis and Design of Switch Mode Power Supplies*, New York: Marcel Dekker, 1993.
- [89] Y. H. Lim and D. C. Hamill, Problems of computing Lyapunov exponents in power electronics, *Proceedings of IEEE International Symposium on Circuits and Systems*, pp. 297–301, 1999.
- [90] C. S. Lin and C. L. Chen, Single-wire current-share paralleling of current-mode-controlled DC power supplies, *IEEE Transactions on Industrial Electronics*, vol. 47, no. 4, pp. 780–786, 2000.
- [91] K. H. Liu and F. C. Lee, Topological constraints on basic PWM converters, *Power Electronics Specialists Conference Record*, pp. 164–172, 1988.
- [92] E. N. Lorenz, Deterministic nonperiodic flow, *Journal of Atmospheric Science*, vol. 2, pp. 130–141, 1963.
- [93] E. N. Lorenz, *The Essence of Chaos*, London: Cambridge University Press, 1993.
- [94] A. Magauer and S. Banerjee, Bifurcations and chaos in the tolerance band pwm technique, *IEEE Transactions on Circuits and Systems Part I*, vol. 37, no. 3, pp. 399–409, 1990.
- [95] J. L. R. Marrero, J. M. Font and G. C. Verghese, Analysis of the chaotic regime for dc-dc converters under current mode control, *IEEE Power Electronics Specialists Conference Record*, pp. 1477–1483, 1996.

- [96] S. K. Mazumder, A. H. Nayfeh and D. Boroyevich, Theoretical and experimental investigation of the fast- and slow-scale instabilities of a dc/dc converter, *IEEE Transactions on Power Electronics*, vol. 16, no. 2, pp. 201–216, 2001.
- [97] S. K. Mazumder, A. H. Nayfeh and D. Boroyevich, A nonlinear approach to the analysis of stability and dynamics of standalone and parallel DC-DC converters, *Proceedings of IEEE Applied Power Electronics Conference and Exposition*, pp. 784–790, 2001.
- [98] R. D. Middlebrook and S. Cuk, A general unified approach to modeling switching-converter power stages, *IEEE Power Electronics Specialists Conference Record*, pp. 18–34, 1976.
- [99] D. M. Mitchell, *DC-DC Switching Converter Analysis*, New York: McGraw Hill, 1988.
- [100] N. Mohan, T. Undeland and W. Robbins, *Power Electronics*, New York: Wiley, 1995.
- [101] F. C. Moon, *Chaotic and Fractal Dynamics*, Chichester: Wiley, 1992.
- [102] I. Nagy, Nonlinear phenomena in power electronics, *Journal Automatika*, vol. 42, no. 3–4, pp. 117–132, 2001.
- [103] H. E. Nusse and J. A. Yorke, Border-collision bifurcations including ‘period two to period three’ for piecewise smooth systems, *Physica D*, vol. 57, pp. 39–57, 1992.
- [104] H. E. Nusse, E. Ott and J. A. Yorke, Border-collision bifurcations: an explanation for observed bifurcation phenomena, *Physical Review E*, vol. 49, pp. 1073–1076, 1994.
- [105] M. J. Ogorzalek, *Chaos and Complexity in Nonlinear Electronic Circuits*, World Scientific Series on Nonlinear Science, vol. 22, 1997.
- [106] M. J. Ogorzalek, Chaos control: how to avoid chaos or take advantage of it, *Journal of Franklin Institute*, vol. 331B, pp. 681–704, 1994.
- [107] M. Orabi, T. Ninomiya and C. Jin, Nonlinear dynamics and stability analyses of boost power-factor-correction circuit, *Proceedings of International Conference on Power System Technology*, pp. 600–605, 2002.
- [108] R. Oruganti and F. C. Lee, State-plane analysis of parallel resonant converter, *IEEE Power Electronics Specialists Conference Record*, pp. 56–73, 1985.
- [109] E. Ott, *Chaos in Dynamical Systems*, Cambridge: Cambridge University Press, 1992.
- [110] E. Ott, T. Sauer and J. A. Yorke (Editors), *Coping with Chaos: Analysis of Chaotic Data and the Exploration of Chaotic Systems*, New York: Wiley, 1994.

- [111] H. A. Owen, A. Capel and J. G. Ferrante, Simulation and analysis methods for sampled power electronic systems, *IEEE Power Electronics Specialists Conference Record*, 1976.
- [112] Y. Panov, J. Rajagopalan and F. C. Lee, Analysis and design of N paralleled DC-DC converters with master-slave current-sharing control, *Proceedings of IEEE Applied Power Electronics Conference and Exposition*, pp. 436–442, 1997.
- [113] T. S. Parker and L. O. Chua, *Practical Numerical Algorithms for Chaotic Systems*, New York: Springer-Verlag, 1989.
- [114] S. Parui and S. Banerjee, Border collision bifurcations at the change of state-space dimension, *Chaos*, vol. 12, no. 4, pp. 1055–1069, 2002.
- [115] H. Peitgen, H. Jürgens and D. Saupe, *Chaos and Fractals: New Frontiers of Science*, Berlin: Springer-Verlag, 1992.
- [116] D. J. Perreault, K. Sato, R. L. Selders and J. G. Kassakian, Switching-rippled-based current sharing for paralleled power converters, *IEEE Transactions on Circuits and Systems Part I*, vol. 46, no. 10, pp. 1264–1274, 1999.
- [117] S. Prentiss, *The Complete Book of Oscilloscopes*, New York: McGraw Hill, 1992.
- [118] A. I. Pressman, *Switching Power Supply Design*, New York: McGraw Hill, 1992.
- [119] Z. Qu, G. Hu, G. Yang, G. Qin, Phase effect in taming nonautonomous chaos by weak harmonic perturbations, *Physics Review Letters*, vol. 74, no. 10, pp. 1736–1739, 1995.
- [120] J. Rajagopalan, K. Xing, Y. Guo, F. C. Lee and B. Manners, Modeling and dynamic analysis of paralleled dc/dc converters with master-slave current sharing control, *Proceedings of IEEE Applied Power Electronics Conference and Exposition*, pp. 678–684, 1996.
- [121] M. H. Rashid (Editor), *The Power Electronics Handbook*, San Diego: Academic Press, 2001.
- [122] R. Redl, Power-factor-correction in single-phase switching-mode power supplies: an overview, *International Journal of Electronics*, vol. 77, no. 5, pp. 555–582, 1994.
- [123] R. Redl and N. O. Sokal, Current-mode control, five different types, used with the three basic classes of power converters, *IEEE Power Electronics Specialists Conference Record*, pp. 771–775, 1985.
- [124] R. A. Rohrer, *Circuit Theory: An Introduction to the State Variable Approach*, New York: McGraw Hill, 1970.

- [125] P. M. de Russo, R. J. Roy and C. M. Close, *State Variables for Engineer*, New York: Wiley, 1966.
- [126] S. R. Sanders and G. C. Verghese, Lyapunov-based control of switched power converters, *IEEE Power Electronics Specialists Conference Record*, pp. 51–58, 1990.
- [127] M. Schroeder, *Fractals, Chaos, Power Laws: Minutes from an Infinite Paradise*, New York: Freeman, 1991.
- [128] R. P. Severns and E. J. Bloom, *Modern Dc-to-Dc Switchmode Power Converter Circuits*, New York: Van Nostrand, 1985.
- [129] L. P. Shil'nikov, A. L. Shil'nikov, D. V. Turaev and L. O. Chua (Editors), *Methods of Qualitative Theory in Nonlinear Dynamics*, Singapore: World Scientific, 1998.
- [130] D. Singer, Stable orbits and bifurcation of maps of the interval, *SIAM Journal of Applied Mathematics*, vol. 35, pp. 260–267, 1978.
- [131] K. Siri, C. Q. Lee and T. F. Wu, Current distribution control for parallel connected converters: Part I, *IEEE Transactions on Aerospace Electronics Systems*, vol. 28, no. 3, pp. 829–840, 1992.
- [132] K. Siri, C. Q. Lee and T. F. Wu, Current distribution control for parallel connected converters: Part II, *IEEE Transactions on Aerospace Electronics Systems*, Vol. 28, No. 3, pp. 841–851, 1992.
- [133] D. Skowronn, D. Li and R. Tymerski, Simulation of networks with ideal switches, *International Journal of Electronics*, vol. 77, no. 5, pp. 715–730, 1994.
- [134] C. Sparrow, *The Lorenz Equations*, New York: Springer-Verlag, 1982.
- [135] S. H. Strogatz, *Nonlinear Dynamics and Chaos*, Reading, MA: Addison-Wesley, 1994.
- [136] Z. Sütő, I. Nagy and E. Masada, Avoiding chaotic processes in current control of ac drive, *IEEE Power Electronics Specialists Conference Record*, pp. 255–261, 1998.
- [137] R. E. Tarter, *Solid-State Power Conversion Handbook*, New York: Wiley, 1991.
- [138] J. M. T. Thompson and H. B. Stewart, *Nonlinear Dynamics and Chaos*, Second Edition, Chichester: Wiley, 2000.
- [139] V. J. Thottuvelil and G. C. Verghese, Analysis and control of paralleled dc/dc converters with current sharing, *IEEE Transactions on Power Electronics*, vol. 13, no. 4, pp. 635–644, 1998.
- [140] B. Tomescu and H. F. VanLandingham, Improved large-signal performance of paralleled DC-DC converters current sharing using fuzzy logic

control, *IEEE Transactions on Power Electronics*, vol. 14, no. 3, pp. 573–577, 1999.

- [141] C. K. Tse, Flip bifurcation and chaos in three-state boost switching regulators, *IEEE Transactions on Circuits and Systems Part I*, vol. 41, no. 1, pp. 16–23, 1994.
- [142] C. K. Tse, Chaos from a buck regulator operating in discontinuous conduction mode, *International Journal of Circuit Theory and Applications*, vol. 22, pp. 263–278, 1994.
- [143] C. K. Tse, Zero-order switching networks and their applications to power factor correction in switching converters, *IEEE Transactions on Circuits and Systems Part I*, vol. 44, no. 8, pp. 667–675, 1997.
- [144] C. K. Tse, *Linear Circuit Analysis*, London: Addison-Wesley, 1998.
- [145] C. K. Tse, Recent developments in the study of nonlinear phenomena in power electronics circuits, *IEEE Circuits and Systems Society Newsletter*, vol. 11, no. 1, pp. 14–21; 47–48, 2000.
- [146] C. K. Tse, Techniques for Experimental Investigation, *Nonlinear Phenomena in Power Electronics*, S. Banerjee and G. Verghese (Editors), Section 4.1, pp. 111–122, New York: IEEE Press, 2001.
- [147] C. K. Tse, Circuit theory of power factor correction in switching converters, *International Journal of Circuit Theory and Applications*, vol. 31, no. 2, pp. 157–198, 2003.
- [148] C. K. Tse and M. di Bernardo, Complex behavior in switching power converters, *Proceedings of the IEEE*, vol. 90, no. 5, pp. 768–781, 2002.
- [149] C. K. Tse and K. M. Adams, On the steady state analysis of switch-mode power converters, *International Journal of Circuit Theory and Applications*, vol. 20, no. 1, pp. 99–105, 1992.
- [150] C. K. Tse and W. C. Y. Chan, Chaos from a current-programmed Ćuk converter, *International Journal of Circuit Theory and Applications*, vol. 23, no 3, pp. 217–225, 1995.
- [151] C. K. Tse and W. C. Y. Chan, Experimental verification of bifurcations in current-programmed boost converters: from quasi-periodicity to period-doubling, *Proceedings of European Conference on Circuit Theory and Design*, pp. 1274–1279, 1997.
- [152] C. K. Tse, O. Dranga and H. H. C. Iu, Bifurcation analysis of a power-factor-correction boost converter: uncovering fast-scale instability, *Proceedings of IEEE International Symposium on Circuits and Systems*, vol. 3, pp. 312–315, 2003.

- [153] C. K. Tse, S. C. Fung and M. W. Kwan, Experimental confirmation of chaos in a current-programmed Ćuk converter, *IEEE Transactions on Circuits and Systems Part I*, vol. 43, no. 7, pp. 605–607, 1996.
- [154] C. K. Tse and Y. M. Lai, Controlling bifurcation in power electronics: a conventional practice re-visited, *Latin American Applied Research*, vol. 31, pp. 177–184, July 2001.
- [155] C. K. Tse, Y. M. Lai and H. H. C. Iu, Hopf bifurcation and chaos in a free-running current-controlled Ćuk switching converter, *IEEE Transactions on Circuits and Systems Part I*, vol. 47, no. 4, pp. 448–457, 2000.
- [156] C. K. Tse, Y. S. Lee and W. C. So, An approach to modelling DC-DC converters using graph theoretic concepts, *International Journal of Circuit Theory and Applications*, vol. 21, no. 4, pp. 371–384, 1993.
- [157] C. K. Tse, Y. Zhou, F. C. .M. Lau and S. S. Qiu, Intermittent chaos and subharmonics in switching power supplies, *Proceedings of IEEE International Symposium on Circuits and Systems*, vol. 3, pp. 332–335, 2003.
- [158] N. B. Tufillaro, T. Abbott and J. Reilly, *An Experimental Approach to Nonlinear Dynamics and Chaos*, New York: Addison-Wesley, 1992.
- [159] R. Tymerski, Volterra series modeling of power conversion systems, *IEEE Power Electronics Specialists Conference Record*, pp. 786–791, 1990.
- [160] R. Tymerski, Application of the time-varying transfer function for exact small-signal analysis, *IEEE Transactions on Power Electronics*, vol. 9, no. 2, pp. 196–205, 1994.
- [161] R. Tymerski and D. Li, State-space models of current programmed pulsedwidth modulated converters, *IEEE Transactions on Power Electronics*, vol. 8, pp. 588–595, 1993.
- [162] S. Wiggins, *Introduction to Applied Nonlinear Dynamical Systems and Chaos*, New York: Springer-Verlag, 1990.
- [163] T. Williams, *EMC for Product Designers*, Butterworth-Heinemann Ltd., 1994.
- [164] R. E. Williamson, R. H. Crowell and H. F. Trotter, *Calculus of Vector Functions*, Englewood Cliffs: Prentice Hall, 1968.
- [165] J. van der Woude, W. L. de Koning and Y. Fuad, On the Periodic Behavior of PWM DC-DC Converters, *IEEE Transactions on Power Electronics*, vol. 14, no. 3, pp. 585–595, 2002.
- [166] M. A. van Wyk and W. H. Steeb, *Chaos in Electronics*, Boston: Kluwer Academic Publishers, 1997.

- [167] A. Wolf, J. Swift, H. Swinney and A. Vastano, Determining Lyapunov exponents from time series, *Physica D*, vol. 16D, pp. 285–314, 1985.
- [168] S. C. Wong and Y. S. Lee, SPICE modelling and simulation of hysteretic current-controlled Ćuk converter, *IEEE Transactions on Power Electronics*, vol. 8, no. 4, pp. 580–587, 1993.
- [169] J. R. Wood, Chaos: a real phenomenon in power electronics, *Proceedings of IEEE Applied Power Electronics Conference and Exposition*, pp. 115–124, 1989.
- [170] C. W. Wu and N. F. Rulkov, Studying chaos via 1-d maps: a tutorial, *IEEE Transactions on Circuits and Systems Part I*, vol. 40, no. 10, pp. 707–721, 1993.
- [171] R. H. Wu, T. Kohama, Y. Kodera, T. Ninomiya and F. Ihara, Load-current-sharing control for parallel operation of dc-to-dc converters, *IEEE Power Electronics Specialists Conference Record*, pp. 101–107, 1993.
- [172] G. H. Yuan, S. Banerjee, E. Ott and J. A. Yorke, Border-collision bifurcations in the buck converter, *IEEE Transactions on Circuits and Systems Part I*, vol. 45, no. 7, pp. 707–716, 1998.
- [173] G. Q. Zhong and F. Ayrom, Experimental confirmation of chaos from Chua’s circuits, *International Journal of Circuit Theory and Applications*, vol. 13, no. 11, pp. 93–98, 1985.

Glossary

Almost periodic function

A function $f(t)$ is an almost periodic function in t if, for any $\epsilon > 0$ and for all t ,

$$|f(t + \tau) - f(t)| < \epsilon$$

for any interval of length $L = L(\epsilon)$ and for some τ independent of t .

Aperiodic function

A function is aperiodic if it is not periodic. See also *periodic function*.

Attractor

An attractor is an invariant set of the state space for a dynamical system which is reached asymptotically as $t \rightarrow \infty$ or $t \rightarrow -\infty$. Any dissipative system, starting from an ensemble of initial points, will shrink to an attractor. Each attractor is surrounded in the phase space by its own basin of attraction [29]. See also *dissipative system*.

Autonomous system

A system is autonomous if it can be described by a differential equation of the form:

$$\frac{dx}{dt} = f(x)$$

where $f(x)$ does not depend on t [53, 135].

Averaged model of a switching system

An averaged model describes the dynamics of a switching system by taking the weighted average of the differential equations describing the system in all sub-intervals of time within a switching period. It effectively removes the dynamical details within a switching period [156].

Basin of attraction

For dissipative systems, more than one attractor may exist for a parameter set. The system eventually approaches one particular attractor, depending upon the initial condition. The closure of the set of initial conditions for which the system approaches to a given attractor is known as the basin of attraction for that attractor [56].

Bifurcation

Bifurcation is the sudden change of qualitative behavior of a system when one or more parameters are varied. Bifurcation literally means splitting into two parts. In nonlinear dynamics, the term has been used to mean splitting of the behavior of a system at a threshold parameter value into two qualitatively different behaviors, corresponding to parameter values below and above the threshold [85].

Bifurcation diagram

A bifurcation diagram is a summary chart of the behavioral changes as some selected parameters are varied [109].

Boost converter

The boost converter is a dc/dc converter whose output voltage is $1/(1 - d)$ times higher than the input voltage, where d is the duty cycle of the main power switch [121]. See also *duty cycle*.

Border collision

Border collision is a bifurcation that involves structural change of the system at the bifurcation point. It is characterized by an alteration of the operation of the system. In switching circuits, such an alteration is manifested by the change in the topological sequence of the switching cycle [103].

Buck converter

The buck converter is a dc/dc converter whose output voltage is a fraction d of the input voltage, where d is the duty cycle of the main power switch [121]. See also *duty cycle*.

Buck-boost converter

The buck-boost converter is dc/dc converter whose output voltage is either higher or lower than the input voltage, depending upon the value of the duty

cycle d . The input to output voltage ratio is given by $d/(1 - d)$ [121]. See also *duty cycle*.

Center manifold

In a local bifurcation involving loss of instability of an attractor, there is a set of critical eigenvalues corresponding to a neutral (non-attracting non-repelling) response under a linear approximation. All essential bifurcation phenomena can be observed in the reduced space defined by the *center manifold* which is the eigenspace associated with those critical eigenvalues [2].

Chaos

See *deterministic chaos*.

Chaotic transient

Chaotic transient is a long irregular transient motion, which eventually leads to an attractor of any type. It can be due to the presence of an unstable chaotic orbit coexisting with an attractor.

Characteristic multiplier

Characteristic multipliers are the eigenvalues of the Jacobian of a discrete-time iterative system. The system is locally stable if all the characteristic multipliers have a magnitude of less than 1 [138].

Co-dimension of bifurcation

The co-dimension of a bifurcation is the number of parameters that must be specified in order to define that bifurcation [65].

Coexisting solutions

Some nonlinear dynamical systems may have two or more solutions coexisting for given fixed parameter values [53].

Conservative system

In a conservative system, energy remains constant along the solution. Typically, a conservative system can be described by

$$\frac{dx}{dt} = \frac{\partial \mathbf{H}}{\partial y}$$

$$\frac{dy}{dt} = -\frac{\partial \mathbf{H}}{\partial x}$$

where \mathbf{H} is called the *Hamiltonian function* or *energy function*. Conservative systems are also called *Hamiltonian systems* [44].

Continuous conduction mode

When a dc/dc converter operates with its inductor current always assuming a non-zero value, it is said to be operating in continuous conduction mode [100].

Controlling chaos

Control of chaos refers to the elimination of chaotic motion in a system. The usual objective is to make the system operate in a desired periodic state [75].

Crisis

A crisis is a bifurcation of an attractor in which the attractor changes abruptly and discontinuously. An *interior crisis* is a *catastrophic-explosive* bifurcation which involves a sudden, instantaneous enlargement of the attractor. A *boundary crisis* is a *catastrophic-dangerous* bifurcation which has a blue sky disappearance of the attractor, giving a sudden jump to a remote unrelated attractor [101].

Ćuk converter

The Ćuk converter is a fourth-order dc/dc converter, which was invented by Slobodán Ćuk in the late 1970s. This converter exhibits non-pulsating input and output currents [37].

Current-mode control

Current-mode control is a popular control method for controlling dc/dc converters. The output voltage error is amplified to give a control signal which is used as a template to directly program the inductor current through a fast control loop. Current-mode control is used mainly for the boost and buck-boost types of converters [99].

Dangerous bifurcation

Dangerous bifurcation is a bifurcation via which a solution abruptly jumps to a remote one [138].

Deterministic chaos

A behavior exhibited by a deterministic system, which is characterized by a random-like motion and lack of long-term predictability, is called chaos. When a system is behaving chaotically, it is extremely sensitive to initial condition, and its largest average Lyapunov exponent is positive [3].

Deterministic system

A deterministic system is a system that can be described without the inclusion of any random process [4].

Difference equation

A difference equation describes the dynamics of a discrete variable. The usual form is: $x_{n+1} = f(x_n, \mu)$, where μ is a set of parameters. The term difference equation is used synonymically with *iterative map*, *discrete-time map*, or *Poincaré map*.

Discontinuous conduction mode

When a dc/dc converter operates with its inductor current assuming a zero value for some interval of time in a switching period, it is said to be operating in discontinuous conduction mode [100].

Dissipative system

A system that dissipates energy as time elapses is a dissipative system. It has a negative divergence, and always tends toward an attractor [162]. See also *divergence*.

Divergence

For a system described by a set of N first-order differential equation, i.e., $\dot{\mathbf{x}} = \mathbf{f}(\mathbf{x})$, the scalar divergence of \mathbf{f} is [164]

$$\text{div}(\mathbf{f}(\mathbf{x})) = \frac{\partial f_1}{\partial x_1} + \frac{\partial f_2}{\partial x_2} + \cdots + \frac{\partial f_n}{\partial x_n}$$

Duty cycle or duty ratio

The duty cycle is defined as the fraction of the switching period during which the main power switch (or the switch concerned) is turned on [128].

Eigenvalue and eigenvector

Let \mathbf{A} be an n -dimensional square matrix. The eigenvalues $\lambda_1, \lambda_2, \dots, \lambda_n$ are the solutions of the characteristic equation

$$\det(\mathbf{A} - \lambda \mathbf{1}) = 0$$

where $\mathbf{1}$ is the unit matrix. For each eigenvalue λ_i , there is a corresponding eigenvector, \mathbf{v}_i , which satisfies

$$(\mathbf{A} - \lambda_i \mathbf{1})\mathbf{v}_i = 0.$$

Equilibrium point or solution

For the dynamical system $\dot{\mathbf{x}} = \mathbf{f}(\mathbf{x})$, the point \mathbf{X} is called an equilibrium point if

$$\mathbf{f}(\mathbf{X}) = 0.$$

Equilibrium points are also called *fixed points*.

Feigenbaum number

See *period-doubling cascade*.

Fixed point

See *equilibrium point*.

Flip bifurcation

Flip bifurcation is a bifurcation characterized by the loss of stability of a period-1 solution and the birth of a period-2 solution. If the newly born period-2 solution is stable, it is called *supercritical flip bifurcation*. If the newly born period-2 solution is unstable, it is called *subcritical flip bifurcation*. Flip bifurcation is also called *period-doubling bifurcation* [138]. See also *bifurcation*.

Fundamental solution

A fundamental solution is a fixed point. For switching converters under an averaged modeling viewpoint, a fundamental solution is equivalent to a period-1 solution.

Hamiltonian system

See *conservative system*.

Harmonic balance

Harmonic balance is a common procedure to approximate the periodic solutions of differential equations. The solution is assumed to take the form

$$x = a_0 + \sum_{i=1}^N a_{2i-1} \cos(i\omega t) + \sum_{i=1}^N a_{2i} \sin(i\omega t).$$

Then, putting it into the differential equation gives terms involving products of powers of $\sin(i\omega t)$ and $\cos(i\omega t)$. These terms can then be expanded to sums of sines and cosines of higher harmonics. Finally, harmonic balance implies equating to zero all coefficients of sines and cosines. This gives expressions for the unknown coefficients in the above approximate expression.

Hopf bifurcation

Hopf bifurcation is a bifurcation characterized by the loss of stability of a focus as a parameter is varied, leading to the birth of a limit cycle. If the newly born limit cycle is a stable one, it is called *supercritical Hopf bifurcation*. If the newly born limit cycle is an unstable one, it is called *subcritical Hopf bifurcation*. In the supercritical case, the system is attracted to a limit cycle after the bifurcation, whereas in the subcritical case, the system goes to some distant part of the state space. In terms of the movement of the eigenvalues as the parameter is varied, Hopf bifurcation is characterized by the transversal crossing of a pair of complex eigenvalues at the imaginary axis [135].

Intermittency

Intermittency is a behavior characterized by long periods of periodic motion with occasional irregular bursts. There are three types of bifurcation that lead to intermittency. The first type is related to tangent bifurcation of a one-dimensional map, which is characterized by the loss of stability when the real eigenvalue of the fixed point moves across the unit cycle at +1. The second type is related to subcritical Hopf bifurcation. The third type is related to subcritical period-doubling bifurcation [65].

Iterative map

See *difference equation*.

Jacobian

For the one-dimensional system $\dot{x} = f(x)$, the Jacobian is $df(x)/dx$ [138]. For a higher-order system described by

$$\dot{\mathbf{x}} = \begin{bmatrix} f_1(\mathbf{x}) \\ f_2(\mathbf{x}) \\ \vdots \\ f_n(\mathbf{x}) \end{bmatrix}.$$

the Jacobian \mathbf{J}_f is a matrix which is given by

$$\mathbf{J}_f = \begin{bmatrix} \frac{df_1}{dx_1} & \frac{df_2}{dx_1} & \dots & \frac{df_n}{dx_1} \\ \frac{df_1}{dx_2} & \frac{df_2}{dx_2} & \dots & \frac{df_n}{dx_2} \\ \vdots & \ddots & & \vdots \\ \frac{df_1}{dx_n} & \frac{df_2}{dx_n} & \dots & \frac{df_n}{dx_n} \end{bmatrix}_{\mathbf{x}=\mathbf{X}}.$$

Laplace transform

The Laplace transform is a mathematical transformation which converts a time-domain representation $f(t)$ to a complex-frequency-domain representation $F(s)$ [144].

$$F(s) = \int_0^{\infty} e^{-st} f(t) dt$$

It is also useful as a tool to solve differential equations. Typically, a differential equation can be transformed to an algebraic one via the Laplace transform.

Limit cycle

A limit cycle is a periodic orbit assumed by an autonomous system.

Linearization

Linearization is a process whereby a nonlinear system is represented by a linear differential equation. The resulting representation is accurate only for describing the system in a small neighborhood of the equilibrium point about which linearization is carried out [135]. For the system $\dot{\mathbf{x}} = \mathbf{f}(\mathbf{x})$, the linearized equation around the equilibrium point $\mathbf{x} = \mathbf{X}$ takes the form

$$\Delta \dot{\mathbf{x}} = \mathbf{J}_f(\mathbf{X}) \Delta \mathbf{x}$$

where $\mathbf{J}_f(\mathbf{X})$ is the Jacobian evaluated at $\mathbf{x} = \mathbf{X}$.

Logistic map

The logistic map is an iterative map given by

$$x_{n+1} = \mu x_n(1 - x_n)$$

where μ is a parameter which can be varied to effect a period-doubling bifurcation [54].

Lorenz system

The Lorenz system is originally proposed to model the convective flow in the atmosphere. It is a three-dimensional system given by

$$\begin{aligned}\frac{dx}{dt} &= -\sigma(x - y) \\ \frac{dy}{dt} &= -xz + rx - y \\ \frac{dz}{dt} &= xy - bz\end{aligned}$$

where σ , r and b are dimensionless parameters [92, 134].

Lyapunov exponent

The Lyapunov exponent is a measure of the sensitive dependence of a system's solution to the initial condition [167].

Neimark-Sacker bifurcation

Neimark-Sacker bifurcation is a bifurcation whereby a periodic limit cycle is replaced by a quasi-periodic solution. It is the same as Hopf bifurcation, but is used mainly in discrete-time systems.

Non-autonomous system

A non-autonomous system is described by a differential equation having an explicit dependence upon time, i.e.,

$$\frac{d\mathbf{x}}{dt} = \mathbf{f}(\mathbf{x}, t).$$

Normal form

The normal form of a nonlinear system is a simplified form of the system which retains the necessary qualitative behavior of the system near a bifurcation point [44]. See also *center manifold*.

Period-doubling bifurcation

See *flip bifurcation*.

Period-doubling cascade

A period-doubling cascade is a common route to chaos, in which a periodic orbit keeps doubling its period through a series of flip or period-doubling bifurcation. As the parameter increases in the direction of the cascade, the bifurcations become more and more closely spaced. The ratio of the successive parameter intervals tends to a limit, which is known as the *Feigenbaum number*, $\delta_\infty = 4.66920\dots$ This limiting ratio is universal and arises in a very wide class of problems [54].

Periodic function

A function $f(t)$ is periodic with period T if

$$f(t + T) = f(t) \quad \text{for all } t.$$

Pitchfork bifurcation

Pitchfork bifurcation is a bifurcation characterized by the loss of stability of an equilibrium point leading to the birth of two equilibrium points. If the newly born equilibrium points are stable, it is a supercritical pitchfork bifurcation. If the newly born equilibrium points are unstable, it is a subcritical pitchfork bifurcation. In the supercritical case, the system assumes a new stable state, whereas in the subcritical case, the system may blow up to a remote solution [135].

Poincaré map

A Poincaré map describes a continuous dynamical system in terms of a discrete map or difference equation. The method is based on a geometrical interpretation in which the trajectory moving in the state space intersects with a plane at discrete instants of time. The relation between two consecutive points intersecting the plane in the same direction is called a Poincaré map. Its final form is mathematically equivalent to *difference equation*.

Poincaré section

A Poincaré section is a plane in the state space on which the trajectory intersects transversally. The consecutive points of intersection define the Poincaré map [109]. See also *Poincaré map*.

Power factor

Power factor is defined as the ratio of the real power to the apparent power. It normally refers to the input side of a converter. The real power is the actual or average power supplied to the converter. The apparent power is the product of the root-mean-square input voltage and the root-mean-square input current [121, 147].

$$\text{Power factor} = \frac{\text{Real input power}}{V_{\text{in,rms}} I_{\text{in,rms}}}$$

Power factor correction

The process whereby the power factor is raised to a value approaching unity is called power factor correction. The converter that performs this process is called power-factor-correction converter [147].

Quasi-periodic function

A function is quasi-periodic if it contains frequency components which are not rationally related [110]. See also *almost periodic function*.

Robustness

Models or solutions that are not sensitive to small variations of parameters are said to be robust.

Route to chaos

A route to chaos is the sequence of bifurcations through which a system becomes chaotic [138].

Saddle-node bifurcation

Saddle-node bifurcation is a bifurcation characterized by a sudden loss or appearance of a solution [1]. It is also called *blue sky bifurcation*.

Stroboscopic map

A stroboscopic map is a discrete map or iterative map obtained by sampling a continuous system periodically [19]. See also *Poincaré map*.

Structural change of switching converters

A switching converter is said to be structurally changed if its topological sequence in a switching cycle is altered. A converter may encounter a structural change at an operational boundary. A trivial case is when a converter changes its operation from continuous conduction mode to discontinuous conduction mode as a result of load variation.

Subharmonic cascade

See *period-doubling cascade*.

Subharmonic operation of switching circuits

A periodic operation is called a subharmonic operation if its period is an integer multiple of the switching period. Subharmonic operation can result from period-doubling bifurcation.

Trajectory

The solution $\mathbf{x}(t)$ of the system $\dot{\mathbf{x}} = \mathbf{f}(\mathbf{x})$, given $\mathbf{x}(0) = \mathbf{x}_0$, plotted on the state space, is called the trajectory of the system. In the steady state, the trajectory, if periodic, is called an orbit.

Transcritical bifurcation

Transcritical bifurcation is a bifurcation characterized by an exchange of stability between two equilibrium solutions [44].

Transient chaos

See *chaotic transient*.

Voltage-mode control

Voltage-mode control is a popular control method for dc/dc converters. The output voltage is compared with a reference level, and the error is amplified to become a control signal which is used to generate the driving signal for the power switch with continuously adjusted duty cycle [118].